Defining the role of LRIG1 dependent EGFR signalling on airway homeostasis and lung cancer development

Laura Succony

Lungs for Living Research Centre
UCL Respiratory
University College London

A thesis presented for the degree of
Doctor of Philosophy
2017

Declaration

I, Laura Succony, confirm that the work presented in this thesis is my own. Where information has been derived from other sources I confirm that this has been acknowledged.

Abstract

Aberrations of EGFR signalling drive cancer development. In squamous cell lung cancer, EGFR is overexpressed. LRIG1 is a negative regulator of EGFR and patient pre-invasive squamous cell lung cancer samples show LRIG1 loss, suggesting involvement in early disease pathogenesis. In skin and gut homeostasis, LRIG1 regulates stem cells. In the upper airway, basal cells act as stem cells and are the putative origin of squamous cell lung cancer. I hypothesise LRIG1 has a key role in the airway homeostasis and its loss tilts this towards pre-invasive squamous cell lung cancer development.

Lrig1 EGFP-ires-CreERT2 mice delineated airway LRIG1 expression. Flow sorted LRIG1-positive and -negative murine basal cells were used in 2D and 3D colony-forming, spheroid and proliferation assays. A murine squamous cell lung cancer model was set up through application of N-Nitrosotris-(2-chloroethyl)urea (NTCU). Pre-invasive lesions and tumour development were compared between wild-type (WT), LRIG1-heterozygous and LRIG1-null animals. Human basal cells obtained from bronchoscopy were sorted according to LRIG1 expression and used directly in colony-forming assays or maintained in primary culture to assess the effect of shRNA knockdown of LRIG1.

LRIG1 is expressed by 50% of airway basal cells. LRIG1-expressing murine basal cells exhibit increased colony-forming capacity ($p=0.0133$), spheroid formation ($p=0.0020$) and proliferation ($p=0.0011$) compared to LRIG1-negative cells. Similarly, LRIG1-expressing human airway basal cells isolated from endobronchial brush biopsy samples exhibit increased colony-forming capacity ($p=0.0067$) and proliferation ($p=0.0153$). Topical application of NTCU to mice recapitulates the development of human pre-invasive and squamous cell lung cancer lesions after 23 weeks. Results show lesions in LRIG1-null mice to be larger than those of WT animals. shRNA knockdown of LRIG1 in cultured human airway basal cells alters cell phenotype, leading to increased colony-forming efficiency and greater proliferation at cell confluence.

LRIG1 has an important role in stem cell homeostasis of the human and murine airway epithelium. Loss of LRIG1 promotes lesion development in a murine squamous cell lung cancer mouse model and alters behaviour of human epithelial cells in culture, indicating a potential target for the treatment of squamous cell lung cancer in humans.

Acknowledgements

I would like to thank my supervisor, Professor Sam Janes, for giving me the opportunity to undertake a PhD at University College London and his advice and support throughout my studies.

A big thank you also to Kate, Sandra, Rob, Krish, Vitor and Manu for their help, advice and friendship over the course of my PhD. I am grateful to everyone in the Lungs for Living Research Group, and more widely within UCL respiratory for making the past 4 years so enjoyable.

I am grateful to Derek Davies and Sukhveer Purewal for their assistance with the flow cytometry experiments, to Professor Nick Wright for teaching me preinvasive lesion pathology and to Rebecca Towns for her assistance with the animal work.

Finally, I would like to thank both Cancer Research UK and the Wellcome Trust for funding my PhD.

Table of contents

Defining the role of LRIG1 dependent EGFR signalling on airway homeostasis and lung cancer development 1

Declaration 2

Abstract 3

Acknowledgements 5

Table of contents 6

1. Introduction 10

1. Introduction 11

1.1 Lung cancer 11

1.1.1 Staging of lung cancers 11

1.1.2 Targeted treatments for lung cancer 12

1.1.3 Molecular pathogenesis of squamous cell lung cancer and potential treatment targets 14

1.1.4 Impact of smoking and genetic changes within the airway epithelium 15

1.1.5 Preinvasive squamous cell lung cancer 15

1.2 The EGF receptor and regulation of signalling 19

1.2.1 The regulation of ERBB signalling 21

1.2.2 LRIG1 structure 23

1.2.3 LRIG1 in the negative regulation of EGFR 24

1.2.4 LRIG1 as a stem cell regulator 28

1.2.5 LRIG1 in cancer 32

1.2.6 The role of LRIG1 in epithelial-to-mesenchymal transition (EMT) 35

1.2.7 The other LRIG proteins 36

1.3 Stem cells of the lung and lung cancer cell of origin 37

1.3.1 Structure of the lung and respiratory epithelium 37

1.3.2 Lung stem cells and the stem cell niche 38

1.3.3 Stem cells of the upper airway 41

1.3.4 Stem cells of the small airways and alveoli 42

1.3.5 The lung cancer cell of origin 45

1.3.6 Lung cancer stem cells 47

1.3.7 Genetic heterogeneity and clonal evolution in lung cancer 48

1.4 Summary 49

1.5 Hypothesis 50

1.6 Aims 50

2. Materials and methods 52

2.1 Chemicals, solvents and plastic ware 52

2.2 Tissue collection 52

2.2.1 Animal breeding strategy 52

2.2.2 Human tissue collection 52

2.3 Genotyping Animals 53

2.3.1 Ear snip digest and PCR 53

2.3.2 Agarose gel electrophoresis 55

2.3.3 Ethanol purification of ear snip DNA 55

2.3.4 Sequencing primer B 55

2.3.5 Immunofluorescent imaging of earnsips 56

2.4 Isolation of murine tissues 56
2.4.1 Isolation of the trachea 56
2.4.2 Isolation of murine lungs following insufflation 56
2.4.3 Isolation of bone marrow cells 57
2.4.4 Isolation of skin samples for histological processing 57
2.4.5 Isolation of skin cells for flow cytometry 57
2.5 Isolation of murine airway basal cells 58
2.5.1 Pronase digest 58
2.5.2 Dispase/DNase/trypsin/collagenase digest 58
2.5.3 Isolation of tracheal cells via collagenase digest 59
2.6 Lineage tracing 59
2.7 Isolation of human brush biopsied epithelial cells 60
2.8 Analysis of cells by flow cytometry 60
2.8.1 Flow cytometry staining 60
2.8.2 Flow cytometry analysis 60
2.8.3 Flow cytometry antibodies 61
2.8.4 Flow cytometry cell sorting 61
2.8.5 Hoescht 33342 cell cycle analysis 62
2.8.6 EdU cell proliferation analysis 63
2.9 Analysis of epithelial cells in situ 63
2.9.1 Tissue processing and haematoxylin and eosin staining 63
2.9.2 Immunofluorescent staining 63
2.9.3 Antibodies used 65
2.9.4 Immunohistochemistry staining 66
2.9.5 Assessing the proliferation of adult airway epithelial cells 66
2.9.6 Assessment of epithelial thickness, proliferation and number of basal cells 66
2.10 Mouse airway epithelial cell culture 67
2.10.1 Tracheosphere assay 67
2.10.2 Colony forming assay 68
2.11 Human airway epithelial cell culture 68
2.11.1 3T3-J2 feeder cell culture 68
2.11.2 Human airway epithelial cell culture in 3T3-J2 co-culture with ROCK inhibition (3T3 + Y) 69
2.11.3 Colony forming assay directly from flow-sorted cells (96-well plates) 69
2.11.4 Colony forming assay in cultured HBECs (6-well plates) 70
2.11.5 XTT assay 70
2.11.6 Invasion assay through Matrigel 70
2.11.7 Organotypic assay 71
2.12 Other tissue culture 72
2.12.1 HEK293T cell culture 72
2.12.2 Human lung fibroblast culture 72
2.12.3 Mycoplasma testing 72
2.13 shRNA knock down of LRIG1 73
2.13.1 Preparation of plasmid DNA 73
2.13.2 Production of virus 73
2.13.3 Titration of virus 74
2.13.4 Viral transduction 74
2.14 Western Blotting 75
2.14.1 Sample preparation 75
2.14.2 Immunoblotting 76
2.14.3 Antibodies used 76

2.15 Single cell RNA sequencing 77
2.16 N-Nitrosotris-(2-chloroethyl)urea (NTCU) in a squamous carcinogenesis model 77
2.16.1 NTCU treatment 77
2.16.2 Assessment of disease extent 78
2.16.3 Assessment of tumour proliferation 81
2.17 Statistics 81

3. Expression of LRIG1 in the murine airway 82

3. Expression of LRIG1 within the murine airway 83
3.1 Background 83
3.2 Aims 85
3.3 Results 85
3.3.1 Establishment of the *Lrig1* EGFP-ires-CreERT2 colony 85
3.3.2 The effect of *Lrig1* haploinsufficiency 86
3.3.3 The establishment of a genotyping strategy for the *Lrig1* EGFP-ires-CreERT2 colony 89
3.3.4 Confirmation that homozygosity for the *Lrig1* EGFP-ires-CreERT2 cassette correlates with loss of protein production 92
3.3.5 Correlation of eGFP with LRIG1 expression 92
3.3.6 Expression of LRIG1 in the airway epithelium 94
3.3.7 Effect of loss of LRIG1 on the airway epithelium 96
3.3.8 Isolation of airway epithelial cells 98
3.3.9 Pronase digestion of the tracheal epithelium 101
3.3.10 Analysis of epitope expression following pronase digestion 101
3.3.11 Alternative methods of epithelial digestion 103
3.3.11 Assessment of growth and differentiation potential of isolated murine basal cells 107
3.3.12 Assessment of LRIG1 expression in airway epithelial cells 109
3.3.13 Lineage tracing from LRIG1-expressing basal cells 112
3.4 Discussion 116
3.5 Summary 121

4. Analysing the effects of LRIG1 expression on the properties of murine basal cells 123
4.1 Background 123
4.2 Aims 125
4.3 Results 125
4.3.1 The effect of LRIG1 expression on the proliferation of airway basal cells 125
4.3.2 The effect of LRIG1 on the stem cell behaviour of airway basal cells 128
4.3.3 Single cell RNA Sequencing: Cell preparation 132
4.3.4 Single cell sequencing: cell quality and gene checks 134
4.3.5 Single cell sequencing: Assessment of cell populations 137
4.4 Discussion 141
4.5 Summary 149

5. Assessment of LRIG1 in the Human Airway 150

5. Assessment of LRIG1 in the Human Airway 151
5.1 Background 151
5.2 Aims 152
5.3 Results 152
5.3.1 Expression of LRIG1 within the human airway 152

5.3.2 Colony-forming efficiency of LRIG1^{+} versus LRIG1^{-} basal cells....155
5.3.3 The proliferation of LRIG1^{+} versus LRIG1^{-} basal cells....157
5.3.4 shRNA knockdown of *LRIG1* in human epithelial cells....159
5.3.5 Effect of *LRIG1* shRNA knockdown on EGFR activation....161
5.3.6 The effect of *LRIG1* shRNA knockdown on colony-forming ability....164
5.3.7 The effect of *LRIG1* shRNA knockdown on cell proliferation; optimising the EdU assay 166
5.3.8 The effect of LRIG1 shRNA knockdown on cell proliferation at confluence....168
5.3.9 The effect of *LRIG1* shRNA knockdown on rate of proliferation....170
5.3.10 The effect of *LRIG1* shRNA knockdown on invasion and differentiation of epithelial cells....173
5.4 Discussion....178
5.5 Summary....184
6. The effect of LRIG1 loss in a murine squamous cell lung cancer model 185
6. The effect of LRIG1 loss in a murine squamous cell cancer model..... 186
6.1 Introduction....186
6.2 Aims....189
6.3 Results....189
6.3.1 NTCU treatment optimisation and establishment of a treatment protocol....189
6.3.2 An optimised treatment course for NTCU....193
6.3.3 NTCU treatment complications....196
6.3.4 Investigation for NTCU-associated disease in other organs....200
6.3.5 Validation of NTCU-induced preinvasive squamous cell lesions....202
6.3.6 Assessment for markers of adenocarcinoma....204
6.3.7 Elucidating the possible cell of origin of preinvasive and squamous cell lung cancers 205
6.3.8 Development of lung adenocarcinoma....209
6.3.9 Association of LRIG1 with preinvasive and invasive squamous cell lung tumours 211
6.3.10 Assessment of the effects of NTCU application....213
6.3.11 Proliferative index of tumours from wild-type, LRIG1-heterozygous and LRIG1-null animals....216
6.4 Discussion....220
6.5 Summary....228
7. Summary/ Future Directions....230
7.1 Summary....230
7.2 Future directions....232
8. Supplementary....235
9. References....239

1. Introduction

1. Introduction

1.1 Lung cancer

Lung cancer is responsible for 22% of all UK cancer deaths, amounting to 46,000 deaths a year. It is the commonest cause of UK cancer death, and in contrast to other malignancies, little improvement in lung cancer survival has been seen over the past four decades. In 1972, the lung cancer 5-year survival was 4.6%, increasing to 9.5% by 2011, but in contrast, leukaemia survival has gone from 12.9 to 51.6% over the same time period (1). These figures highlight the need for improved lung cancer diagnostics and treatment strategies.

There are two main subtypes of lung cancer, which are distinguished by their histological appearances. Small cell lung cancer (SCLC) is responsible for 15% of lung cancer cases, and is termed due to the histological appearance of tightly packed small cells with a large nucleus, whilst non-small cell lung cancer (NSCLC) constitutes around 85% of cases (2). NSCLCs can be further divided into adenocarcinomas, squamous cell carcinomas and large cell carcinomas (2). Squamous cell lung cancer is the commonest form of lung cancer in the UK (1).

The association of smoking with lung cancer has been known since the 1950s (3) and smoking remains the predominant lung cancer risk factor, particularly in relation to SCLC and squamous cell carcinoma. Other risk factors include exposure to radon gas (where risk is increased in smokers) (4), passive smoking (5, 6), air pollution, occupational asbestos exposure and a genetic predisposition (2).

1.1.1 Staging of lung cancers

The extent to which the lung cancer has affected the body is classified according to two staging systems, the first is the TNM (tumour, node, metastases) staging system;

T considers the tumour size, N the presence of any associated lymph nodes and M, whether the disease has metastasised beyond the lungs (7). The second classification system divides the disease into 4 groups; stage 1 is localised to the lungs, stage 2 and 3 are where the tumour has grown larger and may have spread to the lymph nodes, and stage 4 is when the cancer has spread to other areas of the body (8). The stage of lung cancer influences the available treatments. In early stage lung cancer, the goal is to eradicate disease and surgical management is the treatment of choice (9). With more advanced disease and spread to the lymph nodes or other organs chemotherapy or radiotherapy becomes appropriate. 48% of patients present with late stage lung cancer (stage 4) (8) and palliative chemotherapy or radiotherapy treatments, where the aim is to prolong life and treat symptoms, are the only options.

1.1.2 Targeted treatments for lung cancer

Until the 1990s treatment of lung cancer consisted of platinum-based chemotherapies; these were later followed by the introduction of third-generation cytotoxic agents such as gemcitabine that improved lung cancer survival to around 8 months and at this point the lung cancer survival was seen to plateau (10). In recent years the molecular pathogenesis of adenocarcinoma has been investigated. The development of lung adenocarcinoma is frequently associated with a single molecular abnormality, including the presence of activating mutations in Kirsten rat sarcoma viral oncogene homolog (KRas) and the epidermal growth factor receptor (EGFR) (11). Targeting lung cancer treatments to the abnormality within the tumour has been shown to improve survival in appropriately selected patients. These targeted treatments include EGFR inhibitors and inhibitors of the echinoderm microtubule-associated protein-like 4 (*EML4*) and anaplastic lymphoma kinase (*ALK*) (*ELM4-ALK*) fusion transcript (10).

EGFR inhibitors

Activation of the EGFR signalling pathway leads to a number of downstream consequences including proliferation and inhibition of apoptosis, which are important in lung cancer development (12). Activating mutations in the tyrosine kinase domain of the EGF receptor leads to constitutively active signalling. EGFR mutations act as driver mutations in 10% of UK adenocarcinomas, but account for as many as 30-50% of driver mutations in tumours from South-East Asia (13). These mutations occur most frequently in women and non-smokers (2). The administration of tyrosine kinase inhibitors such as gefitinib, have been found to improve survival beyond that of platinum-based chemotherapy agents (14, 15). However, despite the initial response rate, resistance to tyrosine kinase inhibitors occurs after 9-11 months. This is due to the development of a second mutation in the catalytic cleft of the EGFR tyrosine kinase domain, which prevents access of the tyrosine kinase inhibitor (16). The most common mutation is the T790M mutation that prevents binding of the inhibitor molecule (17).

ELM4-ALK inhibition

The *EML4-ALK* fusion transcript is seen in 6.7% of patients with non-small cell lung cancer, predominantly in adenocarcinomas (18). This is an oncogenic rearrangement in chromosome 2 that leads to ligand-independent dimerisation of the *ALK* domain and consequent constitutive cellular proliferation and inhibition of apoptosis through the downstream activation of mitogen-activated protein (MAP) kinases and the phosphatidylinositol 3-kinase (PI3K) signalling pathways. Crizotinib, a drug that targets the ALK rearrangement, has been shown to improve progression-free survival from 3.0 months with conventional chemotherapy to 7.7 months (19).

Cetuximab

Cetuximab is a chimeric human IgG1 antibody that competitively binds to the EGF receptor and prevents ligand binding, receptor phosphorylation and activation of downstream signalling (20). Antibody-receptor complexes are internalised, resulting

in the removal of the EGF receptor from the cell membrane and preventing further activation (21).

1.1.3 Molecular pathogenesis of squamous cell lung cancer and potential treatment targets

The molecular pathogenesis of squamous cell lung cancer is more complex than that of adenocarcinoma, and the development of targeted treatments for squamous cell lung cancer is lagging behind that for adenocarcinoma. Common pathways that are affected in the development of squamous cell lung cancer include those regulating the response to cellular stress (Nuclear factor erythroid 2-related factor 1 (NFE2LL)/ Kelch-like ECH-associated protein 1 (KEAP1)/ Cullin-3 (CUL3)), squamous differentiation (sex determining region Y-box 2 (SOX2)/ NOTCH/tumour protein p63 (TP63)), intracellular signalling (PI3K/protein kinase B (AKT)) and cell cycle regulation (cyclin-dependent kinase inhibitor 2A (CDKN2A)/ retinoblastoma 1 (RB1)) (22, 23).

Potential squamous cell lung cancer therapeutic targets are the PIK3 mutation (4% of squamous lesions) and amplification (33% of lesions), or the overexpression of the fibroblast growth factor receptor 1 (FGFR1) that is seen in 20% of cases (22, 24). The use of FGF inhibitors in xenograft tumour models has led to lesion regression (25) and there are currently early clinical trials of PIK3 inhibitors such as buparlisib and FGFR1 inhibitors, the results for which are awaited (24).

In contrast to adenocarcinoma, EGFR-activating mutations are seen in only 1-2% of squamous cell lung cancers (22), however as many as 88% of squamous cell lung cancers show overexpression of EGFR in the absence of a mutation (26, 27). This EGFR overexpression has been targeted by the administration of cetuximab to patients with squamous cell cancers. In the SQUIRE trial, stage 4 squamous cell lung cancers were randomly assigned to chemotherapy +/- necitumumab (an IgG1 monoclonal antibody to the EGF receptor agent that is related to cetuximab), with

the necitumumab treatment shown to improve survival from 9.9 to 11.5 months (28). Further results obtained from the FLEX trial, which added cetuximab to standard chemotherapy for NSCLC, found a survival benefit that was greatest in patients with squamous cell lung cancer arm compared to those with other histological subtypes (28, 29).

1.1.4 Impact of smoking and genetic changes within the airway epithelium

Smokers are predisposed to a number of respiratory conditions including emphysema, bronchitis and lung cancer. The majority of squamous cell lung cancers are caused by smoking (8), with exposure to cigarette smoke associated with effects on airway epithelial gene expression (30). A recent study has revealed that for every year a smoker smokes one packet of cigarettes per day, there is the accumulation of an extra 150 mutations per lung cell (31). A comparison of samples obtained at bronchoscopy from smokers and never smokers found 97 differentially expressed genes within airway epithelial cells. Upregulated genes in smokers included those for xenobiotic function (e.g. cytochrome P450 family 1 subfamily B member 1 (CYP1B1)), antioxidants (e.g. aldehyde dehydrogenase 3 family member A1 (ALDH3A1)) and electron transport system (e.g. nicotinamide adenine dinucleotide phosphate (NADPH)) (32). On smoking cessation, many of these changes were fully reversed, but a few persisted (33). Work by Boelens *et al* (30) confirmed these findings and, in addition, showed that genes associated with the oxidative stress response, adhesion, cell proliferation and apoptosis were upregulated in the epithelium of current smokers compared with ex-smokers, and that these changes were magnified further on the development of squamous cell lung cancers.

1.1.5 Preinvasive squamous cell lung cancer

One of the reasons lung cancer survival is so poor is its late detection (34, 35). However, squamous cell lung cancer has an early, premalignant phase, where lesions develop from abnormal areas of bronchial epithelium. Histologically, these become

increasingly dysplastic before the development of carcinoma-in-situ (CIS) and the eventual breach of the basement membrane that leads to the development of an invasive tumour. The World Health Organisation has classified lesions into nine categories ranging from normal through to inflammation, basal cell hyperplasia, squamous metaplasia, mild dysplasia, moderate dysplasia, severe dysplasia, CIS and invasive disease (36, 37) (Figure 1.1). The morphology of these lesions changes with increasing severity: initially the nuclei change, with an increase in nuclear to cytoplasmic ratio, the presence of nucleoli and a lack of nuclear orientation, and this is accompanied by an increase in cell crowding and a lack of orientation in the tissue. The initial abnormalities only affect the basal layer, but subsequently increase to involve the full thickness of the epithelium (38). These changes are accompanied by an increased mutational burden.

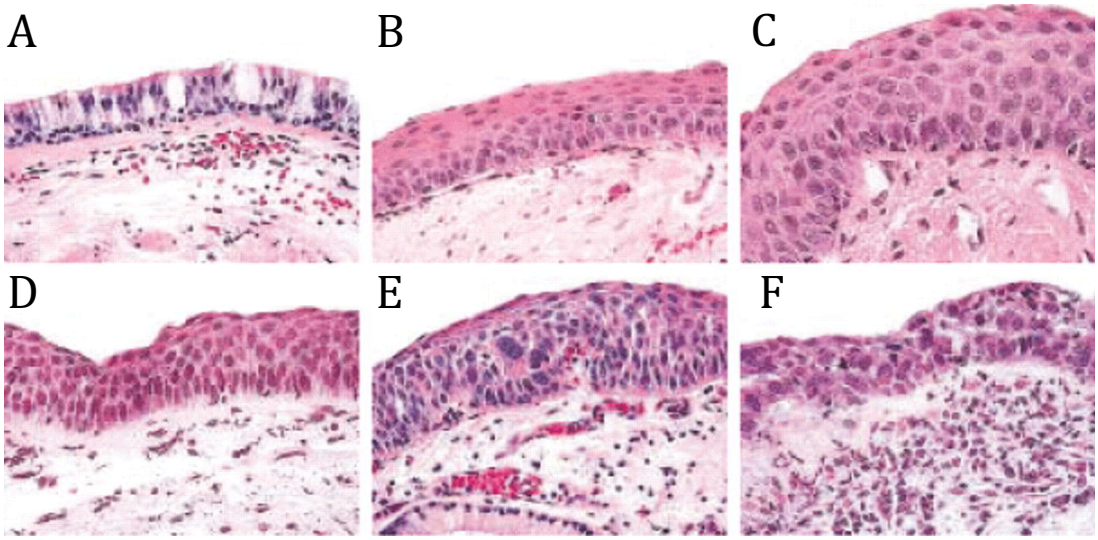

Figure 1.1: Histological changes associated with preinvasive lung cancer

The development of preinvasive lung cancer lesions is associated with progressively more disorganisation within the airway epithelium. A) Normal airway B) Squamous metaplasia C) Mild dysplasia D) Moderate dysplasia E) Severe dysplasia F) Carcinoma-in-situ. Changes according to the WHO classification of preinvasive lung cancer lesions (39).

The natural history of preinvasive lung cancer is uncertain, with Auerbach *et al* reporting from post-mortem studies in the 1960s that most CIS lesions do not progress into invasive cancers (40). Monitoring of preinvasive lesions has previously proved challenging, but with the introduction of autofluorescence bronchoscopy, a technique by which subtle changes in the bronchial mucosa are detected following blue light (490–700 nm) excitation, preinvasive lesions are identifiable from normal epithelium (41, 42). It is difficult to study the natural history of lesions as they are often detected by chance, repeated biopsies are needed at the same site and there is often a high intra-observer variability on the lesion grade (43). Despite these limitations, it has been shown that lesions are often dynamic; some lesions progress to invasive cancer, while others regress. Work by George *et al* showed that 7 out of 36 high-grade lesions were observed to regress over long-term follow up, 6 out of 36 progressed to cancer whilst the remainder were static (44). Interestingly the presence of high-grade dysplasia is a risk factor for the development of invasive lesions elsewhere in the bronchial tree (45). The 'field of cancerisation' hypothesis may explain these findings: due to the entire bronchial tree being exposed to the same precipitating stimulus, a preinvasive lesion in one area is an indicator of the susceptibility of the entire epithelium to disease development (46). This theory is also consistent with the widespread epithelial changes that are seen in smokers. However, recent longitudinal, molecular mapping of both CIS lesions and surrounding normal tissue by gene sequencing and loss-of-heterozygosity analysis has revealed that spatially segregated clonal lesions develop (47). The finding of normal epithelium between lesions, raises the possibility of the field cancerisation occurring through a process of cell migration rather than contiguous spread.

There is currently no consensus on when to treat preinvasive lesions or the stage of the disease when treatment becomes necessary. There are, as yet, no clear biomarkers to suggest whether a lesion will progress, remain static or regress. However, it is interesting to note that when 10 high-grade lesions were examined all were found to have chromosome 3q amplifications. This 3q amplification progressively increased during the evolution of the squamous cell carcinoma and was associated, in three of the patients, with an incremental increase in SOX2

expression (48). Treatment decisions need to consider the likelihood of lesion progression in addition to the fitness of the patient to undergo the treatment modality. The finding that cells from preinvasive lesions may migrate, supports the more aggressive treatment of lesions, before abnormal cells are able to migrate from the site of the lesion to affect other areas within the bronchial tree (47). Current therapeutic strategies include cryotherapy, photo-dynamic therapy, argon plasma coagulation and brachytherapy (43).

Challenges for the chemoprevention of preinvasive lesions include the heterogeneous nature of the lesions and their complex mutational burden (49). If, following a biopsy, there is no targetable mutation, the most appropriate agents are those that target general processes such as inflammation and the augmentation of apoptosis (49). Lesions are associated with an inflammatory infiltrate, therefore trials of inhaled corticosteroids have been administered (43). However, in smokers with at least one preinvasive lesion, administration of the inhaled corticosteroid budesonide for 6 months did not increase lesion regression compared with placebo treatment (50). Other strategies have included the administration of myo-inositol, an inhibitor of PIK3, with a phase 1 trial (of 10 patients) showing an increase in the regression of dysplastic lesions from 48% to 91% over a 3-month period (51). These results do need to be treated with caution, due to the inclusion of only 10 patients. In a larger study of 152 patients, Iloprost, a prostacyclin analogue (prostacyclin levels are reduced in lung cancer), was administered and led to a significant improvement in endobronchial histology, with lesions assigned a pre- and post-treatment score after 6 months. Of note, these effects were only seen in patients who were former smokers, and no differences were detected in those currently smoking (52).

1.2 The EGF receptor and regulation of signalling

The EGF receptor belongs to the avian erythroblastosis oncogene B (ERBB) family of four receptors proteins comprising ERBB1/ EGFR (hereafter referred to as EGFR), ERBB2, ERBB3 and ERBB4. Each receptor consists of a cysteine-rich, extracellular

binding domain, a single pass alpha helix transmembrane domain, a C-terminal signalling domain and, with the exception of ERBB3, a cytoplasmic tyrosine kinase. There are 13 known ligands of ERBB signalling: these include EGF, transforming growth factor α (TGFα) and amphiregulin (12). The activating ligands are shed from the surface of the cell, through the action of a disintegrin and metalloproteinase (ADAM) family of proteases in response to both pharmacological and physiological stimuli (53). The ligands are capable of inducing receptor activity through autocrine (self activation), paracrine (activation of adjacent cells), juxtacrine (where the tethered ligand on one cell is capable of activating a receptor on another) and extracrine (where ERBB activation occurs within exosomes) mechanisms (54). On ligand binding, the receptors dimerise and undergo receptor autophosphorylation, whereby the tyrosine residues in the intrinsic tyrosine kinase domain of one receptor cross-phosphorylates specific residues on its partnering receptor. The ERBB2 receptor is unable to directly bind ligand, therefore heterodimerisation is necessary for its activation (55). Specific ligands trigger different heterodimerisations, for example, EGF will induce the heterodimerisation of EGFR with ERBB2, ERBB3 and ERBB4 (55).

Receptor autophosphorylation activates a number of downstream pathways including the MEK/ERK (MAPK kinase/extracellular signal-regulated kinase), PI3K/AKT, STAT (signal transducer and activator of transcription) and mTOR (mammalian target of rapamycin) signalling cascades (12, 56).

The ERBB signalling pathways are crucial for normal cell proliferation, angiogenesis, differentiation and cell survival (57), they also play a key role in lung development. Mice lacking EGFR have impaired lung development which leads to death *in utero* (58). Whilst ERBB signalling provides an important role in the maintenance of airway homeostasis, aberrations have been linked to lung cancer, lung fibrosis and hypersecretory diseases including cystic fibrosis, chronic obstructive pulmonary disease (COPD) and asthma (59-63).

1.2.1 The regulation of ERBB signalling

Given the complexity of the ERBB signalling pathway, due to the variety of activating ligands, the strength of ligand binding, the dimerisation of receptors and the number of downstream pathways that are activated, it is vital the amplitude of signalling is tightly regulated. In the airway, a physical barrier exists between the ERBB receptor that is located on the basolateral surface of the cell and the ligands that are released apically (12). This means that unless a breach of the epithelium occurs, the ligand and receptor do not come into contact. On breach of the epithelial membrane the ERBB receptor becomes activated, and triggers a signalling cascade that rapidly restores epithelial integrity (61).

Once activated, the phosphorylated receptors are immediately targeted by protein tyrosine phosphatases such as density-enhanced phosphatase (DEP1), that deactivate the receptor (55). The activated ERBB receptors are then internalised, separating the receptor from the apical source of ligands and preventing continued activation (64). The internalised receptors are either recycled back to the cell surface or there is recruitment of adaptor proteins such as growth factor receptor bound protein 2 (GRB2). These adaptor proteins facilitate both the clathrin-mediated endocytosis of the activated ERBB receptor and the subsequent recruitment of the E3 ubiquitin ligase, CBL (Casitas B-lineage Lymphoma). The CBL molecule ubiquitinates the ERBB receptor and targets it to the lysosomes for degradation (65). At this point, de-ubiquitinating enzymes may intervene to remove the ubiquitin tag and allow the receptor to recycle back to the cell membrane (64).

The ligand responsible for receptor activation has been shown to influence receptor fate. EGF remains tightly bound (allowing continued signalling whilst within the vesicle) and triggers the lysosomal degradation pathway, whilst TGFα rapidly dissociates from the receptor, favouring receptor recycling (66). Additional regulation is exerted through timing of ligand expression and tissue specific ligand availability (67), allowing a tight control of receptor-mediated effects.

The synthesis of *de novo* inhibitors that are turned on once the ERBB has been activated provide a further level of ERBB signalling control (68). These include the proteins suppressor of cytokine signalling 4 and 5 (SOCS4 and SOCS5), mitogen inducible gene 6 (MIG6) and leucine rich repeats and immunoglobulin like domains 1 (LRIG1). These proteins are induced within 30 minutes (SOCS4 and SOCS5) to 4 hours (LRIG1 and MIG6) post receptor activation and are capable of binding to all four of the ERBB receptors, inhibiting their activity (69). SOCS4 and SOCS5 belong to a family of intracellular proteins that negatively regulate cytokine receptor signalling. It is suggested these molecules act by binding to the tyrosine residue 1068 of the EGFR (that becomes phosphorylated on receptor activation) and then targeting the receptor for ubiquitination (68). MIG6 is a cytosolic protein that is recruited to the ERBB receptor on ligand activation. It can bind to, and lock the receptor into an inactive configuration, preventing the activation of downstream signalling (70). MIG6 can also target the receptor for endocytosis, with its subsequent breakdown via the ubiquitination pathway (68).

Figure 1.2: Regulation of ERBB Signalling

The ERBB pathway is regulated through a number of mechanisms. 1) The choice of receptor, and the strength of ligand binding, 2) whether the ERBB receptor form hetero- or homodimers, 3) the release of extracellular ligands and segregation of ligands and receptor 4)

During homeostasis several endogenous mechanisms exist to modulate EGFR pathway activity. These include 1) ligand–receptor choice and binding affinity, 2) EGFR homo- and heterodimerisation, 3) extracellular ligand release and receptor–ligand segregation, 4) cytoplasmic and cell surface antagonist abundance, 5) rate of intracellular receptor recycling, and 6) downstream pathway choice causing differential gene expression. MEK/ERK: MAPK kinase/extracellular signal-regulated kinase; PI3K: phosphatidylinositol-3-kinase; JAK/STAT: Janus kinase/signal transducer and activator of transcription.

1.2.2 LRIG1 structure

LRIG1 belongs to a group of three proteins, called the leucine rich repeat and immunoglobulin like domain proteins. These are transmembrane proteins, each with an extracellular portion consisting of 15 leucine rich repeats followed by three immunoglobulin-like domains, a transmembrane region and a cytoplasmic tail. There is 57-67% amino acid identity between the 3 proteins, with LRIG1 the most extensively studied (71). The gene is expressed on chromosome band 3p14, a region of the genome that is frequently mutated in human cancers (72). The *LRIG1* nucleotide sequence encodes 1093 amino acids, and 83% sequence conservation exists between the human and murine amino acid sequences (72). Two different isoforms of LRIG1 have been identified, with molecular weights of 143 kDa and 134 kDa. Both forms are larger than the calculated polypeptide molecular mass of 120 kDa, indicating the presence of post translational modifications such as glycosylation (73). 32 kDa and 111 kDa LRIG1 fragments are also detected on the use of antibodies to the internal and external membrane components respectively. This suggests that LRIG1 is cleaved and there is a shedding of LRIG1's extracellular domain (the 111 kDa portion) (73).

LRIG1 has been identified in all studied tissues of the body (72), the highest protein expression levels are seen in the brain, followed by the kidney, then lung. The protein is found in a perinuclear location and along the basolateral membrane of cells. These sites correspond to those where the ERBB receptors are located (61, 74).

1.2.3 LRIG1 in the negative regulation of EGFR

LRIG1 negatively inhibits all members of the ERBB receptor family, and has also been found to down-regulate the action of other tyrosine kinases. These include the hepatocyte growth factor receptor (MET) (75), proto-oncogene tyrosine-protein kinase receptor Ret (RET) (76), and platelet-derived growth factor receptor alpha

(PDGFRα) receptors (77). Additionally, LRIG1 exerts a negative inhibitory action on the constitutively active mutant form of EGFR, EGFRvIII (78). Once activation of the ERBB receptor occurs, there is an increase in LRIG1 mRNA expression, with a 2-4 fold induction seen in HeLa cells over the course of a few hours (69). Both LRIG1 and MIG6 are labile and undergo proteasomal degradation; the half- life of LRIG1 is 4 hours but further activation of the EGF receptor leads to LRIG1 instability and a shorter duration of action (69).

The mechanism by which LRIG1 regulates ERBB signalling is controversial. All 4 ERBB receptors co-immunoprecipitate with LRIG1, indicating that there is a direct interaction between LRIG1 and the ERBB family member. The deletion of the entire cytoplasmic portion of EGFR does not prevent LRIG1 binding, which shows that ERBB/LRIG1 interaction occurs through the ectodomain of the ERBB (69, 74). Conversely, LRIG1 mutants lacking the leucine rich repeats or the immunoglobulin like domain components can still interact with EGFR. It is only following the deletion of both of these sections that the interaction is inhibited (69).

LRIG1 knock down increases the cell surface expression of EGFR (79), whilst LRIG1 overexpression enhances the EGF-stimulated cellular uptake of EGFR, suggesting that LRIG1 is involved in receptor endocytosis (80, 81). It was initially proposed that LRIG1 triggered EGFR degradation through the ubiquitination of the receptor's cytoplasmic portion. The presence of EGF ligand stimulates EGFR ubiquitination and this stimulation was found to be enhanced by LRIG1 expression (74). Tagged ubiquitin was further found to co-immunoprecipitate with both LRIG1 and EGFR, indicating the formation of a ternary complex between the three (74). To support this finding, there were similar rates of EGFR ubiquitination in the presence of LRIG1 as there was when CBL was ectopically expressed, indicating a similar mechanism of action (69). A role for ubiquitination and the CBL protein has been shown following induced expression of a dominant negative form of CBL, 70Z-CBL. 70Z-CBL is able to bind to EGFR in preference to CBL but it cannot induce receptor ubiquitination. When 70Z-CBL was coexpressed with LRIG1, EGFR was stabilised and not degraded.

This suggests that LRIG1-mediated ubiquitination of EGFR is dependent on a functional CBL (69).

Interestingly, the binding of CBL to EGFR and interaction with LRIG1, in addition to reducing EGFR levels, was shown to reduce levels of LRIG1. A series of LRIG1 truncation mutants showed that CBL binds to LRIG1's cytoplasmic portion. Therefore, to establish whether the binding of LRIG1 to EGFR and CBL led to the degradation of LRIG1, HEK293T cells transfected with LRIG1 mutants were treated with a proteasome inhibitor (to prevent LRIG1 degradation through the alternative proteasomal degradation pathway). These LRIG1 mutants could not bind either CBL or EGFR and showed very limited degradation suggesting that binding of CBL to the LRIG1/EGFR complex also targets LRIG1 depletion (69).

However the work by Stutz *et al*, who analysed the effects of LRIG1 on the mutant EGFRVIII receptor contradicted the above findings (78). The EGFRVIII receptor is a mutated form of EGFR that lacks a portion of the extracellular domain and is therefore unable to bind any ligand. Despite this, the receptor is constitutively active and its activity enhanced by its decreased internalisation rate and altered intracellular trafficking. LRIG1 and EGFRVIII were shown to co-immunoprecipitate, as with the other ERBB receptors, so there is a direct interaction between the two proteins. When the EGFRVIII and LRIG1 were expressed in HEK293T cells, LRIG1 led to a reduction in EGFRVIII levels, with recovery curves showing that EGFRVIII was more sensitive to LRIG1 regulation than wild-type EGFR. However, the investigators showed that the 70Z-CBL protein had no effect on receptor stability, and did not affect the rate of receptor degradation. This is despite EGFRVIII having an entirely functional cytoplasmic domain. Subsequent studies using the wild-type EGFR receptor and 70Z-CBL, failed to show any engagement of LRIG1 with CBL to mediate the degradation of EGFR (78). Further support of these findings is provided by experiments determining the effects of LRIG1 on the degradation of the MET receptor. Until recently, MET receptor degradation was considered to be ubiquitination-dependent. There is a binding motif in the juxtamembrane domain of MET that binds CBL, with an uncoupling of this MET/CBL binding leading to cellular

transformation (82). However, when 70Z-CBL was coexpressed with LRIG1, there was no effect of 70Z-CBL on LRIG1's ability to destabilise the MET receptor. This effect was seen both in the presence and absence of the MET ligand hepatocyte growth factor (HGF) and subsequent CBL RNAi experiments found CBL to have no influence over LRIG1-mediated MET receptor degradation (75). This indicates LRIG1 triggers MET receptor degradation by an alternative mechanism to that of CBL, and suggests that the LRIG1 mediated degradation of EGFR may also be independent of CBL.

The extracellular portion of LRIG1, containing the leucine rich repeats, has been demonstrated to regulate EGFR signalling independently of either receptor internalisation or receptor degradation (83). The action of the protein ADAM17 causes shedding of the LRIG1 ectodomain (84) and this shed portion is thought to act in a paracrine fashion as a 'competitive inhibitor', of ERBB ligand binding. A down regulation of EGFR signalling was seen in A431, HeLa and MDA-468 cancer cell lines in response to administration of the LRIG1 ectodomain, whilst cells that do not express EGFR did not respond to the LRIG1 ectodomain (83). Increasing concentrations of EGF reduced the negative inhibition exerted by exogenous LRIG1 on the EGFR receptor, through the displacement of LRIG1 by the EGF ligand. The LRIG1 ectodomains do not cause a physical down regulation of EGFR, instead it is speculated that LRIG1's soluble ectodomain binds to the EGFR, preventing the binding of ligands and keeping EGFR in an inactive conformation. This is analogous to the ERBB monoclonal antibody cetuximab that inhibits EGFR signalling (85). The extracellular portion of LRIG1 has also been shown to inhibit tumour growth of patient derived glioblastoma xenografts in mice (86). These soluble LRIG1 ectodomains were continually administered via a bead delivery system and demonstrate the inhibitory role of the cleaved portion of the LRIG1 protein and its potential therapeutic effects.

Whilst LRIG1 is subject to proteasomal degradation and its breakdown is accelerated by the presence of CBL, further complexity to LRIG1's control of ERBB signalling arises with the finding that LRIG1 can interact with LRIG3. The two proteins co-

immunoprecipitate, even in the absence of an ERBB receptor, implying potential cross-regulation (80). Rafidi *et al* (80) showed that LRIG3 overexpression leads to increased numbers of both EGFR and ERBB2 receptors at the cell surface of HEK293T cells, directly opposing the actions of LRIG1. Conversely, when LRIG1 was overexpressed, this acted to destabilise LRIG3 and reduced LRIG3 detection at the cell surface.

In summary, whilst LRIG1 clearly regulates cell surface EGFR levels (79), the mechanism of action remains to be determined.

1.2.4 LRIG1 as a stem cell regulator

Stem cells are defined by their ability to self-renew and their capacity to produce daughter cells with more restricted potential (87). Early research into the role of LRIG1 has identified a role for the protein in the regulation of tissue stem cell compartments.

1.2.4.1 LRIG1 in the skin

Our initial understanding of the function of LRIG1 has come from loss-of-function studies in mouse. Suzuki *et al* first detected the LRIG1 gene following a screen for genes that were upregulated during the neural differentiation of the mouse cancer cell line P19 (88). Following Northern blot analysis, LRIG1 was found to be highly expressed in the brain, and in the anticipation of a neurological phenotype, an *Lrig1* knockout mouse was developed (89). Although there were no neurological sequelae caused by loss of *Lrig1*, by 3- 4 weeks of age the *Lrig1* knockout mice were noted to have skin abnormalities, with thickening of the tail skin and alopecia around the facial area. Histological examination revealed marked epidermal hyperplasia and an increased epidermal proliferation on Ki67 staining (89). A comparison of these skin changes was made to those of psoriatic epidermal hyperplasia in humans, with both showing similar histological appearances. It was found that LRIG1 protein

expression was absent in the psoriatic lesions, but was detectable at normal levels in the surrounding, unaffected tissue (89).

A further insight into the role of LRIG1 was obtained through experiments designed to elucidate markers of the keratinocyte stem cell population. Single-cell expression profiling was performed in both stem cells and the more differentiated, transit-amplifying cell population of human epidermal keratinocytes. *LRIG1* transcripts were found to be enriched in the stem cell fraction (79). Subsequent *LRIG1* knockdown using siRNA was noted to increase both cell proliferation and clonogenic capacity, with increased EGFR levels and downstream signalling activation (79). These findings suggested that LRIG1's role may be to regulate stem cell activity and maintain the epidermal stem cells in a quiescent, non-proliferative state that is mediated through LRIG1's regulation of EGFR signalling.

Further studies have shown that LRIG1 regulates the proliferative capacity of epidermal cells (90). 5-bromo-2'-deoxyuridine (BrdU) pulse-chase studies have shown that in LRIG1-null animals, a decrease in the number of epidermal DNA label-retaining cells is seen after a 70 day chase period, compared to wild-type animals indicating that the population is dividing more rapidly and diluting out the BrdU label, suggesting that LRIG1 is necessary for stem cell quiescence. Interestingly, in skin reconstitution assays, where GFP labelled LRIG1 positive cells are isolated and mixed with unlabelled cells, the LRIG1 positive cells were able to contribute to all epidermal lineages, highlighting their potential stem cell phenotype (90).

Recent increases in the understanding of the skin stem cell compartment have shown LRIG1 to mark a population of cells in the upper isthmus of the hair follicle. This compartment maintains the upper pilosebaceous unit that contains the infundibulum and sebaceous gland (91). Lineage-tracing analysis using tamoxifen inducible Cre under the control of the *Lrig1* promoter have shown that during homeostasis this LRIG1-positive subpopulation is responsible for the maintenance of the pilosebaceous unit and is not detectable outside these margins. It is interesting to note that a single LRIG1-expressing cell either maintains the infundibulum or

sebaceous gland, but an individual cell is incapable of contributing to both. This restriction changes on skin wounding, where the LRIG1-expressing cells are able to replace cells lost from other areas, including the hair follicle and interfollicular epidermis (91). Furthermore, this study showed the highly proliferative nature of LRIG1 positive cells, as following a short BrdU pulse, where the LRIG1-expressing cells showed increased labelling compared to both the $CD34^+$ hair follicle stem cells and the interfollicular epidermal skin cells. This is seemingly in contradiction to LRIG1's role as a negative regulator of proliferation and may best be explained by LRIG1 controlling the amplitude of ERBB signalling.

1.2.4.2 LRIG1 in the gut

Intestinal stem cells reside at the crypt base, where they divide to self-renew and to maintain the continuously renewing epithelial surface. As cells move away from the crypt base, they become progressively more differentiated (92). LRIG1 shows a gradient of expression that is highest at the crypt base, but is diluted as the cells move out along the walls. These levels of LRIG1 expression correlate to those of the intestinal stem cell marker leucine rich repeat containing G protein coupled receptor 5 (LGR5) (93). Other intestinal stem cell markers including Achaete-Scute Family BHLH Transcription Factor 2 (ASCL2) and Musashi RNA Binding Protein 1 (MSI1) are also enriched in this area. To investigate the proliferative nature of gut LRIG1 positive cells BrdU pulse chase labelling was used. After a 3 day pulse, 60% of LRIG1 expressing cells were BrdU-labelled, indicating that, as shown in the skin, LRIG1 marks a highly proliferative cell population (93).

Lrig1 loss in the inbred mouse strain FVB/N resulted in a marked increase in crypt size along the length of the intestine, and produced a phenotype so severe that the mice needed to be sacrificed around postnatal day 10. This model was interesting for two reasons; the effects of loss of *Lrig1* in a knockout model are dependent on mouse background (with these changes not seen in the initial *Lrig1* knock out, used by Suzuki *et al*, on an outbred background (89)) and that the phenotypic change

corresponded directly with an expansion of the stem cell compartment. Rescue of the phenotype was achieved either pharmacologically through the administration of gefitinib, an EGFR receptor blocker, or genetically by the crossing of the *Lrig1* knockout animals to hypomorphic EGFR w-2 mice. This directly demonstrates that LRIG1 is exerting its action on the intestinal stem cell compartments through an effect on EGFR signalling (93).

Lineage tracing using tamoxifen inducible Cre under the control of the LRIG1 promoter confirmed that LRIG1 marks a population in the gut with stem cell properties (94). Activation of the lineage marker in LRIG1^{+} cells showed that labelled cells first appeared in the crypt bases, before spreading over a 14-day period to repopulate the entire crypt. All cell types within the crypt were labelled and labelling was still evident after 3 months, indicating the effective labelling of a stem cell (94).

A recent controversy in the field is that the rapidly proliferative LRIG1 positive gut population identified by Wong *et al* (93), contrasts to the findings of Powell *et al*, where their Ki67 and BrdU analyses determined LRIG1 positive cells to be infrequently cycling (94). However, a recently published paper has drawn light on the confusion; Wong *et al* used a commercially available LRIG1 antibody against LRIG1's entire ectodomain, whilst the Powell group developed their own antibody against a 12 amino acid motif within the ectodomain, a site that is possibly affected by glycosylation, and that may affect antibody binding (95). It is likely that the work of Wong et al gives a better indication of the activity of all LRIG1 expressing cells, rather than a potentially more quiescent LRIG1-expressing subpopulation.

1.2.5.3 LRIG1 in the eye

In addition to the findings in the skin and gut, the importance of LRIG1's regulation of the stem cell compartment has been shown in the cornea (96). Gene expression analysis has shown increased *LRIG1* expression in the corneal epithelial cells that

exhibit a stem cell phenotype compared to the corneal cells that are more differentiated. LRIG1 appears to regulate cell fate decisions, with its loss changing cell fate from corneal to keratinised epithelium, and leading to corneal opacification in an *Lrig1* knockout mouse model. These effects are exerted through the action of LRIG1 on the STAT3 inflammatory pathway, as corneal wounding in *Lrig1* knockout animals led to an increased expression of phospho-STAT3. The pharmacological inhibition of STAT3 blockade prevented these changes occurring. Interestingly, *K5 Stat3* transgenic mice that exhibit constitutively active STAT3 signalling, show a similar phenotype to the *Lrig1* knockout animals after corneal injury (96). This is the first research that links LRIG1 with the STAT3 pathway and it remains uncertain as to whether this restricted to the cornea or may be a more widespread action of LRIG1.

1.2.5 LRIG1 in cancer

The first indication of LRIG1 as a potential tumour suppressor arose through the development of adenomas in *Lrig1*-null mice. At five months of age, 80% of the *Lrig1*-null mice had developed duodenal adenomas and by 14 months, these had progressed to adenocarcinomas with invasion of the bowel wall (94). The tumours were associated with increased EGFR expression and indicated a direct effect of LRIG1 absence. Powell *et al* further showed that by inducing the loss of one adenomatous polyposis coli (APC) allele, a tumour suppressor protein in which mutations lead to colonic cancer, in an LRIG1 expressing cell that the stochastic loss of the second APC allele led to multiple colonic tumours. These findings add further weight to LRIG1 marking a gut stem cell, as the lifespan of an LRIG1 expressing cell needs to be sufficiently long in order to acquire the stochastic loss of the second APC allele (94).

In humans, *LRIG1* is localised to the chromosome band 3p14.3, a location frequently deleted in various human cancers (97). Rouam *et al* undertook a large bioinformatics study where 8 datasets were combined to assess prognostic factors in various solid tumours. Remarkably, they found that *LRIG1* was one of 4 key genes (in

addition to *ESPL1*, *KIF4A* and *HJURP*) whose decreased expression led to reduced survival outcomes across five tumour types including breast, bladder, glioma, melanoma and lung cancer (98).

A reduction in LRIG1 protein expression and a worsening of outcome has been shown in cervical cancer (99), astrocytomas (100), nasopharyngeal (101) and oropharyngeal malignancies. LRIG1 is seen in higher concentrations in the well-differentiated squamous cell carcinomas of the skin (102) and loss of LRIG1 is associated with the invasion of ocular surface neoplasia in the eye (103).

1.2.5.1 LRIG1 in lung cancer

Analysis of the gene expression within the airway epithelium shows that *LRIG1* is downregulated in current smokers compared to ex-smokers, and this drop in expression falls further on the development of squamous cell carcinoma (30). Loss of LRIG1 protein expression is seen in preinvasive lung cancer lesions, a loss that is associated with increased EGFR expression (104). This may, in part, explain the finding of increased EGFR expression in squamous cell lung tumours (26, 27).

The isolation of mRNA and protein expression in paired samples of preinvasive and normal epithelium from the same patient have shown both decreased gene expression and a reduced immunoreactivity of LRIG1 in each of the 10 cases examined. In four out of the 10 cases there was loss of heterozygosity (LOH) at the *LRIG1* locus, but unfortunately, due to the small amount of frozen tissue available for assessment, promoter methylation or mutation in the other allele was not identifiable (104). LOH analysis for *LRIG1* was subsequently analysed in 138 lung cancer cell lines as part of the Sanger Cancer Genome Project, with LOH reported at the *LRIG1* locus in 75% of cases (104).

Loss of LRIG1 was shown to reduce contact inhibition in human airway epithelial cells grown at air-liquid-interface. It was observed in LRIG1 expressing cells that

LRIG1 expression co-localised with that of EGFR and E-cadherin at cell confluence, with co-immunoprecipitation experiments showing the formation of a tripartite complex between LRIG1, E-cadherin and EGFR (104). This may provide a further mechanism by which LRIG1 regulates the effects of EGFR and may explain the development of tumours in the gut with loss of LRIG1, as there is a removal of the contact inhibition provided by the EGFR/E-cadherin/LRIG1 complex (104). Whether this complex exists in tissues other than the lung and the downstream consequences of EGFR/E-cadherin/LRIG1 complex formation remain to be determined.

The possibility of LRIG1 as a prognostic biomarker in NSCLC has been raised by Kvarnbrink *et al* (105). In their analysis of LRIG1 protein expression in 347 NSCLC tumours, they detected that high LRIG1 expression was related to a dramatically improved survival of 2.8 years. Initial analysis showed the survival advantage to be most marked in adenocarcinoma, however only the presence of LRIG1 in the tumour cells was considered. The group's subsequent analysis of the Oncomine database, where *LRIG1* mRNA was strongly correlated to an improved squamous cell lung cancer prognosis, prompted their re-examination of the tumour and showed LRIG1 protein expression in the surrounding cell types (stromal and immune cells) was highly correlated to the improved outcome (105).

1.2.5.2 LRIG1 in breast and prostate cancer

In breast and prostate cancer LRIG1 expression is induced by oestrogen and androgens respectively. A recent study has shown in 971, stage 1/2, breast tumours (of all subtypes) that the loss of LRIG1 is associated with an increased risk of both breast cancer relapse, relapse of breast cancer after 5 years, and death (106). However, LRIG1 expression in breast cancer is variable according to both tumour type and the sensitivity of the tumour cells to oestrogen. LRIG1 expression is seen in higher levels in oestrogen receptor positive ($ER\alpha^{+}$) breast cancer than $ER\alpha^{-}$ disease. Krieg *et al* showed that LRIG1 is a target of ERα, so in the presence of oestrogen LRIG1 levels are increased, with LRIG1 acting as an oestrogen-regulated growth

inhibitor (107). Intermediate to high levels of *LRIG1* transcripts in ERα^{+} disease were shown, through the analysis of the Oncomine database, to be associated with an improved relapse free survival time.

The ERBB2 receptor is over expressed in 20-30% of breast cancers and this up regulation is associated with a reduction in both protein and transcript levels of *LRIG1* (108). The reduction in LRIG1 protein in turn contributes to further ERBB2 over expression (108). Kreig *et al* further showed ERBB2 over expression to reduce ERα^{+} induced LRIG1 expression, indicating mechanistically, how LRIG1 expression may be reduced in ERBB2 over expressing tumours (107).

The role of LRIG1 in prostate cancer is interesting. LRIG1 expression is increased by androgen administration and the transduction of the PC3 prostate cancer cell line with *LRIG1* lentivirus causes a slower growth rate. In a cohort of patients that had not undergone treatment, high LRIG1 expression levels were associated with a poor prognosis, however in a cohort that had undergone prostatectomy high LRIG1 expression levels were related to improved outcomes (109). The authors describe a possible explanation for this paradox, whereby in a high androgen environment the inhibitory effects of LRIG1 are not sufficient to counteract the tumour burden, whilst in patients who have undergone treatment the tumour burden is less and LRIG1 is better able to exert its inhibitory role (109).

1.2.6 The role of LRIG1 in epithelial-to-mesenchymal transition (EMT)

Two recent studies have indicated a possible role for LRIG1 in the modulation of epithelial-to-mesenchymal transition (EMT) (110, 111). EMT is the process by which an epithelial cell phenotype changes to become mesenchymal (112). It is associated with a loss of cellular polarity and the reorganization of the cytoskeleton. There is a downregulation of epithelial markers including E-cadherin, Zinc finger protein SNAI1 (SNAI1) and zonula-ocludens (ZO-1), whilst there is upregulation of markers including Twist Family BHLH Transcription Factor 1 (TWIST), fibronectin and matrix

metalloproteinases (MMPs). These changes in expression contribute to cancer progression (112).

Assessment of the effects of LRIG1 within head and neck squamous cell cancers, have shown that the reintroduction of LRIG1 to a nasopharyngeal cell line lacking LRIG1 resulted in a morphology change from spindle-like to cuboidal, with activation of integrins and a downregulation of SNAI1 expression. Conversely, when LRIG1 was knocked down in an LRIG1-expressing cancer cell line, cell migration, invasion and proliferation were enhanced. This was associated with extracellular matrix remodelling activity and an increase in MMP expression, all changes that are associated with the onset of EMT (110).

As discussed above, LRIG1 is associated with poor prognosis from breast cancer, and studies with breast cancer-derived cell lines have implicated LRIG1 as a possible EMT regulator. During EMT of breast cancer cells LRIG1 is downregulated, whilst the re-expression in an LRIG1 negative invasive cell line induces a mesenchymal-to-epithelial transition (reversal of EMT). This is associated with a reduction of tumoursphere formation and an inhibition of invasive growth (111).

1.2.7 The other LRIG proteins

LRIG2 and LRIG3 have been less extensively studied than LRIG1, and their functions have not been fully defined. Genetic inactivation of *Lrig2* in a mouse leads to no phenotype other than reduced weight at 5 days, and an increased likelihood of malnutrition and premature death (77). In humans, *LRIG2* mutations are associated with congenital urofacial syndrome (113), where the clinical features of hydronephrosis and facial grimace, are indistinguishable from those of Heparanase-2 (HPSE2) linked urofacial syndrome. This suggests that there is a functional overlap between LRIG1 and HPSE2, with loss of either protein leading to aberrant growth factor signalling (81, 114).

Following the finding that LRIG2 expression is associated with poor survival outcomes in patients with oligodendroglioma (115), the effects of the lack of LRIG2 on tumour growth were investigated in a murine glioma model. It was found that LRIG2 deficient animals were protected against platelet derived growth factor B (PDGFB) induced tumours, suggesting a potential role of LRIG2 in regulating PDGFB signalling (77). The expression of LRIG2 in cancer has been associated with a worsening of the prognosis from a number of other malignancies. These include an association of LRIG2 expression with the increased invasion of pituitary adenomas (116), poor survival in early stage cervical cancer (117) and a worsening of outcome from non-small cell lung cancer (118).

Lrig3 knockout mutant mice show impaired morphogenesis of the inner ear, where LRIG3 is necessary for lateral canal development, a process independent of ERRB signalling (119). The protein also plays a role in the neural crest formation of *Xenopus* through the modulation of Fgf and Wnt signalling (120). Similarly to LRIG1 and 2, LRIG3 expression has been associated with malignancies. A high number of LRIG3 positive cells in cervical adenocarcinoma specimens are associated with an improved outcome (121), whereas the perinuclear staining of LRIG3 is inversely correlated to the grade of astrocytic tumour and patient survival (100). Two studies looking at the effects of LRIG3 in glioblastoma cell lines have shown that LRIG3 overexpression causes a reduction of glioblastoma cell proliferation (122), whilst *LRIG3* shRNA mediated knockdown leads to increased EGFR expression and cellular proliferation (123). Interestingly, these findings oppose those of Rafidi *et al* who suggest that LRIG3 directly antagonises the action of LRIG1 (80) and it is possible that these contradictions may be explained by a tissue-to-tissue variability in the function of LRIG3.

1.3 Stem cells of the lung and lung cancer cell of origin

1.3.1 Structure of the lung and respiratory epithelium

The lungs are directly exposed to the external environment, with the respiratory epithelium subject to a number of chemicals, viruses, bacteria and other insults over the lifetime of an individual. The presence of an intact epithelium is essential for warming inspired air, performing gaseous exchange in the distal airway, and in the production of mucus that defends against inhaled pathogens (124). In humans, the airways, down to a diameter of 1- 1.5 mm, are lined by a pseudostratified columnar epithelium consisting of ciliated cells, mucous secreting goblet cells, club cells and basal cells. Mucous cells predominate in the larger airways and club cells increase distally. Neuroendocrine cells are scattered throughout the airway, but also form collections around the airway branch points that are termed the neuroepithelial bodies (NEBs). The simple cuboidal epithelium that leads to the alveoli is poorly characterised, but the alveolar epithelium consists of cuboidal alveolar type 2 cells (AT2) and squamous alveolar type 1 cells (AT1) (125). Differences exist between the human and murine airway. In the mouse, the pseudostratified airway epithelium is seen only in the trachea and the mainstem bronchi, with the basal cells limited to these areas. The smaller airways of the mouse are lined by a simple cuboidal epithelium consisting of ciliated and club cells, and there are fewer neuroendocrine cells compared to the human (125).

1.3.2 Lung stem cells and the stem cell niche

Stem cells are vital in maintenance of an intact respiratory epithelium. They are defined by their ability to self-renew and their capacity to produce multiple, more differentiated daughter cells of varying types (87). Our understanding of stem cell behaviour has been derived from studies in the haematopoietic system. In the haematopoietic system there is a quiescent stem cell at the apex of the hierarchy, which divides asymmetrically to produce new stem cells, which, in turn, divide to produce progressively more rapidly dividing progenitor cells. As cells move through this system they become increasingly differentiated and the full complement of blood cell types is produced (126).

In contrast to the haematopoietic system, where the stem cell hierarchies are well defined, the stem cell populations maintaining solid organs and in particular the airway epithelium is more complex. Studies in the airway have been hampered by the slow turnover of the respiratory epithelium, making lineage-tracing studies during homeostasis challenging. Murine lung injury models have been crucial in defining the putative stem cell populations of the airway and through the damaging of a discrete cell population, combined with lineage tracing (124), three possible stem cell niches have been identified within the murine lung (Figure 1.2).

A stem cell niche is a particular area within a tissue where the stem cells reside. The stem cells interact with the cells of the niche where they are kept in a quiescent and dormant state. The role of the niche is to protect the stem cells from exhaustion or death, and on activation of the stem cell population, promote cellular differentiation and influence the fate of daughter cells (127). Within the mouse lung, stem cell niches are reported in the submucosal glands of the trachea where there is an increased density of basal cells, the neuroepithelial bodies (NEBs) that are located at airway branch points, and the bronchoalveolar duct junctions (BADJs) that are positioned where the bronchioles transition into the gas exchanging alveoli (128, 129).

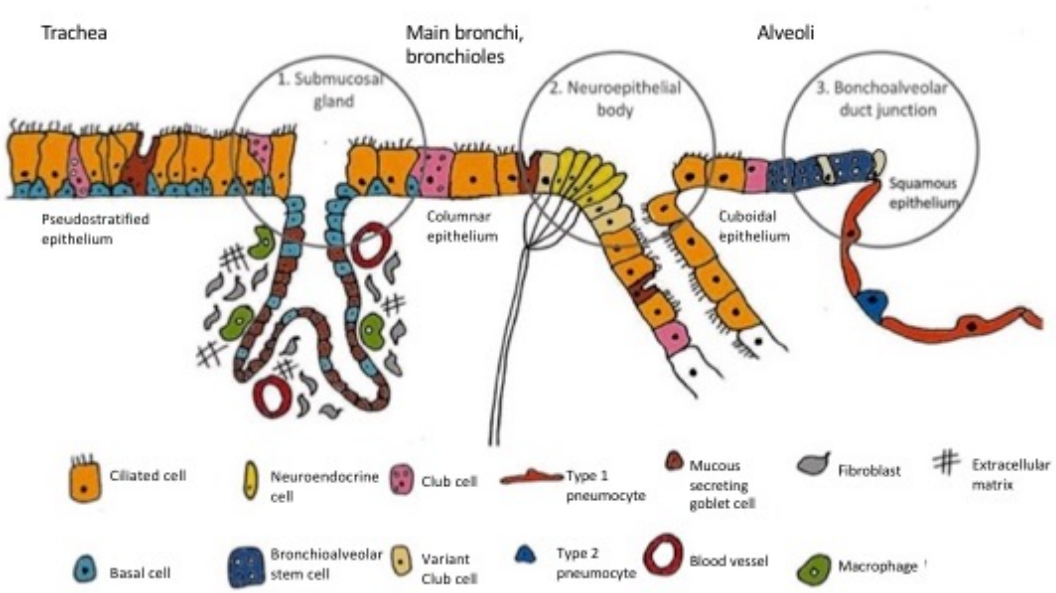

Figure 1.2: Schematic showing the different epithelial cell types within the murine bronchial tree

Image shows the different cells types moving from the trachea, with a high density of basal cells seen in the upper airways, to the alveoli. The position of the three stem cell niches are indicated. These are the upper airway submucosal gland, the neuroepithelial body positioned at airway branch points and the bronchoalveolar duct junction situated at the point where the small airways become alveoli. Figure adapted from reference (124).

1.3.3 Stem cells of the upper airway

Basal cells constitute 30% of the upper airway epithelium and are identified by the expression of the markers p63, nerve growth factor receptor (NGFR) and keratins 5 and 14 (KRT5 and KRT14) (130). The basal cells are considered the upper airway stem cell, as shown through lineage-tracing experiments using *KRT5-CreER*^{T2}*;Rosa26R-LacZ* mice. Exposure of these mice to sulphur dioxide (SO_2) leads to the loss of both secretory and ciliated cell populations, whilst leaving the basal cells intact. Over the course of a 7 day period, the basal cells proliferate and repair the damaged epithelium including the replacement of lost secretory and ciliated cells (130). Notch signalling promotes the luminal differentiation of basal cells, as shown through the pharmacological inhibition of Notch in a tracheosphere assay. The Notch-inhibited tracheospheres fail to form a lumen and remained as clumps of $p63^+$ basal cells, whereas the controls hollowed and formed $p63^-KRT8^+$ progenitors. This is also seen in vivo, where mindbomb E3 ubiquitin protein ligase 1 (*Mib1*) deficient mice (that are unable to activate Notch signalling) were less able to repopulate the airway epithelium following SO_2-mediated airway damage (131). The levels of Notch signalling regulate the differentiation of $p63^+$ basal cells into either secretory or ciliated lineages. The $p63^+$ basal cell may either show intracellular Notch 2 activation, and ultimately develop into a secretory cell, or exhibit c-myb expression and differentiate into a ciliated cell (132).

Whilst basal cells have been shown to replace ciliated and secretory cells populations, recent research has shown that following the complete ablation of basal cells (using doxycycline-dependent diphtheria toxin expression targeted to $KRT5^+$ cells) there is a dedifferentiation of luminal secretory cells to a basal cell phenotype. These dedifferentiated cells persist and act as functional stem cells, capable of producing new ciliated, secretory and basal cells (133). This suggests that airway epithelial cells exhibit more plasticity than previously considered.

The stem cell phenotype of basal cells has also been shown in the human airway. When integrin $\alpha6^+$, $NGFR^+$ basal epithelial cells are isolated from the human airway

and grown in tracheosphere culture there is evidence of ciliated differentiation after 25 days, findings that are absent in the integrin $\alpha6^-$, $NGFR^-$ population (130). Additionally, when human basal cells are isolated and grown at air-liquid interface, using a rat trachea as a scaffold, the basal cells are capable of forming a fully differentiated mucociliary epithelium (134).

Further insight into the maintenance of the human airway has been obtained from Teixeira *et al* (135), who have shown that in the large airways homeostasis is maintained by the stochastic division of basal cells, spread throughout the airways that self renew and differentiate. The experiments used clonal lineage analysis, where the airway epithelium was stained for the presence of cytochrome C oxidase (CCO), a gene that becomes stochastically mutated in mitochondrial DNA and passed to daughter cells. Clones of CCO negative cells were visible within the airway epithelium and mathematical modelling showed that these clones were associated with airway basal cells. The basal cells did not appear to be pre-programmed stem cells, but were equipotent in their ability to maintain epithelial integrity. However, it remains uncertain as to whether these cells are responsible for the repair of airway damage, or whether a more defined stem cell pool is activated (125).

1.3.4 Stem cells of the small airways and alveoli

The small airways contain two stem cell niches, one situated within the NEB and the other at the BADJ. Again our knowledge of the small airway stem cell populations has been derived predominantly from murine injury models, and it remains uncertain as to how closely correlated these findings are to the human airway.

The small airways are predominantly lined by Clara cell 10 KDa (CC10) expressing club cells and Forkhead Box J1 (FOXJ1) expressing ciliated cells. Naphthalene administration to a mouse leads to acute club cell toxicity. On club cell death, the ciliated cells are seen to spread across the respiratory epithelium but they fail to divide to replace the lost club cell population (136). 72 hours post-injury there is an

expansion of cells at the NEB, including both the calcitonin gene related peptide (CGRP) expressing neuroendocrine cells and a variant CC10-expressing club cell population (137). The variant club cells lack the cytochrome P450 2F2-immunoreactive protein that metabolises naphthalene, leading to naphthalene resistance and their survival. To determine whether the neuroendocrine cells, or the variant club cells re-epithelialise the airway following damage, complete club cell obliteration was achieved through the administration of ganciclovir to transgenic mice expressing herpes simplex kinase under the regulatory control of the mouse CC10 promoter (this depletes all club cells, including the variant club cells). The CGRP-expressing neuroendocrine cells were unable to replace the lost cells, indicating that the CC10 variant club cell population is vital to the regeneration of the airway epithelium (138).

Moving distally, the most terminal bronchioles lack a NEB and following naphthalene exposure, it is the variant club cells that are situated at the BADJ which proliferate, indicating a possible further stem cell niche at this location (139). Subsequently, Kim *et al* have reported the finding of a unique cell population at the BADJ, cells that they have termed bronchioalveolar stem cells (BASCs) (129). These cells express both surfactant protein C (SPC), that is associated with alveolar type 2 cells (AT2), and CC10. On either naphthalene-induced airway damage or the alveolar injury-inducing bleomycin, the BASCs proliferate, implying they have a role in both distal airway regeneration, and the replacement of both club cells and alveolar epithelium. It was further shown that when BASCs were isolated and grown *in vitro* in Matrigel, they were able to generate club cells, AT2 cells and AT1 cells (129).

Whilst the above experiments suggest the BASC to be a distal airway stem cell, subsequent lineage-tracing of the club cell population at the BADJ (including the marking of the previously identified BASCs) using a transgenic mouse line expressing tamoxifen inducible Cre from the CC10 locus, has contradicted these findings. Following naphthalene damage, CC10 expressing cells are able to regenerate the bronchiolar epithelium, but following hyperoxia (that causes alveolar cell damage), alveolar cell replacement does not arise from the BADJ, but it is the AT2 cells that

divide and replace the lost AT1 cells (136). Influenza infection causes more severe alveolar damage than oxygen, and following influenza exposure it has been suggested that replacement of lost AT2 cells can occur from the CC10 expressing club cells (140). Another group used the same CC10 lineage-tracing mice and exposed the animals to bleomycin injury. In this case, both AT1 and AT2 cells were lineage-traced from the CC10 population (141). Therefore the mode of airway regeneration may be dependent on both the degree and mechanism of injury. To confirm the significance of the BASC population direct labelling and lineage-tracing from the BASC would be necessary. However, to date, no unique markers of the BASC population have been identified.

To further complicate our understanding of distal airway repair, $p63^+$ cells have been shown to arise in the distal airway following influenza infection. These p63 cells organise into $KRT5^+$ pods that subsequently enlarge and contribute to the repair of the alveolar epithelium (142). Isolation of these $p63^+$ cells from the mouse, rat and human distal lung shows the capacity of these cells to generate alveolar structures *in vitro* (142).

Whilst activation of the stem cell populations occurs on airway damage, during airway homeostasis, it has been suggested that a group of 'committed' airway progenitors maintains the integrity of the epithelium (143). Experiments using GFP chimeric mice, shows that the severity of airway injury influences the cell population that is activated and contributes to airway regeneration. Mice were exposed to naphthalene, and the degree of airway injury assessed by the animals weight loss. When mice were severely injured, with a greater than 10% weight loss, large GFP patches were seen centred around the airway branch points (at sites of NEBs) and at the BADJ. When the mice were less severely injured (less than 10% weight loss) there was no association of the GFP patches to either of the stem cell niches. This suggests that the airway stem cells only become activated following severe airway damage and less severe injury triggers the proliferation of a more widespread, differentiated population (143). The findings are supported by the observation that club cells are able to regenerate the ciliated population within the main airways

without activating the basal stem cells (136) and that AT2 cells are able to divide and replenish lost AT1 cells in the alveoli (144).

It currently remains uncertain as to how these findings relate to the stem cell populations of the human. Kajstura *et al* identified a population of c-kit expressing cells from the human airway that exhibited the stem cell features of self-renewal, clonogenicity and multipotency both *in vitro* and *in vivo* (145). Flow cytometry-isolated human airway c-kit positive cells were administered to mice that had undergone cryogenic damage to their lung tissue. The cells were seen to engraft and replace not only the airway epithelium, but also the pulmonary vasculature and pulmonary interstitium (145). However the validity of these findings has been thrown in doubt by the observation that c-kit positive cells also express the leucocyte marker CD45 (135) and that lineage tracing from the c-kit positive cells shows they do not contribute to the lung epithelium during either homeostasis or repair, but that they maintain a vascular endothelial cell fate (146). Neither BASCs nor variant club cells have been identified in the human lung and this is a focus of ongoing research (147).

1.3.5 The lung cancer cell of origin

A key characteristic of lung stem cells is their longevity. This means that over the course of their lifetime, these cells are long-lived enough to accumulate the necessary mutations needed to drive the development of lung cancer (148). More differentiated cell have a shorter lifespan and have less likelihood of acquiring the necessary mutational burden.

In humans there is a proximal to distal tumour pattern of tumour development, with squamous cell carcinomas found in the trachea and upper airway, small cell lung cancers in the intermediate airways and adenocarcinomas more distally. This suggests that the tumour cell of origin may be a cell type found at each location, with the tumour subtypes sharing characteristics to each of the stem cell

populations involved in the repair of each of the areas of the bronchial tree (128). The use of murine models, with the overexpression of an oncogene or the removal of a tumour suppressor, has provided insight into the cell of origin of lung cancer.

Squamous cell carcinomas originate in the large airways and are characterised by a high number of basal cells and the stepwise morphological changes through basal cell hyperplasia, metaplasia, dysplasia and carcinoma in situ during the development of malignancy (44). Both preinvasive and squamous cell carcinomas maintain a basal cell phenotype with persistent KRT5 expression (149), whilst squamous cell carcinomas are also situated at submucosal duct gland junctions or intracartilaginous boundaries. These are areas of high basal cell concentration, suggesting basal cells are the likely cell of origin of squamous cell lesions (128).

Small cell lung cancers arise in the bronchioles and express markers, including CGRP, that are seen in the neuroendocrine population. *Rb1* loss of function negatively regulates neuroendocrine cell differentiation and in common with *Trp53* loss, is frequently found in SCLCs (150). Targeting the sequential loss of both *Rb1* and *Trp53* in a murine model to club cells, neuroendocrine cells and AT2 cells demonstrated that tumours arose most consistently, and with the shortest time-lag, from the neuroendocrine cells. These tumours exhibited SCLC features on histology, expressed SCLC cell markers and readily metastasised (151). SCLCs did not arise when disruption of *Rb1* and *Trp53* was targeted to club cells and only infrequently caused lesions when targeted to the AT2 cell population. Collectively, these results indicate that the neuroendocrine population is the likely SCLC cell of origin.

Lung adenocarcinomas are associated with the expression of the markers CC10 and SPC, with 25-50% of lesions associated with an activating mutation in KRAS (152). BASCs were initially proposed as the adenocarcinoma cell of origin, due to their co-expression of CC10 and SPC, and the observation that naphthalene increases tumour formation in a murine $KRas^{G12D}$ model (where *KRas* is constitutively active) (129). However following the activation of $KRas^{G12D}$ in both $CC10^{+}$ and SPC^{+} epithelial cells of murine lungs, hyperplasia was detected in the BASC population and terminal

bronchiole club cells, whilst adenocarcinomas only developed from the AT2 cells (153), suggesting that this population is the likely adenocarcinoma cell of origin.

1.3.6 Lung cancer stem cells

The cancer stem cell (CSC) hypothesis is a concept that describes cells within a tumour that drive the tumour's growth and metastatic potential. To be defined as a CSC, the cells need to be capable of self-renewal, the generation of differentiated progeny and the production of tumours in xenotransplantation models (124, 154). CSCs may originate either from a stem cell, or a more differentiated long-lived progenitor cell that has accumulated sufficient mutations over the course of its lifespan to become tumorigenic. CSCs have been identified in a number of malignancies including brain, haematopoietic cancers, breast and lung tumours (154).

Due to their longevity and their role in replacing lost cells, stem cells utilise several protective mechanisms. These include high levels of anti-apoptotic proteins and ABC transporter proteins that are involved in toxin efflux. It has been suggested that CSCs also express high levels of ABC transporter proteins that remove chemotherapeutic agents from the cells, making the CSCs resistant to therapy. Therefore, following chemotherapy the tumour bulk is reduced, but the resistant CSCs remain and on treatment cessation, repopulate the tumour, resulting in disease relapse (124). Cells with CSC characteristics may also explain the finding that tumour cells are often found in the peripheral circulation, but are not always associated with metastatic deposits. The circulating tumour cells may need to have CSC characteristics to be able to seed metastases elsewhere (155).

Several markers have been used to identify cells within a lung cancer that have CSC characteristics, these include CD133, CD44, CD166, aldehyde dehydrogenase (ALDH) and being of a 'side population' (SP) phenotype (154). SP cells are recognised by their ability to efflux Hoescht 33342 through their ABC transporters and are

identifiable using flow cytometry techniques. Isolation of the SP from cultured lung cancer cells has revealed these cells to have increased tumorigenicity in a xenograft model, increased invasion capacity, and an ability to form both SP and non-SP cells on culture (whilst non-SP cells only produced non-SP cells on culture) (156). SP cells isolated from squamous cell lung cancers have also been shown to be resistant to chemotherapy, but become sensitised following the administration of the ABC transporter activity blocker verapamil (157). CD133 has an unknown function (154), but is detected on the surface of many tumours. Isolation of $CD133^+$ cells from primary non-small cell lung cancer shows these cells to have both a greater tumorigenic potential in SCID mice and have an upregulation of genes involved in stemness, adhesion and cell motility compared to their $CD133^-$ counterparts (158). The $CD133^+$ cells also exhibit a higher number of ABC transporters. When cisplatin (a chemotherapeutic agent removed through ABC transporter activity) was administered to $CD133^+$ xenotransplanted mice the tumours were shown to reduce in size, but the remaining cisplatin-resistant cells were entirely $CD133^+$. Of note, following the examination of $CD133^+$ cells in tumours from NSCLC patients, it was revealed that those with a higher proportion of $CD133^+$ cells had a tendency towards a shorter progression-free survival (158).

The cancer stem cell hypothesis is an important consideration for the development of successful cancer therapies. Conventional treatments target the rapidly proliferating cell population and are unlikely to eradicate the more quiescent, often ABC transporter-expressing, CSC population.

1.3.7 Genetic heterogeneity and clonal evolution in lung cancer

A further consideration in the administration of successful cancer therapy is the genetic heterogeneity that exists within a tumour. Tumours, due to their rapid proliferation, will develop several mutations (159), a number of these will be passenger, with no impact on the behaviour of the tumour mass, but a few will be cancer driver events that have a selective advantage over the other tumour cells, and lead to 'clones' with variability across the tumour (159-161). When sequencing

several areas from resected renal cell carcinomas wide-ranging intratumour heterogeneity was revealed across the tumour bulk, with 63-69% of these mutations heterogeneous and not seen in every sample (162). This study gave rise to the terminology 'branched evolution', and the concept of a phylogenetic tree in cancer, where a few, key mutations are common across all cells, but where the branches of the tree are representative of clones that have arisen later in the tumours natural history and are not shared by the entire tumour mass (162). For a cancer treatment to be successful, focus should be on therapies that target mutations found in the lesion trunk rather than those detected in the branches, where the cancer cell subsets are seen.

1.4 Summary

Lung cancer has a poor prognosis, with new treatments desperately needed. Squamous cell lung cancer has a preinvasive period, and if the disease is detected and treated at this stage, lesions may be prevented from progressing. Preinvasive squamous cell lesions and squamous cell lung cancers are associated with an overexpression of EGF receptors. LRIG1 negatively regulates EGFR signalling and has been shown to be important in the regulation of the stem cell compartments of the skin and gut, and is also associated with both the development and outcome of a number of malignancies. It has been shown that LRIG1 is lost in the development of preinvasive lung cancer and that LRIG1 loss is associated with a worsening of NSCLC prognosis.

It is possible that LRIG1 regulates the stem cell compartment of the human airway. A loss of the protein may lead to dysregulation of the lung stem cell compartment. This may influence the behaviour of the putative cancer stem cells and lead to the development of malignancy. By understanding the role of LRIG1 within airway homeostasis and how its loss leads to preinvasive disease, new therapeutic avenues may be opened.

1.5 Hypothesis

I hypothesise that LRIG1 expression controls airway cell homeostasis and its loss contributes to the initiation of pre-invasive lung cancer.

1.6 Aims

1. To delineate LRIG1 expression in normal and cancerous airways
2. To determine the role of LRIG1 in homeostasis and cancer initiation
3. To identify the mechanism by which LRIG1 regulates airway epithelial growth and cancer initiation

2. Materials and methods

2. Materials and methods

2.1 Chemicals, solvents and plastic ware

All chemicals used were of analytical grade or above and obtained from Sigma Aldrich (unless otherwise stated). Water was distilled and deionised using a Millipore water purification system (Millipore LTD, US). Laboratory plastic ware was from BD Biosciences.

2.2 Tissue collection

2.2.1 Animal breeding strategy

Two, eight week old male mice containing an EGFP–ires-CreERT2 'knock in' cassette at the translational start site of exon 1 of the *Lrig1* locus (91) (Figure 3.1.A. Gene construct) on an FVB/N C57BL/6 background were a kind gift from Dr Kim Jensen, BRIC, Copenhagen. These mice were crossed with FVB/N females (Harlan, UK) producing heterozygous, experimental animals. These heterozygous mice were then crossed to produce homozygous animals (Figure 3.1.B).

For lineage tracing experiments, a homozygous breeding pair of Rosa-26td tomato mice was purchased (Stock number 07909, Jackson laboratories, USA). Homozygous LRIG1 EGFP-ires-CreERT2 animals were then crossed with homozygous Rosa-26td tomato animals, creating offspring heterozygous for Rosa 26 tdtomato reporter and the EGFP-ires-CreERT2 cassette.

Animals were kept in individually ventilated cages at the central biological services facility at University College London. Animals were kept on a 12-hour light/dark cycle at 25°C and were provided with food and water ad libitum. All animal studies were performed in accordance with British Home Office procedural and ethical guidelines.

2.2.2 Human tissue collection

Ethical approval was obtained through the National Research Ethics Committee (REC references 06/Q0505/12). Samples of human bronchial cells were taken from areas of normal bronchial epithelium, and either used directly for analysis (bronchial brush experiments) or expanded and then frozen to create a tissue bank. Cells were taken from this cell bank for cell culture experiments.

2.3 Genotyping Animals

2.3.1 Ear snip digest and PCR

Mouse ear snip samples were placed into 50 µl of ear snip buffer (1M Tris pH 8.0, 5M NaCl, 10% SDS and proteinase K at 20 mg/ml) and were incubated at 55°C for 1 hour. After 1 hour the samples were vortexed and incubated for a further 2 hours. 150 µl of DNase/RNase free water (Life Technologies, UK) was added and samples and heated for 20 minutes at 95°C to inactivate the proteinase K (P6556, Sigma, UK). The samples were then freeze-thawed, and centrifuged at 300 x *g* for 5 minutes to remove any undigested fragments. 1 µl of extracted DNA was used for each PCR reaction.

Primers were used at a concentration of 20 ng/µl and added to 12.5 µl OneTaq PCR 2x mastermix (M0270L, New England Biolabs, UK), or OneTaq PCR 2x master mix with GC buffer (M0483S, New England Biolabs, UK), 9.5 µl ddH_2O to make up to 25. 1 µl of extracted DNA was used for genotyping from the Cre insert and 20 ng of DNA was used for the other reactions.

Gene		Reference	Sequence	Bases
Cre insert	5	Professor Kim Jensen	GCC TGC ATT ACC GGT CGA TGC AAC GA	700
Cre insert	3	Professor Kim Jensen	GTG GCA GAT GGC GCG GCA ACA CCA TT	
LRIG1 wild-type	5	Designed using Primer 3	CGG CGC GTT CCA GAC AAG	355
LRIG1 wild-type	3	Designed using	CAC CCA CAA GTC TCC CAG	

		Primer 3		
Rosa 26 tdtomato mutant	5	The Jackson Laboratory	GGC ATT AAA GCA GCG TAT CC	196
Rosa 26 tdtomato mutant	3	The Jackson Laboratory	CTG TTC CTG TAC GGC ATG G	
Rosa 26 tdtomato wild-type	5	The Jackson Laboratory	AAG GGA GCT GCA GTG GAG TA	297
Rosa 26 tdtomato wild-type	3	The Jackson Laboratory	CCG AAA ATC TGT GGG AAG TC	

PCR reaction protocols

	Cre reaction		LRIG1 WT		Rosa WT/ Mutant	
Step	Temperature (°C)	Time (s)	Temperature (°C)	Time (s)	Temperature (°C)	Time (s)
1	94	30	94	30	94	30
2	94	30	94	30	94	30
3	67	30	62	30	61	30
4	68	60	68	30	68	30
		repeat 2-4 30 cycles		repeat 2-4 30 cycles		repeat 2-4 30 cycles
5	68	300	68	300	68	

Primers were designed around the native copy of *Lrig1* using the first ATG start codon of exon 1 of *LRIG1*. The Primer 3 package was used for primer design (163, 164) and three potential primers selected for subsequent optimisation; primer A, B and C.

Primer	Bases	Direction	Sequence
A	353	5’	GAG TCG GGC GTC CAT GTC
		3’	CAA AGG CGA TAC TCA CAG GC
B	355	5’	CGG CGC GTT CCA GAC AAG
		3’	CAC CCA CAA GTC TCC CAG
C	393	5’	CTG GAG TCG GGC GTC CAT
		3’	AGC AGC CCC GTC TTA ATG

2.3.2 Agarose gel electrophoresis

Gel separation electrophoresis was used to confirm the PCR products were of the expected size. A 1% gel was made by dissolving 1.5 g of agarose in 150 mls 1x TBE. The solution was heated in the microwave to dissolve the agarose and 4.5 µl 10,000 x gel red added (Biotium, California, USA). The solidified gel was placed in a tank filled with 1 x TBE running buffer and 10 µl PCR product loaded, in DNA loading buffer (BIO-37045, Bioline UK). A DNA marker (BIO-33053, Bioline, UK) was included and the gel run for 45 minutes at 140 volts. The DNA bands were visualised using the Gene Genius UV source and camera (Syngene, UK).

2.3.3 Ethanol purification of ear snip DNA

Taking the supernatant from the initial DNA digest, 50 µl 3 M sodium acetate and 500 µl ice cold 100% ethanol were added and the samples incubated at – 20°C for 30 minutes. The samples were then centrifuged at 14,800 rpm for 15 minutes and the supernatant removed. The DNA was washed by re-suspension in 70% ethanol and centrifuged at 14,800 rpm for a further 5 minutes. The supernatant was again removed and the pellet left to air-dry overnight. The following day the pellet was rehydrated in 50 µl of ddH_20 and DNA quantity and purity assessed using the Nanodrop. 20 ng of purified DNA was used for subsequent PCRs.

2.3.4 Sequencing primer B

The entire 25 µl PCR product from the primer B reaction was loaded into a 1% agarose gel. The gel was run at 140 volts for 45 minutes and the DNA band visualised by examination under UV light. The band that corresponded to the predicted bases (350 bp) was carefully cut from the membrane and the sample weighed. The DNA was isolated from the sample following the QIAquick Gel Extraction Kit protocol (28704, Qiagen, UK). The sample was sequenced at Life

Biosciences with results compared to the anticipated product using the software Chromas (South Brisbane, Australia).

2.3.5 Immunofluorescent imaging of earnsips

Earsnips were placed onto a glass slide and mounted in ddH_20 and coverslipped. Microscopy was performed using a Carl Zeiss Axioskop 2 fluorescent microscope. Images were obtained using a QImaging camera and QCapture Pro 6.0 and analysed using Adobe Photoshop CS6.

2.4 Isolation of murine tissues

All mice were used at 6-8 weeks old and sacrificed using a 200 µl intraperitoneal injection of 200 mg/ml pentobarbital (Euthatal, Merial, UK) followed by laparotomy and exsanguination.

2.4.1 Isolation of the trachea

The trachea was identified and cuts made above at the larynx and below at the main carina, and the oesophagus and associated soft tissues were removed. For culture or flow cytometry analysis the tracheas were harvested into DMEM (41966, Gibco) supplemented with 100 U/ml penicillin and 100 µg/ml streptomycin (15070, Gibco) or for histology, was placed directly into 4% paraformaldehyde (PFA).

2.4.2 Isolation of murine lungs following insufflation

Lung insufflation followed the methods described by Giangreco et al (165). In brief, the murine trachea and lungs were exposed, whilst taking care not to damage the lung tissue. The trachea was cannulated and 4% PFA infiltrated from a height of 10 cm. Once the lungs were seen to expand, insufflation continued for 3 minutes before the trachea was tied off and the cannula removed. The lungs and heart were removed from the point of tracheal intubation and placed into 4% PFA.

2.4.3 Isolation of bone marrow cells

Both femurs were isolated from the mouse, and the soft tissues cleaned away. The ends of the bone were cut off. Using a syringe and a 25 G needle, F12 media was flushed through the bone causing the bone to become translucent and the bone marrow cells to be released. Fetal Bovine Serum (FBS, 10270, Gibco) was added to the media, to a final concentration of 10% and the solution pipetted vigorously to create a single cell suspension.

2.4.4 Isolation of skin samples for histological processing

The dorsal skin was shaved to remove fur and using forceps the skin 'tented'. A patch of skin of approximately 5 cm in diameter was removed. The skin was stretched flat onto stiffened paper and placed into 4% PFA for processing.

2.4.5 Isolation of skin cells for flow cytometry

The collected skin sample was washed first in iodine surgical solution and then twice with distilled water, followed by immersion in 70% ethanol for 2 minutes and two further washes in distilled water. Using a petri dish, the subcutaneous fat was scraped off with a scalpel until the remaining tissue became translucent. The skin was floated, hair side up on 0.25% trypsin (T4049, Sigma, UK) and incubated overnight at 4°C. The following day the skin samples were washed in F12 media (21765, Gibco) supplemented with 10% FBS, 100 U/ml penicillin and 100 µg/ml streptomycin, inactivating the trypsin. The hairy side of the skin was scraped to lift off the epithelial cells and the fragments cut into small pieces using two scalpels. The samples were collected in media and residual hairs/solid pieces removed through passing through a 70 µm cell strainer. The cells were centrifuged at 300 x *g* for 10 minutes at 4°C, followed by removal of the supernatant and resuspension in supplemented F12 media.

2.5 Isolation of murine airway basal cells

2.5.1 Pronase digest

The isolated tracheas were cleaned under a dissecting microscope (Leica MZ6) to remove any remaining soft tissues and cut along the long axis. The tracheas were placed in 0.15% pronase (10165921001, Roche, UK) in serum free, supplemented DMEM and incubated at 4°C for 16 hours. FBS was then added to the pronase solution, to a final concentration of 10% and the tube vortexed to detach remaining epithelial cells. The residual trachea was then transferred to a further falcon containing DMEM/FBS and vortexed again. This process was repeated four times and the samples combined. The remaining tracheal soft tissues were disposed of. The cell suspension was centrifuged at 300 x *g*, for 10 minutes at 4°C following which the media was removed and the cells resuspended in DNase solution (stock: 10 mg crude pancreatic DNase I (Sigma, UK), 2 mls 1% BSA and 18 mls FAD) at 200 µl per trachea. After 5 minutes the sample were centrifuged at 300 x *g* for 5 minutes and the cells resuspended in DMEM/FBS. The sample was filtered through a 40 µm filter, and cells counted. The presence of epithelial cells was confirmed by checking for ciliated cells on light microscopy. The isolated cells were either used for flow cytometry analysis or cell culture.

2.5.2 Dispase/DNase/trypsin/collagenase digest

Method was adapted from those previously reported (166-168). The tracheas were isolated as previously described and cut along the long axis, and then incubated in dispase 16 units/ml (Corning, UK), made up in serum free DMEM for 30 minutes. The tracheas were then transferred to DNase solution (as above) for 20 minutes. The samples were checked under the dissecting microscope, and once the epithelium had become 'ruffled' it was gently removed from the underlying tissues with fine forceps using the dissecting microscope. The epithelial sheets were collected using a pipette into a 0.1% trypsin/ EDTA (Sigma, UK) solution, in serum free DMEM, and placed in a 37°C water bath for 30 minutes. The remainder of the

trachea was minced and placed into a 0.25% collagenase solution (Roche, UK), in serum free DMEM and was placed in the water bath for 30 minutes (solution was made at 30 mg/ml in PBS, use 917 µl of media and 83 µl of collagenase solution). Samples were vortexed every 15 minutes to ensure tissue breakdown.

Once the digestion steps were complete, the samples were either combined or analysed separately (in experiments to establish the maximal basal cell yield from a trachea). The samples were then filtered through 40 µm cell strainers and the enzymes neutralised by the addition of FBS, to a final concentration of 10%. The cells were centrifuged at 300 x *g* for 10 minutes and resuspended in media according to the volume required for flow cytometry.

2.5.3 Isolation of tracheal cells via collagenase digest

Tracheas were cleaned and minced into small pieces with a scalpel (168). The samples were incubated in a 0.25% collagenase solution (as above) at 37°C for 90 minutes. Every 15 minutes the samples were vortexed. The samples were then filtered and the enzymes neutralised by the addition of FBS, for use of the cells in flow cytometry.

2.6 Lineage tracing

During optimisation, 4-Hydroxytamoxifen (4OH-tamoxifen) was made up in corn oil to concentrations of 1mg, 0.1 mg, and 0.01 mg. 200 µl of tamoxifen solution was injected intraperitoneally to 6-8 week animals heterozygous for both the eGFP–ires-CreERT2 cassette and the Rosa 26 tdtomato reporter. The animals were observed for 2 weeks before sacrifice. The skin was isolated for flow cytometry analysis and the trachea, bowel and skin isolated for histological examination.

Following the selection of the 1 mg dosage for use in the airway, mice were treated with 1 mg 4OH-tamoxifen and culled 2 days later. Their tracheas were isolated for histological examination.

2.7 Isolation of human brush biopsied epithelial cells

Two bronchial brushings were collected from a normal area of bronchial mucosa into collection media (αMEM supplemented with penicillin/streptomycin and amphotericin B) on ice. Brushes were vortexed vigorously to release the cells, with the brushes remaining *in situ* in the collection falcon and then centrifuged at 300 x *g* for 5 minutes. The cells were resuspended in red cell lysis buffer (Sigma, R7757) and incubated at room temperature for three minutes. Cells were resuspended in 10% FBS diluted in 1% BSA in PBS for blocking in preparation for flow cytometry staining.

2.8 Analysis of cells by flow cytometry

2.8.1 Flow cytometry staining

Mouse

Isolated epithelial cells were blocked for 10 minutes in complete DMEM. Primary antibodies were applied at room temperature for 20 minutes, followed by washing 3 times in complete DMEM. Secondary antibodies were subsequently applied for 20 minutes. After staining the cells were washed 3 further times in DMEM. Secondary-only stains were used when non-conjugated antibodies were included. DAPI at a concentration of 1:1000 was added to the sample immediately prior to running the experiment.

Human

Cells were blocked for 10 minutes in 10% FBS diluted in 1% BSA in PBS. All antibodies used were conjugated and applied for 20 minutes in 1% BSA in PBS at 4°C. After staining, samples were washed 3 times in 1% BSA in PBS. DAPI at a concentration of 1:1000 was added immediately prior to running the experiment.

2.8.2 Flow cytometry analysis

Samples were analysed using the LSR FACS machine (BD LSR Flow cytometer, UK) and were gated according to forward and side scatter characteristics to exclude cell debris and doublets. Where possible, a minimum of 1,000 events in the population of interest was collected for each sample analysed. All gates were set using fluorescence minus one controls. Sample analysis was performed using FlowJo Software (Tree Star Inc., Oregon, USA).

2.8.3 Flow cytometry antibodies

Antigen	Colour	Antibody	Reactivity	Concentration
CD31	PE	102407, Biolegend, UK	mouse	1:100
CD31	PE	303106, Biolegend, UK	human	1:100
CD31	BV421	303124, Biolegend, UK	human	1:100
CD31	PE-Cy7	102417, Biolegend, UK	mouse	1:100
CD45	PE	103105, Biolegend UK	mouse	1:100
CD45	PE	368510, Biolegend UK	human	1:100
CD45	BV421	304032, Biolegend UK	human	1:100
CD49f	APC	17-0495-80, EBioscience	mouse/ human	1:100
EpCAM	BV711	BD Biosciences, UK	mouse	1:100
Isolectin GS-IB4	Biotin	I21414, Invitrogen, UK	mouse	1:100
GS-IB4 secondary	Streptavidin	Q10101MP, Invitrogen, UK		1:100
CD24	PeCy7	101821, Biolegend, UK	mouse	1:100
SSEA1	PerCP efluor700	46-8813-41, eBioscience, UK	mouse	1:50
LRIG1	PE	FAB7498P, R and D Systems	human	1:100
NGFR	PE-Cy7	345110, Biolegend, UK	human	1:100

2.8.4 Flow cytometry cell sorting

Cells were processed as previously and sorting took place using a BD FACS Aria II Flow Cytometer.

Mouse

After the final wash the cells were resuspended in flow cytometry sorting buffer (45 mls media, 5 mls 25 mM HEPES, 40 µl 2 mM EDTA). When cells were used for tracheosphere assays they were sorted into media with 20% FBS, for colony forming assays were sorted directly into 96 well plates and for sc-RNA seq into media containing 5% FBS.

Human

After the final wash, cells were resuspended in flow cytometry sorting buffer (45 mls 1% BSA in PBS, 5 mls 25 mM HEPES, 40 µl 2 mM EDTA). Cells were sorted directly into 96 well plates for colony forming assays.

2.8.5 Hoescht 33342 cell cycle analysis

Mouse

Cell samples were blocked for 10 minutes in supplemented DMEM and Hoechst 33342 added to a final concentration of 10 µg/ml. The samples were incubated at 37 °C for 45 minutes. After Hoescht 33342 incubation, the samples were transferred to ice with application of antibodies as described previously. PI, at a final concentration of 1 µg/ml was used as a viability marker and added immediately prior to running the sample. The Hoechst 33342 data was acquired in linear.

Human

After the blocking step, samples were incubated with Hoescht 33342 added to a final concentration of 10 µg/ml at 37°C for 30 minutes. After incubation, the samples were transferred to ice and antibodies applied as described previously. Sytox red (S34859, ThermoFisher, UK) was used 1:100 as a viability marker, it was added

immediately prior to running the sample. The Hoescht 33342 data was acquired in linear.

2.8.6 EdU cell proliferation analysis

Cells were plated in triplicate in a 6-well plate and grown in BEGM. Once confluence was reached, the media was changed and 24 hours later EdU (Life Technologies Click-iT EdU Alexa Fluor 647; C10424) added to a final concentration of 10 µM. The cells were incubated for 2 hrs and then trypsinised and stained according to the manufacturers instructions.

2.9 Analysis of epithelial cells in situ

2.9.1 Tissue processing and haematoxylin and eosin staining

The isolated tissue samples were left in 4% PFA at 4°C for 24 hours. The formalin was subsequently replaced with 70% ethanol and the samples processed in paraffin wax, using an automated system (Leica TP 1050). 4 µm sections were cut from the embedded sections and mounted on polylysine slides for staining. Haematoxylin and eosin (H&E) staining was performed using an automated staining system (TissueTek).

2.9.2 Immunofluorescent staining

Cytospun cells

Isolated airway epithelial cells were pelleted and resuspended in media at a concentration of 500,000 cells/ml. 100 µl of this solution was applied to each funnel, and the cytospin set at 400 rpm for 5 minutes. Cells were fixed in 4% PFA for 15 minutes, and washed three times in PBS. The slides were incubated in blocking solution (36 mls PBS, 4 mls FBS, 80 µl fish skin solution, 80 µl Triton X) and stained overnight with primary antibodies, made up in blocking solution.

The following morning, the slides were washed three times in PBS and secondary antibody applied in block solution at a concentration of 1:300 for 3 hours. The cells were washed twice more in PBS. DAPI at a concentration of 1:10,000 was applied to the slide for 10 minutes. The cells were washed in PBS once more and mounted with immunomount (Thermo Scientific, UK).

Paraffin embedded sections

4 µm sections were dewaxed and rehydrated by immersion in xylene followed by decreasing concentrations of ethanol through to water, performed by an automated staining system (TissueTek).

Antigen retrieval was performed using either citrate buffer (10 mM sodium citrate, adjusted to pH 6), or EDTA (1 mM EDTA adjusted to pH 8) and samples heated in the microwave on high power for 2 periods of 10 minutes. The samples were left to cool for 15 minutes and the samples blocked (36 mls PBS, 4 mls FBS, 80 µl fish skin gelatin solution) at room temperature for 1 hour. Primary antibody was applied overnight and the following morning samples were washed 3 times, with application of secondary antibodies and cover slipping as above.

When staining for GFP, antigen retrieval was performed via incubation in 0.2% Triton X in PBS and for 10 minutes at room temperature. After blocking, anti eGFP primary antibody (ab13970, Abcam, 1:1000) was applied in blocking solution overnight. Due to difficulties with antigen retrieval when using eGFP, the concentration of KRT5 antibody for dual staining needed to be increased to 1:500. MUC5AC was effective at previous concentrations and no antigen retrieval was performed when staining for eGFP and FOXJ1 expression.

Frozen sections

Frozen sections were left to dry, fixed for 10 minutes in 4% PFA and washed 3 times in PBS. Slides were then blocked in blocking solution (36 mls PBS, 4 mls FBS, 80 µl fish skin solution, 80 µl Triton X) for 1 hour and then primary antibodies applied.

Imaging

All images were captured using a Leica TCS SP8 confocal microscope (Department of Cell and Developmental Biology, UCL) or Carl Zeiss Axiovert A1 microscope and Axiocam 503 camera (Carl Zeiss, UK). Images were analysed using ZEN lite Imaging Software (Carl Zeiss, UK) or Adobe Photoshop CS6.

2.9.3 Antibodies used

Antigen	Antibody	Species	Concentration	Antigen Retrieval
eGFP	Abcam ab13970	Chicken	1:1000	0.2% Triton X
FOXJ1	EBioscience 14-9965-80	Mouse IgG1	1:50	Nil
LRIG1	R and D Systems AF3688	Goat	1:200	0.2% Triton X/ citrate
Tdtomato	Rockland 600-401-379	Rabbit	1:1000	0.2% Triton X
Ki67	Abcam ab15580	Rabbit	1:100	Citrate
Ki67	Biolegend 151202	Rat IgG2b	1:200	Citrate
GS-IB4	L2895 Sigma, 488 conjugate		1:75	Citrate
KRT5	Abcam ab24647	Rabbit	1:1000	Citrate/ 0.2% Triton X
KRT5	Biolegend 905501	Rabbit	1:1000	Citrate/ 0.2% Triton X
ACT	T6793 Sigma	Mouse IgG2b	1:800	Citrate/ 0.2% Triton X
p63	Abcam ab53039	Rabbit	1:50	Citrate
EGFR	LS Bio LS-B2914	Sheep	1:400	Citrate/ 0.2% Triton X
Phospho-EGFR	Invitrogen 36-9700	Rabbit	1:500	Citrate
SPC	Santa Cruz SC-7706	Goat	1:50	Citrate
TTF1	Novocastra NCL-L-TTF-1	Mouse IgG1	1:200	Citrate
CC10	Santa Cruz SC-9772	Goat	1:400	Citrate

CC10	Santa Cruz SC-365992	Mouse IgG1	1:400	Citrate
Annexin 5	Abcam ab14196	Rabbit	1 µg/ml	Citrate
BrdU	Bio-Rad BU1/75 (ICR1)	Sheep	1:200	Citrate

All secondary antibodies for immunofluorescence were AlexaFluor conjugates.

2.9.4 Immunohistochemistry staining

4 µm tissue sections were dewaxed and antigens retrieved via sodium citrate retrieval. Slides were washed once with PBS and endogenous peroxidases blocked for 10 minutes in 1% hydrogen peroxide. The samples were washed again in PBS and then were blocked for 30 minutes in blocking solution (1% casein (VectorLabs), 1% BSA, 2% goat serum (VectorLabs) in PBS). The primary antibody was applied overnight in blocking solution at 4°C. The following morning slides were washed 3 times with PBS, and a streptavidin conjugated secondary antibody applied at a 1:200 dilution in block solution (BA-1000 VectorLabs) for 45 minutes. After washing a further 3 times in PBS, avidin/biotin blocking was performed according to kit instructions (SP-2001, VectorLabs). Cells were washed 3 x in PBS and stained with 3, 3'-diaminobenzidine (DAB) (SK-4100, VectorLabs), according to kit instructions. Slides were counterstained using the automated staining system (TissueTek).

2.9.5 Assessing the proliferation of adult airway epithelial cells

6-8 week old mice were injected with 10 ul/gram of BrdU (Invitrogen, UK) and observed for 5 hours. After 5 hours, the tracheas were isolated and placed in 4% PFA for embedding. A bowel sample was taken as a positive control for the BrdU staining.

2.9.6 Assessment of epithelial thickness, proliferation and number of basal cells

Sections were stained for H&E or appropriate stains (Ki67 or KRT5). Epithelial thickness was measured using NDP Viewing Software (Hamamatsu, UK). Depth was measured from the basement membrane to the lumen, perpendicular to the

tracheal length. Measurements were taken in 6 locations and an average obtained for each trachea.

For BrdU, Ki67 and KRT5 staining, 6 images of the epithelium were taken across the length of the trachea, and images overlaid. The numbers of epithelial cells seen above the basement membrane were counted (based on DAPI staining) and the numbers of either BrdU, Ki67 or KRT5 positive cells above the basement membrane were counted. These cell counts were expressed as a percentage of the total epithelial cell number in that section, and an average of the 6 images was recorded.

2.10 Mouse airway epithelial cell culture

All tissue culture plastics, tissue culture grade trypsin, tissue culture antibiotics and FBS were purchased from Invitrogen, unless otherwise stated. Sterile tissue culture flasks and plates were purchased from Nunc (ThermoFisher). All tissue culture plates were coated with rat tail collagen type 1 (354263, BD) prior to seeding of cells.

3T3-J2 feeder layers were prepared as below. Flow cytometry sorted murine basal cells or murine airway epithelial cells obtained following pronase digest, were plated on feeder layers in mouse tracheal epithelial cell culture media (MTEC) (169, 170). MTEC consisted of DMEM (41966, Gibco) and F12 (21765, Gibco) in a 1:1 ratio with penicillin/streptomycin (15070, Gibco), supplemented with 15 mM HEPES, 3.6 mM sodium bicarbonate,10 μg/ml insulin (I6634, Sigma), 5 μg/ml transferrin (T1147, Sigma), 0.1 μg/ml cholera toxin (C3012, Sigma), 25 ng/ml epidermal growth factor (354001 Becton-Dickinson), 30 μg/ml bovine pituitary extract (13028014, ThermoFisher), 5% FBS (10270, Gibco), and freshly added 0.01 μM retinoic acid (R2625, Sigma). Media was changed every 3 days. At confluence, cells were expanded and then passaged at a 1:5 ratio onto fresh 3T3-J2 feeder layers.

2.10.1 Tracheosphere assay

Flow cytometry-sorted murine basal epithelial cells were plated at 1,250 cells/ well in matrigel (#354230, BD Biosciences) and cultured in MTEC, for 7 days. After 7 days the media was changed to MTEC differentiation media, consisting of DMEM (41966, Gibco) and F12 (21765, Gibco) in a 1:1 ratio with penicillin/streptomycin (15070, Gibco), supplemented with 15 mM HEPES, 3.6 mM sodium bicarbonate,5 µg/ml insulin (I6634, Sigma), 5 µg/ml transferrin (T1147, Sigma), 0.025 µg/ml cholera toxin (C3012, Sigma), 5 ng/ml epidermal growth factor (354001 Becton-Dickinson), 30 µg/ml bovine pituitary extract (13028014, ThermoFisher), 1mg/ml BSA and freshly added 0.01 µM retinoic acid (R2625, Sigma). At day 14 tracheospheres were counted, photographed, washed in ice cold PBS and fixed in 4% PFA. Spheres were processed in Histogel (HG-4000-012, Fisher Scientific) prior to paraffin embedding.

2.10.2 Colony forming assay

Epithelial cells were sorted directly into each well of a 96-well plate containing mitotically inactivated 3T3-J2 fibroblasts and MTEC media. MTEC was replaced 2-3 times a week. At day 10 the colonies were fixed in 4% PFA for 15 minutes and then stained with crystal violet (HT90132, Sigma, UK) at room temperature for 10 minutes. The plates were washed in tap water until it ran clear and then left to air-dry. The numbers of colonies, which consisted of more than 10 cells were counted.

2.11 Human airway epithelial cell culture

2.11.1 3T3-J2 feeder cell culture

3T3-J2 feeder cells were cultured in DMEM (41966, Gibco) supplemented with 100 U/ml penicillin, 100 µg/ml streptomycin (15070, Gibco) and 9% bovine serum (26170, Gibco). The cells were cultured at 37°C, in 5% CO_2. The media changed 3 times a week and cells were used up to passage 12. To generate feeder layers, confluent cells were mitotically inactivated by treatment for 2 hours with 4 µg/ml mitomycin (M4278, Sigma). Following inactivation, the cells were trypsinised and

plated at a density of 20,000 cells/cm^2, in DMEM growth media. The epithelial cells were added to the feeder layers the following day.

2.11.2 Human airway epithelial cell culture in 3T3-J2 co-culture with ROCK inhibition (3T3 + Y)

3T3-J2 feeder layers were prepared as above. Cells were cultured at 37 °C in 5% CO_2 in epithelial culture medium consisting of DMEM (41966, Gibco) and F12 (21765, Gibco) in a 3:1 ratio with penicillin/streptomycin (15070, Gibco) and 7.5% FBS (10270, Gibco) with the supplementation of 5 μM Y-27632 (ROCK inhibitor, Y1000, Cambridge Bioscience), 25 ng/ml hydrocortisone (HO888, Sigma), 0.125 ng/ml epidermal growth factor (10605, Sino Biological), 5 μg/ml insulin (I6634, Sigma), 0.1 nM cholera toxin (C8052, Sigma), 250 ng/ml amphotericin B (10746254, Fisher Scientific) and 10 μg/ml gentamycin (15710, Gibco). Media was changed three times a week.

When experiments necessitated a pure epithelial cell population, the 3T3-J2 feeder layers were removed by differential trypsinisation (171). In brief, cells were washed with PBS and 0.05% Trypsin/EDTA added. The cells were incubated at 37 °C and the feeder cells seen to detach. The trypsin was removed and cell layers washed with PBS and further trypsin added, after a further 5 minutes the epithelial cells were seen to detach.

All epithelial culture using the generated *LRIG1* shRNA cell lines, was performed with the parent cells, the *LRIG1* shRNA knockdown cells and the *LRIG1* expressing non-silencing controls at the same passage number.

2.11.3 Colony forming assay directly from flow-sorted cells (96-well plates)

Epithelial cells were sorted directly into each well of a 96-well plate containing mitotically inactivated 3T3-J2 fibroblasts and 50:50 conditioned media (from a confluent layer of human epithelial cells filtered through a 40 μm filter) and 3T3 + Y

media, and supplemented with additional ROCK inhibitor at a concentration of 5 µM. After 7 days the media was replaced with 3T3 + Y media. Throughout the experiment media was replaced 2-3 times a week. At day 14 the colonies were fixed and stained with crystal violet, and colonies counted as above.

2.11.4 Colony forming assay in cultured HBECs (6-well plates)

6-well plates were coated with collagen and seeded with mitotically inactivated 3T3-J2 cells in 10 % DMEM. Human epithelial cells were seeded at 1,000 cells/well in FMED. The media was changed on days 3, 5, 7 and 9. On day 10 the plates were fixed in 4 % PFA and then stained with crystal violet. After washing in tap water and air-drying the number of colonies per well were counted. Colonies greater than 10 cells were included.

2.11.5 XTT assay

7,500 cells were plated in BEGM (CC-2540B, Lonza, with all the aliquots added to the BEBM), in triplicate, per well of a collagen-coated 96-well plate. Cells were left overnight to adhere, and then the media changed and XTT (A8088, Applichem) added according to the manufacturers instructions. Three control wells containing BEGM media were included as blanks. After a 4 hour incubation, the absorbance of samples were measured using a Titertec Multiscan MCC/340 plate reader (Labsystems, Turku, Finland) at wavelengths of 490 and 630 nm. The 630 nm measurement was subtracted from the 490 nm to obtain the absorbance reading. Percentage change was expressed as a proportion of the initial reading. Readings were taken at 1, 2, 3, 4, 7, 9, 11 and 14 days.

2.11.6 Invasion assay through Matrigel

Matrigel (#354234, BD Biosciences), was mixed 1:1 with serum free media (containing 3:1 DMEM to F12 with penicillin/streptomycin) on ice, with 200 µl added to the upper chamber of a transwell plate. The matrigel solution was left to set for

30 minutes at 37°C. Epithelial cells were seeded at 50,000 and 100,000 cells above the Matrigel in serum free media. The wells were filled with 500 µl of complete epithelial media containing ROCK inhibitor. After 96 hours the Matrigel was carefully removed using a cotton bud, and the media replaced with 4% PFA. The membranes were left at room temperature for 20 minutes and then stained with crystal violet and washed gently in tap water until the water ran clear. The membranes were left to air-dry overnight. The following morning the membranes were treated with 350 µl of 10% glacial acetic acid. 100 ul of this solution was added, in triplicate to a 96 well plate and the absorbance read at 550 nm.

2.11.7 Organotypic assay

A solution containing rat tail collagen type 1 (354263, BD), Matrigel (#354234, BD Biosciences), 10 x DMEM, 10% FBS complete DMEM, and human fibroblasts at a concentration of 5 x 10^6 cells/ml was prepared on ice, in a volume ratio of 3.5:3.5:1:1:1. 1M NaOH was added to the solution in 100 µl aliquots until the mixture became a pink colour. 1ml of the gel mix was added per well of a 24-well plate and plates were incubated at 37°C for 1 hour to allow the gels to solidify. 1ml of 10% FBS complete DMEM was then added to each well and the plates returned to the incubator overnight.

The following day, 2 cm squares of nylon were sterilised by autoclaving. A collagen mix was prepared consisting of collagen/10x DMEM/FCS/10% FBS complete DMEM, in a ratio of 7:1:1:1. 250 µl of the collagen solution was added per nylon sheet and left at 37°C for 30 minutes. 1% glutaraldehyde solution (G5882, Sigma, UK) was used to wash the sheets, with incubation in the 1% glutaraldehyde solution at 4°C for 1 hour. The sheets were washed in PBS to remove any excess glutaraldehyde and stored in serum free DMEM until required.

The DMEM overlying the gels was removed and 750,000 epithelial cells in FMED + Y media were added to each gel, in triplicate. After 48 hours the media was changed. At 96 hours, the gels were detached from the wells and raised onto a metal grid

within a 6-well plate. A collagen-coated square was added to each of the grids and then the gel added on top. Tracheosphere media (172) was added to each well of the 6-well plate, so that the collagen membrane was covered, but the upper surface of the gel, with the over-lying epithelial cells was exposed to air. Tracheosphere medium consisted of 50% BEBM (CC-2540B, Lonza) and 50% DMEM (41966, Gibco) supplemented with BEGM supplements (minus triiodothyronine, gentamycin, amphotericin and retinoic acid). 100 nM retinoic acid (R2625, Sigma) was added immediately before each use.

The media was replaced every 2-3 days. After 24 days, the media and metal grids were removed from the gels. The membranes were fixed in 4% PFA for 6 hours and then paraffin embedded.

2.12 Other tissue culture

2.12.1 HEK293T cell culture

HEK293T cells were grown in DMEM (41966, Gibco) supplemented with penicillin/streptomycin (15070, Gibco) and 10% FBS. On cell confluence, cells were trypsinised and passaged at a 1:10 ratio.

2.12.2 Human lung fibroblast culture

Primary human lung fibroblasts derived from healthy donor lungs were a kind gift from Professor Robin McAnulty (University College London, UK). The fibroblasts were cultured in DMEM with 100 U/ml penicillin and 100 µg/ml streptomycin (Gibco; #15070) and 10% FBS.

2.12.3 Mycoplasma testing

Cells in culture were routinely tested for mycoplasma contamination. This was performed through either the MycoAlert Mycoplasma Detection Kit (LT07-318,

Lonza), according to manufacturers instructions, or using published PCR techniques (173).

2.13 shRNA knock down of LRIG1

2.13.1 Preparation of plasmid DNA

Three LRIG1 plasmids, V2LHS_229246, V3LHS_332387 and V3LHS_404471, purchased as bacterial stabs, were used. These were arbitrarily labelled 1, 2 and 3 for the purposes of assessment. Initially an LB broth, containing 25 g of LB broth (Sigma, UK) dissolved in 1 litre of water and adjusted to pH 7 was produced. This solution was autoclaved and left to cool. 1 ml of 100 mcg/ml ampicillin (concentration 1:10000) was added to the solution. 3 mls of the broth was aliquoted into 3 falcons and a sample of the bacterial stab added to each. The solution was incubated at 37°C, in an orbital incubator at 230 rpm for 5 hours. 200 mls of fresh broth was added to autoclaved 500 ml glass bottles. 25 µl of the resulting bacterial solution was added to each of these bottles and incubated overnight at 37°C, 230 rpm. The following day, the DNA was extracted using the Qiagen HiSpeed Plasmid Maxi Kit 12663 (Qiagen, UK), according to the manufacturers instructions. The DNA concentration was quantified via Nanodrop.

2.13.2 Production of virus

HEK293T cells were seeded into 4 T175 flasks, containing DMEM (41966, Gibco) supplemented with penicillin/streptomycin (15070, Gibco) and 10% FBS. The flasks were left to reach 80- 90% confluence. For each T175 flask, 20 µg of plasmid DNA (UCLH shRNA library), 7 µg pmD.G and 13 µg of PCMV_dR8_74 packaging plasmids (Plasmid Factory, Germany) were added to 1 ml of 150 mM NaCl, vortexed for 10 seconds and passed through a 0.22 µm filter. 80 µl of jet PEI was added to 1 ml of 150 mM NaCl solution. The jet PEI solution was added to the plasmid DNA/NaCl solution, vortexed for 10 seconds and incubated for 20 minutes at room temperature. The NaCl/DNA/jet PEI solution (2 mls) was added to 13 mls DMEM and

replaced the media in each T175 flask. The flasks were incubated for 4 hours at 37°C, and after this period the media replaced with 20 ml fresh DMEM. After 24 hours the media was replaced with 12mls of fresh media, and following another 24 hours the media was collected for virus isolation. In total, two 12 ml aliquots of media were collected from each flask at 48 and 72 hours post initial virus incubation.

The ultracentrifuge was set to 4°C and Beckman centrifuge tubes were washed in 70% IMS and left to dry in a hood. The collected media was centrifuged at 300 x *g* for 10 minutes at 4°C. The supernatant was removed and filtered through 0.45 µm filters, and then transferred to the dry centrifuge tubes and centrifuged at 17,000 rpm for 2 hours at 4°C (SW28 rotor, Optima LE80K Ultracentrifuge, Beckman). After centrifuging, virus was resuspended and stored in aliquots at -80°C for further use.

2.13.3 Titration of virus

50,000 HEK293T cells were seeded per well of a 12-well plate. The following day the media was replaced with virus- containing media, with 2, 1, 0.5, 0.25, 0.125 µl of virus and 4 µg/ml of polybrene. After 48 hours, the cells were trypsinised and prepared for flow cytometry. A GFP reporter is contained within the plasmid, so the percentage of GFP expressing cells was elucidated by flow cytometry. The viral titre in particles/ml was calculated using the formula: -

$$\text{Viral titre} = \frac{\%\text{ of positive cells} \times \text{number of cells plated}}{\text{volume of virus added (in ml)}}$$

2.13.4 Viral transduction

50,000 epithelial cells were seeded onto mitotically inactivated 3T3-J2 feeder layers in 6-well plates. The following day, virus was added at a multiplicity of infection (MOI) of 3. The J2 feeder layers were included in the assessment of MOI. The virus was added with 4 µg/ml polybrene. The media was exchanged with fresh FMED after 4 hours. Transduction success was confirmed through both the expression of GFP

protein that was seen detectable immunofluorescence and through immunoblotting for LRIG1.

2.14 Western Blotting

2.14.1 Sample preparation

Cerebella

6- 8 week old adult mice were euthanised and their brains removed and placed in ice-cold PBS. Cerebella were dissected and lysed in P40 extraction buffer consisting of 50 mM Tris-HCl pH 8.0, 150 mM NaCl, 1% IGEPAL, 1 mM Na_2VO_3, 25 mM NaF with the addition of protease and phosphatase inhibitor cocktail (#1861281, ThermoFisher). The samples were frozen at -80°C, defrosted on ice, macerated and centrifuged at 13000 × *g* for 3 min. The cleared supernatants were collected for Western blotting.

Cells used in the assessing the success of shRNA knock down

HBECs were grown in 3T3 + Y conditions. When confluent, the 3T3 cells were removed by differential trypsinisation and the media replaced. The following morning the HBECs were washed twice in ice cold PBS and cell lysis performed using RIPA buffer (R0278, Sigma) containing a protease and phosphatase inhibitor cocktail (ThermoFisher). The cells were left at – 80°C for 1 hour prior to cell scraping. After cell scraping, the lysates were transferred to microfuge tubes and stored at – 20°C for future use. When needed, the samples were defrosted on ice and centrifuged at 14,000 x *g* for 10 minutes at 4 degrees. The cleared lysates were transferred to a clean microfuge tube.

Samples used in the assessment of the effects of EGF

HBECs were grown in 3T3 + Y conditions. When confluent, the 3T3 cells were removed by differential trypsinisation, the cells washed with complete media to neutralise the trypsin and then starved for 16 hours in DMEM (41966, Gibco) with penicillin/streptomycin (15070, Gibco). Cells were stimulated with 10 ng/ml EGF for 30 minutes. After 30 minutes, the cells were washed twice in ice cold PBS and underwent cell lysis as above.

2.14.2 Immunoblotting

The protein concentration of samples was determined by BCA assay and samples diluted in dH_20 to equivalent concentrations. The samples were mixed with 5 x laemmlli buffer (3.125 mM Tris- base pH 6.8, 10% (w/v) SDS, 20% (v/v) glycerol, 50 mM Dithiothreitol (DTT), in dH_20) and heated to 80°C for 10 minutes. The proteins were separated on 4-12% Bis- Tris gels (Invitrogen) and transferred onto a nitrocellulose membrane using the iBlot transfer system (Invitrogen), or the XCell II blot module according to manufacturers instructions (EI9051, ThermoFisher).

The blots were blocked for 1 hour at room temperature in blocking buffer, tris-buffered saline (Cell Signalling Technologies) containing 0.1% Tween 20 (TBST) and 5% non-fat dry milk in TBST. Antibodies were added in 5% BSA in TBST overnight at 4 degrees. The membranes were washed 3 times in TBST and then incubated for 1 hour at room temperature with an HRP conjugated secondary antibody in 5% milk. The membranes were then washed 3 further times in TBST and the developed using Luminata Western HRP Chemiluminescence Reagent (Millipore). Protein bands were detected using an ImageQuant LAS 4000 system (GE Healthcare). When blots were re-probed, they were stripped in stripping buffer for 10 minutes at room temperature (21059, ThermoFisher), reblocked, and a further antibody applied as above.

2.14.3 Antibodies used

Antibody	Species	Supplier	Code	Concentration

LRIG1 (anti mouse)	Rabbit	Abcam	Ab36707	1 µg/ml
LRIG1 (anti human)	Rabbit	Cell Signalling Technologies	#12752	1:1000
α-tubulin	Rabbit	Cell Signalling Technologies	#9099	1:1000
EGFR	Rabbit	Cell Signalling Technologies	#4267	1:1000
phospho-EGFR	Rabbit	Cell Signalling Technologies	#2234	1:1000
ERK ½	Rabbit	Cell Signalling Technologies	#9102	1:1000
phospho- ERK 1/2	Rabbit	Cell Signalling Technologies	#9101	1:1000

2.15 Single cell RNA sequencing

Flow cytometry sorted epithelial cells were transported in collection media to either the Genome Centre, University of London (UK), or to The Mill Hill Laboratory, Francis Crick Institute (UK). In both institutions the experiments were run by a technician. The cells were inserted into a C1 Fluidigm according to the manufacturers instructions. Medium sized C1 Fluidigm plates were used (Fluidigm, UK) and an ERCC control added to samples (Invitrogen, UK). The cDNA library was prepared using the Nextera XT DNA Library Preparation Kit. Prior to sequencing, the cDNA quality was assessed using a bioanalyser. cDNA sequencing was performed on an a HiSeq2500 (Illumina, UK). Data was received in the form of FASTQ files. These were given to bioinformaticians at the Bill Lyons Informatics Centre UCL for data analysis.

2.16 N-Nitrosotris-(2-chloroethyl)urea (NTCU) in a squamous carcinogenesis model

2.16.1 NTCU treatment

6 week old female, LRIG1-null, LRIG1-heterozygous and wild-type FVB/N C57BL/6 mice were treated. 24 hours prior to the first dose, murine dorsal skin was shaved. NTCU (sc-212265 Santa Cruz) was diluted in acetone to a concentration of 0.013 M, with aliquots stored at -20°C in Nunc Cryovials (ThermoFisher) for future use. 75 µl of NTCU was applied twice weekly, between the shoulder blades of the mouse

(within a class II microbiological safety cabinet). The NTCU solutions were kept on ice at all times. Skin was allowed to dry before the animal placed back into its cage. Acetone was used as a control. Prior to application, the animals were weighed and skin checked to ensure no irritation. Skin was shaved once a week, 24 hours before dosing and bedding changed every 2 weeks. Animals underwent 12 weeks of treatment (24 doses), followed by an 11 week monitoring period, where twice-weekly weights were continued. After 23 weeks animals were culled via pentobarbital injection. 4 hours prior to sacrifice, BrdU (000103, ThermoFisher) was administered intraperitoneally.

2.16.2 Assessment of disease extent

Lung blocks were sectioned until the trachea and main bronchi were visible (Figure 2.1.A). To assess disease extent, two continuous 4 µm sections were taken followed by a further 2 sections 200 µm from the first. The first of each of these were stained with H&E, and the second stained for KRT5 by immunohistochemistry.

Abnormal airways were determined by the presence of KRT5 staining distal to the cartilage containing trachea and the left and right main bronchi. Slides were scanned using a NanoZoomer (Hamamatsu, UK), and NDP Viewing Software (Hamamatsu, UK) was used to draw around the KRT5 stained bronchial tree. The entire bronchial tree (beyond the cartilage containing areas) was then measured. The percentage of abnormal airway defined by the length of the KRT5 stained airway was then divided by the total length of the bronchial tree (Figure 2.1.Bi and 2.1.Bii). An average of the percentage of KRT5 stained airway was then obtained from the two sections that were 200 µm apart.

The KRT5 stained areas were then compared to the corresponding H&E image. Staining was divided into flat atypia, low-grade and high-grade dysplasia. The percentage of each type of lesion was then divided by the total length of abnormal bronchial tree, to obtain the proportion affected by each lesion type. Flat atypia was defined as any KRT5 staining of the airway beyond the cartilage containing bronchial

tree that was one cell layer in thickness. Low-grade dysplasia, encompassed metaplasia, mild and moderate dysplasia and consisted of KRT5 staining of more than one cell in thickness, but with clear differentiation/organisation of cells from the basal layer to those adjacent to the lumen. High-grade dysplasia was severe dysplasia or carcinoma in situ, with KRT5 staining of more than one cell thickness, with disorganization; the nuclei were large and there was no evidence of organisation of cells between those along the basal layer and the lumen (Figure 2.1.C).

When the abnormal areas of KRT5 staining eroded through the basement membrane these were defined as cancers. Using the NDP Viewing Software, the total surface area of the lung and lesion areas were calculated. Cancers were counted as individual lesions if they were greater than 200 µm apart. The number of tumours were counted across two sections of lung that were separated by 200 µm. An average size number of tumours for each mouse (from the average of the two sections was determined.

The size of each tumour was considered as a single entity and analysed according to the genotype of the mouse. Therefore the tumours were divided into three groups, dependent on the genotype of the parent. This is similar to the method reported by Alcolea *et al* in their analysis of clonal patches in the oesophagus (174). The percentage of lung affected by cancer was determined by averaging the percentage of surface area covered be invasive cancers in two sections, 200 µm apart (Figure 2.1.B iv).

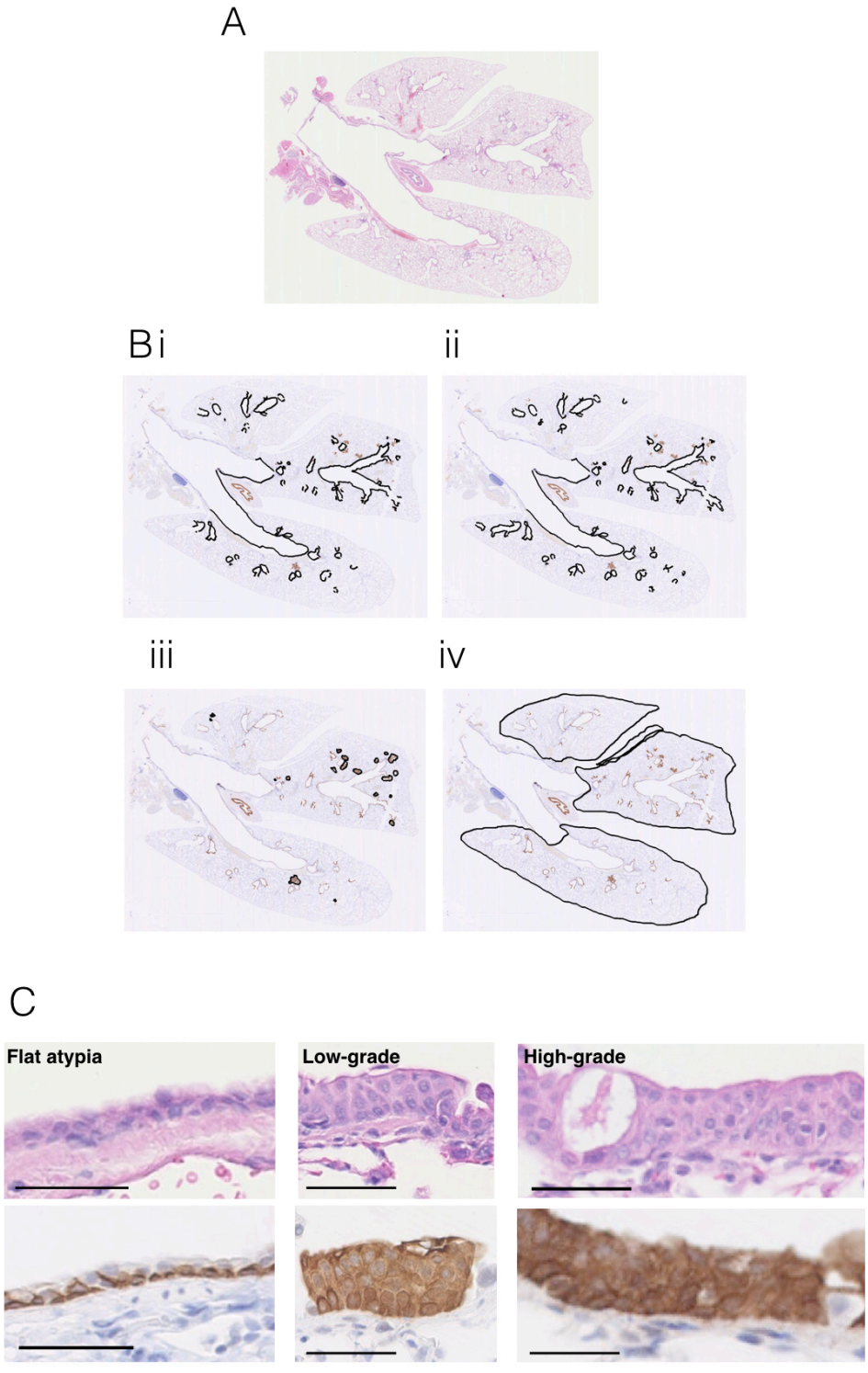

Figure 2.1: Assessment of NTCU induced disease

A) Transverse sections of lungs were cut until a section containing the cross section of the trachea and the right and left main bronchi were reached. B) i) Keratin 5 stained lung was drawn around using NDP image software, this was then compared to the length of the entire bronchial tree that was visible in ii). iii) shows the assessment of the surface area of lung cancers, with the perimeter of the lesion drawn around by using NDP image software, whilst iv) shows how the entire lung was drawn around to work out the total surface area of the lungs. Scale bars = 0.5 cm. C) Examples, from left to right of flat atypia lesions, low grade dysplasia and high grade dysplasia, scale bars = 100 µm

2.16.3 Assessment of tumour proliferation

Sections, from LRIG1-null, LRIG1-heterozygous and wild-type mice were stained for immunofluorescence with Ki67, Annexin V, KRT5 and DAPI. The number of DAPI stained cells within a KRT5 stained tumour were counted, along with the number of Ki67 and Annexin V positive cells. These were expressed as a percentage of the DAPI positive cells making up the tumour.

2.17 Statistics

Statistical analysis was performed using GraphPad Prism (GraphPad Software, CA, USA) and Microsoft Excel. Mouse and human tissue culture data were analysed using t-test and one-way ANOVA. NTCU data was assessed for normality using the D'Agostino & Pearson test, followed by the Kruskal-Wallis or one-way ANOVA as appropriate. Percentages underwent arcsine transformation to enable assessment. Results were considered statistically significant when $p \leq 0.05$. All data points are represented as mean ± standard error of mean.

3. Expression of LRIG1 in the murine airway

3. Expression of LRIG1 within the murine airway

3.1 Background

The role of leucine-rich repeats and immunoglobulin-like domains protein 1 (LRIG1) in the skin and the gut has been defined through the use of mouse models. *In situ* hybridisation has shown expression of LRIG1 in the stem cell niche of the small intestine and colon (93). Whilst LRIG1 is expressed throughout the skin, it is seen in the highest concentrations in the melanoma-associated chondroitin sulfate proteoglycan (MCSP)-positive keratinocyte stem cell population (90). *Lrig1* knockout mouse models have shown the role of LRIG1 in the regulation of the stem cell compartments, where loss of LRIG1 leads to the hyperproliferation of both skin (89) and gut epithelia (93). To assess how LRIG1 could lead to preinvasive lung cancer, LRIG1's expression in the normal airway and its association with the stem cell compartments of the airways needs to be delineated. Then, through the use of an LRIG1-null mouse model, the effect of loss of LRIG1 in the airway, and how loss of LRIG1 leads to preinvasive cancer, can be established.

The external domain of LRIG1 is susceptible to cleavage by trypsin and there are few reports of the successful use of antibodies against LRIG1 in immunohistochemistry, flow cytometry analysis or western blotting. To make detection easier, LRIG1 has previously been tagged with the FLAG protein (104) and research groups have generated their own LRIG1 antibody (94), although with limited success (175). Due to these difficulties, this project makes use of the *Lrig1* EGFP-ires-CreERT2 mouse, where an EGFP-ires-CreERT2 cassette is placed behind the start codon of *Lrig1* (91). This means that when the *Lrig1* promoter is activated, the reporter protein eGFP is expressed instead of LRIG1, labelling the cell. The CreERT2 component of the cassette allows lineage tracing of LRIG1-expressing daughter cells, should the animal to be crossed with a reporter strain. As an *Lrig1* EGFP-ires-CreERT2 heterozygous mouse only has a single copy of the cassette, functional LRIG1 is still produced. By using the expression of eGFP, these *Lrig1* EGFP-ires-CreERT2 mice have been used to

identify the presence of LRIG1-expressing cells in the epidermis through both immunohistochemistry and flow cytometry (91). Previous work has found there to be no effect of *Lrig1* haploinsufficiency, with no detectable differences between *Lrig1* wild-type and *Lrig1*-heterozygous animals (104). When both copies of the *Lrig1* gene are replaced by the *Lrig1* EGFP-ires-CreERT2 cassette no functional LRIG1 protein is produced; this means an animal homozygous for the *Lrig1* EGFP-ires-CreERT2 cassette is the equivalent of an LRIG1-null mouse.

Basal cells are the stem cells of the upper airway (176) so by extrapolating from studies in the skin and gut, where the highest LRIG1 expression is seen in the stem cell compartments, the airway basal cells would be expected to have the greatest LRIG1 expression. Airway basal cells are further considered to be the cell of origin of squamous cell lung cancer (177, 178). Therefore, the loss of LRIG1 seen in preinvasive cancer could affect the airway basal cells, leading to their dysregulation and the development of preinvasive disease. To understand the effects of LRIG1 in the murine airway, the expression of LRIG1 in the airway epithelium needs to be determined and airway basal cells need to be isolated to analyse this in more detail. By comparing LRIG1-expressing basal cells (from heterozygous animals) to LRIG1-null basal cells (from mice homozygous for the *Lrig1* EGFP-ires-CreERT2 cassette), the effect of loss of LRIG1 on the behaviour of the airway stem cell compartment and how its loss may lead to preinvasive lung cancer can be determined.

To fully establish the role of LRIG1 in the airway, I intended to perform lineage tracing using the CreERT2 component of the gene cassette. This would characterise the stem cell potential of an LRIG1-expressing cell, as when *Lrig1* EGFP-ires-CreERT2 mice are crossed with reporter animals the progeny of an LRIG1-expressing cell will be permanently labelled. When lineage tracing in animals heterozygous for *Lrig1* EGFP-ires-CreERT2 cassette, the potential of an LRIG1-positive cell to maintain the epithelium during homeostasis, during repair and on cancer induction can be assessed. Subsequent lineage-tracing experiments using animals homozygous for the *Lrig1* EGFP-ires-CreERT2 cassette could then be used to determine how the

lineage tracing changes when LRIG1 is deleted and the effect of the loss of LRIG1 in homeostasis, repair and cancer induction.

3.2 Aims

- To establish and characterise *Lrig1* EGFP-ires-CreERT2 mice
- To assess the expression of LRIG1 within the murine trachea and lung, particularly in the airway stem cell compartments
- To isolate LRIG1-expressing basal cells from the trachea to enable a more detailed assessment of the properties of LRIG1-expressing cells
- To assess the behaviour of LRIG1-expressing cells in a lineage-tracing model

3.3 Results

3.3.1 Establishment of the *Lrig1* EGFP-ires-CreERT2 colony

To study LRIG1 in the airway epithelium, reporter mice, where one copy of native *Lrig1* is replaced with an *Lrig1* EGFP-ires-CreERT2 cassette (Figure 3.1.A) were used. These *Lrig1* EGFP-ires-CreERT2 heterozygous animals, a gift from Professor K. Jensen, The University of Copenhagen, were on an FVB/N C57BL/6 background and were crossed with commercially available FVB/N animals. The viability of the *Lrig1*-knockout offspring is dependent on background: animals inbred on a pure FVB/N background have a severe phenotype, with the development of a grossly distended bowel and malabsorption that necessitates culling at around P10 (93), whereas outbred *Lrig1* knockout animals survive into adulthood (89, 90). FVB/N mice were selected due to their susceptibility to the development of chemically induced squamous cell carcinomas (179, 180), which would become of relevance in later carcinogenesis experiments.

Following the cross of the *Lrig1* EGFP-ires-CreERT2 cassette animals with the FVB/N animals, heterozygous progeny were produced. These were crossed again creating wild-type, LRIG1-heterozygous and LRIG1-null animals (Figure 3.1.B). The LRIG1-null

animals had no phenotypic characteristics other than a reduced weight at weaning (Figure 3.1.C), there was no evidence of the previously described skin thickening, dermatitis or bowel abnormalities (89, 93). There were, however, fewer LRIG1-null animals produced than anticipated by Mendelian genetics (Figure 3.1.D). To increase the number of LRIG1-null animals, breeding pairs were set up between LRIG1-null and LRIG1-heterozygous animals. Between 30-50% of these litters were lost prior to weaning, which contravened Home Office Guidelines. The breeding strategy was initially abandoned, but subsequently returned to and, with improved animal husbandry, was a greater success.

3.3.2 The effect of *Lrig1* haploinsufficiency

The loss of LRIG1 initiates hyperproliferation of the skin and gut (89, 93), however, it has previously been reported that there is no effect of *Lrig1* haploinsufficiency (104). To confirm this finding, airway cell proliferation in wild-type and LRIG1-heterozygous animals was compared (Figure 3.1.E and 3.1.F). Assessment of the rate of proliferation followed a 6-hour pulse of BrdU. BrdU uptake was noted in approximately 0.8% of airway epithelial cells. There was no difference in epithelial cell proliferation between LRIG1-heterozygous and wild-type mice and no differences between male and female animals.

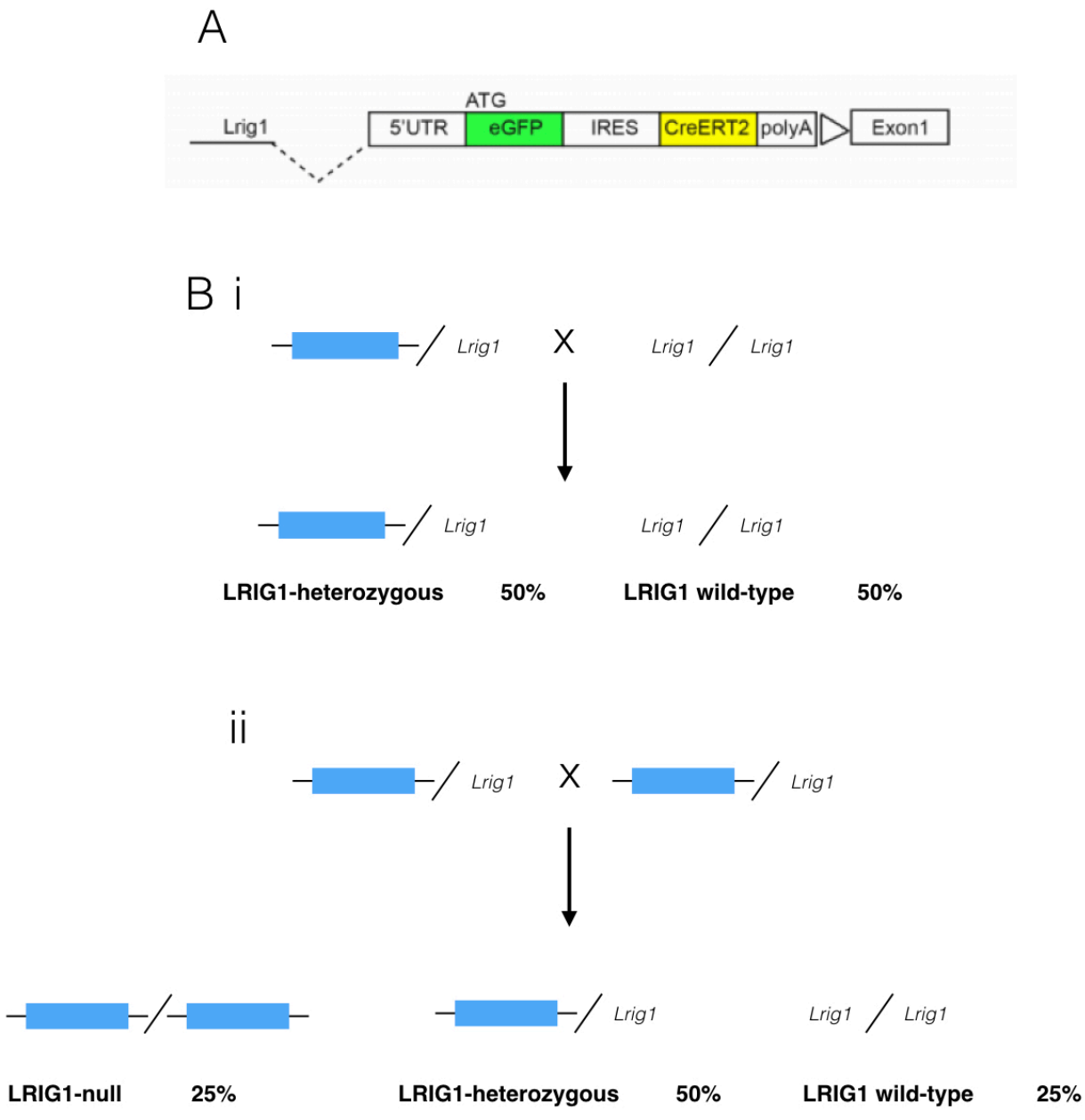

Figure continued over page.

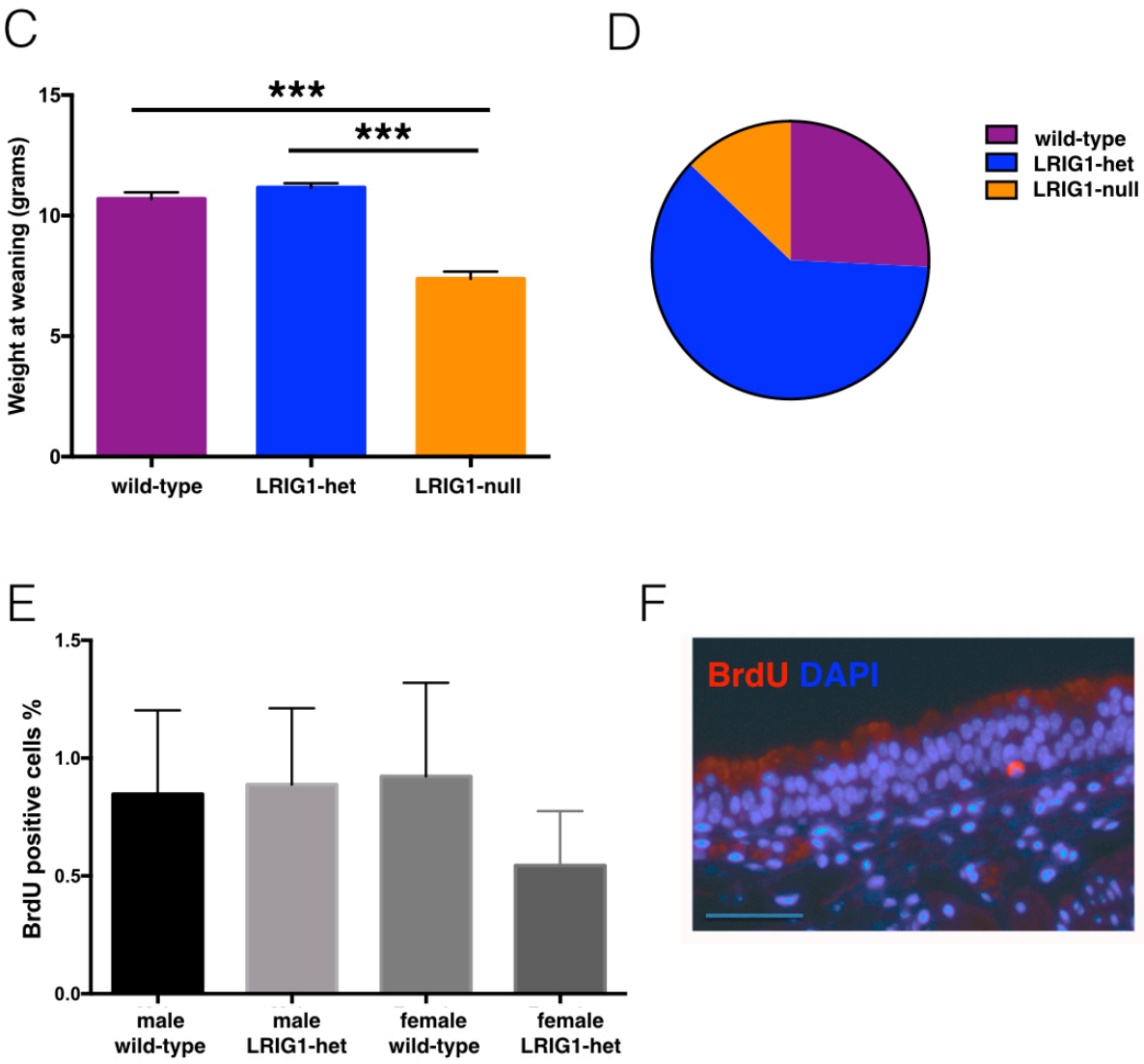

Figure 3.1: Characterisation of the *Lrig1* EGFP-ires-CreERT2 colony

A) The EGFP-ires-CreERT2 cassette situated at the start of exon 1 of *Lrig1*, placed behind the first ATG start codon. Image reproduced, with permission from reference (91). B) The breeding strategy used to produce LRIG1-null, LRIG1-heterozygous and LRIG1-wild-type mice. The initial cross involved breeding mice heterozygous for the EGFP-ires-CreERT2 cassette with wild-type FVB/N animals. The litters produced were 50% heterozygous for the EGFP-ires-CreERT2 cassette and 50% wild-type. The mice heterozygous for the EGFP-ires-CreERT2 cassette were bred with other heterozygous animals. This cross would lead to, according to Mendelian ratios: 25% LRIG1-null mice (with two copies of the EGFP-ires-CreERT2 cassette, but no LRIG1 expression), 50% LRIG1-heterozygous mice (with one copy of the EGFP-ires-CreERT2 cassette and a functional LRIG1 allele) and 25% LRIG1-wild-type mice (without a copy of the EGFP-ires-CreERT2 cassette). C) Weight at weaning (at 3 weeks) of mice in the *Lrig1* EGFP-ires-CreERT2 colony. The weight of LRIG1-null animals was significantly lower than the LRIG1-heterozygous or wild-type mice. Statistical analysis was performed using a Kruskal-Wallis test, following assessment of normality using the D'Agostino & Pearson normality test with Dunn's post- test; n= 25 – 119 mice; mean +/- SEM; *** indicates p< 0.0001. D) Proportion of animals of each genotype, n= 194. E) Assessment of the proliferation of epithelial cells, showing the percentage of BrdU-positive epithelial cells after a 6-hour chase, divided into gender and *Lrig1*-wild-type or -heterozygous genotype. Statistical analysis was performed using a Kruskal-Wallis test, with Dunn's post-test; n= 3 mice; mean +/- SEM. F) A single BrdU-positive proliferating epithelial cell (BrdU;red), DAPI (blue) used as a counterstain. Scale bar = 50 µm.

3.3.3 The establishment of a genotyping strategy for the *Lrig1* EGFP-ires-CreERT2 colony

The presence of the EGFP-ires-CreERT2 cassette was identifiable using primers to the Cre recombinase component. This allowed wild-type and LRIG1-heterozygous animals to be discriminated (Figure 3.2.A). To discriminate LRIG1-heterozygous from LRIG-null animals, a second round of genotyping was necessary and new primers were designed. The EGFP-ires-CreERT2 cassette is situated at the ATG start codon of the first exon of *Lrig1*, so using the Primer3 design tool, primers were designed around the native *Lrig1* gene. LRIG1-heterozygous animals have one normal *Lrig1* allele and therefore a PCR product would be detectable on a gel, whereas the LRIG1-null animals, without a normal *Lrig1* allele, would be negative for this PCR product. The final genotyping strategy therefore required two steps: the first to identify wild-type mice and the second to distinguish LRIG1-heterozygous from LRIG1-null mice (Figure 3.2.B).

Initially, three sets of forward and reverse primers were designed. These all encompassed the native *Lrig1* allele. The sequences were designed to overlap at the point where the EGFP-ires-CreERT2 cassette was inserted in the native allele, meaning a product would only be detectable if the native allele was present. Each primer was trialled on the extracted DNA of two LRIG1-heterozygous mice and the PCR products were run on an agarose gel. However, each of the product bands were poorly defined (Figure 3.2.C). In the first Cre PCR reaction, the extracted ear snip DNA was used directly, and a clear, well-defined band was seen in the agarose gel (Figure 3.2.A). However, when the ill-defined bands were seen in the second reaction, the DNA purity was assessed using a Nanodrop. This measurement implied the DNA contained impurities, therefore any contaminating salts were removed using the ethanol precipitation method. The initial Cre PCR reaction may have been successful due to the strength of primer binding to the DNA, however, the second PCR reaction involved amplifying a region of DNA that was 'GC rich' (made up of 75% G or C bases). A GC-rich area affects the ability of the primers to anneal, so in combination with impurities in the DNA, may have led to the ill-defined bands. By

removing the impurities through ethanol precipitation and adjusting the PCR mastermix to one suitable for GC-rich areas, the PCR product became cleaner (Figure 3.2.D).

Primer B produced the cleanest product, but two bands were present in the lane. The lowest band corresponded to the predicted size of 355 bp. To ensure the primer was annealing to the correct section of DNA, sequencing of the PCR product was performed at Source Biosciences. This revealed that primer B was annealing to the correct DNA target (Figure 3.2.E). Different annealing temperatures were assessed to see if the band could become clearer and eliminate the contaminant band; 62°C was found to be most effective (Figure 3.2.F). The optimisation of the PCR reaction led to clear PCR product bands and allowed successful genotyping (Figure 3.2.G).

The accuracy of genotyping was essential to ensure the appropriate animals were used in downstream experiments. Therefore, visual genotyping was used as an additional step. eGFP, and the presence of the EGFP-ires-CreERT2 cassette, was confirmed by analysing the ear snips by immunofluorescence (Figure 3.2.H). The low weaning weights of the LRIG1-null mice supported the PCR confirmation of genotype.

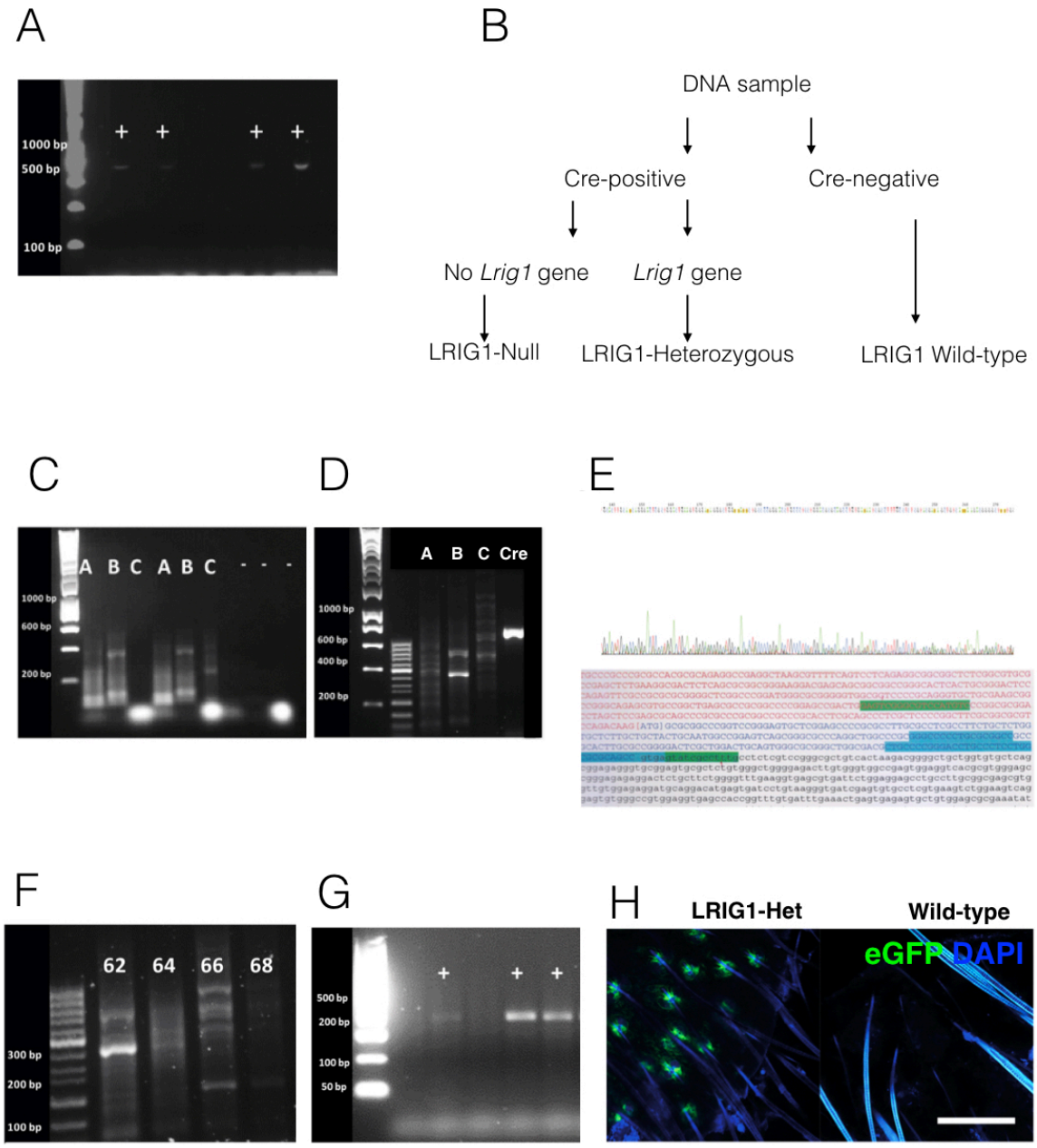

Figure 3.2: Genotyping the *Lrig1* EGFP-ires-CreERT2 colony

A) Agarose gel demonstrating the presence of the Cre protein in *Lrig1* EGFP-ires-CreERT2 heterozygous animals. The PCR product is visible at 700 bp in animals containing the *Lrig1* EGFP-ires-CreERT2 cassette. B) Genotyping strategy to distinguish wild-type, LRIG1-heterozygous and LRIG1-null animals. If the Cre insert is present, a second PCR reaction is necessary to distinguish LRIG1-heterozygous from LRIG1-null mice. C) Initial genotyping using the designed primers A, B and C. DNA from two mice was used for analysis. Negative controls were used for each of the three primers. Note multiple bands in each of the lanes. D) Optimisation of primers using the improved quality DNA. Clearer bands were seen when using primers B and primer C. The Cre primers were used as a positive control to ensure the DNA was of high quality. E) Sequencing results from Source Biosciences. Top graph shows transcript obtained. The bottom diagram indicates correspondence of the sequence with the expected DNA transcript. Green highlighting indicates primer B forward and reverse. The [ATG] start codon of *Lrig1* exon 1 is indicated. The blue highlights areas of matching of the sequenced product to the expected transcript. This shows the LRIG1 primers anneal to the anticipated part of the transcript. F) Trial of annealing temperatures using primer B. The clearest PCR product band is seen at 62°C. G) Final, optimised PCR reaction showing samples positive for the native *Lrig1*, including a positive control. H) Immunofluorescence of ear snip samples, showing endogenous eGFP expression in *Lrig1* EGFP-ires-CreERT2 animals located around the hair follicle. There is no eGFP expression in wild-type animals.

3.3.4 Confirmation that homozygosity for the *Lrig1* EGFP-ires-CreERT2 cassette correlates with loss of protein production

The use of mice with a double EGFP-ires-CreERT2 cassette (LRIG1-null animals) has not previously been reported, with heterozygous animals used for all experiments in the skin (91). It was essential to ensure that the LRIG1-null animals did not express LRIG1 protein. The insert is a knock-in behind the start codon of *Lrig1*, where the *Lrig1* DNA beyond the EGFP-ires-CreERT2 cassette remains in place. Whilst it is unlikely that functional LRIG1 is produced, given both a probable frame-shift following the insertion and that the LRIG1-null animals have a subtle phenotype (lower weaning weight), confirmation of loss of LRIG1 protein production through Western blotting was necessary.

The highest LRIG1 protein expression in humans is seen in the cerebellum (181) and in the mouse significant *LRIG1* mRNA levels are seen in the brain (182). Therefore, cerebella were collected from 6 animals; 2 wild-type, 2 LRIG1-heterozygous and 2 LRIG1-null mice and protein extracted. Western blotting demonstrated LRIG1 protein expression in the wild-type mice, a reduction in the heterozygous mice and a complete absence in the LRIG1-null mice (Figure 3.3.A).

3.3.5 Correlation of eGFP with LRIG1 expression

The *Lrig1* EGFP-ires-CreERT2 mice express eGFP following activation of the *Lrig1* promoter, therefore, in heterozygous animals, eGFP expression should co-localise to that of native LRIG1 expression. This has previously been shown in the skin of *Lrig1* EGFP-ires-CreERT2 animals (91), but to confirm this finding in the airway, tracheas from LRIG1-heterozygous animals were stained for both LRIG1 and eGFP.

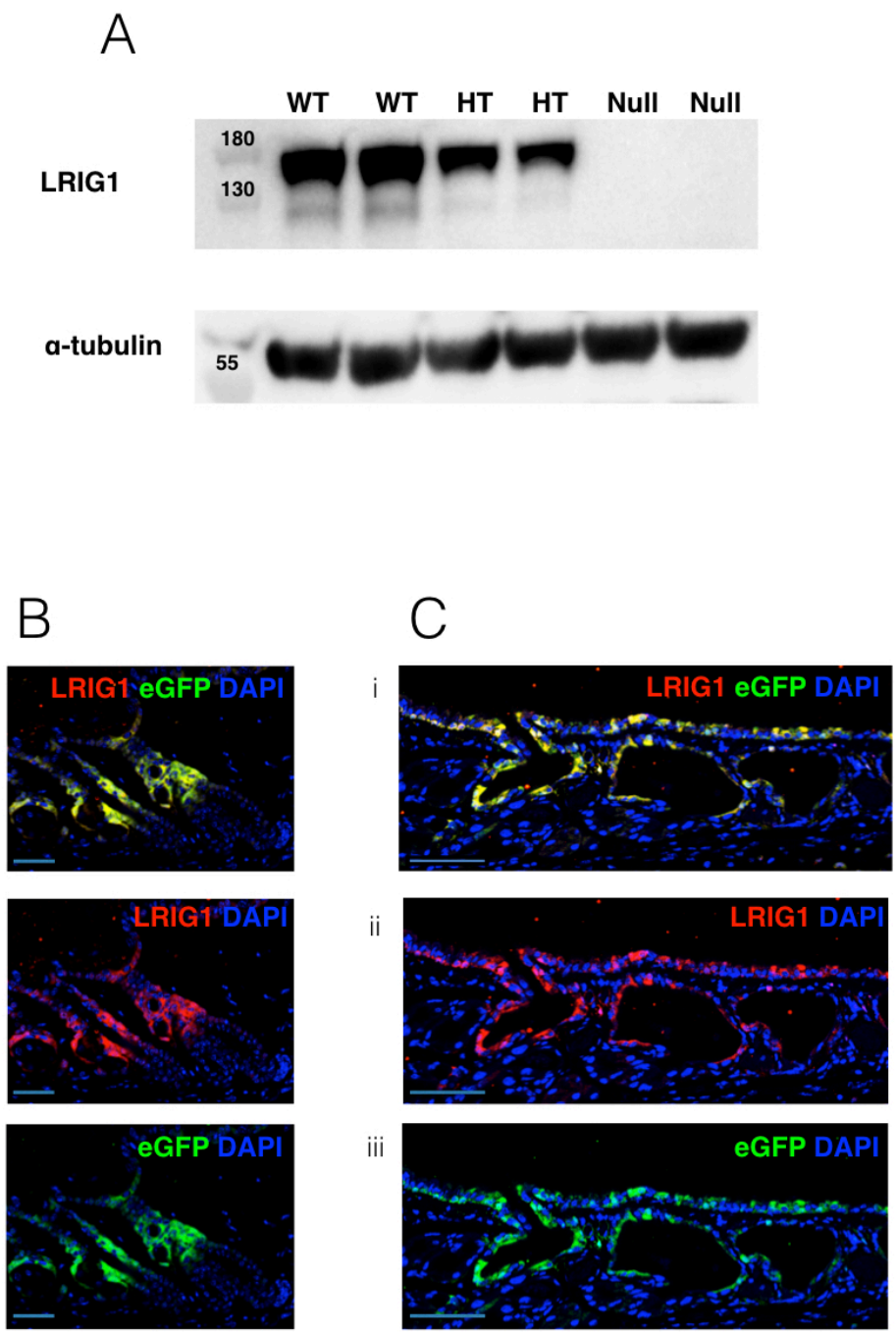

Figure 3.3: Confirmation of absence of LRIG1 protein in the LRIG1-null animals and correlation of eGFP with LRIG1 expression

A) Detection of LRIG1 in lysates of murine cerebella from wild-type, LRIG1-heterozygous and LRIG1-null mice. The greatest LRIG1 protein expression is seen in the wild-type animals (142 kDa); there is slightly less expression in the LRIG-heterozygous mice and a complete absence in LRIG1-null animals. α-tubulin used as a loading control (50 kDa). n= 2. B) Immunofluorescence staining of the hair follicles, which is consistent with that previously reported. Dual staining for LRIG1 (red) and eGFP (green), indicating a complete overlap between the staining of these proteins, scale bar = 50 µm, image representative of n = 3. C) Immunofluorescence staining of the trachea with dual staining for LRIG1 (red) and eGFP (green), showing correlation of LRIG1 expression to eGFP, scale bar = 50 µm, image representative of n = 3.

The expression of eGFP in the skin co-localised with that of LRIG1 (Figure 3.3.B), consistent with the previously reported study (91). When the tracheas were examined (Figure 3.3.C), there was a similar overlap between eGFP and LRIG1 expression, indicating eGFP is an appropriate reporter of LRIG1 in the airway. Of note, LRIG1 is expressed on the cell and nuclear membranes, whilst eGFP is cytoplasmic. When the staining is closely examined, the different cellular locations of the two proteins can be determined.

3.3.6 Expression of LRIG1 in the airway epithelium

In humans, loss of LRIG1 is an early event in the development of preinvasive lung cancer (104). These preinvasive lesions occur in the trachea and upper airways, where the airway basal cells are situated. In the mouse, airway basal cells are restricted to the trachea and first division of right and left main bronchi. To understand the expression of LRIG1 in the mouse airways and to be able to relate this to the human airway, tracheas were isolated from LRIG1-heterozygous mice and were stained for eGFP in combination with keratin 5 (KRT5) to identify basal cells, forkhead box J1 (FOXJ1) to identify ciliated cells, and mucin 5AC (MUC5AC) to mark goblet cells.

LRIG1 expression was confirmed across all epithelial cell populations (Figure 3.4.A-D). This contrasts to the findings in the skin and the gut where there is a clear association with the stem cell compartments (91, 93). Beneath the basement membrane eGFP staining is seen both in the cartilage rings and some stromal cells (Figure 3.4.C, arrowed). LRIG1 expression in the skin is concentrated within the sebaceous glands of the epidermis (91), however, within the tracheal submucosal glands (where the basal cells are concentrated) an increased eGFP expression is not visualised compared to the rest of the epithelium (Figure 3.4.B).

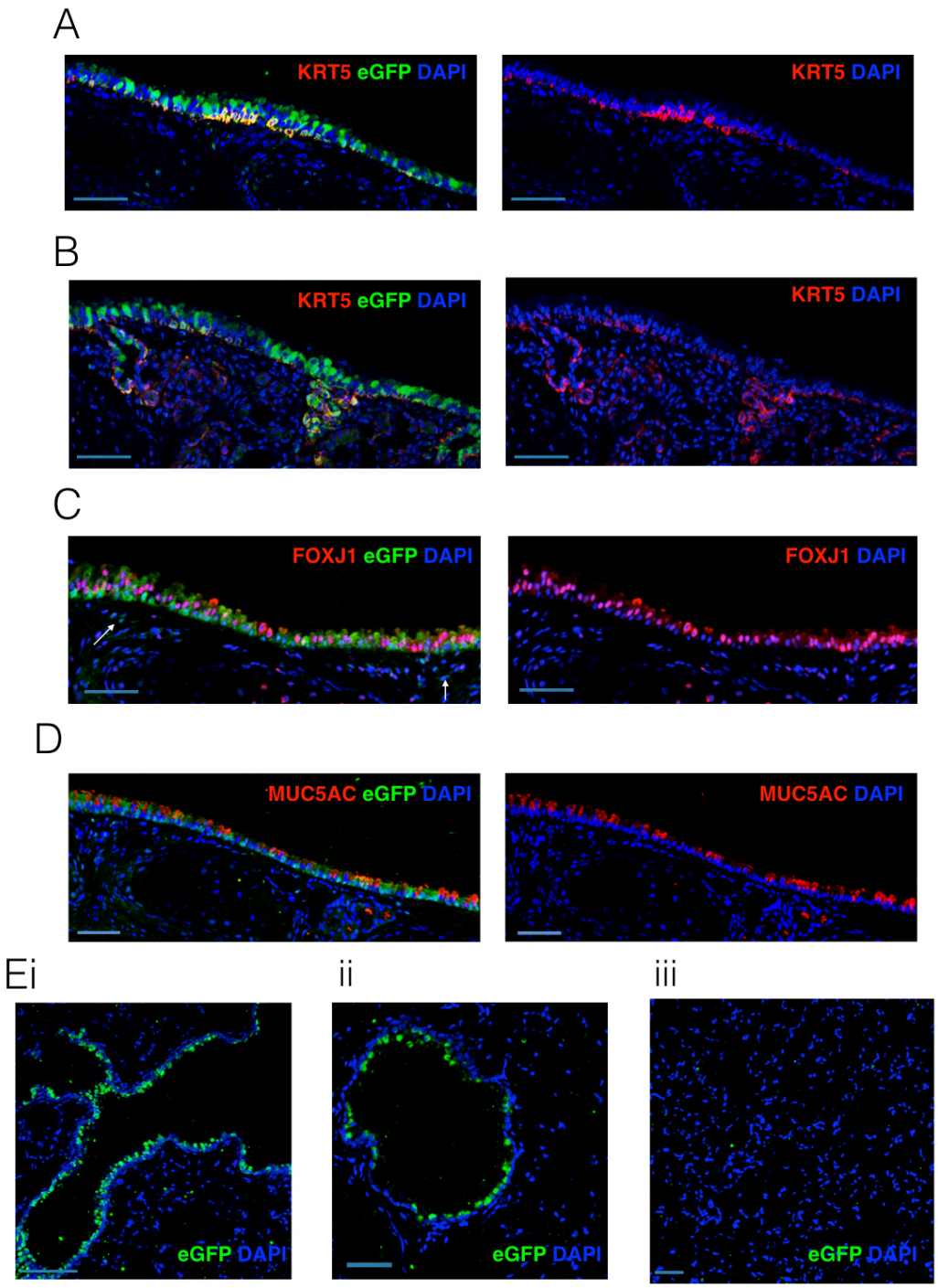

Figure 3.4: Coexpression of LRIG1 with other airway epithelial markers and LRIG1 in the distal airway

A) Immunofluorescence staining of the tracheal epithelium for eGFP (green) and KRT5 (red). DAPI used as a counterstain. Scale bar = 50 µm, image representative of n = 3. B) Immunofluorescence staining for eGFP (green) and keratin 5 (KRT5; red) within the submucosal glands. DAPI used as counterstain. Scale bar = 50 µm, image representative of n = 3. C) Immunofluorescence staining showing coexpression of eGFP (green) with forkhead box J1 (FOXJ1; red), a marker of ciliated epithelial cells. Arrows indicate eGFP-stained stromal cells. DAPI used as a counterstain. Scale bar = 50 µm, image representative of n = 3. D) Immunofluorescence staining of the tracheal epithelium for eGFP (green) and mucin 5AC (MUC5AC; red). DAPI used as a counterstain. Scale bar = 50 µm, image representative of n = 3. E) Immunofluorescence staining of eGFP (green) in the distal airway showing (in i and ii),eGFP expression in the distal bronchioles, indicating the expression of LRIG1 in the distal airway, but no eGFP is in the distal lung parenchyma. Staining performed in LRIG1-heterozygous mice (iii). Scale bar = 50 µm, image representative of n =3.

To establish the expression of LRIG1 in the distal airways, sections including both the bronchioles and alveolar epithelium, were stained for eGFP. LRIG1 was seen throughout the distal airway, located within the bronchiolar epithelium (Figure 3.4.Ei). The staining appeared homogeneous and was not increased at the bronchoalveolar duct junctions, which would suggest a concentration of expression within this stem cell compartment. There was no LRIG1 staining within the lung parenchyma (Figure 3.4.Eii).

3.3.7 Effect of loss of LRIG1 on the airway epithelium

To examine the effects of loss of LRIG1 on the airway epithelium, tracheas from LRIG1-null and LRIG1-heterozygous animals were compared. The loss of LRIG1 has been shown to cause the hyperproliferation phenotype through an increase in EGFR signalling. This has been previously shown in the airway epithelium where *Lrig1*-knockout mice have increased epithelial staining for phosho-EGFR, compared to wild-type controls (104). On repeat of the phospho-EGFR staining, the staining was variable across the length of the epithelium, but collectively there was no difference seen between the phospho-EGFR staining of LRIG1-heterozygous and LRIG1-null animals (Figure 3.5.A). The intensity of EGFR staining was greater in the LRIG1-null animals, indicating that absence of LRIG1 may lead to an upregulation in the density of EGF receptors.

LRIG1-null mice have been shown to have increased airway epithelial thickness compared to LRIG1-heterozygous controls, with an increased proliferation seen on Ki67 staining (104). An increase in epithelial depth was confirmed in the *Lrig1* EGFP-ires-CreERT2 mice where heterozygous animals had a mean epithelial depth of 21.71 µm compared to 27.86 µm in the LRIG1-null animals (Figure 3.5.B).

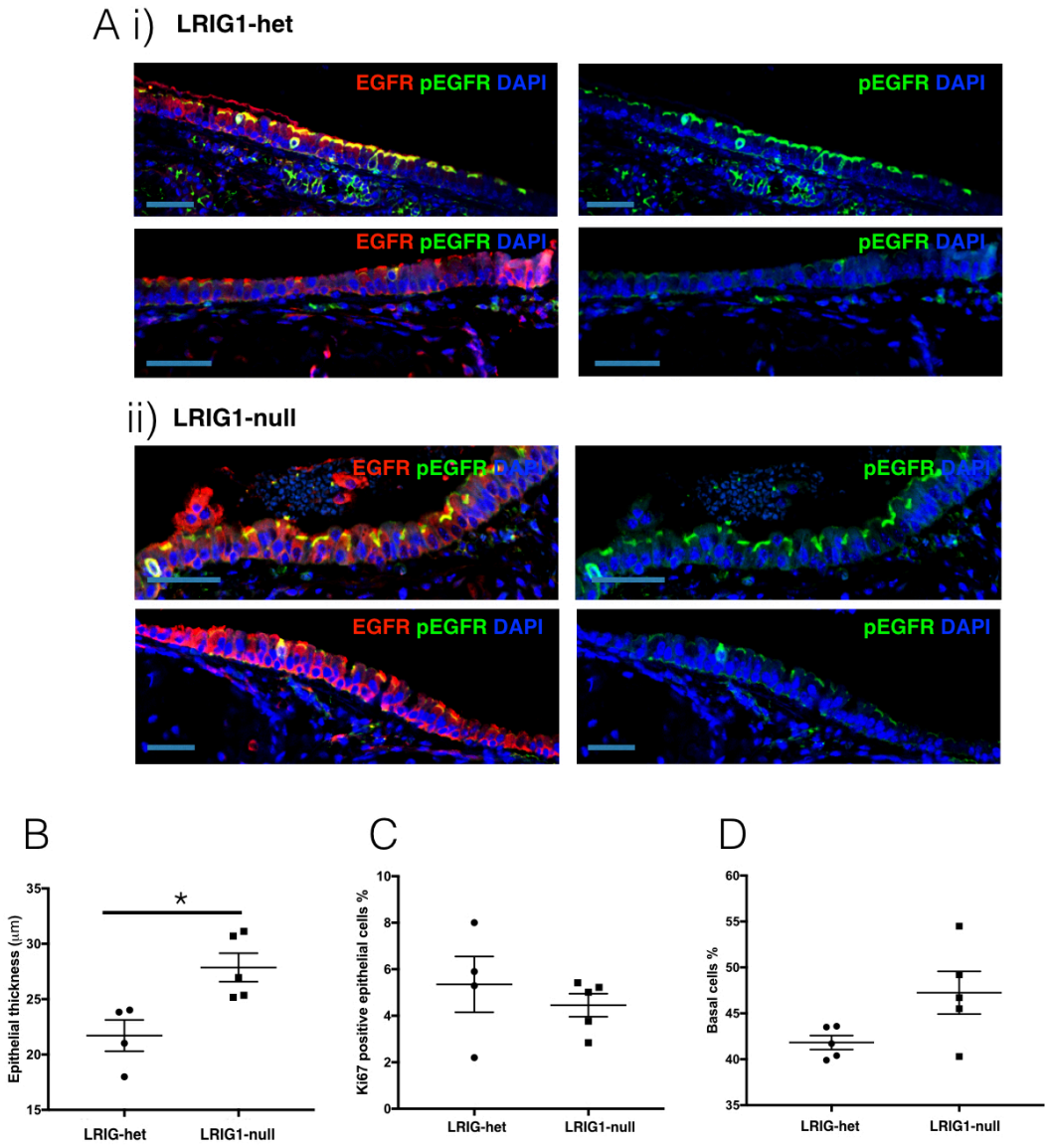

Figure 3.5: Comparison of tracheal epithelium between LRIG-heterozygous and LRIG1-null mice

A) Immunofluorescence staining of murine tracheal epithelium for phospho-EGFR (green) and EGFR (red). DAPI used as a counterstain, i) shows images from two LRIG1-heterozygous tracheas and ii) shows images from two LRIG1-null. Scale bar = 50 µm, images representative of n = 3. B) The comparison of epithelial thickness between LRIG1-heterozygous and LRIG1-null mice. Statistical analysis performed using the unpaired t-test; n= 4-5; * indicates $p<0.05$; mean ± SEM. C) The percentage of the epithelium consisting of $KRT5^{+}$ basal cells in LRIG1-heterozygous and LRIG1-null animals. Statistical analysis performed using the unpaired t-test; n= 4-5; mean ± SEM. D) The percentage of $Ki67^{+}$, proliferating cells within the tracheal epithelium of LRIG1-heterozygous and LRIG1-null mice. Statistical analysis performed using the unpaired t-test; n= 4-5; mean ± SEM.

The increase in epithelial depth in the previous study was attributed to increased proliferation (104), but here there was no difference in the number of Ki67-positive cells in the airways of LRIG1-heterozygous and LRIG1-null animals (Figure 3.5.C). There was, however, a large spread of proliferation rates within the heterozygous animals that ranged from 2.2% to 8.0%, which may indicate a number of outliers.

An increase in the size of the stem cell compartment has been detected in the gut of *Lrig*-knockout mice. To assess whether there was an effect of LRIG1 loss on the stem cell compartment of the murine trachea, the proportion of KRT5-positive basal cells was counted in LRIG1-heterozygous and LRIG1-null mice (Figure 3.5.D). Although no statistically significant differences were seen, there was a trend towards an increased proportion of KRT5-positive basal cells in the tracheas of LRIG1-null animals (with p=0.0576) compared to the LRIG1-heterozygous mice.

3.3.8 Isolation of airway epithelial cells

As LRIG1 is expressed across the tracheal epithelium, to understand how loss of LRIG1 influences the development of preinvasive lung cancer, I needed to compare LRIG1-expressing epithelial cells (from heterozygous mice) to cells where LRIG1 is absent (in LRIG1-null mice). The murine epithelium contains a heterogeneous cell population, including basal, ciliated and secretory cells. To allow a direct cell comparison, and to avoid confounding from multiple cell populations, I needed to compare cells of the same type. Basal cells are the putative cell of origin of squamous cell lung cancer (128) and the earliest indication of preinvasive disease is basal cell hyperplasia (36). Therefore, any changes associated with development of preinvasive squamous cell lesions are likely to occur in the basal cells, so a flow cytometry strategy was devised to identify and isolate this population. This would allow a defined population of $eGFP^+$ LRIG1-expressing basal cells from LRIG1-heterozygous mice to be compared to $eGFP^+$, but LRIG1-negative, basal cells from LRIG1-null mice (cells that should have expressed LRIG1, but where the active gene has been disrupted, and that are $eGFP^+$ due to the activation of the *Lrig1* promoter).

To allow their use in *in vitro* cell culture comparison studies, it was important that the airway basal cells remained viable, so a strategy using extracellular markers was employed. A staining strategy was devised that involved the negative selection of $CD31^{+}CD45^{+}$ cells, eliminating the endothelial and haematopoietic populations, respectively, and then positively selecting for either $EpCAM^{+}$ or integrin $\alpha6^{+}$ and then using *Griffonia Simplicifolia* isolectin $(GS\text{-}IB4)^{+}$ to identify basal cells (Figure 3.6.A). The expression of eGFP could later be used to collect $LRIG1^{+}$ and $LRIG1^{-}$ basal cell populations. Lectins are specific carbohydrate-binding proteins found on the cell surface and, although identification occurs through protein binding rather than epitope/antibody interactions, GS-IB4 can be used to identify airway basal cells (133, 183-185). The specificity of GS-IB4 for airway basal cells was confirmed by assessing its binding in association with $KRT5^{+}$ cells in the tracheal epithelium (Figure 3.6.B). This showed that all $KRT5^{+}$ basal cells were stained with GS-IB4 and that it was a suitable marker to use. A few cells beneath the basement membrane were positive for GS-IB4, but these would be excluded by positive selection for the $EpCAM^{+}$ or integrin $\alpha6^{+}$ epithelial populations (which would not be found on these cells).

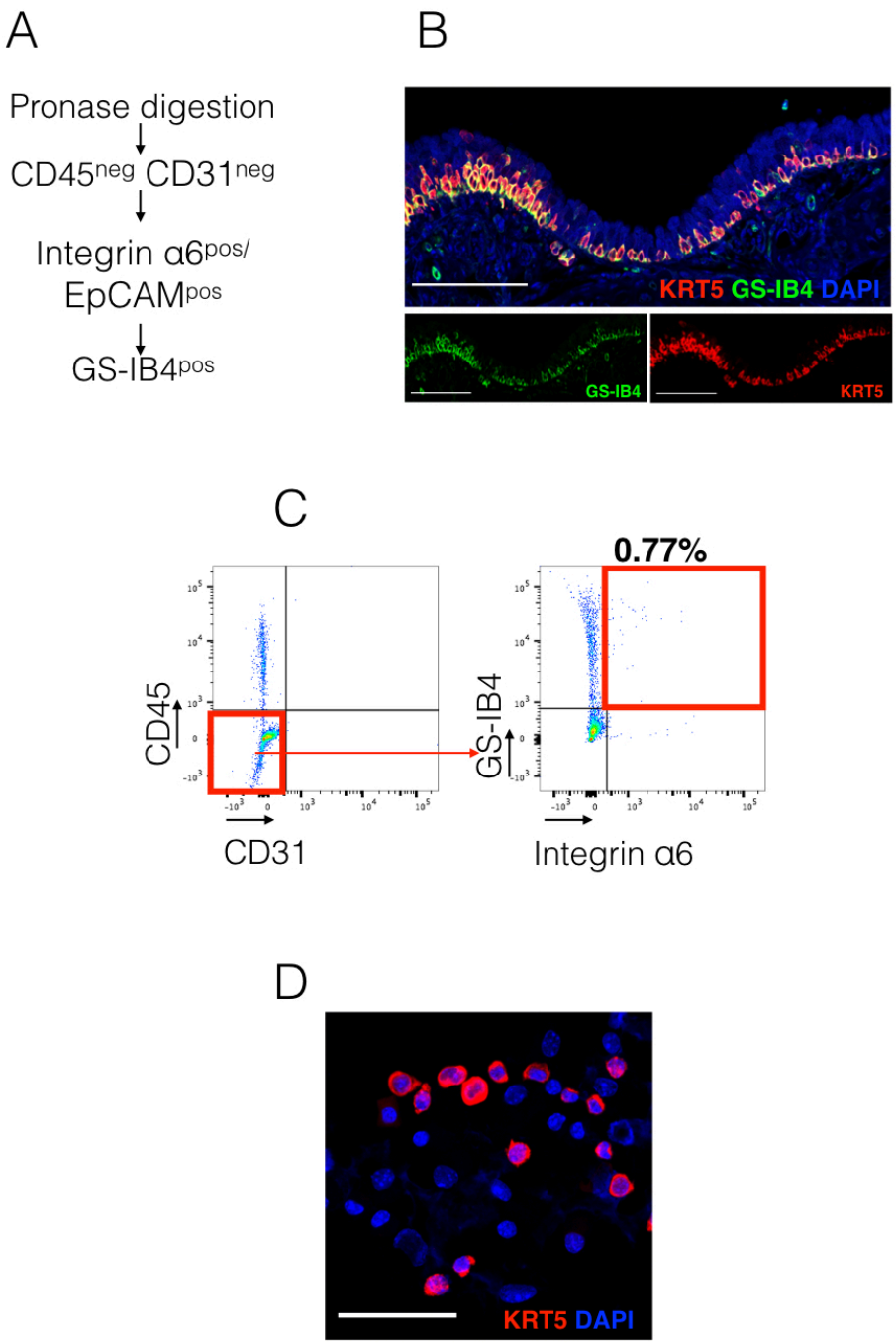

Figure 3.6: Isolation of basal cells from the tracheal epithelium

A) Sorting strategy to obtain a pure, viable population of airway basal cells. B) Immunofluorescence staining of murine trachea for *Griffonia Simplicifolia* isolectin B4 (GS-IB4; green) and keratin 5 (KRT5; red), showing staining of the same epithelial populations and the suitability of GS-IB4 as a basal cell marker. Scale bar = 100 µm. C) Flow cytometric analysis of the cell populations obtained following pronase digestion of the murine airway. Red boxes indicate the populations of interest, while red arrows show the population taken forward. Antibodies were used in the following colours: CD31-PECy7, CD45-PE, GS-IB4-qdot 605, and Integrin α6-APC. D) Immunofluorescence staining for KRT5 in murine airway epithelial cells following pronase digestion, in a cytospun sample. Scale bar = 50 µm.

3.3.9 Pronase digestion of the tracheal epithelium

The enzyme pronase has been traditionally used for creating a single cell suspension of tracheal epithelial cells for use in cell culture or downstream applications (170, 186-188). When using pronase, a single trachea is expected to yield around 2.5 x 10^5 tracheal epithelial cells (189) and basal cells constitute 30% of airway epithelial cells (130). However, when using flow cytometry to identify the basal cell population from pronase-digested tracheas, the basal cell fraction was extremely low. After excluding the immune and endothelial cells, the proportion of basal cells was only 0.77% (Figure 3.6.C). To confirm how many basal cells would be expected in a pronase-digested cell suspension, a fresh pronase-isolated, epithelial cell sample was cytospun, fixed and stained for the intracellular basal cell marker KRT5 (Figure 3.6.D). $KRT5^+$ cells were then counted and found to constitute 40% of the cell suspension, in line with the expected yields (130). It became apparent pronase may be cleaving the epitopes required for flow cytometry analysis, meaning a reduction in overall cell yield.

3.3.10 Analysis of epitope expression following pronase digestion

To explore the effect of pronase on epitopes of interest, a cell source that did not require enzymatic digestion was necessary. Isolation of bone marrow cell populations can be obtained through simply flushing the extracted long bones of a mouse with saline (190, 191). CD31, CD45 and integrin α6 (192) are all expressed by bone marrow populations, whilst GS-IB4 binds to antigens on bone marrow endothelial cells (193) and macrophages (194). EpCAM is an epithelial cell marker and is not detectable in any bone marrow cell population. For this reason, the effects of pronase on the EpCAM epitope were not assessed.

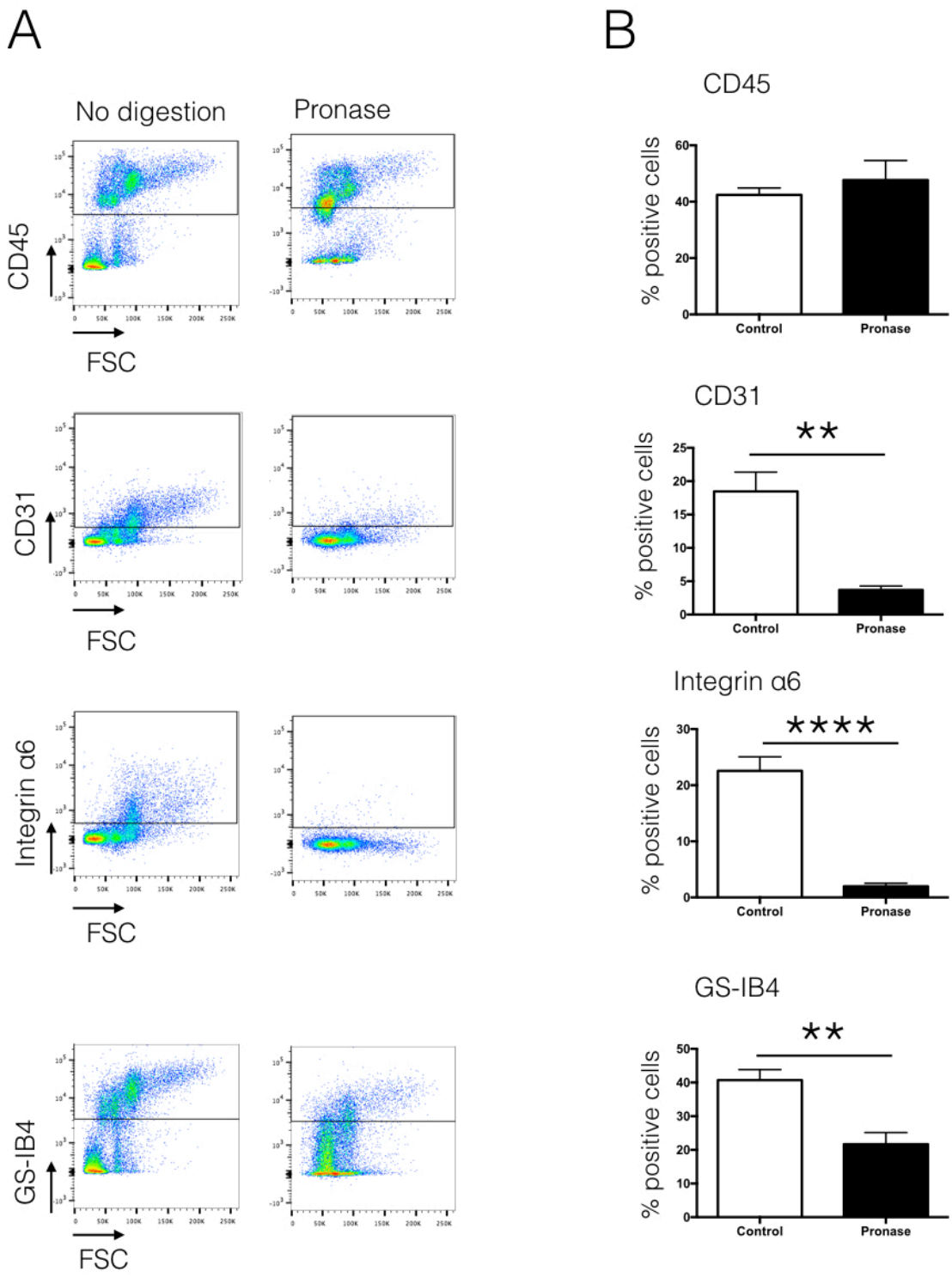

Figure 3.7: Investigation of epitope cleavage in bone marrow cells

A) Flow cytometry plots showing a reduction in cells following pronase digestion of bone marrow cells. Antibodies were used in the following colours: CD31-PECy7, CD45-PE, GS-IB4-qdot 605, and Integrin α6-APC. B) Quantification of the proportion of bone marrow cells expressing epitopes of interest with or without pronase digestion in flow cytometry experiments (n = 6 for CD45, integrin α6 and GS-IB4, and n = 3 for CD31). Statistical analysis performed using the unpaired t-test; ** $p < 0.01$, **** $p < 0.0001$; mean ± SEM.

Bone marrow cells were isolated, treated overnight in 0.15% pronase (as per the tracheal samples), or were left in serum-free medium as a control and then stained the following morning for flow cytometry. These results showed CD45 was resistant to the effects of pronase; however, following pronase incubation, CD31, integrin α6 and GS-IB4 expression were significantly reduced compared to the undigested controls (Figures 3.7.A and 3.7.B). These results imply that pronase cleaves either the epitopes or protein-binding sites (of GS-IB4) and may explain the lower than expected population of basal cells detected by flow cytometry (Figure 3.6.C).

3.3.11 Alternative methods of epithelial digestion

As pronase digestion was unsuitable to identify a basal cell population by flow cytometry, alternative strategies were explored. A simple collagenase digestion, where entire rat tracheas were minced prior to collagenase incubation (195), and a more complex dispase/DNase/trypsin method (166, 167) used in mice and human airways were identified from the literature. The dispase/DNase/trypsin method involved using dispase and DNase to detach sheets of epithelium from the underlying stroma and then incubating these sheets with trypsin to create a single cell suspension. However, when trialling the dispase/DNase/trypsin method, the epithelium failed to detach in complete sheets and I became concerned there were still basal cells attached to the underlying stroma. I was further concerned that the basal cells buried deep within the crypts of the trachea may also not be removed with the epithelial sheets. To ensure all basal cells were being collected, after the removal of the epithelial sheets the remaining tracheal pieces were incubated in collagenase. It was intended that the collagenase would break down the stroma and release any basal cells within the crypts together with any remaining cells that failed to detach when the epithelial sheets were removed.

In total, 3 methods were compared. These were the collagenase method, the reported dispase/DNase/trypsin method, and the dispase/DNase/trypsin method followed by collagenase digestion of the remaining tracheal pieces. Each of these

methods was compared to the initial pronase digestion. The amount of cell death, the total number of cells and the total number of basal cells obtained per trachea was considered.

The greatest cell death occurred following the collagenase digestion (Figure 3.8.B). This was possibly related to the incubation time needed to ensure that the tissue had sufficiently broken down into a single cell suspension (195). Using pronase or the dispase/DNase/trypsin/collagenase method led to the greatest number of viable cells, however, pronase digestion yielded the lowest number of basal cells (Figure 3.8.A and 3.8.B). The low yield of basal cells following pronase digestion is likely to be caused by epitope cleavage, meaning that although present, the basal cells cannot be identified. The highest number of basal cells was obtained using the dipase/DNase/trypsin/collagenase method (Figure 3.8.B). This method produced an average of 19,021 cells per trachea, compared to 442 cells following pronase digestion. Adding collagenase to digest the remaining tracheal pieces was of benefit (Figure 3.8.C), with a clear basal cell population identifiable by flow cytometry and the basal cell yield increasing by as much as 3 fold (an increase in the average number of basal cells from 6,274 to 19,021 cells per trachea).

Method	Number of cells
Pronase	442
Collagenase	7,495
Dispase/DNase/Trypsin	6,274
Dispase/ DNase/ Trypsin/ Collagenase	19,021

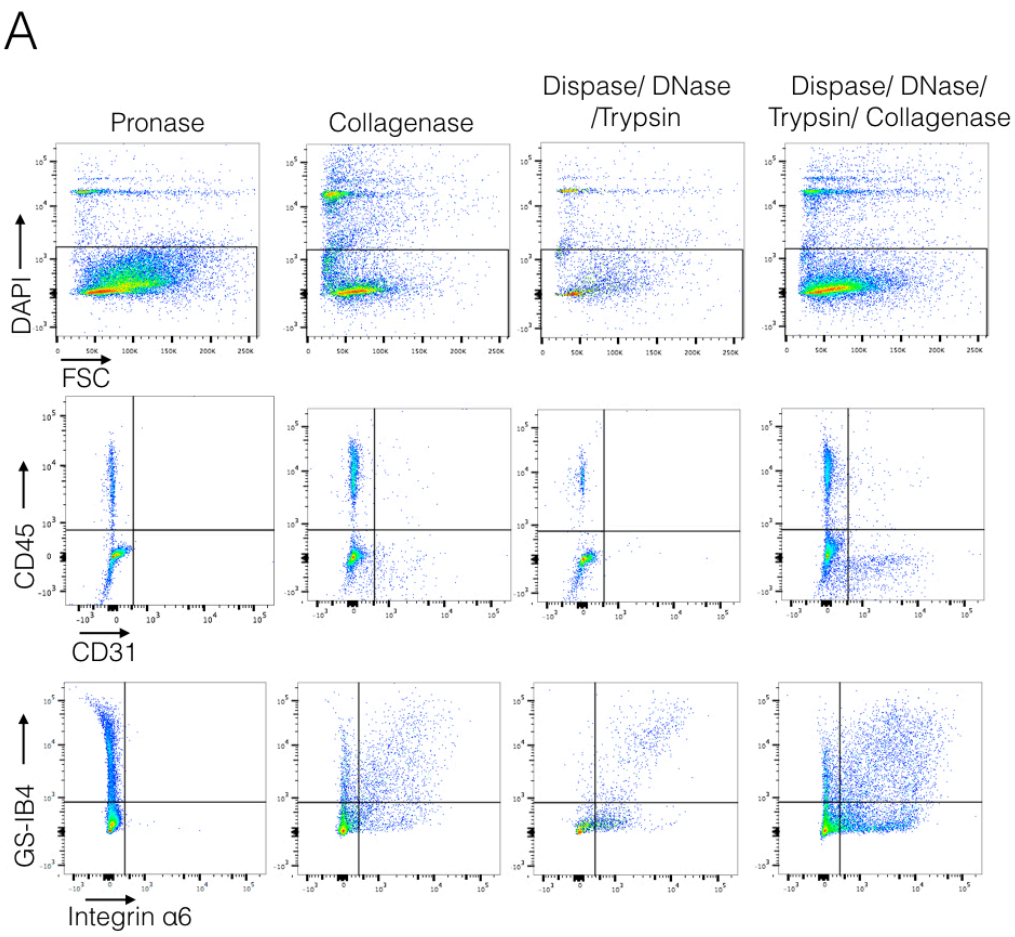

Figure 3.8: Comparison of digestion methods to obtain basal cells from the murine tracheal epithelium

A) Flow cytometric comparison of digestion strategies (pronase, collagenase, dispase/DNase/trypsin and dispase/DNase/trypsin/collagenase) for murine airway basal cell isolation. Living cells were analysed by selection of the $DAPI^-$ population (upper panel), non-endothelial and non-haematopoietic cells were selected by their lack of expression of CD31 and CD45, respectively (middle panel), and basal epithelial cells were analysed by their expression of both integrin α6 and GS-IB4 (bottom panel). Antibodies were used in the following colours: CD31-PECy7, CD45-PE, GS-IB4-qdot 605, and integrin–α6-APC. B) Quantification of cell death, the total number of living cells and the total number of basal epithelial cells obtained per trachea, using each digestion strategy (n=6). Each digestion strategy was compared to pronase digestion. Statistical analysis was performed by ordinary one-way ANOVA, with Dunnett's multiple comparison test; * $p<0.05$, ** $p<0.01$, **** $p<0.0001$; mean +/- SEM. C) Flow cytometry plots to identify the additional basal cell population obtained by digestion of the remaining tracheal pieces. n = 6.

Figure continued over page.

B

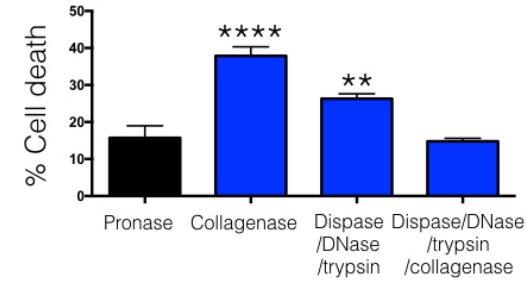
% Cell death
50
40
30
20
10
0
****
**
Pronase
Collagenase
Dispase /DNase /trypsin
Dispase/DNase /trypsin /collagenase

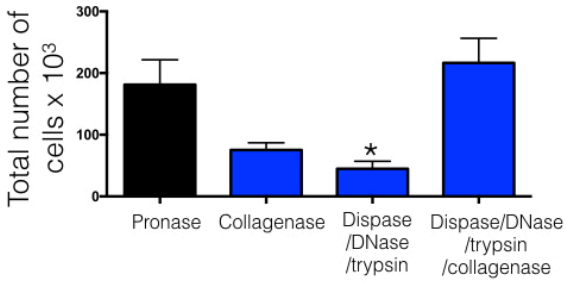
Total number of cells x 10³
300
200
100
0
*
Pronase
Collagenase
Dispase /DNase /trypsin
Dispase/DNase /trypsin /collagenase

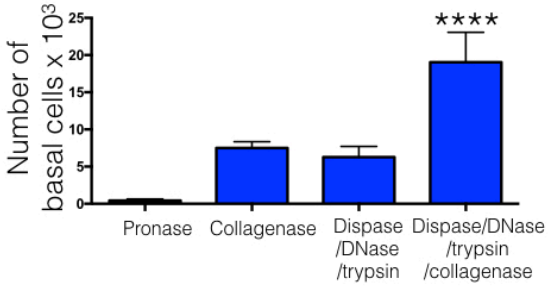
Number of basal cells x 10³
25
20
15
10
5
0
****
Pronase
Collagenase
Dispase /DNase /trypsin
Dispase/DNase /trypsin /collagenase

C

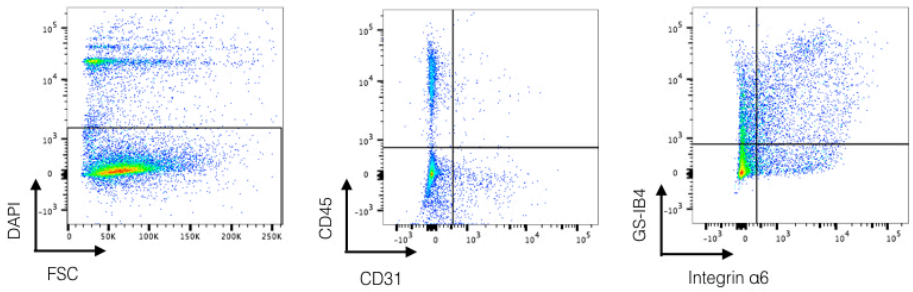
DAPI
FSC
CD45
CD31
GS-IB4
Integrin α6

3.3.11 Assessment of growth and differentiation potential of isolated murine basal cells

To ensure that the FACS-sorted basal cells retained their growth and differentiation potential (after the digestion and sorting steps), the cells were used in 2D and 3D cell culture assays. Basal cells were directly used in a tracheosphere assay where the tracheospheres hollowed and then differentiated over a 3-week period (Figure 3.9.A). Differentiation was confirmed by immunofluorescence staining for MUC5B (secretory cells) and acetylated tubulin (ACT, ciliated cells) (Figure 3.9.B).

There are limited reports of 2D murine airway basal cell culture (196-198). Most methods relate to the use of the air-liquid interface model in which basal cells are obtained directly from a mouse, without cell sorting or *in vitro* expansion. There are few reports of cultured basal cells being passaged successfully, with those that are grown in 2D culture losing the ability to differentiate (196). To assess whether the isolated basal cells could be grown *in vitro* and used in subsequent colony-forming assays (Chapter 4), the basal cells were co-cultured on mitomycin C-inactivated 3T3-J2 feeder layers in mouse tracheal epithelial cell (MTEC) medium (170). Colonies were noted to appear after 7-10 days (Figure 3.9.C).

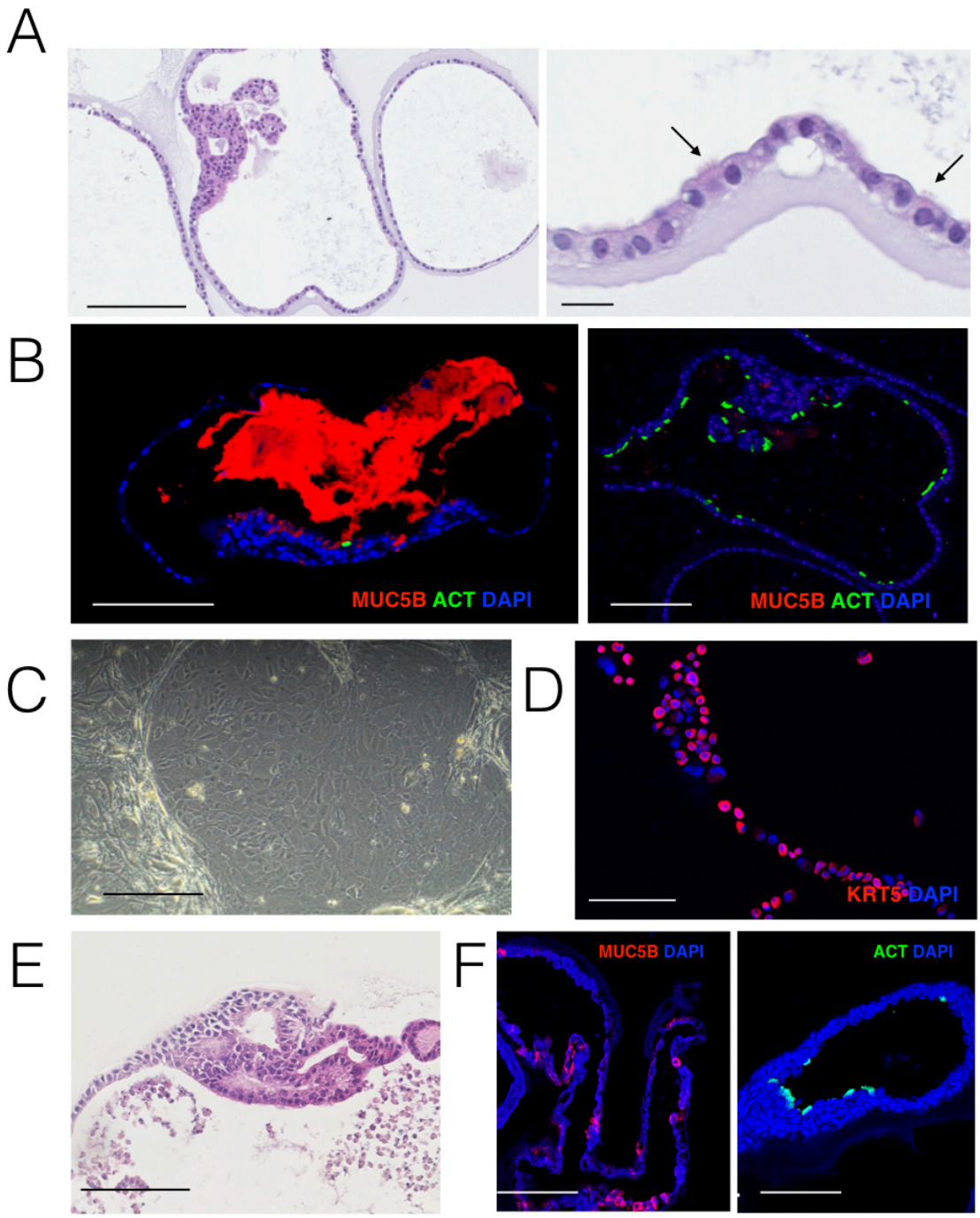

Figure 3.9: Expansion of murine basal epithelial cells in culture following dispase/DNase/trypsin/collagenase digestion and fluorescence-activated cell sorting

A) Haematoxylin and eosin (H&E) staining of fluorescence-activated cell-sorted murine basal cells grown in a 3D tracheosphere assay, showing evidence of differentiation and cilia formation (arrows). Scale bars = 100 µm and 20 µm. B) Immunofluorescence staining of mucosecretory (MUC5B; red; left) and ciliated (ACT; green; right) cells in 3D tracheospheres. Scale bars = 100 µm. C) Brightfield microscopy shows a colony of murine epithelial cells expanded on a 3T3-J2 feeder layer. Scale bar = 100 µm. D) Immunofluorescence staining of cytospun cultured murine epithelial cells following differential trypsinisation to remove 3T3-J2 cells, cultured epithelial cells are keratin 5-positive (KRT5; red) basal cells. Scale bar = 100 µm. E) H&E staining of passaged murine basal cells grown in a 3D tracheosphere assay. Scale bar = 100 µm. F) Immunofluorescence staining of mucosecretory (MUC5B; red; left) and ciliated (ACT; green; right) cells in 3D tracheospheres generated from passage 5 cultured murine basal cells. DAPI used as counterstain. Scale bars = 100 µm.

As the sorted epithelial cells readily formed colonies, I assessed whether murine epithelial cells could be serially passaged and whether they could retain their differentiation capacity following culture on mitomycin C-inactivated 3T3-J2 feeder layers. I performed initial experiments using FACS-sorted epithelial cells and, although I found that these formed small colonies (as in the colony-forming assays), they then failed to develop into confluent monolayers. As the cell number following FACS sorting was low, to assess whether it was possible to culture mouse basal cells *in vivo*, I increased the seeding density by using pronase-digested epithelial cells and plated these directly, without cell sorting, onto 3T3-J2 feeder layers. Colonies appeared after a few days and differential trypsinisation (171) allowed the epithelial cells to be separated from the supporting 3T3-J2 feeder cells. The basal cell phenotype of the growing colonies was confirmed by the expression of KRT5 on cell cytospin (Figure 3.9.D). Cells were passaged at a 1:5 ratio and, at passage 5, were used in tracheosphere assays. Mucociliary differentiation of these tracheospheres was confirmed through the expression of MUC5B and ACT (Figures 3.9.E and 3.9.F).

3.3.12 Assessment of LRIG1 expression in airway epithelial cells

Having optimised a strategy for the isolation of airway basal cells, the expression of eGFP as a reporter for LRIG1 in this population could also be established. eGFP-positive epithelial cells were seen on a cytospin following pronase digestion (Figure 3.10.A) and flow cytometry confirmed that LRIG1 (through the constitutive presence of eGFP) could be identified in the basal cell population (Figure 3.10.B). Of note, as eGFP is not an extracellular marker, and is resistant to trypsin and pronase (199), there was no effect of enzymatic digestion on its expression. The proportion of $eGFP^+$ cells seen by flow cytometry mirrored that seen by immunofluorescence (Figure 3.5).

Although $eGFP^+$ basal cells were detectable in LRIG1-heterozygous mice using flow cytometry, a significant percentage of these were $eGFP^-$, and hence LRIG1-negative, with LRIG1-expressing basal cells making up only 50% of the total basal cell

population (Figure 3.10.C). This was also the case in LRIG1-null animals, where eGFP$^+$ (cells where the *Lrig1* promoter is active, although with no active LRIG1 expression) and eGFP$^-$ populations were detectable.

Using immunofluorescence, LRIG1 was identified in other epithelial cell populations: in both secretory and ciliated cells. To confirm this finding by flow cytometry, the eGFP$^+$ epithelial population was identified and the component cell types analysed. Of the eGFP$^+$ cells, basal cells constitute 20%, CD24-positive (ciliated cells) make up 50% and there is a smaller, SSEA1-positive (secretory cell) population (Figures 3.10.D and 3.10.E).

The highest expression of LRIG1 may be expected in the cells that are the most 'stem like'. In the skin, LRIG1 is expressed across all epithelial cell populations, but is at the highest concentration in the cells that express other stem cell markers (90). To identify whether LRIG1 expression was highest in basal cells, only the most eGFP$^+$ cells were analysed (Figure 3.10.F). If LRIG1 was most concentrated in the basal cells, when taking the top 25% of eGFP$^+$ cells there would be an enrichment of basal cells. However, the proportion of eGFP$^+$ cell types did not change across any of the groups, including in the basal cells. This indicates that the level of eGFP expression (and by inference the LRIG1 expression) is similar across all epithelial populations.

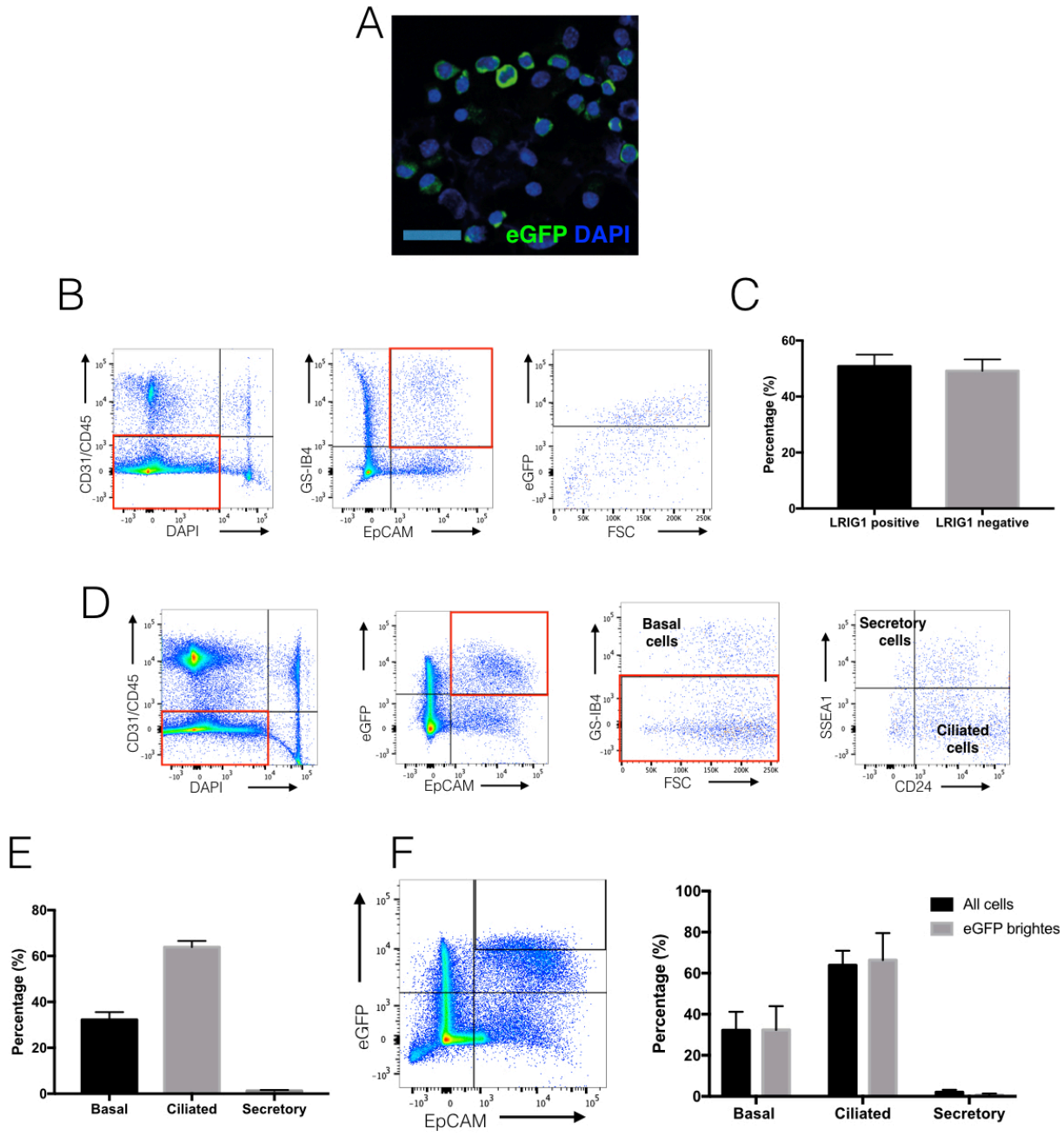

Figure 3.10: Identification of LRIG1 expression in epithelial populations by flow cytometry

A) Immunofluorescence for eGFP (green) in a cytospun sample following pronase digestion of the tracheal epithelium. DAPI used as counterstain. Scale bar = 50 µm. B) Flow cytometry plots showing the identification of a $CD31^{-}CD45^{-}DAPI^{-}$ population (shown in red; left plot), an $EpCAM^{+}GS\text{-}IB4^{+}$ population (shown in red; middle plot) and an eGFP-positive and -negative population (left plot). The red boxes indicate the population taken forwards for analysis. n= 5. C) The proportion of LRIG1-positive and -negative basal cells obtained from the tracheal epithelium. D) Flow cytometry plots showing the identification of a $CD31^{-}CD45^{-}DAPI^{-}$ population, followed by selection of an $EpCAM^{+}eGFP^{+}$ population and the identification of the proportion of GS-IB4 basal cells. Then, in the $GS\text{-}IB4^{-}$ population, the proportion of GFP-positive ciliated cells (CD24-positive) and secretory cells (SSEA1-positive), n = 5. Antibodies were used in the following colours: CD31- and CD45- PE, GS-IB4- qdot 605, EpCAM-APC, SSEA1-PerCP efluor700 and CD24-PECy7. E) Percentage of each type of epithelial cell in the tracheal epithelium that is eGFP-positive. Mean ± SEM. F) When the most eGFP positive epithelial cells are selected, there is no enrichment in the proportion of either basal, ciliated or secretory cells.

3.3.13 Lineage tracing from LRIG1-expressing basal cells

To assess whether LRIG1 labels a stem cell population in the respiratory epithelium, a lineage-tracing model was also used. Lineage tracing allows cell fate determination and was performed by crossing *Lrig1* EGFP-ires-CreERT2 mice with Rosa26 tdtomato reporter mice (Figure 3.11.A). In brief, when 4-hydroxytamoxifen (4OH-tamoxifen) is given it activates a Cre-lox system causing release of a Cre recombinase protein from the CreERT2 4OH-tamoxifen-responsive element. The Cre recombinase then catalyses the removal of a stop codon placed between the Rosa26 gene and an inserted transgene, in this case, the red fluorescent protein, tdtomato. Rosa26 is ubiquitously expressed (200) meaning activation of tdtomato is possible in all cells where Cre is present. When the *Lrig1* promoter is active the cell will express eGFP and following the administration of 4OH-tamoxifen the cell will also express tdtomato. The removal of the stop codon is a permanent change, so all daughter cells, arising from the LRIG1-expressing parent cell, will express tdtomato, irrespective of whether the *Lrig1* promoter is active or whether eGFP is being expressed.

To set up *in vivo* lineage tracing, I first established the appropriate 4OH-tamoxifen dose to use. In the skin, Cre-lox activation occurs following the administration of 0.1 mg 4OH-tamoxifen (91). However, the tracheal epithelial turnover is lower compared to the skin, so doses of 1, 0.1 and 0.01 mg 4OH-tamoxifen were trialled. 1 mg of 4OH-tamoxifen successfully activated the transgene and, after two weeks, there was clear expression of tdtomato in tracheal cells adjacent to the basement membrane (Figure 3.11.B). Gut samples were taken as a positive control and here, due to the higher epithelial turnover, clear crypt labelling was identified (Figure 3.11.B).

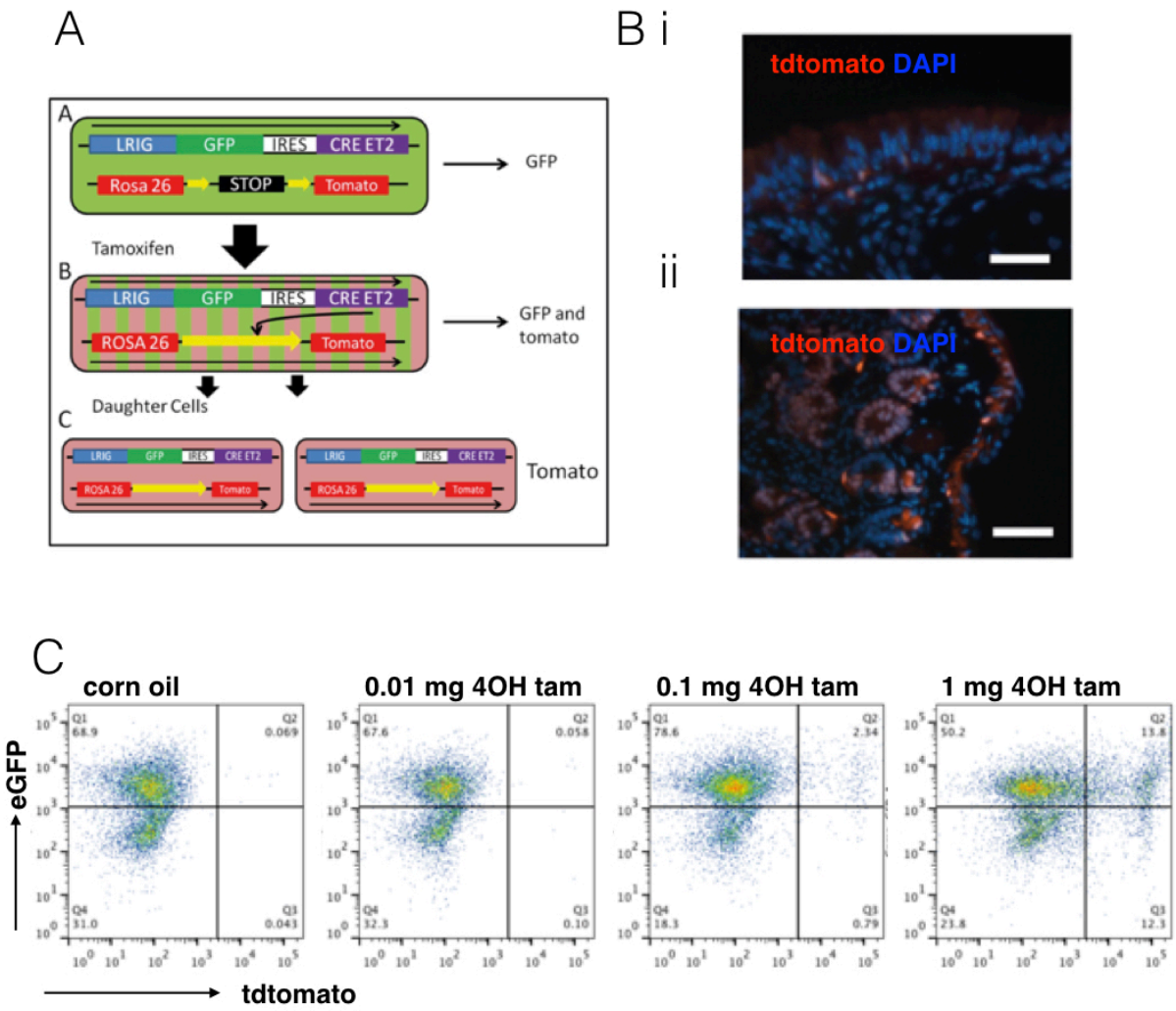

Figure 3.11: *In vivo* lineage tracing

A) The action of the tdtomato reporter gene. When the *Lrig1* promoter is active eGFP is expressed from the cell. On administration of 4OH tamoxifen the stop codon is removed from the reporter gene. If the cell has an active *Lrig1* promoter and the stop codon is removed the cell will express eGFP and tdtomato. The removal of the stop codon is permanent, so all daughter cells will express the tdtomato protein, irrespective of the expression of the *Lrig1* gene. B) Clear activation of the tdtomato protein in the airway i) and gut ii), (without antibody staining). DAPI used as a counterstain. Scale bar = 50 µm. Samples shown are representative images, n= 3. C) Flow cytometry analysis of tdtomato activation in the skin, following increasing concentrations of 4OH tamoxifen administration, n= 3. Note, following 1 mg of 4OH tamoxifen an $eGFP^+$/$tdtomato^+$ cell population is seen, in addition to a singly labelled $tdtomato^+$ population, implying these are the daughter cells of LRIG1-expressing cells that are no longer expressing LRIG1 (as not $eGFP^+$).

To confirm the activation of tdtomato in association with eGFP, skin epithelial cells were analysed by flow cytometry. There was no expression of tdtomato (indicating reporter gene activation) in the corn oil or 0.01 mg 4OH-tamoxifen dosing regimens after 2 weeks and minimal dual labelling in mice treated with 0.1 mg 4OH-tamoxifen (2% of cells). However, using a 1 mg dose of 4OH-tamoxifen, dual labelling with eGFP and tdtomato was detectable in 13% of the population and, notably, 12% of cells were singly stained for tdtomato. This suggests the singly tdtomato-expressing cells were the progeny of the initially labelled parents (Figure 3.11.C).

Extrapolating from studies in the skin and gut, LRIG1 was anticipated to be expressed in the airway stem cells. However, I have shown here that LRIG1 expression is seen throughout the respiratory epithelium. If LRIG1 were expressed across the epithelium, lineage tracing may be futile as tdtomato would be expressed in several populations. This means the cell of origin of the lineage trace could not be determined and the resultant patches of lineage-traced cells would be meaningless.

To assess the cell type where the tdtomato reporter is being activated, animals were administered 1 mg of tamoxifen and observed for 2 days. At this point they were culled and their tracheas extracted, paraffin-embedded and sectioned. Sections were stained for tdtomato (to assess for activation of the transgene), together with KRT5 (basal cells) and FOXJ1 (ciliated cells). Only singly labelled cells were detectable. The majority of tdtomato stained cells were KRT5-positive (Figure 3.12.A), however, there were occasional cells that were KRT5-negative (Figure 3.12.B, arrowed). When dual staining was performed with tdtomato and FOXJ1, an occasional cell was both tdtomato- and FOXJ1-positive (Figure 3.12.C), suggesting activation of the transgene in the ciliated cell population. This indicates that the transgene is activated in cells other than basal cells and that any lineage-traced progeny would have an uncertain origin.

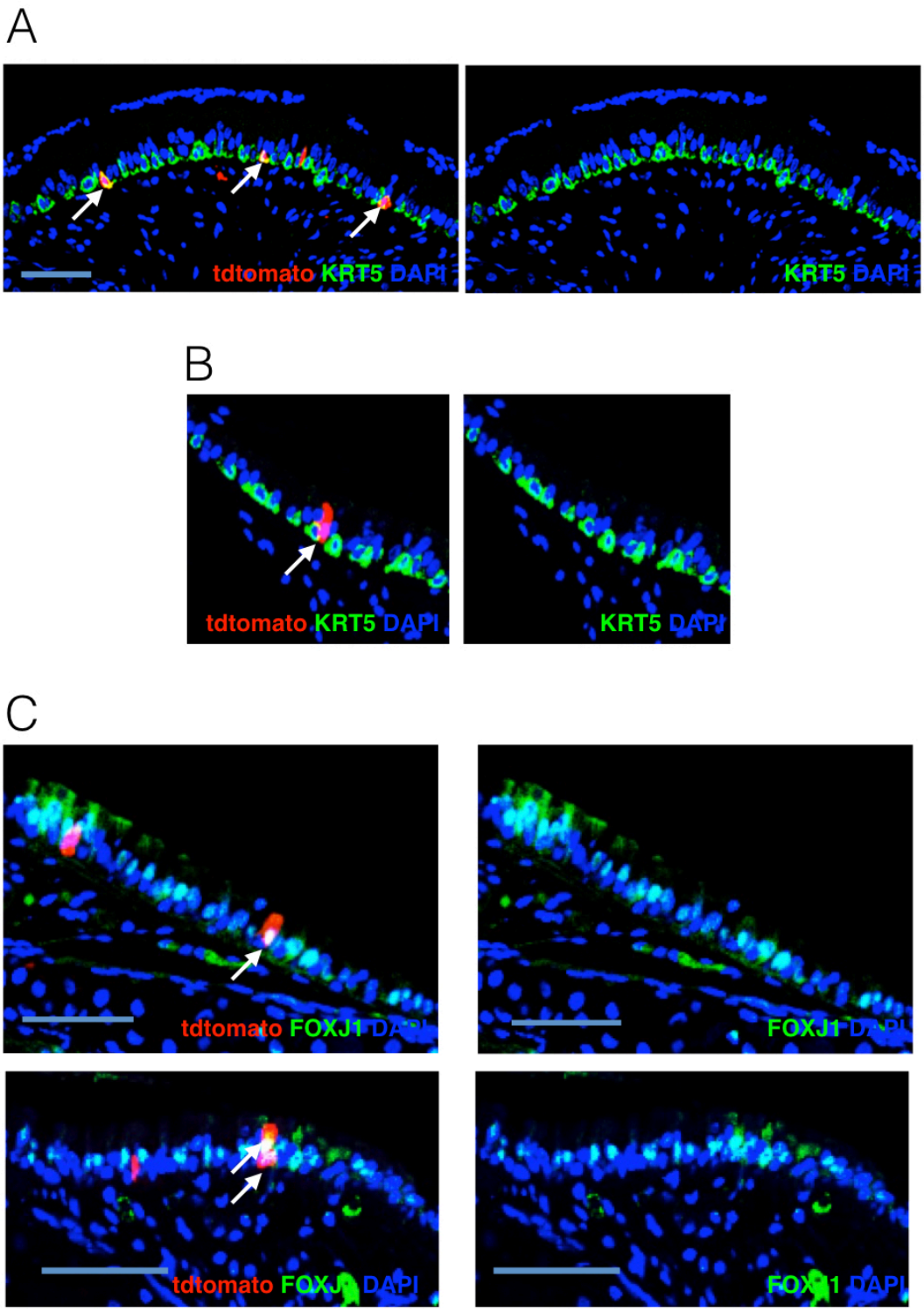

Figure 3.12: Activation of tdtomato in cells other than the basal cells

A) Immunofluorescence staining of tracheal epithelium showing tdtomato (red) and keratin 5 expression (KRT5; green). Arrows indicate cells dual stained for tdtomato and KRT5. B) Not all tdtomato (red) stained cells are KRT5-positive (green). Single, KRT5-negative (green), tdtomato-positive (red) epithelial cell are seen. The arrow indicates a tdtomato stained cell that is not positive for KRT5. C) Immunofluorescence staining of the tracheal epithelium for forkhead box J1 (FOXJ1) to identify ciliated cells (green) and for tdtomato (red). Tdtomato-positive, FOXJ1-positive epithelial cells are seen after 48 hours of tamoxifen exposure, indicated by arrows, suggesting activation of the transgene in cells other than the basal cells. DAPI used as counterstain in all images. Scale bars = 50 µm, images representative of n= 3.

3.4 Discussion

I have successfully set up a colony of *Lrig1* EGFP-ires-CreERT2 mice on a mixed FVB/N and C57BL/6 background, with the generation of wild-type, LRIG1-heterozygous and LRIG1-null animals. The phenotype of the LRIG1-null mice is mild, with the only change being a reduced weight at weaning; this equilibrates by 6-8 weeks. The previously seen gut hyperplasia in *Lrig1* knockout mice (93) is not seen in these C57BL/6 FVB/N animals, possibly due to their mixed background. My results confirm there is nil effect of haploinsufficiency of *Lrig1*.

The eGFP reporter successfully identifies the expression of LRIG1 and, although eGFP has been shown to degrade over a period of 24 hours (201), immunofluorescence staining shows a clear correlation between LRIG1 and eGFP expression. As the airway epithelial turnover is so low, and studies were carried out in the absence of damage or other airway insult, any subtle differences in the breakdown time of eGFP and LRIG1 are unlikely to have a significant impact at homeostasis.

Based on the findings in other organs, LRIG1 was only anticipated to be expressed by the airway basal cells, however, it is detectable across all epithelial cell types in the upper airway epithelium by both immunofluorescence and flow cytometry. LRIG1 is further seen throughout the epithelium of the distal airway. The protein does not appear concentrated in the areas of known stem cell compartments in either the tracheal submucosal glands, the airway branch points or at the bronchoalveolar duct junctions. This is in contrast to the skin and gut findings, where there is clear association of LRIG1 with the stem cell compartments (90, 93). As the break down of eGFP is over a 24-hour period and varies according to cell type, it is possible that the slow breakdown of eGFP may lead to the persistent marking of differentiated cells that no longer express LRIG1, if they originated from an LRIG1-expressing, $eGFP^+$ basal cell. However, if this were the case, the differentiated cell types would probably be less eGFP bright, but when flow cytometry was used to select the 25% most $eGFP^+$ cells, there was no enrichment of the basal cell population and the relative proportions of all cell types remained static. This indicates that there is

LRIG1 expression across epithelial cell types. In further support of this, when an LRIG1 antibody was used to assess LRIG1 expression in the epithelium there was homogeneous staining across all epithelial cells.

It is notable that although LRIG1 is expressed across the airway, when basal cells are considered independently, there are two populations: 50 % of the total basal cells are LRIG1-positive, while 50% are LRIG1-negative. With LRIG1 shown to mark a more 'stem cell'-like population of the skin and gut, this poses the question as to whether the expression of LRIG1 in this basal cell population confers a phenotype. Whilst basal cells were previously considered a homogeneous population, the possibility of basal cell heterogeneity has been raised. One study used clonal dynamics to show that basal stem cells give rise to a 'basal luminal precursor' prior to their differentiation into other cell types (202). This basal luminal precursor, although expressing basal cell markers, can be differentiated from the basal stem cell through expression of keratin 8 (202). A further study looking at basal cell heterogeneity has identified keratin 14 as marking a subpopulation of basal cells. This population makes up 20% of the basal cells, and is associated with a unipotent basal cell population at homeostasis; but this population becomes multipotent and can regenerate the tracheal epithelium on airway damage (203). Therefore, it is possible that the 50% of basal cells that express LRIG1 may exhibit different properties to the LRIG1-negative population. As loss of LRIG1 may lead to preinvasive cancer, the cell type of origin needs to originally express LRIG1, meaning that there might be a change in phenotype when LRIG1 is lost. Therefore the LRIG1-expressing basal cells are likely to be more significant than LRIG1-negative basal cells in preinvasive lung cancer development.

Loss of LRIG1 leads to skin hyperproliferation (89) and gut abnormalities (93). It has previously been shown that the tracheal epithelium in an LRIG1-null mouse is thicker than that in an LRIG1-heterozygous animal (104). I have confirmed this finding in the *Lrig1* EGFP-ires-CreERT2 animals. However, in contrast to this data, there was not a noticeable increase in the number of proliferative cells, suggesting that the rate of epithelial turnover did not explain this difference. I did, however, notice an

increased number of KRT5-positive basal cells in the LRIG1-null mice and, although not significant, it suggests that there may be an increase in the airway's basal stem cell pool. This may indicate that LRIG1 is behaving in the airway in a similar manner to its role in the skin and gut, where it has a regulatory role in these stem cell compartments. An expansion of the KRT5-positive cells in the LRIG1-null mice may suggest that LRIG1 loss leads to increased basal cell numbers in the airway. To confirm these findings, increased numbers of animals would need to be examined. To confirm whether LRIG1 regulates the basal cell compartment of the airway, in addition to the number of proliferative epithelial cells, the proliferation of the basal cells could be specifically determined. Whilst the number of mice used here were similar to the numbers used by Lu *et al* (104), there may be some strain-to-strain variability in the effects of LRIG1 loss and an increase in the sample size would increase the power of these preliminary findings. Strain-to-strain variability may also explain the differences in the phospho-EGFR staining shown here to that of Lu *et al*. In contrast to their findings, I detected no differences in the staining between the LRIG1-heterozygous and LRIG1-null animals, there was however, an increased intensity of staining for EGFR in the LRIG1-null tracheas. To conclusively show that loss of LRIG1 exerts its effects through loss of its inhibitory action on EGFR signalling in the airway epithelium, a larger number of animals could be examined and stained for other downstream protein such as extracellular signal–regulated kinases (ERK) and phospho-ERK, which I have shown is upregulated in the human epithelium upon *LRIG1* shRNA knockdown (Chapter 5). Using the murine epithelial cell culture techniques documented above I may also be able to culture sufficient cells from LRIG1-null and LRIG1-heterozygous animals to allow Western blotting for both EGFR and ERK.

A key advantage in the use of *Lrig1* EGFP-ires-CreERT2 mice is the ability to perform lineage tracing and to establish the role of LRIG1 in marking the stem cell compartment. I intended to use lineage tracing in a squamous lung carcinogenesis model to identify whether preinvasive and invasive squamous cell lung cancer lesions originate from an LRIG1-expressing basal cell. Thus, the role of LRIG1 in regulating a potential cancer stem cell of origin could be considered in wild-type,

LRIG1-heterozygous and LRIG1-null mice. Initially, the basal cells were the only airway cell population that I expected to be marked, however, as I have identified by both immunofluorescence and flow cytometry, LRIG1 is expressed throughout the airway epithelium and does not appear to be concentrated in the basal cell population. Therefore the origin of a clone would not be clear and the information obtained by lineage tracing would be of limited use in the assessment of a cancer cell of origin. Whilst it is possible that the 48- hour post 4OH-tamoxifen time point is not short enough to exclude the differentiation of an LRIG1-expressing basal cell to a labelled ciliated cell, this is unlikely as only single cells were seen and the tracheal epithelial turnover at homeostasis is extremely low. In further support of this finding, when KRT5-expressing basal cells are labelled with an eGFP reporter, labelled secretory cells and ciliated cells were not seen until 3-6 weeks and then they were rare (202).

Although lineage tracing may not clearly delineate the fate of an LRIG1-expressing cell, by comparing the clone sizes derived from LRIG1-heterozygous and LRIG1-null mice, an indication of the role of LRIG1 in airway epithelial regulation may be obtained. As LRIG1 is anticipated to regulate the stem cell compartments, clones from cells lacking LRIG1 may be larger than those from LRIG1-heterozygous animals. The growth dynamics of a clone from an LRIG1-null mouse compared to a heterozygous mouse may differ similarly to when larger clonal patches are seen in human smokers compared to non-smokers in airway dynamic studies (135) and when loss of Notch leads to a clonal advantage within the oesophageal epithelium (204). The activation of the reporter gene in cells other than basal cells would have less of an impact in these experiments. The lineage tracing experiments were initially abandoned, as they were unable to answer whether preinvasive lung cancers developed from LRIG1-expressing basal cells. However, it may be useful to revisit these experiments compare the size of epithelial clones from LRIG1-heterozygous and LRIG1-null mice, both at homeostasis and following injury to determine the effect of LRIG1 loss on clonal behaviour.

The difficulties encountered with pronase digestion of the trachea have been addressed through the optimisation of a method involving dispase/DNase/trypsin/collagenase digestion steps. The problems encountered with pronase digestion highlight wider issues when analysing cell populations obtained through tissue digestion. The choice of enzyme affects the cell population that is collected and should influence the choice of markers used to obtain this population. For digestion of the airway, the choice of enzyme used has previously been shown to affect the population of epithelial cells obtained when TROP2-positive epithelial cells were isolated from the mouse trachea. TROP2 (found in the highest concentrations in the upper murine airway) is extremely sensitive to trypsin, but much more resistant to pronase digestion. To account for this, when these cells are isolated the upper third of the trachea is separated from the lower part and each section digested differently (167).

The addition of the collagenase step to the reported dispase/DNase/trypsin strategy is of importance and greatly increased the basal cell yield. The basal cells located within the submucosal glands may have different characteristics to those lining the tracheal surface (205) and LRIG1 expression has clearly been seen in these areas. It is vital that these remaining basal cells are considered in any subsequent comparisons.

To fully assess the characteristics of isolated basal epithelial cells it is necessary to use them in downstream assays and to be able to grow them in cell culture. I have shown that this is possible through the use of 3T3-J2 mouse embryonic fibroblast co-culture. The isolated basal cells can then be used in tracheosphere assays where they show evidence of mucociliary differentiation. Until recently, the differentiation capacity of cultured murine epithelial cells had not been reported. A recent method (206) describes replacing the growth of murine epithelial cells on mitotically inactivated J2-3T3 feeder layers, as used here, with pharmacological inhibition of the SMAD and Rho-associated protein kinase (ROCK) signalling pathways and the growth of cells on a laminin matrix. Growing cells on either J2-3T3 feeder layers or the pharmacological inhibition of the SMAD and ROCK pathways using a laminin matrix

will enable the number of basal cells obtained from a single mouse to be increased through *in vitro* expansion. This may ultimately reduce the number of animals required for experiments and improve animal welfare issues, in accordance with the '3 R's' (207). The successful culture of mouse basal cells allows the properties of LRIG1-expressing cells to be explored further. The identification of a method to isolate and culture these basal cells in both 2D and 3D assays will allow comparison of the effect of LRIG1 on murine basal cell behaviour.

3.5 Summary

- LRIG1-wild-type, -heterozygous and -null mice can be generated from the *Lrig1* EGFP-ires-CreERT2 colony.
- The eGFP reporter co-localises with LRIG1 expression.
- LRIG1 expression is seen throughout the tracheal epithelial populations. It is also seen within the distal bronchioles.
- Only 50% of airway basal cells express LRIG1.
- Due to the expression of LRIG1 across the epithelial populations, lineage tracing cannot be used to assess the stem cell potential of LRIG1-expressing basal cells.
- A viable, pure population of basal cells can be isolated from the tracheal epithelium. These cells can be used in 2D and 3D assays.

4. Analysing the effects of LRIG1 expression on the properties of murine basal cells

4. Analysing the effects of LRIG1 expression on the properties of murine basal cells

4.1 Background

Despite expression patterns in the skin and gut suggesting that LRIG1 localises in the highest concentrations to the stem cell compartments (90, 91, 93), I have shown that in the airway LRIG1 expression is seen across the ciliated, secretory and basal epithelial cells. However, following analysis of the airway basal cell population, LRIG1 is detectable in only half of these cells. Until recently the airway basal cell population was considered as a homogeneous group. However, Ghosh *et al* have shown that 20% of the keratin 5 (KRT5) basal cell population co-express KRT14 (203); these KRT5/KRT14 expressing cells unipotent in the steady state, but that become multipotent after injury. In addition, Watson *et al* (202) have identified keratin 8 (KRT8) as marking 50% of basal cells, with these cells exhibiting a more differentiated phenotype. It is therefore possible that the LRIG1-expressing basal epithelial cells have distinct properties compared to LRIG1-negative basal cells. To understand the role of LRIG1 in airway epithelial cell homeostasis, the differences between $LRIG1^{+}$ and $LRIG1^{-}$ basal cells need to be explored, and this necessitates airway basal cell isolation (Figure 4.1).

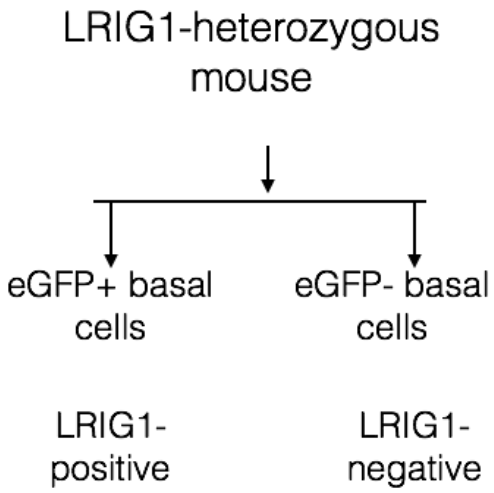

Figure 4.1. LRIG1$^+$ epithelial cells were compared to LRIG1$^-$ from an LRIG1-heterozygous mouse

The airway basal cells are the putative origin of squamous cell lung cancer and LRIG1 is lost in the development of preinvasive lesions (104). Therefore, to understand how the loss of LRIG1 influences basal cell behaviour and how this loss may lead to preinvasive lung cancer, LRIG1$^+$ cells from LRIG1-heterozygous mice were isolated and compared to the eGFP$^+$ basal cells isolated from LRIG1-null mice (Figure 4.2).

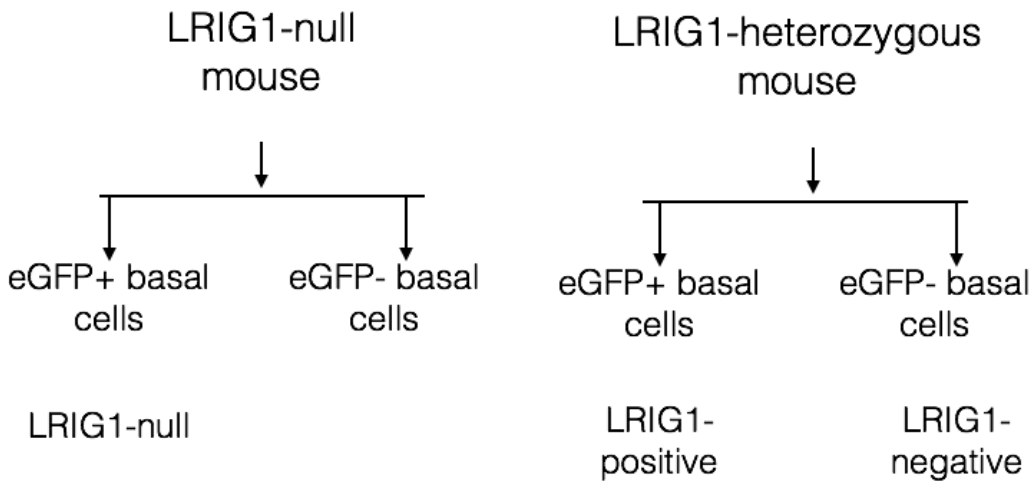

Figure 4.2. LRIG1$^+$ epithelial cells from an LRIG1-heterozygous mouse were compared to eGFP$^+$ epithelial cells (in which LRIG1 expression has been lost) from an LRIG1-null mouse.

Initially the behaviour of these basal cell populations was investigated using cell culture techniques. Then, to understand how the loss of LRIG1 leads to preinvasive disease, the gene expression profiles of each population was determined. The aim of these experiments was to create a list of candidate targets that could be explored in more detail, potentially identifying therapeutic candidates and leading to the identification of molecules and inhibitors that are able to reverse the effects of LRIG1 loss.

4.2 Aims

- To assess whether LRIG1^{+} basal cells behave differently to LRIG1^{-} (both cell types from an LRIG1-heterozygous mouse) and whether LRIG1 expression confers a more stem cell-like phenotype
- To assess whether the absence of LRIG1 (in eGFP^{+} basal cells from an LRIG1-null mouse) alters cell behaviour
- To assess the difference in gene expression between LRIG1^{+} and LRIG1^{-} basal cells (from a heterozygous mouse)
- To assess the difference in gene expression between LRIG1^{+} cells (from an LRIG1-heterozygous mouse) and eGFP^{+} cells (from an LRIG1-null mouse), to understand the changes that occur in preinvasive lung cancer

4.3 Results

4.3.1 The effect of LRIG1 expression on the proliferation of airway basal cells

Cells expressing LRIG1 within the murine gut and skin are more proliferative than LRIG1-negative cells (91, 93). This appears counterintuitive, due to LRIG1 being a negative inhibitor of EGFR signalling, but it is possible that LRIG1 moderates the amplitude of EGFR signalling, therefore is seen at higher levels in more proliferative cells.

To assess whether LRIG1 marks more proliferative basal cells in the airway, cells were isolated from murine tracheas. Initially basal cells were isolated from LRIG1-heterozygous mice and the cell cycle distribution of $LRIG1^+$ and $LRIG1^-$ cells (based on eGFP expression) compared using Hoescht 33342 uptake (Figure 4.3.A). $LRIG1^+$ basal cells were found to be significantly more proliferative than $LRIG1^-$ basal cells, with a greater proportion of cells in the G2/M phase of the cell cycle ($p=0.0011$) (Figure 4.3.B).

To assess whether LRIG1 loss influences cell proliferation, $eGFP^+$ cells from LRIG1-null mice (with no LRIG1 expression, but an active LRIG1 promoter) were compared to the $LRIG1^+$ basal cells from an LRIG1-heterozygous mouse. This comparison revealed no differences in proliferation (Figure 4.3.C).

The $eGFP^+$ LRIG1-null basal cells were then compared to the $eGFP^-$ LRIG1-null basal cells from the LRIG1-null mouse and were found to be significantly more proliferative (Figure 4.3.D).

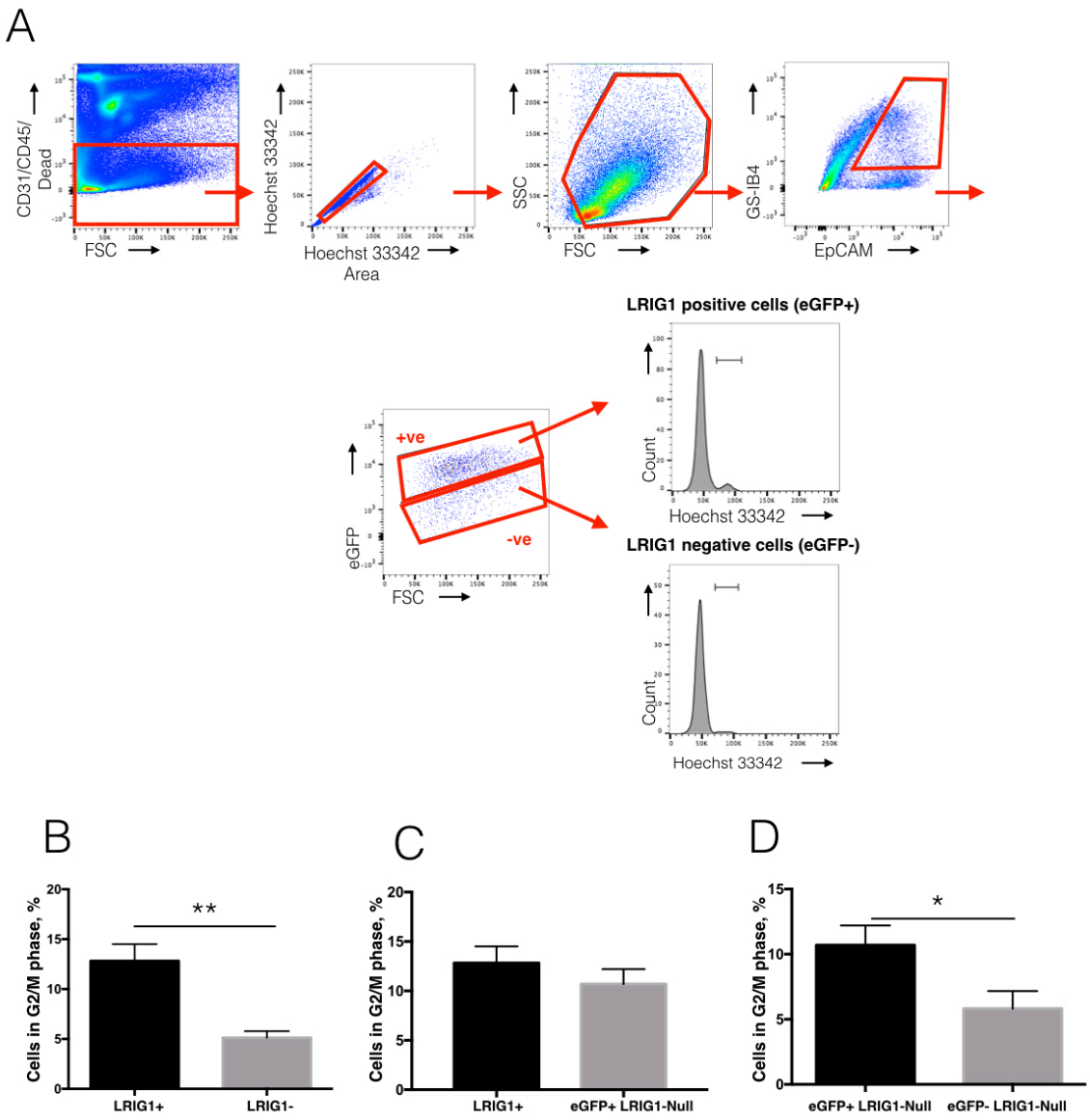

Figure 4.3: Proliferation of airway basal cells

A) Example of Hoescht 33342 staining in airway basal cells from LRIG1-heterozygous mice. CD31/CD45/Dead cells were negatively selected for, followed by the plotting of Hoescht 33342 area against width which was used to exclude doublets and then the plotting of FSC against SSC to eliminate cell debris. GS-IB4^{+} and EpCAM^{+} indicate the basal cell population, whilst eGFP is used as a marker of LRIG1 expression. eGFP-positive and -negative populations are gated and cell proliferation determined by analysis of the peaks Hoescht 33342 uptake. Cells in the G2/M phase are indicated in the second peak of the Hoescht 33342/cell count flow cytometry plot. The red gates indicate the population taken forward for analysis. Antibodies were used in the following colours; CD31 and CD45- APC, Live/Dead-PI, GS-IB4^{+}-qdot605 and EpCAM-BV711. B) Proliferation of LRIG1^{+} compared to LRIG1^{-} basal cells from LRIG1-heterozygous mice, showing the proportion of cells in the G2/M phase of the cell cycle. Mean ± SEM. Statistical analysis performed using the paired t test, ** indicates $p < 0.005$, $n = 6$. C) Proliferation of LRIG1^{+} basal cells (from LRIG1-heterozygous mice) compared to eGFP^{+} basal cells from LRIG1-null mice. Mean ± SEM. Statistical analysis was performed by the unpaired t test, $p = 0.3685$, $n = 6$. D) Proliferation of eGFP^{+} basal cells compared to eGFP^{-} basal cells from LRIG1-null mice. Mean ± SEM. Statistical analysis performed by the paired t-test, * indicates $p < 0.05$, $n = 6$.

4.3.2 The effect of LRIG1 on the stem cell behaviour of airway basal cells

4.3.2.1 Spheroid-forming assays

To compare the stem cell potential of the LRIG1^{+} and LRIG1^{-} basal cells from LRIG1-heterozygous mice, fluorescent activated cell sorted (FACS) basal cells were seeded into a spheroid-forming assays (Figure 4.4.A). LRIG1^{+} basal cells were seen to form significantly more spheroids than LRIG1^{-} basal cells (with $p = 0.0020$) (Figure 4.4.B).

To assess the effect of LRIG1 loss on spheroid-forming ability, eGFP^{+} LRIG1-null basal cells were also seeded into spheroid-forming assays and compared to LRIG1^{+} basal cells from LRIG1-heterozygous mice. No significant difference in the spheroid-forming efficiency was detectable between the two populations (Figure 4.4.C).

Although comparable spheroid-forming efficiencies were seen in LRIG1^{+} cells from LRIG1-heterozygous mice and the eGFP^{+}, LRIG1-null basal cells to those reported in the literature (208, 209), at high seeding densities spheroids form from epithelial cells that pool together, rather than from a single cell of origin (210). Due to the potential of spheroids to form from pooled epithelial cells, colony-forming assays were performed to further investigate the 'stem cell' potential of these populations of cells.

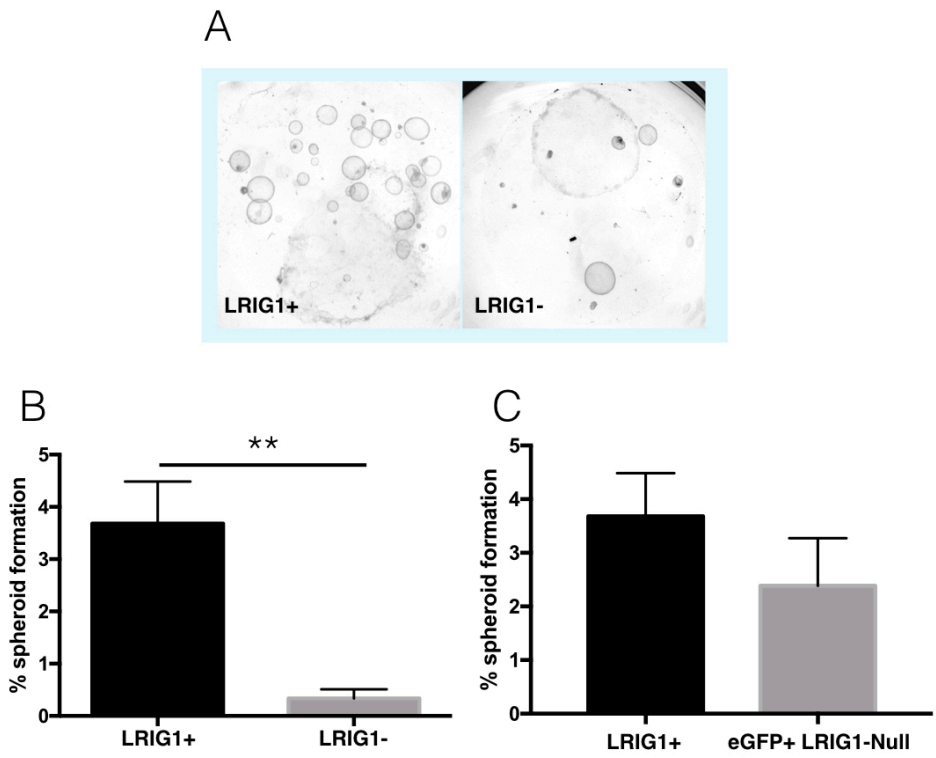

Figure 4.4: Formation of spheroids from airway basal cells

A) Example of growth of spheroids from airway basal cells in Matrigel following flow cytometry sorting into LRIG1^{+} and LRIG1^{-} populations from LRIG1-heterozygous mice. Note the increased spheroid numbers from LRIG1^{+} cells. B) Comparison of spheroid-forming efficiency between LRIG1^{+} and LRIG1^{-} basal cells from LRIG1-heterozygous mice. Mean ± SEM. Statistical analysis performed by the paired t-test, ** indicates $p < 0.005$, $n = 10$. C) Comparison of spheroid-forming efficiency between LRIG1^{+} and eGFP^{+} cells from LRIG1-null mice. Mean ± SEM. Statistical analysis performed by the unpaired t-test, $p = 0.3176$, $n = 10$ in the LRIG1^{+} group and $n = 6$ in the LRIG1-null cells.

4.3.2.2 Colony-forming assays

Colony forming assays assess a cell's stem cell potential as they determine the ability of a population to self renew (211) . Sorted epithelial cells were initially seeded into 6 well plates, where they were grown on 3T3-J2 feeder layers (as optimised in Chapter 3). However, due to the low numbers of LRIG1^{+} and LRIG1^{-} basal cells obtained from each murine trachea, the numbers of mice needed to ensure replicates could be performed was prohibitive. To overcome this problem, I chose to use a single cell colony forming assay instead. Individual basal cells were sorted directly into each well of a 96-well plate containing mitotically inactivated 3T3-J2 feeder cells and mouse tracheal epithelial cell (MTEC) media (169). LRIG1^{+} and LRIG1^{-} basal cells from LRIG1-heterozygous animals were collected as well as eGFP^{+} basal cells from LRIG1-null mice (Figure 4.5.A).

After two weeks of culture, colonies that were greater than 10 cells were counted. Significantly more colonies grew from LRIG1^{+} basal cells compared to the LRIG1^{-} population in LRIG1-heterozygous mice (Figure 4.5.B). There was no difference in the number of colonies forming in LRIG1^{+} basal cells (from LRIG1-heterozygous animals) compared to the eGFP^{+} basal cells from LRIG1-null mice (Figure 4.5.C).

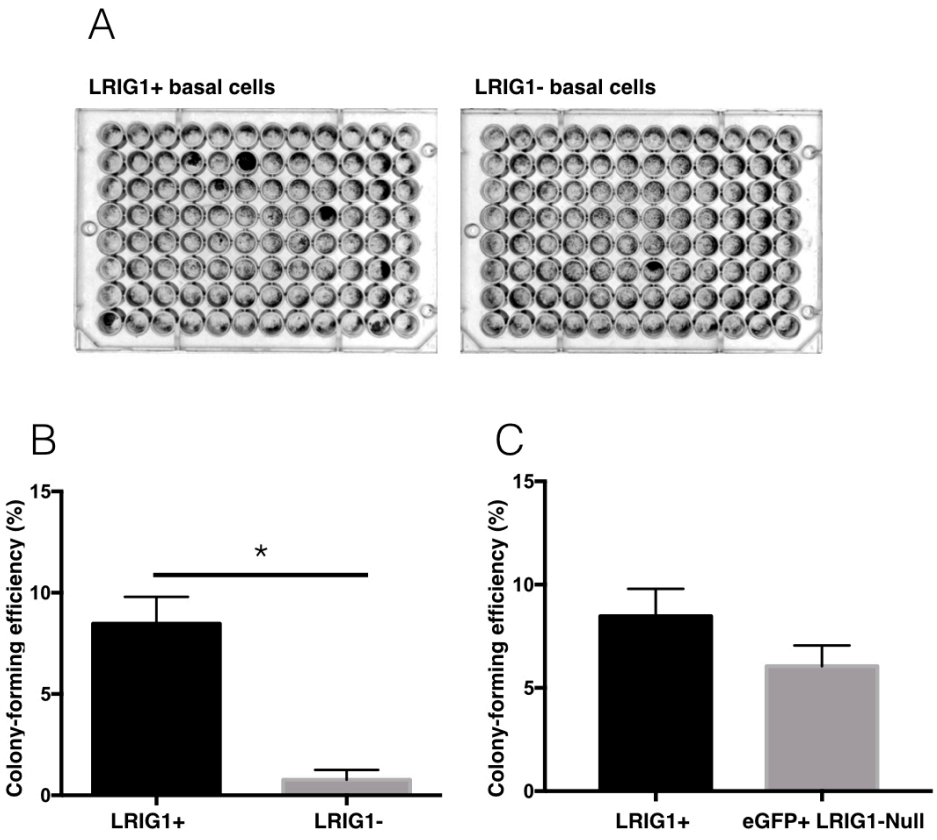

Figure 4.5: Colony-forming efficiency in airway basal cells

A) Example of colony-forming assay. Colonies that were greater than 10 cells were counted. B) Comparison of colony-forming efficiency in LRIG1^{+} and LRIG1^{-} epithelial cells from LRIG1-heterozygous animals. Mean ± SEM. Statistical analysis performed by paired t-test, * indicates $p < 0.05$, $n = 4$. C) Comparison of colony-forming efficiency between LRIG1^{+} from LRIG1-heterozygous and eGFP^{+} basal cells from LRIG1-null mice. Mean ± SEM. Statistical analysis performed by the unpaired t-test, $p = 0.1946$, $n= 4$.

4.3.3 Single cell RNA Sequencing: Cell preparation

To address my initial hypothesis that the loss of LRIG1 leads to preinvasive lung cancer, I first intended to look at differential gene expression between airway basal epithelial cells that expressed LRIG1 and cells in which LRIG1 had been lost (in the LRIG1-null animals). However, after demonstrating that LRIG1^{+} basal cells have distinct properties to LRIG1^{-} basal cells from LRIG1-heterozygous mice I further compared the gene expression profiles of these two populations to gain further insights into the biological differences between these cell populations.

In total the gene expression of 3 groups was compared (Figure 4.6.A). To assess for the effects of loss of LRIG1, group 1 (eGFP^{+} basal cells from LRIG1-null mice) was compared with group 2 (LRIG1^{+} basal cells from LRIG1-heterozygous mice) basal cells. This would determine the gene expression changes likely to be occurring in preinvasive lung cancer and could lead to the identification of potential therapeutic candidates. To understand the differences in behaviour that I found between LRIG1^{+} and LRIG1^{-} basal cells, group 2 (LRIG1^{+} basal cells from LRIG1-heterozygous mice) was compared to group 3 (LRIG1^{-} basal cells from LRIG1-heterozygous mice).

Initially, I had planned to analyse pooled populations of murine basal cells and to use the extracted RNA for microarray analysis. However, the recommended total amount of RNA for a microarray is in the range of micrograms (212) and, as a limited number of basal cells could be obtained from one trachea (Chapter 3), of which only 50% would express LRIG1, a large number of mice would be needed. The experiment would also need to be performed in triplicate, increasing further the number of animals required. Alternative strategies to a microarray were considered and single cell RNA sequencing (sc-RNA seq) appeared the best option. The advantages to sc-RNA seq were two fold: firstly, the technique allows gene expression analysis in cell numbers too low for conventional microarray purposes (as the results from individual cells can be pooled to understand the population characteristics); secondly, any heterogeneity within the three groups of basal cells could be determined (213).

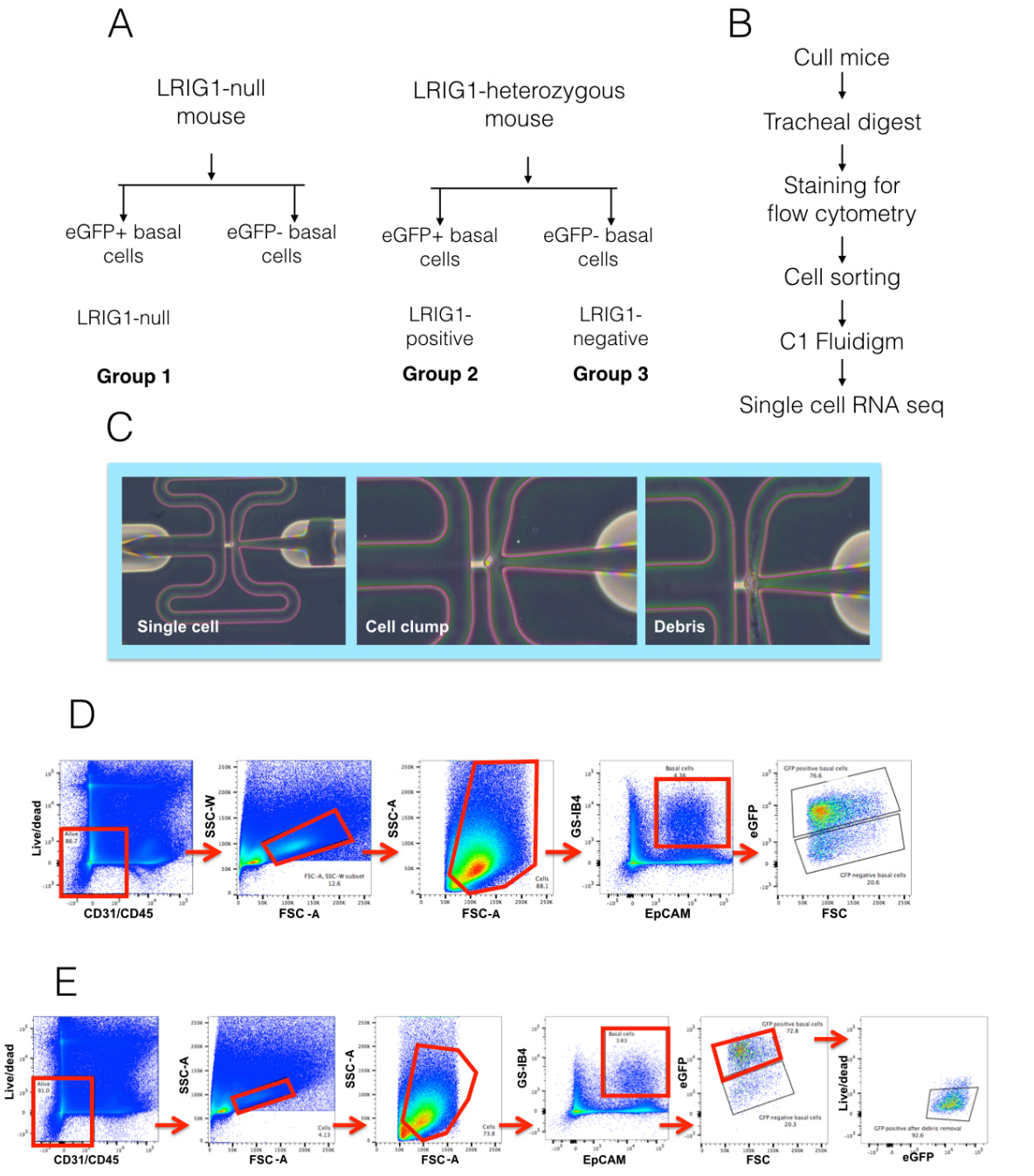

Figure 4.6: Preparation of cells for single cell RNA sequencing

A) The division of cells into 3 groups for single cell RNA seq. Group 1: eGFP^{+}, LRIG1-null basal cells. Group 2: LRIG1^{+} cells from LRIG1-heterozygous mice. Group 3: LRIG1^{-} cells from LRIG1-heterozygous mice. B) Process of sample preparation for single cell RNA seq. C) Collection of single cells, cell clumps and debris within the wells of the C1 Fluidigm. D) Initial flow cytometry sorting strategy for single cell RNA Seq. Live, CD31^{-},CD45^{-} cells are gated, and FSC against SSC-width selected to ensure the removal of cell doublets. Next, FSC against SSC removes cell debris and EpCAM^{+} and GS-IB4^{+} cells identifies the basal cell population. LRIG1^{+} and LRIG1^{-} populations are sorted on the expression of eGFP. The red gates indicate the population taken forward for analysis. Antibodies were used in the following colours; CD31 and CD45-PE, Live/dead-DAPI, EpCAM-APC, GS-IB4-qdot605. E) Adjustments to the sorting strategy to ensure a reduced amount of debris is collected. The doublets gate was tightened, as was the FSC/SSC gate. The red gates indicate the population taken forward for analysis. Once an eGFP positive population had been selected, this was then re-analysed against the DAPI, ensuring the removal of any dead cells.

The strategy for sc-RNA seq followed the flow diagram displayed in Figure 4.6.B. To obtain single cells for analysis, $eGFP^+$ and $eGFP^-$ basal cells from digested murine tracheas were sorted by FACS, and the isolated cells loaded into a C1 Fluidigm, a microfluidic device where a cDNA library is prepared. Advantages to the use of a C1 Fluidigm over other methods includes a high level of inter-sample reproducibility and a low volume of sample preparation, which lowers false positives and bias (213).

Initial attempts revealed a very low single cell capture rate on the C1 Fluidigm. When the wells were examined there were empty wells, cell clumps and debris (Figure 4.6.C). Optimisation of the initial FACS strategy (Figure 4.6.D) was performed and sample quality improved by adjustment of the sorting buffer (through reducing the serum concentration) and a tightening of the flow cytometry gates (Figure 4.6.E). This included the addition of a final gate where the $eGFP^+$ population was examined against the live-versus-dead stain. This step dramatically reduced the amount of debris in the sample. The C1 Fluidigm steps were performed in two different institutions (due to the possibility of technician error). cDNA libraries were prepared within the C1 Fluidigm plates and libraries sequenced on the HiSeq 2500. The data for the single cell sequencing were obtained in FASTQ format and passed to a bioinformatician for analysis.

4.3.4 Single cell sequencing: cell quality and gene checks

After the exclusion of any doublets or debris, 225 cells were considered suitable for analysis. These cells were screened further by the assessment of the number of genes detected in each cell sample (Figure 4.7.A). The median number of genes detected per sample was around 4,000, which is consistent with that previously reported for sc-RNA seq experiments (214). Any cell that expressed less than 2,000 genes was of poor quality (where a poor quality reaction occurred or where there was low RNA sampling) and removed. After exclusion of 27 cells for low gene expression levels, 199 cells remained (Figure 4.7.A).

An External RNA Controls Consortium (ERCC) spike-in was added to the C1 Fluidigm reaction. These spike-ins assess the quality of transcript detection following sequencing. The spike-ins contain 92 transcripts, so any cell expressing less than 25 transcripts was excluded as the quality of the reaction and sample labelling was likely to be poor. This removed a further 37 samples, leaving 154. Of these 154 cells, 28 were not suitable for analysis, as were dead or contained debris on visual inspection of the cells in the C1 Fluidigm, and 126 cells remained (Figure 4.7.A).

Genes that were detected in less than 10 of the 126 cells were removed from the overall data set (Figure 4.7.B). Therefore, after quality assessment checks 126 cells remained and 13090 genes were included. The number of cells in each population is shown in Figure 4.7.C.

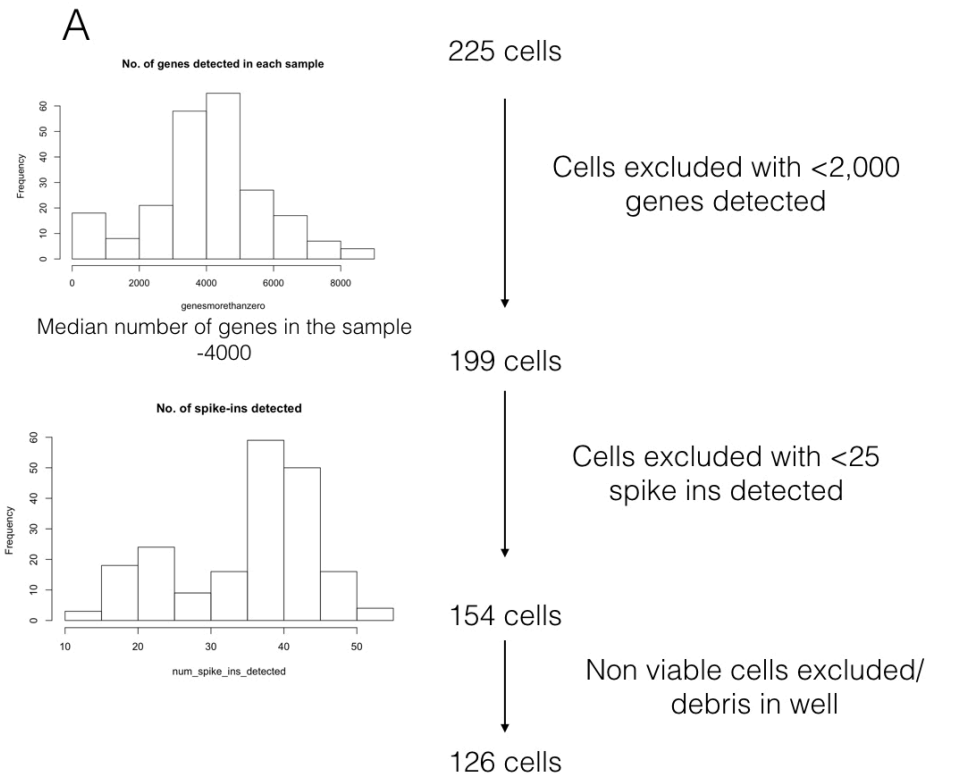

C

Group	Number of cells
1	28
2	46
3	52

Figure 4.7: Selection of cell population suitable for sc-RNA seq analysis

A) 225 collected single cells across five C1 Fluidigm plates were reduced to 126 cells that were suitable for further analysis. Initially, cells were excluded where less than 2,000 cells were detectable in the sample, followed by the exclusion of cells where less than 25 ERCC RNA spike-ins were detected. Cells unsuitable following visual inspection on the C1 Fuildigm were also excluded. B) Graph showing the number of genes detected in each sample. When genes were detected in fewer than 10 cells, these genes were excluded from the analysis. The data analysis was performed and graphs drawn by Dr Stephen Henderson, Bill Lyons Informatics Centre, UCL. C) Table to show the number of cells in each of the 3 groups.

4.3.5 Single cell sequencing: Assessment of cell populations

In addition to the above quality controls, I wanted to confirm that the cells being analysed were, as anticipated, epithelial. This would show that the FACS strategy was adequate and confirm that the correct populations were being analysed. Therefore, cells were assessed for the expression of the epithelial genes, *Krt5*, *Krt8*, *Krt14*, *Trp63*, *Epcam*, *Itgα6*, *Cd151*, *Tacstd2*, *Egfr*, *Met* and *Aqp3*. Of the 154 cells suitable for analysis, only one cell did not express any epithelial genes (and was excluded) (Figure 4.8.A), indicating the analysed cells were epithelial.

The expression of the different epithelial markers was then determined in each of the three groups. No significant differences in expression were detectable across any of the epithelial genes. It is notable that levels of both *Krt8* and *Krt14*, each shown to mark a subpopulation of basal cells (202, 203), were comparable between the three groups, indicating that LRIG1 does not co-localise with known markers of basal cell heterogeneity (Figure 4.8.B).

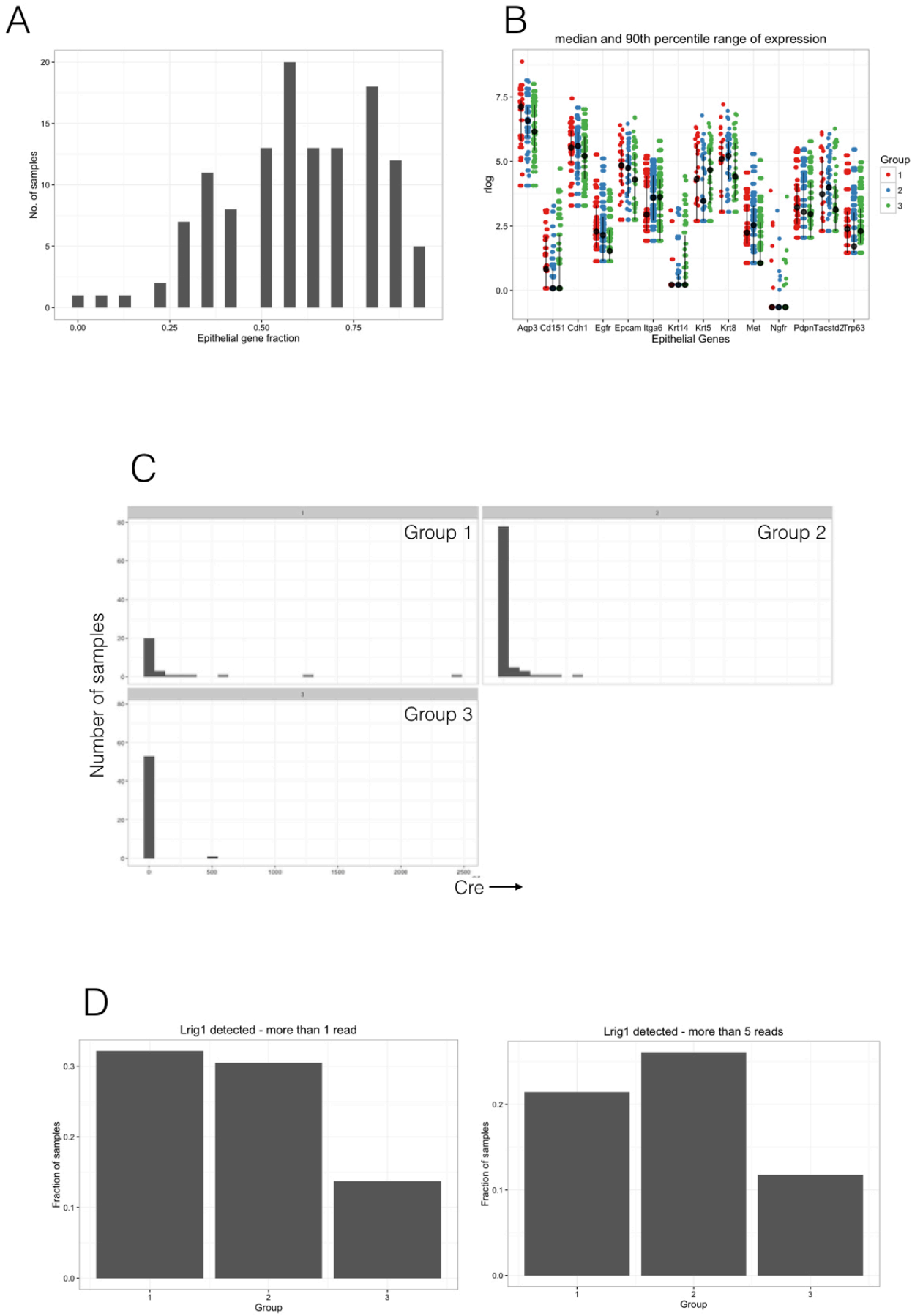
A
No. of samples
Epithelial gene fraction
B
median and 90th percentile range of expression
rlog
Aqp3 Cd151 Cdh1 Egfr Epcam Itga6 Krt14 Krt5 Krt8 Met Ngfr PdpnTacstd2Trp63
Epithelial Genes
Group
C
Group 1
Group 2
Group 3
Number of samples
Cre
D
Lrig1 detected - more than 1 read
Lrig1 detected - more than 5 reads
Fraction of samples
Group

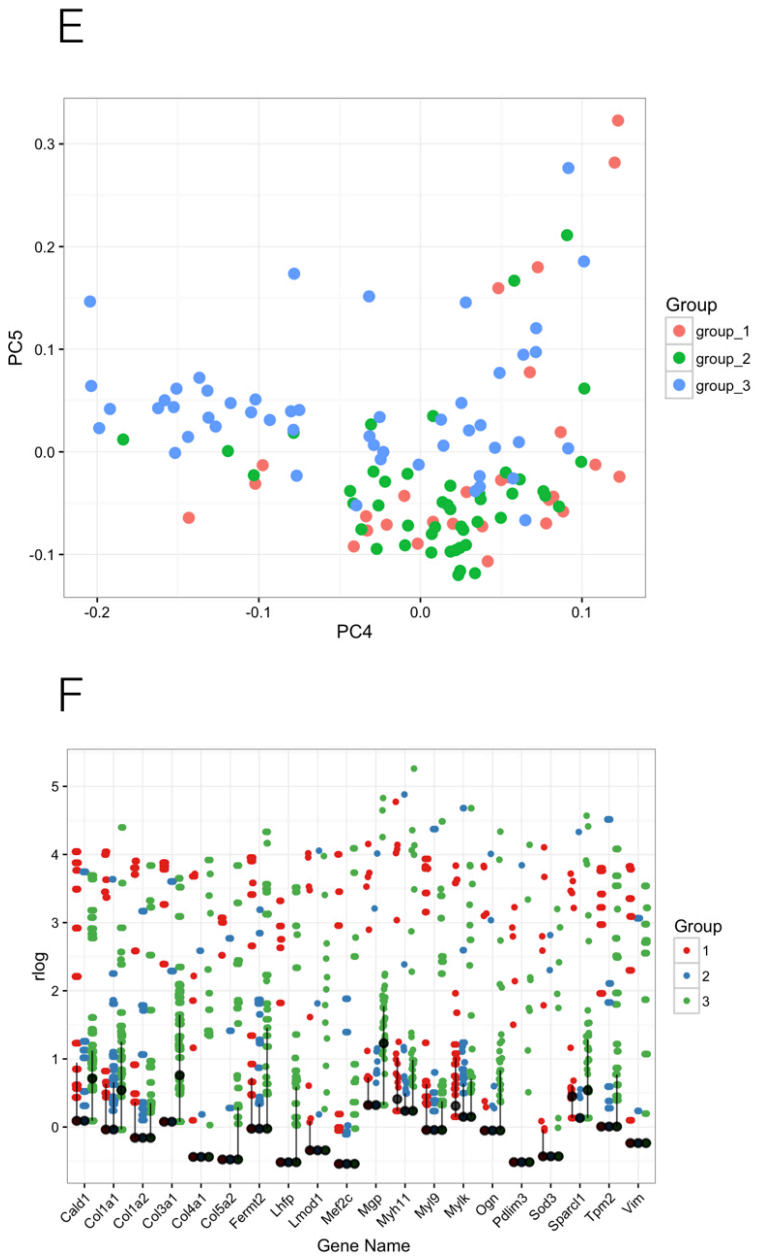

Figure 4.6: Expression of specific genes within the single cell RNA sequencing population

A) Assessment of the expression of genes associated with the airway epithelium in the 154 isolated cells to be used in the sc-RNA seq experiments. The proportion of the number of epithelial genes out of *Krt5*, *Krt8*, *Krt14*, *Trp63*, *Epcam*, *Itgα6*, *Cd151*, *Tacstd2*, *Egfr*, *Met* and *Aqp3* that each cell expressed. B) The median and 90th percentile range for the above genes split between the three groups. Note there are no significant differences in the gene expression of the groups. In particular, the expression of *Krt8* and *Krt14* is similar in all three groups. C) The number of Cre transcripts detectable in the cell populations of groups 1, 2 and 3 and combined. There are more Cre transcripts in group 2, although the majority have no Cre transcripts. D) *Lrig1* detection within each of the three populations. The graph on the left shows the proportion of cells expressing at least one transcript of *Lrig1*, whilst the graph on the right shows the proportion of cells that are expressing more than 5 transcripts of *Lrig1*. E) Random forest plot of PC4 plotted against PC5, showing some separation of group 3 from groups 1 and 2. F) Gene expression that is most associated with group 3. Level of gene expression, mean ± 90th percentiles in each of the three groups. The genes most associated with group 3 are *Col1a1*, *Col1a3*, *Mgp* and*Tpm2*. The data analysis was performed and graphs drawn by Dr Stephen Henderson, Bill Lyons Informatics Centre, UCL.

Next, to confirm that flow cytometry was able to adequately discriminate between $eGFP^+$ and $eGFP^-$ cells, the cells were examined for the expression of *eGFP* transcripts. However, the *eGFP* sequence failed to align to any transcripts, and *eGFP* was undetectable in the samples. To ensure this was not the result of an *eGFP* sequence anomaly, the transcripts were aligned to the Cre component of the LRIG1 cassette. Although some transcripts were seen, these were detected at very low levels, and most cells did not express any Cre transcripts. There was a slightly higher proportion of Cre transcripts in group 2 ($LRIG1^+$ basal cells from LRIG1-heterozygous mice), but this was not high enough to differentiate this population (Figure 4.8.C). As these results were unclear, the expression of *Lrig1* transcripts was analysed across the three groups. *Lrig1* transcripts should only be detected in group 2 ($LRIG1^+$ cells from LRIG1-heterozygous mice), but would still give an indication as to how successful the sorting had been and how well defined the populations were. Unfortunately *Lrig1* transcripts were seen in all populations (Figure 4.8.D) and were detectable in as many as a third of cells from group 1 ($eGFP^+$, LRIG1-null basal cells). In group 2 ($LRIG1^+$ basal cells from LRIG1-heterozygous mice), where cells should be producing *Lrig1* transcripts, only a third showed evidence of *Lrig1* transcript expression, and in group 3 ($LRIG1^-$ basal cells from LRIG1-heterozygous mice), transcripts were detectable. To assess if this was non-specific, the number of transcripts of *Lrig1* required to confirm positive detection was increased from 1 read to greater than 5. Whilst this slightly increased the number of cells that expressed the transcript in group 2 ($LRIG1^+$ basal cells from LRIG1-heterozygous mice), the relative proportions of cells expressing *Lrig1* transcripts did not change significantly (Figure 4.8.D).

To assess for differences in the groups, principal component analysis (PCA) was used to look for clustering. PCA showed that group 3 ($LRIG1^-$ basal cells from LRIG1-heterozygous mice) was separated from the other two groups (Figure 4.8.E). These were the cells with the most distinctive phenotype in the *in vitro* experiments and showed a reduced colony- and spheroid-forming ability and a reduced proliferation. There were 4 genes; collagen alpha 1 chain (*Col1a1)*, collagen alpha 3 chain (*Col3a1)*, matrix gla protein (*Mgp)* and β-tropomyosin (*Tpm2)* (Figure 4.8.F) were found to be

most associated with group 3 (LRIG1$^-$ basal cells from LRIG1-heterozygous mice). Both *Col1a1* and *Col1a3* are genes for secreted proteins for collagen production and the formation of the extracellular matrix (215), whilst the *Mgp* gene encodes a secreted protein that regulates the organisation of bone tissue (216), and *Tpm2* has a role in the cell cytoskeleton and is involved in muscle contraction (217). None of the genes were able to distinguish the population with certainty on their own, but collectively could identify the group with 65% accuracy, compared to a 33% accuracy expected should the cells have been completely random.

4.4 Discussion

LRIG1 marks a population of airway basal cells from LRIG1-heterozygous mice that is more proliferative and shows an increased stem cell-like phenotype with increased spheroid- and colony-forming ability. The increased proliferative capacity of LRIG1$^+$ basal cells is consistent with that reported in the skin and the gut (91, 93).

Assessment of the effect of loss of LRIG1 on basal cell behaviour analysed through the use of eGFP$^+$ basal cells from LRIG1-null mice showed there is no effect of the loss of LRIG1 on either the proliferation or spheroid- or colony-forming capacity of airway basal cells. This contrasts with the findings of Jensen *et al*, who show that, in the skin, when keratinocytes are isolated from an *Lrig1*-knockout mouse, there is an increase in colony-forming capacity (90).

The lack of effect of LRIG1 loss on airway basal cells (when LRIG1$^+$ and eGFP$^+$ cells from LRIG1-null mice are compared) may be due to LRIG1 simply marking an airway basal cell population, without having a regulatory function. Although LRIG1 does have a clear role in other tissues, the effects may be organ-specific. If the LRIG1 protein were redundant in the airway, its loss would have no biological impact. The proliferation of eGFP$^+$ LRIG1-null basal cells and eGFP$^-$ LRIG1-null basal cells (Figure 4.3.D) is very similar to that of the proliferation of the LRIG1$^+$ and LRIG1$^-$ basal cells from LRIG1-heterozygous animals (Figure 4.3.B). If LRIG1 were simply marking a

basal cell population, these findings would be expected, as the loss of the 'marker' would have no biological effect, and a redundancy of LRIG1 exists. The lack of phenotype in the LRIG1-null eGFP$^+$ basal cells may further be explained by the loss of LRIG1 in the *Lrig1* EGFP-ires-CreERT2 mouse being constitutive, rather than conditional. In this mouse, any LRIG1 protein expression would have been absent throughout the animal's life, so compensatory upregulation of other cellular proteins may have occurred (for example the negative inhibitor of EGFR signalling, MIG6 (218)). To clearly assess the change in LRIG1 expression, an alternative mouse model with conditional loss of LRIG1 should be used. This would also more closely mirror the changes that are seen in the human airway on the loss of LRIG1 during the development of preinvasive disease.

However, eGFP expression in LRIG1-null animals goes against LRIG1 being redundant in the airway. eGFP is expressed on activation of the LRIG1 promoter, therefore if the cell was not trying to express LRIG1, the promoter would not be active (indicative of a possible ongoing biological need for LRIG1). It is also interesting to note that the tracheal epithelium is thicker in LRIG1-null mice compared to LRIG1-heterozygous animals (Chapter 3), which is in line with the findings of Lu *et al* (104). As there is increased epithelial thickness, there is an *in vivo* airway phenotype caused by the loss of LRIG1. It is possible that this phenotype is reflective of the loss of LRIG1 in the multiple cell types that constitute the respiratory epithelium, rather than just the basal cells that are analysed here.

Although there are a number of limitations to the sc-RNA seq data (discussed later), the above factors may explain why no differential gene expression is seen between groups 1 (eGFP$^+$ cells from LRIG1-null mice) and 2 (LRIG1$^+$ basal cells from LRIG1-heterozygous mice). If LRIG1 is simply marking the cell it is not influencing the transcripts that are produced and no differences would be seen between the two groups. Alternatively, if there was an upregulation of other factors that compensate for the constitutive loss of LRIG1 then these may have been apparent in the sc-RNA seq data, and this was not seen in the data, suggesting that compensation is not occurring.

In general, the single cell RNA seq results are disappointing. I was initially concerned the quality of the data would be poor due to the prolonged sample preparation time and the need to perform different components of the experiment across 3 different institutions. Surprisingly, the Bioanalyser measurements of RNA integrity were good and the samples did not appear to be unduly affected by the length of time between the cell harvest and their insertion into the C1 Fluidigm.

The FACS strategy initially appeared successful and the single cells appear to be an almost pure epithelial cell population, however, there was no alignment of the eGFP transcript to cellular gene expression. Possible explanations for this include the stability of the *eGFP* mRNA, with degradation possibly occurring prior to the cDNA synthesis step. Around 7 hours elapsed between the harvesting of the airway basal cells and their insertion into the C1 Fluidigm. The half-life of *eGFP* mRNA has been demonstrated to be around 5 hours (219), therefore detection of at least a small number *eGFP* transcripts would still be expected. The eGFP protein was also detectable by flow cytometry and allowed sorting of $eGFP^+$ and $eGFP^-$ populations (using a fluorescence minus one control to set the gates), so *eGFP* mRNA was clearly being produced at least prior to cell harvest. I have previously shown a clear correlation between eGFP protein and LRIG1 protein expression, so eGFP should be reflective of LRIG1 protein production (Chapter 3). As the cells contained the large cassette at the *Lrig1* locus, instead of aligning to the *eGFP* sequence, I attempted to align to the Cre component of the cassette. Although some Cre transcripts were expressed, the majority (> 90% of cells) in groups 1 and 2 (where the insert is present) were negative for Cre transcripts, making this alignment unsuitable too. This suggests that either the Cre transcript is expressed at very low levels or is unstable.

It is concerning that the level of *Lrig1* transcript did not distinguish between the three populations. Group 2 ($LRIG1^+$ basal cells from LRIG1-heterozygous mice) should show the presence of *Lrig1* transcript in all of the cells, but was seen in only a third, and group 1 ($eGFP^+$ cells from LRIG1-null mice) showed similar *Lrig1* transcript

levels to group 2 (LRIG1^{+} basal cells from LRIG1-heterozygous mice), despite these cells not producing *Lrig1*. *Lrig1* transcripts were also seen in group 3 (LRIG1^{-} basal cells from LRIG1-heterozygous mice). The FACS strategy is unlikely to be at fault, as the eGFP gate was set based on the fluorescence minus one controls and there was a clear separation of eGFP^{+} and eGFP^{-} cell populations (Figure 4.5.D). If the eGFP were to degrade during the prolonged experimental time course, it would mean that there are LRIG1 false-negative cells in group 3 (LRIG1^{-} basal cells from LRIG1-heterozygous mice) and may explain the small number of cells with LRIG1 expression seen in this population. The possibility that LRIG1 was still being expressed in the LRIG1-null animals was considered as a cause for the presence of *Lrig1* transcript, but immunoblotting clearly confirmed no LRIG1 protein production in LRIG1-null mice (Chapter 3). The detection of *Lrig1* transcript in group 1 (eGFP^{+}, LRIG1-null basal cells) is probably due to the position of the EGFP-ires-CreERT2 cassette: the *Lrig1* EGFP-ires-CreERT2 cassette is situated behind the start codon of *Lrig1*, so despite there being no LRIG1 protein produced, a simple frame- shift mutation would mean the mRNA is still present (but not transcribed due to the mutation) and the transcript is detectable on sequencing. This would account for there being a similar number of transcripts seen in groups 1 (eGFP^{+}, LRIG1-null basal cells) and 2 (LRIG1^{+} basal cells from LRIG1-heterozygous mice). In group 1 (eGFP^{+}, LRIG1-null basal cells) the frame-shifted transcript aligns, whilst in group 2 (LRIG1^{+} basal cells from LRIG1-heterozygous mice) the 'real' *Lrig1* mRNA aligns. LRIG1 belongs to a family of three proteins designated LRIG1-3 and these proteins share a degree of mRNA transcript similarity. The percentage identity between *Lrig1* and *Lrig2* is 57.26% and between *Lrig1* and *Lrig3* is 59.72% (220). This means it is unlikely that these transcripts are being detected in place of *Lrig1*. Additionally, *Lrig2* and *Lrig3* are likely to be expressed at similar levels across the three populations, therefore any confounding is likely to be comparable between the groups.

The low detection of *Lrig1* transcript (along with other genes in the gene expression analysis) within group 2 (LRIG1^{+} basal cells from LRIG1-heterozygous mice) may be explained by the stability of the *Lrig1* transcript or that a low number of transcripts are present per cell. *Lrig1* transcripts are detectable by sc-RNA seq (221), this has

been shown in the sequencing of gut epithelial cells where *Lrig1* transcript expression levels correlate to those of *Lgr5* and *Hopx*, implying *Lrig1* transcript stability should not pose a problem. A further consideration is the length of the *Lrig1* transcript. There are different methods by which sc-RNA seq is performed and the cDNA is amplified. My samples underwent the SMART-seq method of RNA amplification, where there is the attachment of a universal primer sequence to either end of the transcripts prior to cDNA amplification. This gives a wide coverage of the transcriptome, but is subject to a transcript length bias, where there are low read counts for long RNAs (222). The *Lrig1* transcript is 4966 base pairs and the average mammalian mRNA size is 1400 base pairs (223); the length of *Lrig1* transcript may therefore result in lower than anticipated *Lrig1* reads.

Unfortunately, sc-RNA seq does not give a fully comprehensive view of the transcriptome. Whilst sc-RNA seq is reflective of highly expressed genes, during the sequencing process the loss of RNA transcripts may be as high as 50-60%. These losses have been shown to be greatest for low abundant transcripts (at a concentration of less than 5-10 copies/cell) (224). In addition, when transcripts are expressed at low levels (with less than 10 copies per cell) the sensitivity of sc-RNA seq is limited, and it becomes challenging to distinguish between the 'technical noise' of the experiment and any biological variability, for example, when cells of the same type are at different phases of the cell cycle leading to variations in gene expression that are detected in the sequencing. It then becomes challenging to determine a differentially expressed gene from those with background variability (224).

4 different genes were reported as differentially expressed between groups 2 ($LRIG1^+$ basal cells from LRIG1-heterozygous mice) and 3 ($LRIG1^-$ basal cells from LRIG1-heterozygous mice). It is remarkable that there are so few, given that these two populations have different phenotypes. I was expecting to see changes in either the proliferation or stem cell signatures, but three of the genes (*Col1a1*, *Col1a3* and *Mgp*) encode secretory proteins that are involved in the extracellular matrix formation or bone production and the fourth (*Tpm2*) is found in the cytoskeleton

(215-217). The significance of these genes is uncertain, and due to the difficulties that I have encountered in the sc-RNA seq process may not be of biological relevance in distinguishing the three groups.

On consideration, sc-RNA seq may not have been the most appropriate choice of assay when attempting to distinguish the subtleties between very similar cell populations. Single cell RNA sequencing was used successfully by Treutlein et al to analyse the populations of the distal airway (214). The different cell types of the distal airway were identifiable through differential gene expression, but each of the cell types within the distal airways has very different transcriptomes. By contrast, my experiments were analysing a single cell type, and attempting to detect smaller changes in a more homogeneous population. In order to meaningfully do this a far greater cell number would be required.

A significant limitation of this sc-RNA seq analysis is that genes were only included in the assessment if they were detectable in more than 10 cells. By restricting the analysis to this extent, the overall sensitivity and the ability to detect small changes in a heterogeneous population is reduced. In one of the analysed groups there were only 28 cells, therefore if a gene is discriminatory for this population (and only expressed in these cells) it would need to be detected in almost a third of cells to be considered (and by the nature of sc-RNA seq the detection of transcripts in each cell is extremely variable). Treutlein *et al* used 80 cells in their analysis and considered genes that were expressed in more than 2 cells (214); this would have allowed smaller changes and fluctuations in the cell populations to be identified.

There are alternatives to sc-RNA seq and, should time have allowed, could have been considered in the analysis of the airway basal cell populations. Using qPCR, as demonstrated by Watson *et al* (202) on single, isolated airway epithelial cells could be an alternative, however this introduces bias, as the probes used for the qPCR need to be selected by the investigator and there is a limit to the number of reactions that can be run on each sample. Watson *et al* successfully isolated single epithelial cells by digesting a murine trachea and loading these onto a C1 Fluidigm

(202) for subsequent qRT-PCR. A selection of 67 genes were chosen for analysis and, although only 17 basal cells were included in their population (making it is difficult to determine how representative these few cells are of the entire basal population), clear differences in the gene expression profiles revealed that KRT8 identified an airway basal cell subpopulation. Jensen *et al* isolated single keratinocytes and amplified cDNA to use in microarray platforms. In total, the amplified cDNA from 12 cells was analysed (six cells from two populations of interest). The differences in expression levels were only considered significant after a 7-fold increase (due to the sensitivity of transcript detection), the data collection was unbiased and led to the identification of LRIG1 as a discriminator between the stem cell and transit-amplifying populations of the skin (79). The advantages of this technique have been shown in a more recent publication (225) where single cell expression profiling of 18 cells showed heterogeneity within undifferentiated keratinocytes and showed that the expression of delta-like 1 (*Dll1*) was associated with genes associated for endocytosis, integrin-mediated adhesion and receptor tyrosine kinase signalling.

McConnell *et al* (208), have recently published sc-RNA seq data looking at heterogeneity within the murine airway club cell population according to the presence or absence of p53 expression. They identified 4 different club cell subpopulations, with the four clusters containing various proportions of markers for the proximal and distal airway club cell subtypes. The relative proportions of these populations changed on the loss of *p53*. These experiments are interesting as the methods used were very similar to mine, with both designed to detect small variations within subpopulations of the airway epithelium (club cells compared to basal cells). Both protocols required enzymatic digestion to release the epithelial cells, followed by FACS for an $EpCAM^{+}$, $eGFP^{+}$ cell population and then the use of the C1 Fluidigm for sample preparation prior to sequencing. However, in contrast to my results, McConnell *et al* were able to detect distinct patterns and perform pathway analysis, finding that loss of *p53* influenced cell cycle-regulatory genes. Therefore small differences should be identifiable within my sc-RNA seq samples.

In summary, the conclusions I can draw from the sc-RNA seq data are limited. I have been unable to successfully confirm that the cells used expressed eGFP, Cre or indeed LRIG1 at the anticipated levels. Whilst there are potential explanations, this raised some concerns about the validity of the findings. There is an indication that group 3 ($LRIG1^-$ basal cells from LRIG1-heterozygous mice) may separate from groups 1 ($eGFP^+$, LRIG1-null basal cells) and 2 ($LRIG1^+$ basal cells from LRIG1-heterozygous mice), but this is not a clear, well-defined separation and this does not occur based on the expression of a single gene, but instead through small elevations in the expression of a number of genes. There are no clearly differentially expressed genes between groups 1 ($eGFP^+$, LRIG1-null basal cells) and 2 ($LRIG1^+$ basal cells from LRIG1-heterozygous mice) that are the $eGFP^+$ cells from LRIG1-null mice and the $LRIG1^+$ from LRIG1 heterozygous mice. It was intended that the differences between groups 1 ($eGFP^+$, LRIG1-null basal cells) and 2 ($LRIG1^+$ basal cells from LRIG1-heterozygous mice) would give an understanding as to the effects of loss of LRIG1 and the development of preinvasive lung cancer. By looking at the differences in the gene expression profiles I was hoping to build the rest of the project on looking for therapeutic candidates that may reverse the changes seen in preinvasive disease. By analysing groups 2 ($LRIG1^+$ basal cells from LRIG1-heterozygous mice) and 3 ($LRIG1^-$ basal cells from LRIG1-heterozygous mice), I was expecting to be able to explain the differences in proliferation and stem cell characteristics of $LRIG1^+$ and $LRIG1^-$ cells that I have demonstrated using cell culture assays. Unfortunately, there are only four genes that appear to distinguish groups 2 ($LRIG1^+$ basal cells from LRIG1-heterozygous mice) and 3 ($LRIG1^-$ basal cells from LRIG1-heterozygous mice) and in isolation it is difficult to determine their biological significance.

I have shown a method for the isolation of single tracheal cells and optimised the FACS process. I have also shown that despite the prolonged experimental times, the RNA quality is preserved. Re-analysis of this preliminary data set to include genes that are expressed in more than two cells would improve the sensitivity of my data and should be performed. In addition, I have demonstrated that my FACS strategy gives a clear epithelial population, so I could analyse the sorted cells using alternative methods of gene expression analysis.

4.5 Summary

- LRIG1^{+} basal cells are more proliferative than LRIG1^{-} basal cells (from LRIG1-heterozygous mice).
- LRIG1^{+} basal cells show an increased spheroid- and colony-forming efficiency compared to LRIG1^{-} cells.
- The loss of LRIG1 in eGFP^{+} basal cells from LRIG1-null mice does not influence either cell proliferation or spheroid- or colony-forming efficiency.
- sc-RNA seq may not be sensitive enough to distinguish between the three cell populations (at the cell numbers used) and alternative methods to determine differential gene expression should be explored.

5. Assessment of LRIG1 in the Human Airway

5. Assessment of LRIG1 in the Human Airway

5.1 Background

The loss of leucine rich repeats and immunoglobulin-like domains 1 (LRIG1) has been associated with the development and the aggressiveness of a number of human malignancies. In the airway, LRIG1 loss is seen in the development of preinvasive squamous cell cancers (104) and it has a prognostic impact on the outcome of non-small cell lung cancer (NSCLC) (105, 226). Our understanding of the effects and role of LRIG1 have largely been determined through the use of *Lrig1* knockout mouse models or *in vitro* cell lines derived from tumour cells. A number of differences exist between the mouse and human airway, particularly in relation to the anatomy and the extent of pseudostratified epithelium that contains basal cells-the putative cell of origin of squamous cell carcinoma. In the mouse, the basal cells are located within the trachea, but in humans they are distributed further down the airway into the smaller bronchi (227).

I have shown that in the mouse, LRIG1-expressing basal cells have a clear phenotype. The murine LRIG1-expressing cells are more proliferative and exhibit an increase spheroid-forming and colony-forming capacity. By assessing whether the human airway also contains populations of $LRIG1^{+}$ and $LRIG1^{-}$ basal cells and whether these populations have different phenotypes, I can determine if the results I have shown in mice are relevant to humans.

After examining the role of LRIG1 in the normal human airway, the effect of loss of LRIG1 can be determined. *LRIG1* gene expression is downregulated in squamous cell lung cancers compared to that of the normal epithelium (30) and during the development of preinvasive lung cancer lesions, *LRIG1* gene expression is reduced (104). By using *LRIG1* shRNA knock down in primary human bronchial epithelial cells (HBECs) obtained from patients, the changes that occur when LRIG1 is lost in the airway can be mirrored in an *in vitro* system.

Primary derived HBECs can undergo only limited passages in the traditionally used bronchial epithelial cell growth medium (BEGM) culture conditions before they undergo senescence (171). With increasing passage, HBECs show a reduction in their ability to differentiate into the different cell types of the respiratory epithelium. The use of 3T3 + Y culture conditions (171, 228, 229), where HBECs are grown on a mitotically inactivated 3T3-J2 feeder layer in the presence of the RHO-associated protein kinase inhibitor, Y-27632, enables on-going passage and means that they are capable of ciliated differentiation (171). The use of Y-27632 has been further shown to facilitate the lentiviral transduction of keratinocytes (230) and airway epithelial cells (231). Therefore, by using 3T3 + Y culture conditions, knockdown of LRIG1 expression in primary HBECs can be achieved.

5.2 Aims

- To assess where LRIG1 is expressed in the human airway
- To assess whether LRIG1^{+} basal cells have a different phenotype to LRIG1^{-} basal cells
- To knockdown *LRIG1* expression in primary human airway cells using shRNA techniques
- To examine how loss of LRIG1 influences cell behaviour

5.3 Results

5.3.1 Expression of LRIG1 within the human airway

To confirm the presence of LRIG1 in the human airway (104), sections of human bronchial epithelium were analysed by immunofluorescence (Figure 5.1.A). This showed clear LRIG1 expression in the basal cells that are adjacent to the basement membrane. Although appearing to be more concentrated within the basal cell compartment, the expression of LRIG1 was visible within the other cell types of the epithelium. Of note, and similarly to in the mouse, there were LRIG1-positive cells

beneath the basement membrane. These were keratin 5 (KRT5) negative, and likely to be fibroblasts (Figure 5.1.A).

To establish whether there was an LRIG1-expressing and LRIG1-negative airway basal cell population, as in the mouse, human airway epithelial cells were examined by flow cytometry. Human bronchial epithelial cells were obtained at bronchoscopy via endobronchial brushings. In contrast to murine airway epithelial cells, where their collection had proved challenging due to the need for enzymatic digestion, the human endobronchial brushings were simply placed into medium and vortexed to release the brushed cells; this negated the need for a digestion step. The brush biopsies were taken from a normal area of airway epithelium in patients undergoing bronchoscopy either for the initial investigation of possible airway disease or as part of our surveillance programme for preinvasive lesions. Abnormal areas of possible preinvasive disease were excluded using autofluorescence bronchoscopy and a bronchial biopsy was taken from the same area. If the associated bronchial biopsy showed any preinvasive disease, malignancy or other abnormality, the samples were not included in subsequent analysis. Once collected, the cells were stained for flow cytometry. $CD45^+$, $CD31^+$ cells and dead cells were excluded and basal cells were identified using the markers integrin α6 and nerve growth factor receptor (NGFR) (130). The basal cells were then divided into $LRIG1^+$ and $LRIG1^-$ populations (Figure 5.1.B).

The $LRIG^+$ and $LRIG1^-$ populations were less clearly defined than in the mouse, and a 'shift' in the population on LRIG1 staining was seen, rather than two well-defined populations. To determine the $LRIG1^+$ and $LRIG1^-$ populations the flow cytometry gate was set using the 'fluorescence minus one' control. Overall, the proportions of $LRIG1^+$ and $LRIG1^-$ cells were similar (50%) in each donor, however a large inter-patient variability was seen (Figure 5.1.C).

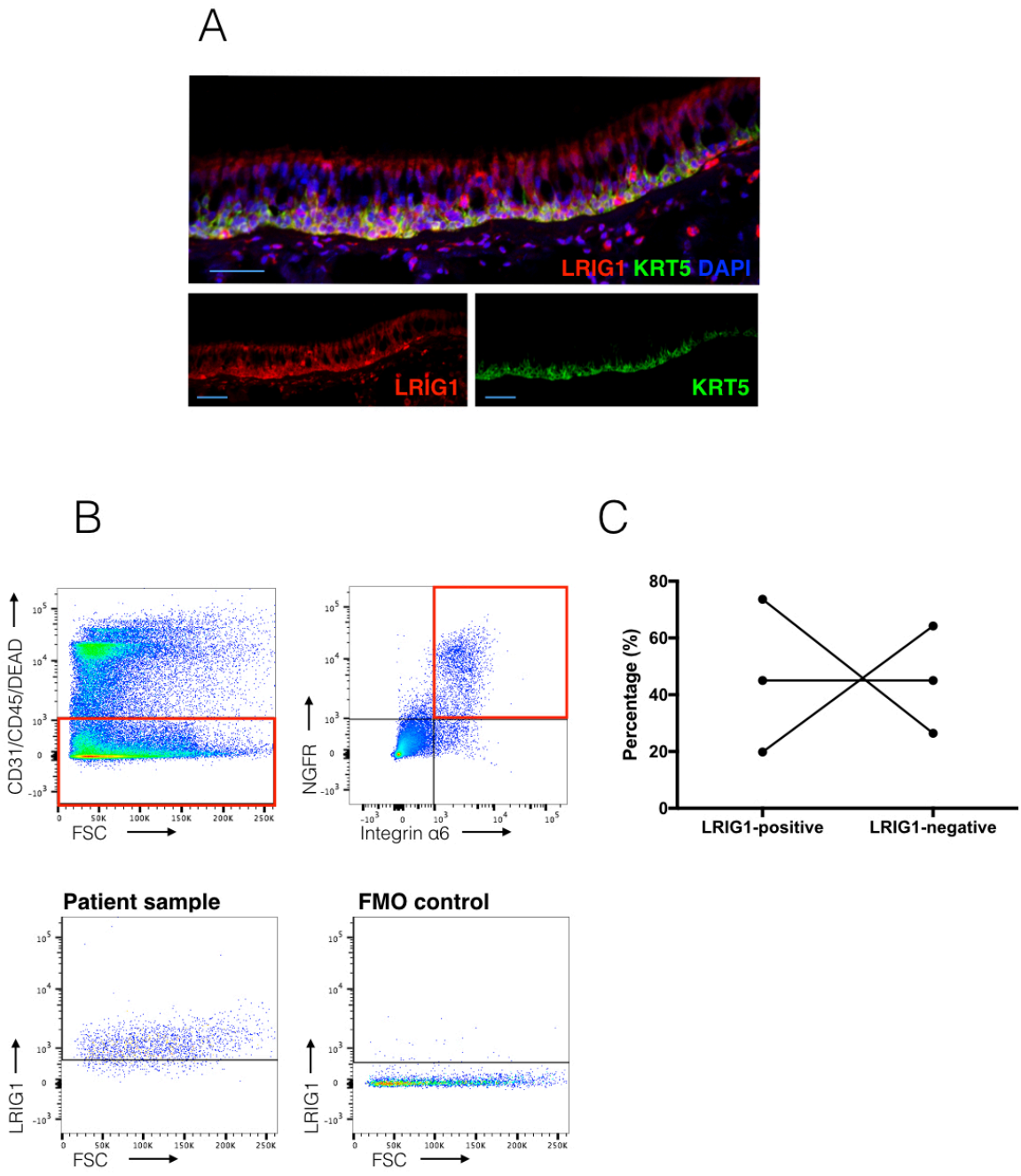

Figure 5.1: Expression of LRIG1 in human airway basal cells

A) Immunofluorescence staining of a fresh frozen section of human airway for LRIG1 (red) and keratin 5 (KRT5; green). Note increase in LRIG1 staining within the basal cell compartment (dual stained with KRT5). Smaller images show LRIG1 staining (red) and KRT5 staining (green). DAPI used as a counterstain. Scale bar = 50 µm. B) Flow cytometry to detect a population of LRIG1$^+$ basal cells within the human airway epithelium. Red boxes show population that is taken forwards. Initially there is negative selection for CD31$^+$, CD45$^+$ and live/dead cell populations. There is then positive selection for integrin α6$^+$, NGFR$^+$ basal cells. The basal cells are next assessed for LRIG1 expression. The final flow cytometry plot shows the population of basal cells in the 'fluorescence minus one' (FMO) control for PE. The FMO was used to place the gate for the LRIG1$^+$ and LRIG1$^-$ populations. Antibodies were used in the following colours: CD31- and CD45-BV421, Live/dead-DAPI, integrin α6$^+$-APC, NGFR-PE-Cy7, LRIG1-PE; n = 5. C) Proportions of LRIG1$^+$ and LRIG1$^-$ basal epithelial cells obtained from brush biopsies; n = 3.

5.3.2 Colony-forming efficiency of LRIG1$^+$ versus LRIG1$^-$ basal cells

In the murine airway, LRIG1 marks a more clonogenic population of basal cells. To investigate whether this finding was similar in the human, human basal cells were sorted into LRIG1$^+$ and LRIG1$^-$ populations. The brushes were taken from areas of normal epithelium with the patient characteristics shown in supplementary table 1. Cells were sorted into 96-well plates, directly onto mitotically inactivated 3T3-J2 feeder cells and grown in medium containing Y-27632. At 2 weeks, the numbers of colonies that formed from LRIG1$^+$ cells were compared to those from LRIG1$^-$ cells (Figure 5.2.A). For one of the patient samples, there were fewer than the 96 basal cells required to fill a plate, therefore the maximum possible number of cells was sorted and equal numbers of LRIG1$^+$ and LRIG1$^-$ basal cells collected. The percentage of cells that formed colonies was expressed as a percentage of the total number of cells plated. Overall LRIG1$^+$ basal cells were significantly more clonogenic than LRIG1$^-$ ($p = 0.0067$) (Figure 5.2.B).

As there was no clearly defined LRIG1$^+$ and LRIG1$^-$ cell populations, index sorting was used to establish whether a correlation existed between the degree of LRIG1 expression and how likely the cell was to form a colony. The index sorting showed no relationship between the degree of LRIG1 expression and colony development (Figure 5.2.C), and the cells that grew were spread across the plot.

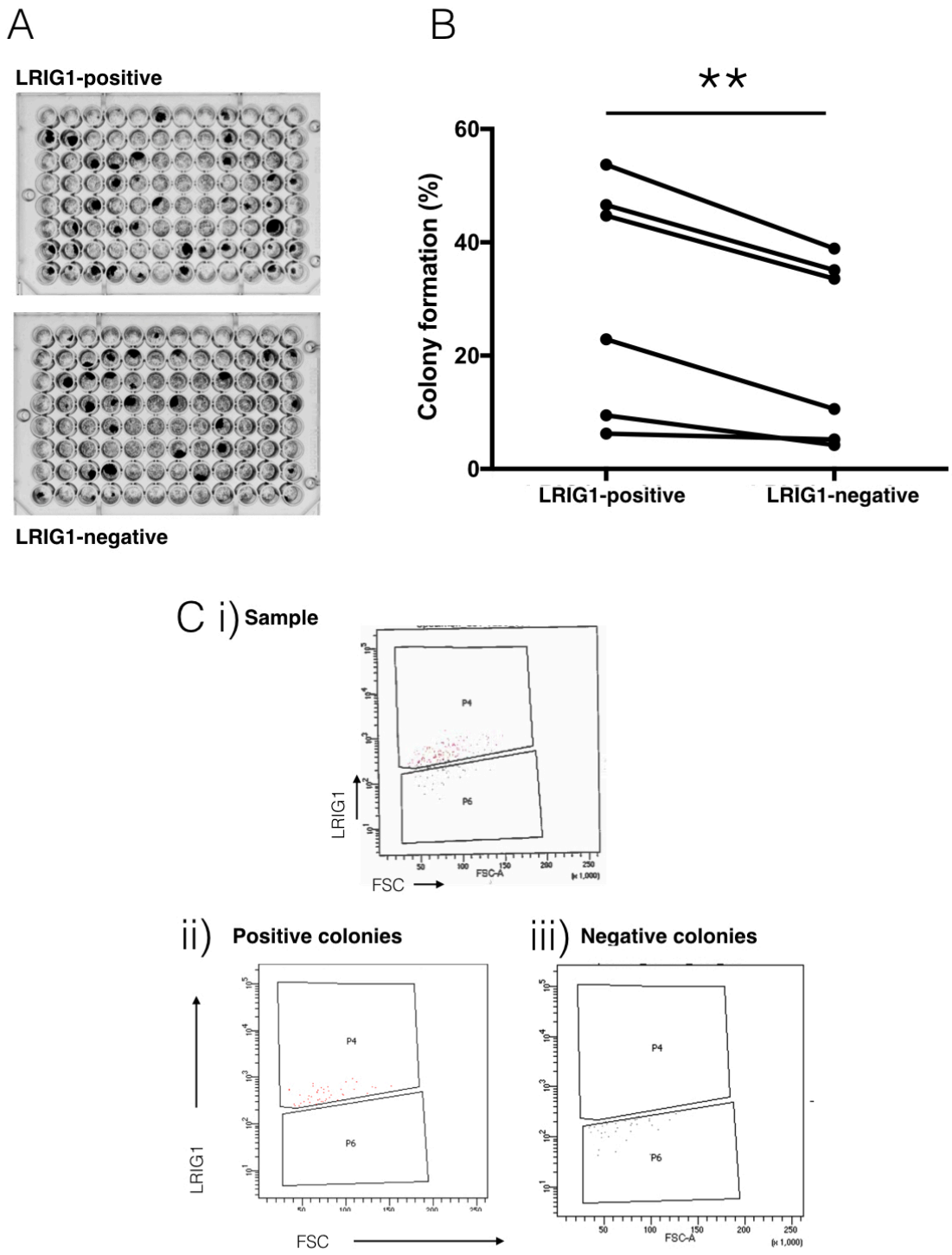

Figure 5.2: Colony formation in LRIG1$^+$ and LRIG1$^-$ epithelial cells obtained at bronchoscopy

A) Examples of colony formation within a 96-well plate. After 2 weeks, the cells are fixed and stained with crystal violet and cells that have formed colonies can be clearly seen. The number of colonies forming from LRIG1$^+$ basal cells (upper image) are then compared to the number of colonies forming from LRIG1$^-$ basal cells (lower image). Image representative of n = 6. B) Colony formation in flow cytometry sorted LRIG1$^+$ and LRIG$^-$ basal cells. Dots indicate individual patients with the positive and negative samples for each patient joined by a line. Statistical analysis was performed using a paired t-test, ** indicates $p<0.01$. C) Index sorting shows the degree of LRIG1 staining is not related to the likelihood of a cell forming a colony. i) Flow cytometry plot for airway basal epithelial cells, with the upper gate showing LRIG1-positive basal cells and the lower gate LRIG1-negative. ii) Flow cytometry plot showing the levels of expression of LRIG1 in the LRIG1$^+$ basal cells that grew into colonies. iii) Flow cytometry plot showing the levels of expression of LRIG1 in the LRIG1$^-$ basal cells that grew into colonies.

5.3.3 The proliferation of LRIG1$^+$ versus LRIG1$^-$ basal cells

LRIG1-expressing epithelial cells within the murine skin and gut are more proliferative than LRIG1-negative basal cells (91, 93) and I have also shown that LRIG1$^+$ basal cells in the murine airway are more proliferative than LRIG1$^-$ basal cells. To establish whether LRIG1$^+$ basal cells in the human airway were more proliferative than LRIG1$^-$ basal cells Hoescht 33342 was used. Cells were obtained from bronchial brushings, with patient characteristics for this experiment detailed in supplementary table 1. Endothelial and immune cells were removed by excluding the CD31$^+$ and CD45$^+$ populations respectively, and a viability dye was used to eliminate dead cells. As previously, basal cells were selected by their positive expression of integrin α6 and NGFR. Due to the limited number of cells obtained from a brush, samples were excluded that contained less than 750 basal cells. The basal cells were then divided into LRIG1$^+$ and LRIG1$^-$ populations and Hoescht 33342 staining used to establish the proportion of proliferative cells in the G2/M phase of the cell cycle (Figure 5.3.A).

In total, samples were obtained from 8 patients. 3 of these were excluded due to low basal cell numbers (although the proliferation phenotypes within the LRIG1$^+$ and LRIG1$^-$ populations showed the same behaviour as samples containing higher basal cell numbers). A further patient was excluded due to the Hoescht 33342 staining being inadequate (the two peaks that corresponded to Hoescht 33342 uptake were not visible). Collating the 4 patients with adequate basal cell numbers and Hoescht 33342 staining, it was clear that LRIG1$^+$ basal cells were more proliferative than LRIG1$^-$ basal cells (Figure 5.3.B). This is statistically significant ($p = 0.0153$) and confirms the findings in the murine airway, skin and gut, where LRIG1$^+$ epithelial cells are more proliferative than LRIG1$^-$.

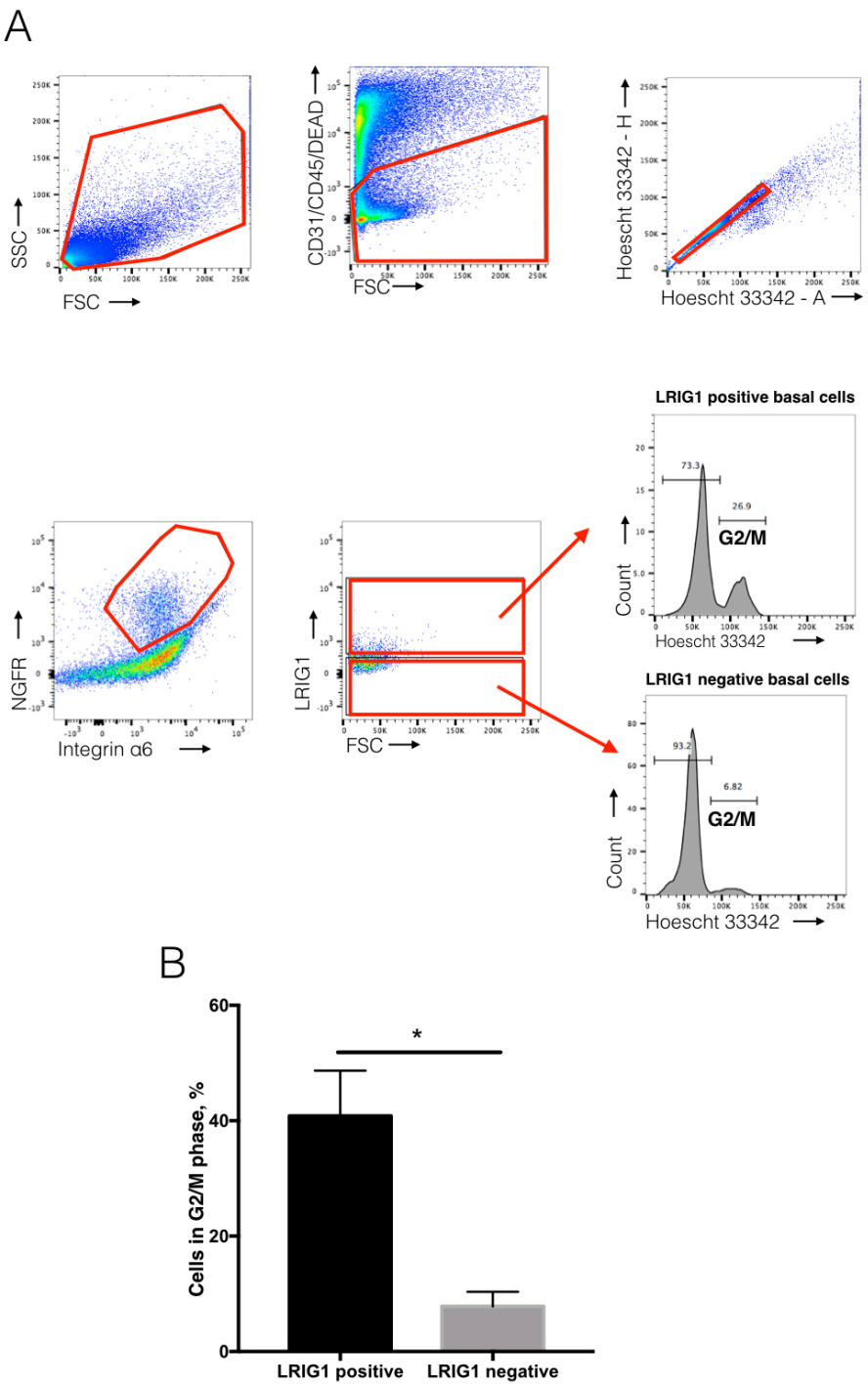

Figure 5.3: Proliferation of LRIG1$^+$ and LRIG1$^-$ human basal cells obtained at bronchoscopy

A) Flow cytometry plots showing the proliferation of LRIG1+ and LRIG1- basal cells. The first plot shows FSC against SSC, with removal of the cell debris (bottom left corner), followed by the negative selection of CD31$^+$ and CD45$^+$ cells and dead cells. Single cells are obtained through comparing the Hoescht 33342-Area to Hoescht 33342-Height. Next, basal cells are isolated through the selection of integrin α6$^+$ and NGFR$^+$. The basal cells are assessed for expression of LRIG1, and LRIG1$^+$ and LRIG1$^-$ cells analysed for Hoechst 33342 uptake. Red gates indicate the population of interest that is analysed in the next plot. The proliferative cells in the G2/M phase of the cell cycle are indicated on the plot. Antibodies were used in the following colours: CD31- and CD45- APC, live/dead-sytox red, integrin α6$^+$-APC-Cy7, NGFR-PE-Cy7, LRIG1- PE. Plots representative of n = 4. B) Proliferation of human LRIG1$^+$ and LRIG1$^-$ basal cells. Statistical analysis was performed using a paired t-test, * indicates $p<0.05$, mean ± SEM, n = 4.

5.3.4 shRNA knockdown of *LRIG1* in human epithelial cells

As LRIG1 is lost in preinvasive lung cancer, I wanted to determine the effect on cell behaviour when LRIG1 is lost in airway basal cells. In Chapter 4 I showed there was no effect of the absence of LRIG1 in a constitutively null LRIG1 animal, possibly due to other factors compensating for the loss or a redundancy of LRIG1 in the airway. By knocking down LRIG1 expression in human basal cells I wanted to more closely recapitulate the LRIG1 loss that occurs in preinvasive lung cancer and allow the effect of LRIG1 loss in airway epithelial cells to be examined in more detail.

Primary HBECs, isolated from patients at bronchoscopy, were obtained from the laboratory's primary cell bank. The cell isolation strategy and culture conditions lead to the culture of a pure airway basal cell population (171). In total, samples from 4 patients were included in the assessment of the effect of *LRIG1* shRNA knock down. Their details are included in supplementary table 1. The cells were grown on mitotically inactivated 3T3-J2 feeder layers in medium containing a rho-associated kinase inhibitor, Y-27632 (3T3 + Y culture conditions) and all 4 patient samples were shown to express LRIG1 by immunoblotting prior to shRNA knock down (Figure 5.4.C). Due to the heterogeneous nature of primary HBECs, and that these differences may lead to variability in susceptibility to *LRIG1* shRNA knock down, lentivirus was made from all three commercially available *LRIG1* shRNA plasmids. The production of virus was confirmed by successfully transducing HEK293T cells and the addition of serial viral dilutions to plated HEK293T cells allowed the viral titre to be quantified (Figure 5.4.A).

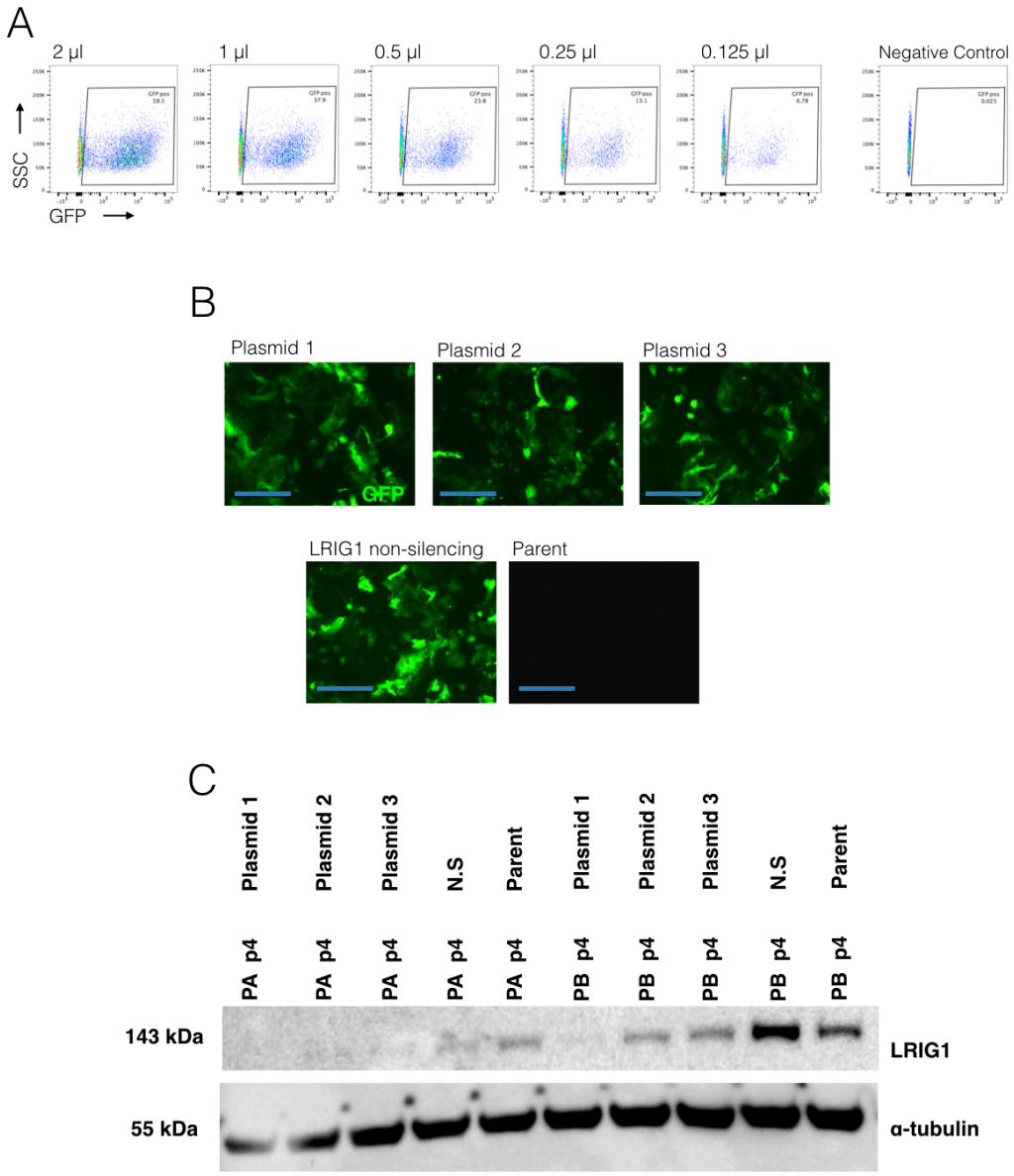

Figure 5.4: *LRIG1* shRNA knockdown in primary human bronchial epithelial cells (HBECS)

A) Flow cytometry plots showing successful production of virus in HEK293T cells. GFP indicates the transduced population. Amount of virus added to each well of a 6-well plate indicated above the plot. Serial dilutions added to allow the calculation of viral titre. B) Successful transduction of human epithelial cells (PA). GFP (green) indicates the successful transduction. All 3 plasmids are associated with a successful transduction. Parent control remains untransduced. Scale bar = 50 µm. Images representative of 4 patient samples. C) Immunoblotting showing the successful knockdown of LRIG1 protein in transduced samples. LRIG1 is seen at a weight of 143 kDa. Lanes correspond with samples 1. PA p4 plasmid 1 (where p4 indicates the cell passage number), 2. PA p4 plasmid 2, 3. PA p4 plasmid 3, 4. PA p4 non-silencing (N.S), 5. PA p4 parent cells, 6. PB p4 plasmid 1, 7. PB p4 plasmid 2, 8. PB p4 plasmid 3 9. PB p4 non-silencing (N.S), 10. PB p4 parent cells. Blot representative of two blots, one for cell lines PA and PB and other for cell lines PC and PD.

Once quantified, all three viruses were used to transduce human epithelial cells at an MOI of 3. As the epithelial cells were transduced on a feeder layer of mitotically inactive 3T3-J2 feeder cells, the number of feeder cells was included in the calculation of MOI. A non-silencing, scrambled shRNA control was used alongside the *LRIG1* knockdown samples at the same MOI. All the *LRIG1* shRNA plasmids, as well as the non-silencing control, contained a GFP reporter. At 48 hours post transduction the cells became GFP-positive, indicating transduction success (Figure 5.4.B). After 72 hours of puromycin selection, the cells were expanded for use in subsequent assays.

Knockdown of LRIG1 was confirmed by immunoblotting for LRIG1 protein (Figure 5.4.C). As the 3T3-J2 cells express LRIG1 (LRIG1 is a negative inhibitor of PDGFRα found in fibroblasts (77)), once the transduced epithelial cells were confluent, the feeder layers were removed by differential trypsinisation. Trypsin cleaves LRIG1, so following J2-3T3 removal, the medium was replaced and the epithelial cells incubated overnight to allow LRIG1 protein recovery. The following morning the cells were lysed and protein samples collected for immunoblotting. The effects of the shRNA knockdown by all three *LRIG1* shRNA plasmids were compared to both the non-silencing control and to the parental non-transduced cells (Figure 5.4.C). The transduction and assessment of LRIG1 protein knockdown was repeated in all four patients. In each of the four patient-derived HBEC samples, plasmid 1 showed the greatest LRIG1 knockdown and therefore the HBECS transduced with plasmid 1 were expanded and used in subsequent experiments.

5.3.5 Effect of *LRIG1* shRNA knockdown on EGFR activation

LRIG1 downregulates epidermal growth factor receptor (EGFR) signalling and, following the loss of LRIG1, an upregulation and activation of EGFR signalling, as well as activation of the downstream extracellular signal-regulated kinase (ERK) pathway, has been detected in keratinocytes (79). To confirm that loss of LRIG1 in HBECs was exerting its effects through action on the EGFR signalling

pathway, cells were immunoblotted for EGFR, phospho-EGFR (Y1068 site), p44/42 ERK and phospho-p44/42 ERK.

Protein levels were assessed in patient samples that had been starved for 16 hours prior to incubation with and without 10 ng/ml of EGF for 30 minutes and then lysates were collected. This dose and timing has previously been shown to trigger phospho-EGFR activation in human airway epithelial cells (232). Following *LRIG1* shRNA knockdown there was an increase in both phospho-EGFR and phospho-ERK proteins, confirming that loss of LRIG1, a negative inhibitor of EGFR, leads to both an upregulation in EGFR signalling, along with the activation of downstream pathways (shown through increased phospho-ERK). This effect was not seen in the absence of EGF stimulation (Figure 5.5). Two patient samples were analysed, with the displayed blots representative of both (each run in duplicate).

Of note, I have seen through these optimisation experiments that the degree of LRIG1 expression detectable by immunoblotting is associated with degree of cell confluence. When the cells are not confluent, there is a dramatic reduction in LRIG1 protein. Cells were lysed at similar levels of confluence, although as discussed later, the *LRIG1* shRNA knockdown cells proliferate more rapidly than the parent or the *LRIG1*-expressing non-silencing controls.

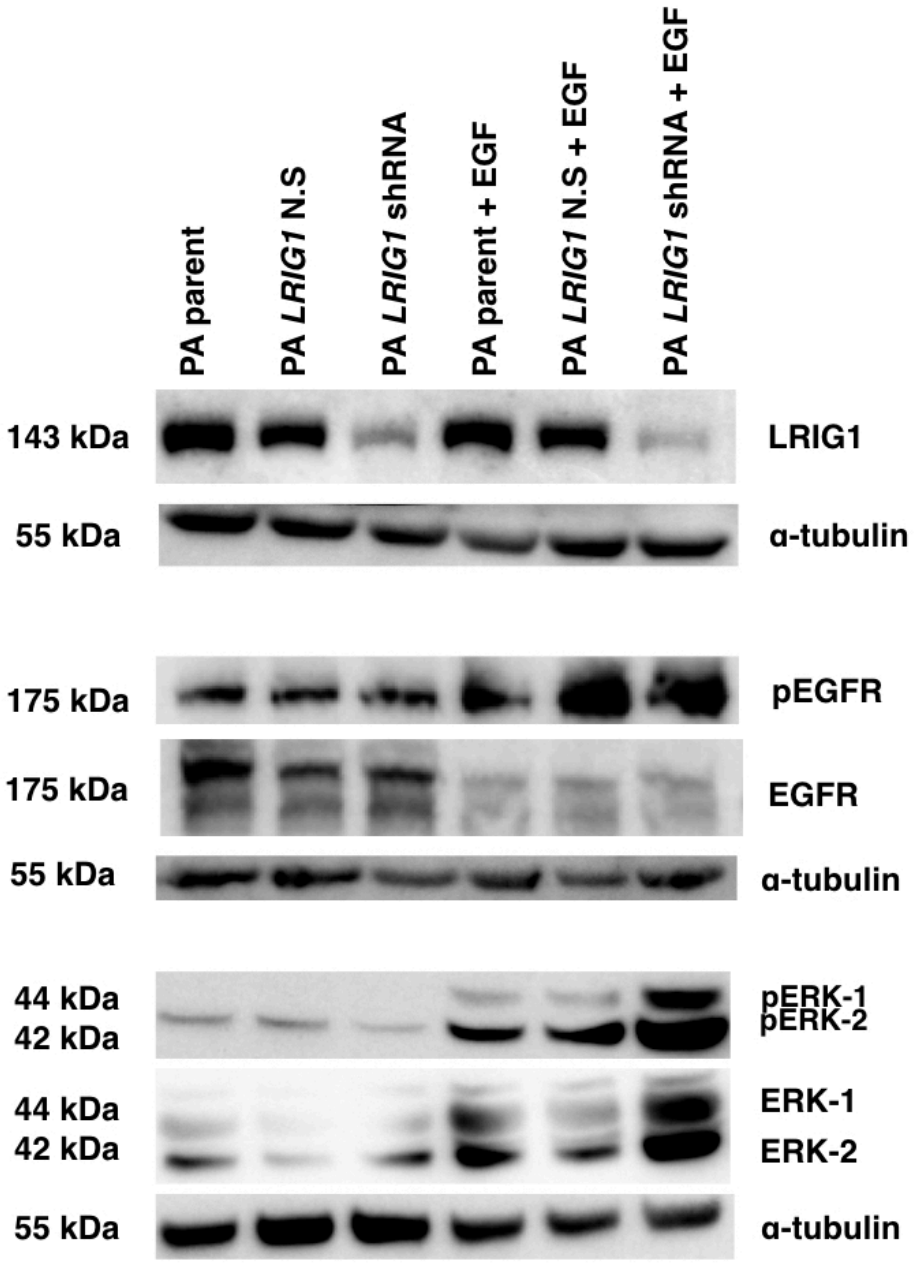

Figure 5.5: shRNA knockdown of *LRIG1* leads to increased EGFR activation

Immunoblotting for LRIG1 (143 kDa), EGFR (175 kDa), phospho-EGFR (175 kDa), ERK (42 and 44 kDa) and phospho-ERK (42 and 44kDa) in lysates from parent, *LRIG1* non-silencing (N.S) and *LRIG1* shRNA-transduced cells. Samples were starved for 16 hours and stimulated with or without EGF at 10 ng/ml for 30 minutes. Protein loading control was α-tubulin, displayed beneath the blots. Blots representative of n = 2, with experiments performed twice in two different patient cell lines. Blot shown for PB p7

5.3.6 The effect of *LRIG1* shRNA knockdown on colony-forming ability

LRIG1 siRNA knockdown in skin keratinocytes, compared to a non-scrambled control, leads to increased colony formation (79). Colony forming assays measure a cell's stem cell potential as they measure the ability of the cell to self-renew (211). In both mice and humans, I have shown that LRIG1^{+} basal cells are more clonogenic than LRIG1^{-} basal cells. To assess whether the knockdown of *LRIG1* in an LRIG1-expressing population of human basal cells (as demonstrated in Figure 5.4.C) leads to increased colony formation, the number of colonies formed in *LRIG1* shRNA knockdown cells was compared to that of the *LRIG*-expressing non-silencing shRNA control.

Cells were grown on mitotically inactivated 3T3-J2 feeder layers in 6-well plates. The number of colonies formed from 1000 seeded cells was counted at 10 days. The *LRIG1* shRNA knockdown cells were compared to the *LRIG1*-expressing non-silencing controls (Figure 5.6.A). Although not significant, there was a clear trend in the data, with *LRIG1* shRNA knockdown in all 4 of the patient cell lines leading to an increase in colony formation (Figure 5.6.B).

A

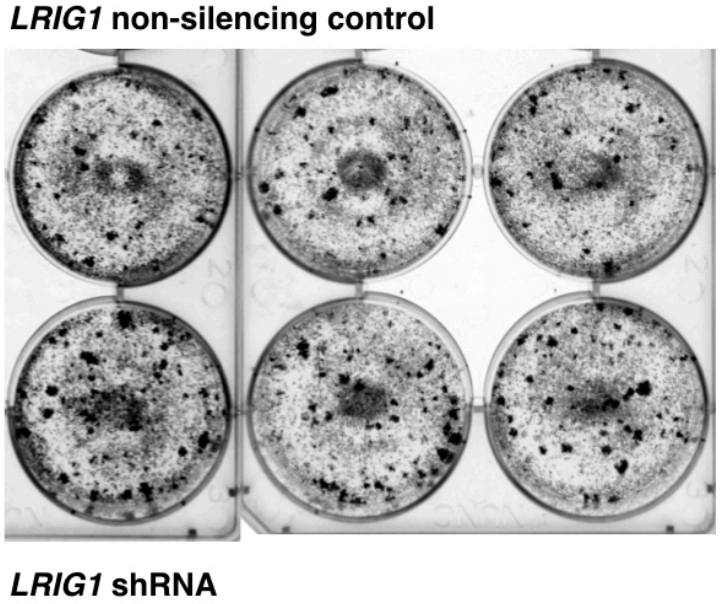

B

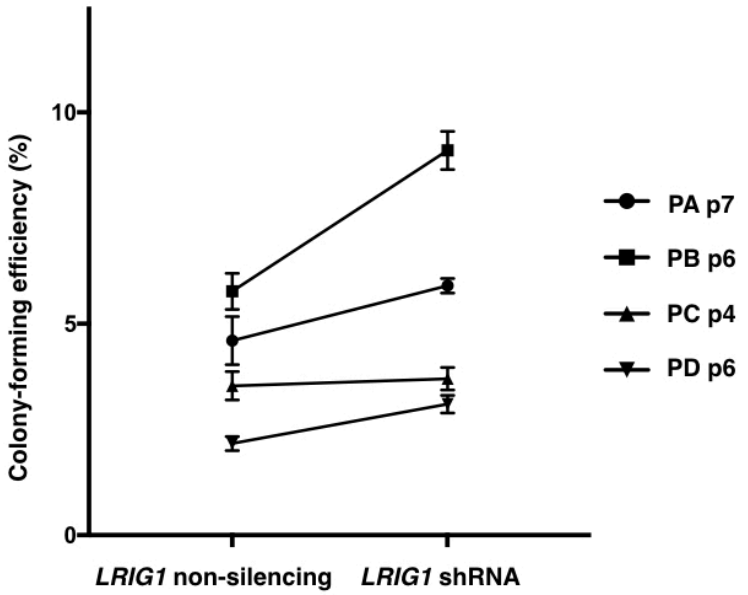

Figure 5.6: Knockdown of *LRIG1* leads to increased colony formation in HBECs

A) Example of colony-forming assay. 1,000 HBECs were plated, in triplicate, per well of a 6-well plate. These were fixed and stained with crystal violet. Colonies that grew to greater than 10 cells were included in the analysis. B) The colony-forming efficiency in HBEC cells with and without *LRIG1* knockdown. Samples performed in triplicate with mean ± SEM displayed. Statistical analysis was performed using a paired t-test, p = 0.1269, n = 4.

5.3.7 The effect of *LRIG1* shRNA knockdown on cell proliferation; optimising the EdU assay

Lu *et al* have shown that when using cells from an *Lrig1*-knockout mouse, the loss of LRIG1 prevents cell-cell contact inhibition and leads to on-going proliferation at cell confluence (104). If this were to occur within the human epithelium this may explain the development of preinvasive lesions and how loss of LRIG1 may lead to a poor outcome from NSCLC.

To assess cell proliferation and the effects of contact inhibition, cells were incubated with EdU, a synthetic thymidine analogue, for analysis by flow cytometry. To confirm reported incubation and uptake times (171), EdU uptake was examined and optimised in one patient. As the addition of Y-27632 leads to increased cellular proliferation beyond the proliferation rate seen in the traditionally used BEGM culture conditions (231) and with growth of cells on 3T3-J2 feeder layers having an additive effect (233), I was concerned that 3T3 + Y culture conditions may cause an artificial increased proliferation phenotype, and that any subtle differences in proliferation resulting from the loss of LRIG1 may be lost. To establish if this may be an issue, this preliminary experiment assessed cells grown in both 3T3 + Y and BEGM conditions, both at sub-confluence and confluence.

This trial showed no difference in the EdU uptake of *LRIG1* shRNA knockdown cells or the *LRIG1*-expressing non-silencing control cells grown in 3T3 + Y conditions, either at subconfluence or confluence (Figure 5.7.A and 5.7.B), possibly as a consequence of the above mentioned factors. In fact, at confluence, in 3T3 + Y conditions, no EdU^+ cells were detected in either *LRIG1* shRNA knockdown cells or the non-silencing control cells, suggesting no proliferation was occurring and cells were contact inhibited. In BEGM, EdU uptake was noted to be similar at sub-confluent conditions (Figure 5.7.C), but the proliferation in the *LRIG1* shRNA knockdown conditions at cell confluence was twice that of the *LRIG1*-expressing, non-silencing controls (Figure 5.7.D).

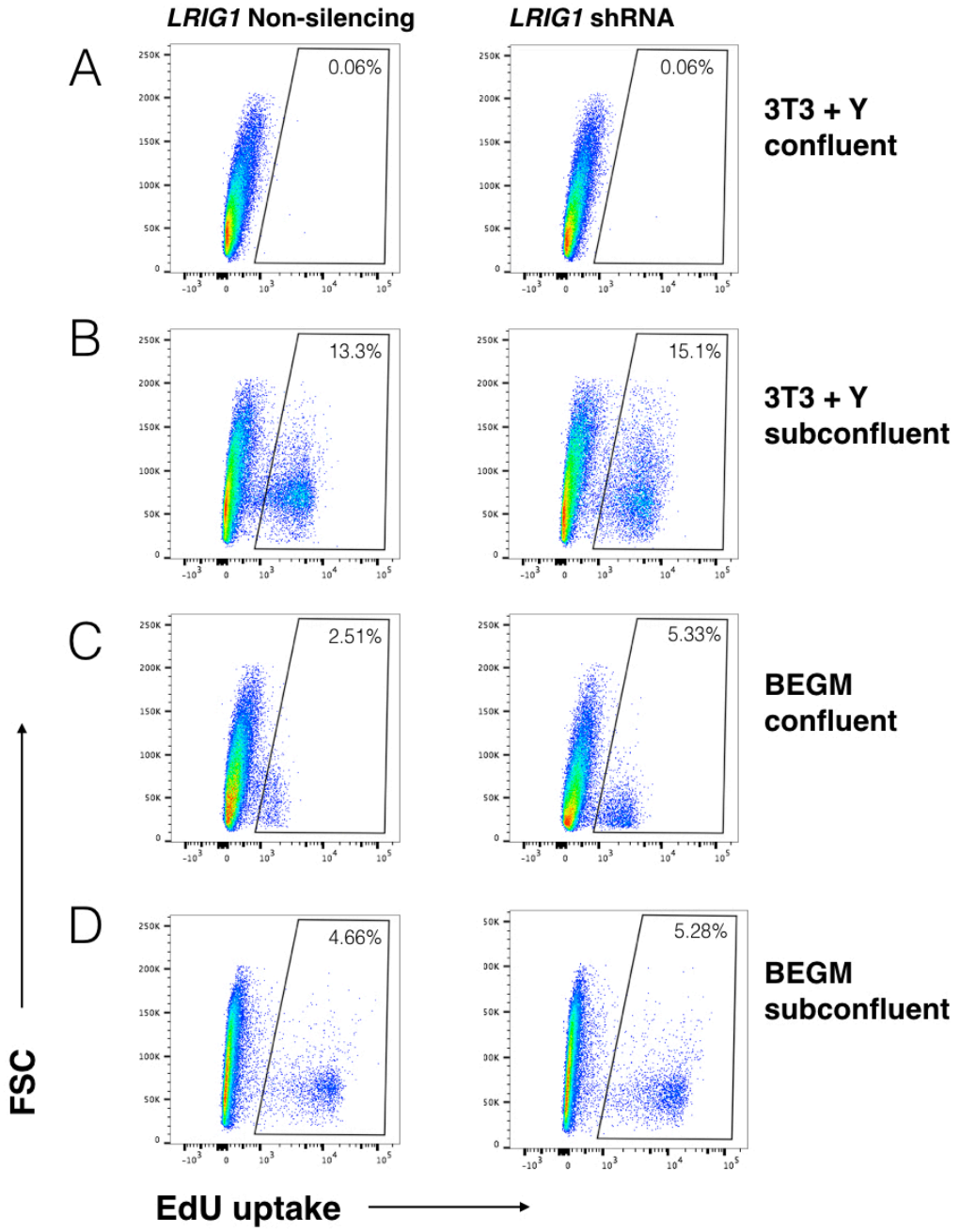

Figure 5.7: Optimisation of EdU proliferation assay

The assessment of EdU uptake in HBECs compared uptake between a non-silencing control and samples where LRIG1 was knocked down. 4 conditions were compared; A) Confluent cells grown in 3T3 + Y, B) Sub confluent cells grown in 3T3 + Y, C) Confluent cells grown in BEGM, D) Sub confluent cells grown in BEGM.

5.3.8 The effect of LRIG1 shRNA knockdown on cell proliferation at confluence

As there was an on-going proliferation at cell confluence in the BEGM conditions (as shown by Lu *et al* in mouse airway epithelium (104)), the growth of cells in BEGM at cell confluence was selected to compare the difference in proliferation in cells from multiple donors. Despite the percentage of EdU-positive cells being comparable at sub-confluence in my preliminary experiments, it was clear that the epithelial cells were growing at different rates. The *LRIG1* shRNA knockdown cells reached confluence more quickly than the *LRIG*-expressing non-silencing controls, despite seeding at the same cell density. I was concerned that the higher cell number of the *LRIG1* shRNA knockdown cells may exert a greater inhibitory effect on proliferation. Therefore, the final cell number in each sample prior to flow cytometry was counted and recorded.

The percentage of cells positive for EdU uptake in each of the cell populations at cell confluence was small (Figure 5.8.A). However, in each of the patient samples examined, the EdU uptake in the *LRIG1* shRNA knockdown sample was greater than that of the *LRIG1*-expressing, non-silencing control (Figure 5.8.B). This shows ongoing proliferation in *LRIG1* shRNA knockdown cells despite cell confluence. When combining the data from three patients, there was a marked increase in the percentage of EdU-positive cells in the *LRIG1* shRNA knockdown cell lines compared to the *LRIG*- expressing, non-silencing controls (Figure 5.8.C).

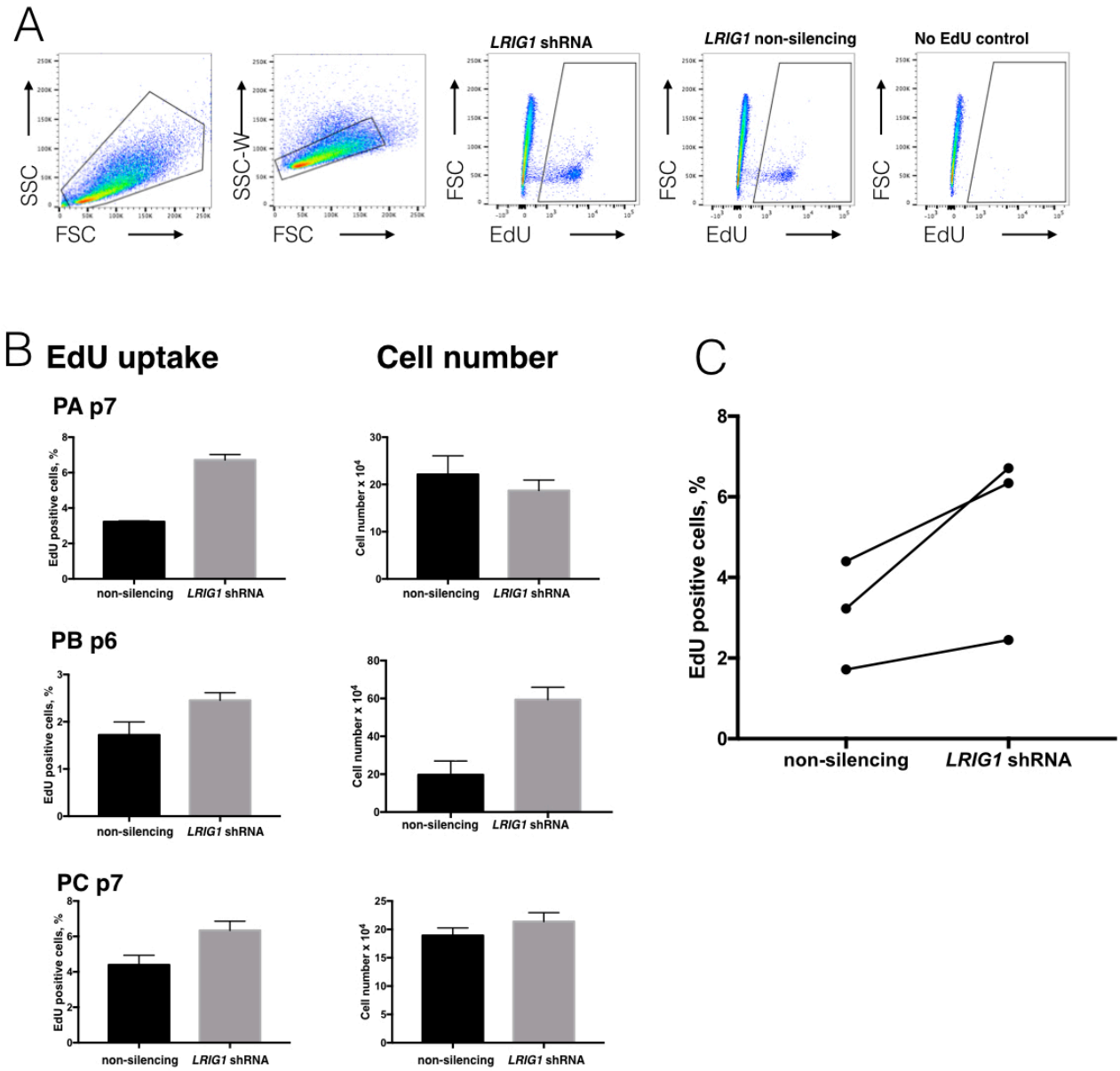

Figure 5.8: Assessment of EdU uptake at cell confluence

A) Flow cytometry plots showing assessment of EdU uptake in HBECs grown in BEGM at cell confluence. Example plot from patient PC p7. Debris and any remaining 3T3-J2 cells were gated out using FSC/SSC dimensions, doublets excluded and then EdU (Alexa 647) uptake assessed. B) Plots showing percentage of EdU positive cells at cell confluence in each of the 3 individual patients. On the right are plots of total cell numbers. Experiments repeated in triplicate, mean ± SEM. C) Combined data for 3 individuals, indicating that within the shRNA LRIG1 knock down cells, the cells continue to proliferate at cell confluence. Statistical analysis was performed using a paired t- test, n=3.

Cell numbers in the *LRIG1* shRNA knockdown cells and the *LRIG1*-expressing non-silencing controls were similar in samples PC and PA. There was a more marked difference in sample PB, with a much higher number of *LRIG1* shRNA knockdown cells. Despite this, the *LRIG1* shRNA sample still had a much greater percentage of EdU-positive cells, meaning any excess negative inhibition caused by the larger cell number was out-weighed by the increased proliferation at cell confluence of the *LRIG1* shRNA knockdown cells.

5.3.9 The effect of *LRIG1* shRNA knockdown on rate of proliferation

As noted above, the *LRIG1* shRNA knockdown cells grew faster than the *LRIG1*-expressing, non-silencing control cells. The use of siRNA in basal keratinocytes has shown that keratinocyte proliferation increases on loss of LRIG1 (79). To assess this in more detail, XTT assays were used to compare the rates of proliferation in the *LRIG1* shRNA knockdown and *LRIG1*-expressing non-silencing control cell lines. Instead of examining cell proliferation at a single time point, XTT assays allow the assessment of cell number at multiple time points, allowing proliferation rate to be assessed. As in the previous experiments the XTT assay was carried out in BEGM.

Cellular XTT metabolism (and by inference cell number) was detected by a spectrophotometer. Readings were compared to a baseline absorbance measurement recorded at day 1, and the percentage change in absorbance values determined. By days 7 and 10 the rate of growth in the *LRIG1* shRNA knockdown cells was greater than that of the *LRIG1*-expressing, non-silencing control cells. This occurred across all 4 donor cell lines, although the difference was less marked in PA, where the rate of proliferation in both the *LRIG1* shRNA knockdown and the *LRIG1*-expressing non-silencing control cells were similar. Proliferation reached a peak at day 9 in 3 of the 4 donor cell lines, and it was at this time point when the greatest difference in proliferation rate between the *LRIG1* shRNA knockdown and *LRIG1*-expressing non-silencing control groups was seen (Figure 5.9.A). Once cells reached confluence, as assessed by eye, between days 9 and 11, the cell numbers decreased,

and the percentage difference in XTT uptake reduced. This is likely due to the cells being intolerant of persistent levels of high confluence. The *LRIG1*-expressing non-silencing cells appeared less tolerant of high levels of cell confluence and did not reach the same cell numbers as the *LRIG1* shRNA knockdown cells. The difference in decline between *LRIG1* shRNA and *LRIG1*-expressing cells is likely due to the *LRIG1* shRNA knockdown cells reaching a higher cell number by day 9 (Figure 5.9.A).

Combining the 4 patient samples gives a clearer indication of the effects of *LRIG1* shRNA knockdown (Figure 5.9.B). *LRIG1* shRNA knockdown increases the rate of proliferation between days 3 and 4, and a marked difference in proliferation is displayed between days 4 and 7. The rate of increase reduces from day 7–9, but is still greater in the *LRIG1* shRNA knockdown arm compared to the *LRIG1*-expressing non-silencing control. At day 9, the difference between the *LRIG1* shRNA knockdown cells and the *LRIG1*-expressing non-silencing control is statistically significant. After this point the number of cells begin decreases, the difference in the rate of decrease is significant at day 11.

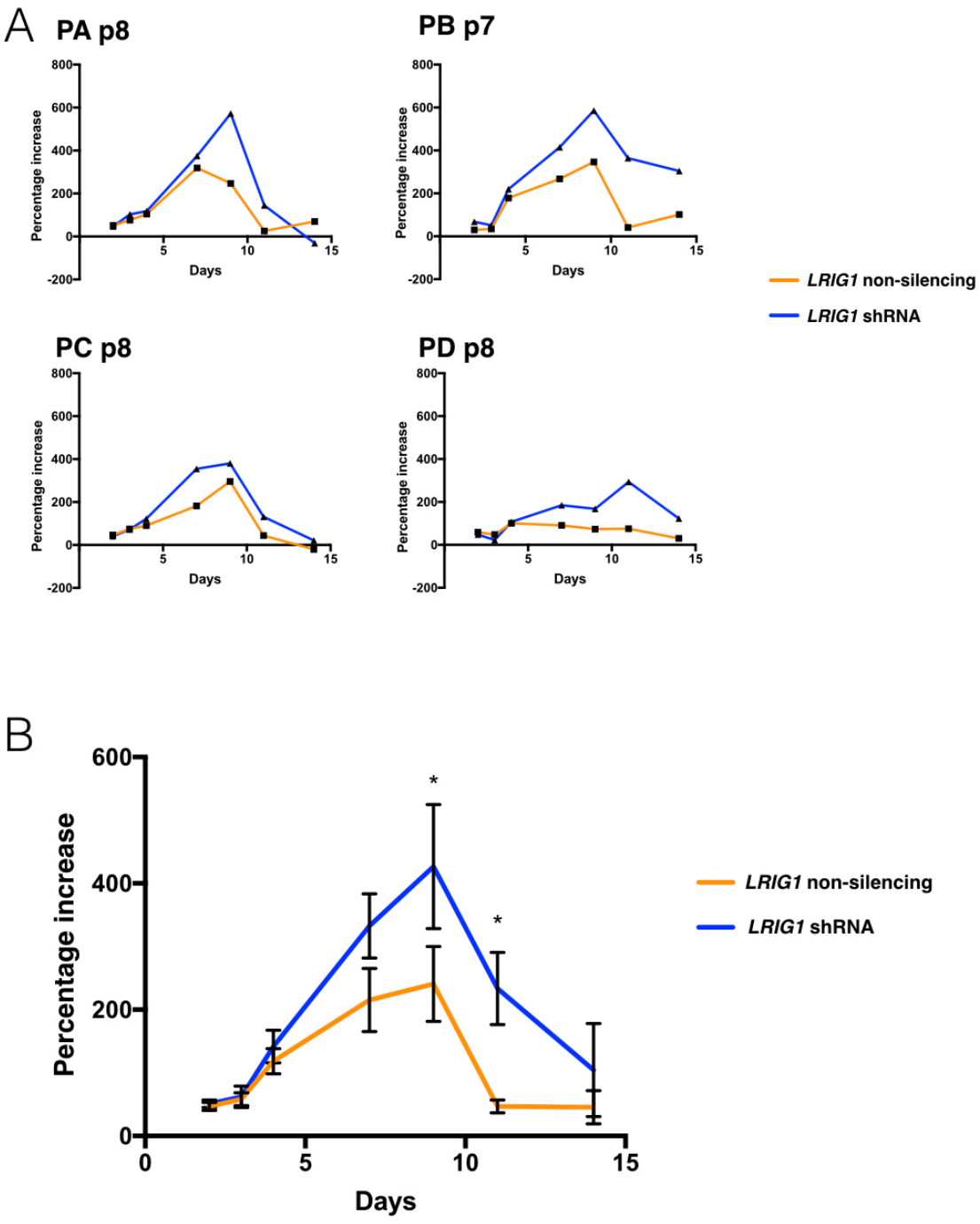

Figure 5.9: Proliferation rate of HBECs following *LRIG1* shRNA knockdown

A) Plots of each of the 4 patient samples including the *LRIG1* shRNA knockdown and the *LRIG1*-expressing non-silencing control showing the percentage change in the XTT absorbance reading from values at day 1. Samples performed in triplicate and the mean value plotted. Measurements taken on days 2, 3, 4, 7, 11 and 14. B) Plot showing the combined data for the 4 patients, mean ± SEM. Statistical analysis was performed using a 2-way ANOVA with Sidak's multiple comparison's test, * indicates $p < 0.05$.

5.3.10 The effect of *LRIG1* shRNA knockdown on invasion and differentiation of epithelial cells

The loss of LRIG1 has been shown to influence both migration and invasion in human cancer cell lines (110, 111). It was seen that, on LRIG1 loss, genes associated with epithelial-mesenchymal transition (EMT) were upregulated and the assessed cell lines took on a more migratory and invasive phenotype. However, despite these findings, I would hypothesise that the loss of LRIG1 from human airway cells is unlikely to result in invasion as LRIG1 loss is seen in preinvasive squamous cell carcinomas, occurring before a detectable break in the basement membrane is seen. If LRIG1 directly influenced invasion, its loss would only become evident in samples where the basement membrane has already been breached.

To assess whether LRIG1 has a role in invasion and whether it modulates an EMT phenotype in the human airway basal cells, invasion assays were performed using the *LRIG1* shRNA knockdown cells. Initially, cells suspended in serum-reduced medium were left to migrate through a Matrigel-covered transwell to a serum-containing medium below the membrane. Two different cell concentrations of 50,000 and 100,000 cells/well were trialled as were 2 different time points, 72 and 96 hours. However, at the experimental end-point, the HBECs were seen to form spheroid-like structures within the Matrigel (Figure 5.10.A). After removing, washing and staining the membrane with crystal violet, there was no indication that migration had occurred from one side of the membrane to the other (Figure 5.10.A). The membrane of a control well, without epithelial cells, was identical to that of a transwell where cells were seeded. These preliminary results showed there was no evidence of increased invasion of *LRIG1* shRNA knockdown cells through Matrigel.

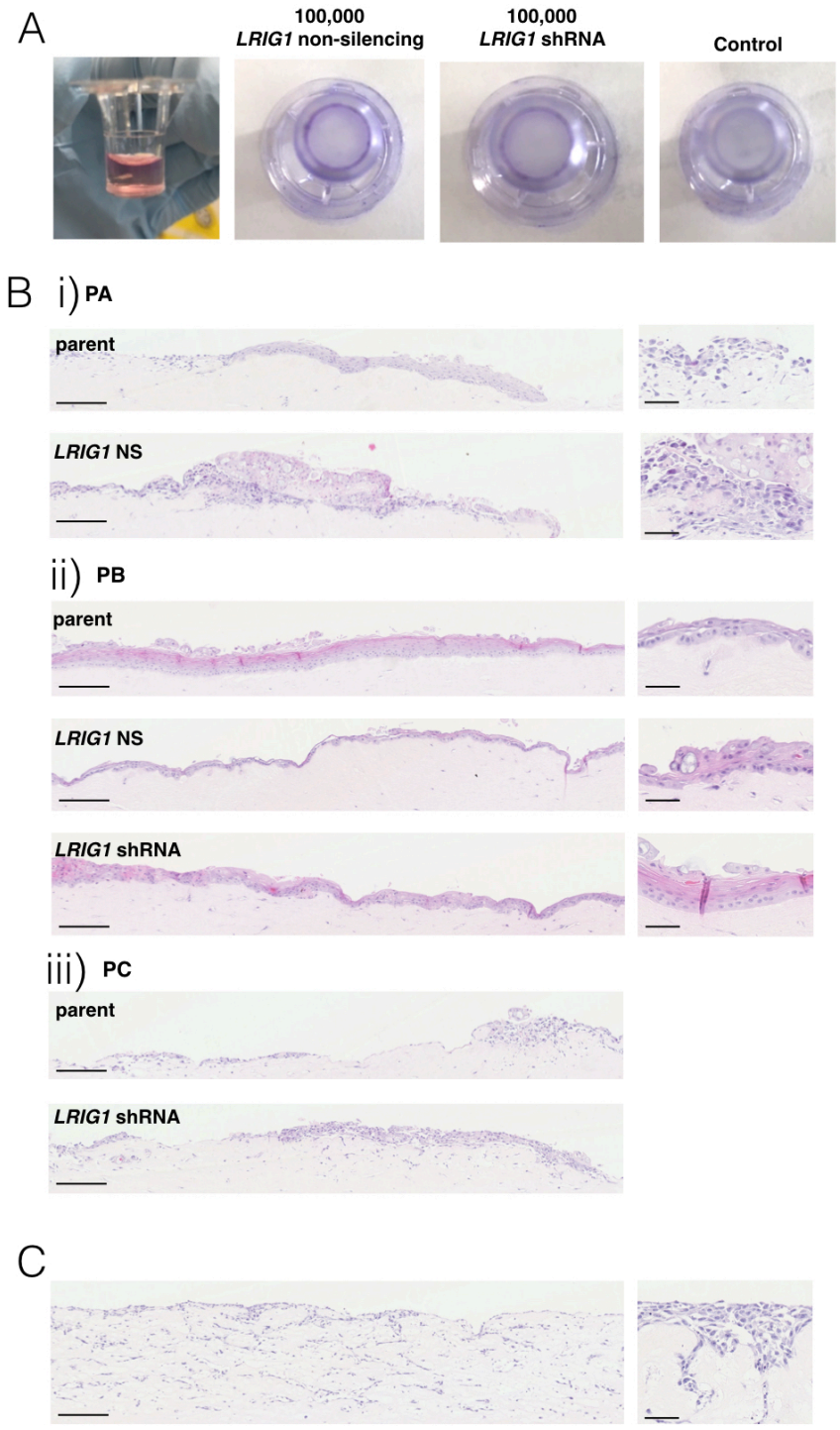

Figure 5.10: Effect of *LRIG1* shRNA knockdown on invasion of HBECS

A) Optimisation of invasion assay through a Matrigel-coated transwell. From left to right: cells appear to migrate to the centre of the Matrigel plug and form spheroids; no evidence of cells on the under surface of the transwell, and on right, no difference between transwells with cells and control membranes (where no cells were seeded). B) Organotypic invasion assays showing the growth of epithelial cells on a collagen/Matrigel matrix with embedded fibroblasts. Picked examples of organotypic assays to show different features. i) PB p7 epithelial cells showing parent, non-silencing (NS) and shRNA treated cells. i) PC p8 parent and NS cells. ii) PA p8 parent and shRNA cells. Scale bar = 200 µm. Images on right show close-up of the larger image. Scale bar = 50 µm. C) Positive control SK-MES-1 cells that have previously been shown to invade a Matrigel matrix. Note the presence of epithelial cells in layers, deep beneath the surface of the matrix. The close-up image shows tumour projections, reaching into the matrix. Scale bars = 200 µm (left) and 50 µm (right).

To ensure there was no increase in the invasive potential of *LRIG1* shRNA knockdown cells, organotypic invasion assays were carried out. Organotypic assays attempt to replicate the tumour/stroma interface, and can assess an epithelial cell's invasive potential (234, 235). By growing epithelial cells on a Matrigel/collagen matrix embedded with fibroblasts and then subsequently exposing this matrix to air, conditions are created that more closely mirror an *in vivo* environment than growing cells submerged on tissue culture plastic. Basal cells grown using this method are capable of differentiating into all of the airway epithelial cell types (171). Therefore, the point of the assay was two-fold. The first was to assess invasion potential, whilst the second was to ensure that lentiviral-transduced HBECs were still capable of differentiating into a respiratory epithelium. If the non-silencing shRNA control cells were unable to form a differentiated epithelium, it may imply that the lentiviral transduction was adversely affecting HBEC behaviour.

The organotypic assays were cultured for 24 days, at which point a layer of cells was seen above the matrix. Following the fixing, embedding and sectioning of the matrix scaffolds, transverse cross-sections were stained with haematoxylin and eosin to assess both invasion and possible differentiation (Figure 5.10.B). Although the conditions were analysed in triplicate, a wide variability existed from well to well. In some areas the epithelial lining was intact with evidence of organisation, whilst in others the membrane was denuded (Figure 5.10.B). The positive control, a squamous cell lung cancer line SK-MES-1 that has shown invasive characteristics in reported invasion assays (236), was seen to clearly invade the matrix with the presence of deep, finger-like projections and accompanying tumour islands (Figure 5.10.C). Amongst the 4 donor cell lines there was no convincing evidence of invasion, and no differences in the behaviour of *LRIG1* shRNA knockdown cells and *LRIG1*-expressing non-silencing control cells. In the majority of assays, the cells appeared to sit in organised layers along the surface of the matrix. In PC there were some areas of less complete epithelial coverage and a suggestion that a few epithelial cells may have encroached into the matrix. This was variable between the triplicate repeats and showed no correlation with whether the cells were from parent, *LRIG1* shRNA knockdown cells or *LRIG1*-expressing non-silencing control

cells. The cells from patient PA grew less well and the epithelial covering of the matrix was extremely sparse. In areas that the matrix was less well covered, similarly to in PC, there were a few cells that had possibly moved into the matrix.

In all 4 patients, there appeared to be some evidence of differentiation. This was variable amongst the triplicate repeats and again showed no clear correlation with whether *LRIG1* was knocked down. To confirm these findings, immunofluorescence was performed for MUC5B and ACT (Figure 5.11). There is a suggestion that the basal cells were still capable of secretory and ciliated differentiation, with cells expressing these proteins seen in at least one of the triplicate repeats in each of the conditions across the 4 patients. This shows that lentiviral transduction of epithelial cells does not alter the differentiation ability of transduced cells.

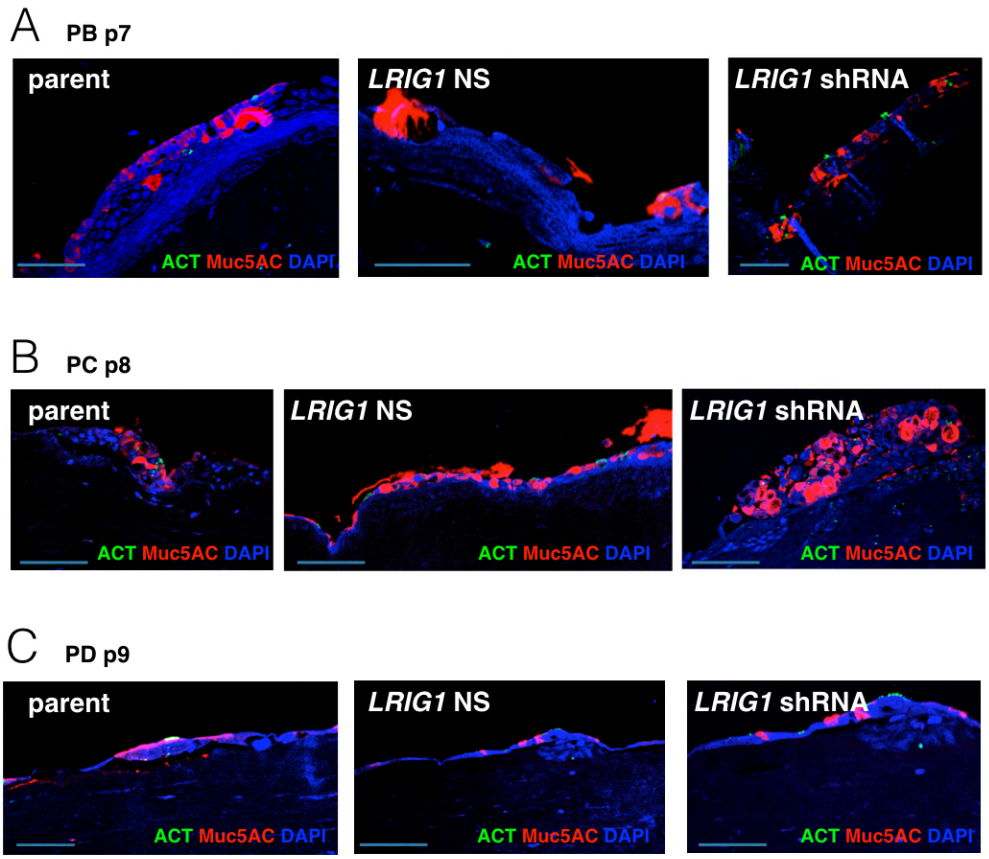

Figure 5.11: Differentiation of parent, *LRIG1* non-silencing and *LRIG1* shRNA knockdown cells in the organotypic assay

Immunofluorescent staining of transverse sections of organotypic assays, suggestive of early mucociliary differentiation. MUC5AC (red; goblet cells) and ACT (green; ciliated cells) stained cells are seen in sections, from parent, non-silencing (NS) and *LRIG1* shRNA- transduced cells. Labelling indicates cells from different donors A) PB p7, B) PC p8, C) PD p9. Scale bar = 100 µm.

5.4 Discussion

I have shown that LRIG1 is expressed within the human airway epithelium. Similarly to the mouse, LRIG1 appears to be expressed across the epithelium, but there are populations of both LRIG1^{+} and LRIG1^{-} basal epithelial cells. The proportion of LRIG1-expressing basal cells mirrors that of the mouse. When these human airway basal cells are isolated by flow cytometry, the LRIG1^{+} cells are more clonogenic than LRIG1^{-} and are more proliferative. This implies that either LRIG1 confers properties to a more stem cell-like basal population or marks those with a more stem-cell like phenotype.

Using 3T3 + Y culture conditions, I have shown it is possible to knock down a gene, in this case *LRIG1*, in primary HBECs. Analysing the effects of knockdown of *LRIG1* suggests that the protein confers properties to the basal cell population, as its loss produces a population that is more clonogenic, shows increased proliferation and is less inhibited by cell-cell contacts. If LRIG1 simply marked a basal cell population in the human airway, any knockdown would have no effect. Immunoblotting for EGFR and downstream ERK have demonstrated that the loss of LRIG1, as anticipated, exerts an effect on the EGFR signalling pathway, with increased phosphorylation of both EGFR and ERK in response to EGF stimulation. Lentiviral transduction of HBECs does not affect the ability of HBECs to differentiate, with parent, non-silencing and *LRIG1* shRNA cells populations all showing evidence of mucociliary differentiation. The isolated loss of LRIG1 does not appear to influence invasion.

I was concerned that the LRIG1^{+} and LRIG1^{-} cells obtained from the *Lrig1* eGFP-ires-CreERT2 null mouse may have given limited information due to the constitutive nature of *Lrig1* loss (Chapter 3). By using *LRIG1* shRNA knockdown in human airway cells, any constitutive compensation would not have occurred, and conditions would be more reflective of those in the human airway, where LRIG1 expression is lost in the development of preinvasive disease.

Whilst the mice used in this project were genetically similar, used at the same age and had similar environmental exposures, the patients varied in age, smoking history, gender, genetic background and other environmental factors. These factors need to be considered when analysing the data. Intriguingly, it has been shown in mice that older animals have a reduced proportion of tracheal $KRT5^{+}p63^{+}$ epithelial cells, meaning the age of the patient may have a bearing on the number of basal cells collected from a bronchial brush (237). The smoking history is also interesting; *LRIG1* gene expression is downregulated in areas of 'normal epithelium' from smokers, compared to ex-smokers and these levels fall further on the development of squamous cell lung tumours (30). This may partly explain some of the variability in the number of LRIG1-expressing cells seen by flow cytometry. Many of the patients from whom samples were obtained had a normal bronchial tree (proven on bronchial biopsy) whilst other samples were obtained during autofluorescence bronchoscopies from areas of 'normal' epithelium in patients with known preinvasive disease (again shown on bronchial biopsy). Increasing the patient numbers for each of the experiments may reduce the effect of these potentially confounding factors. Should time have allowed, it would have been useful to use a greater number of samples from patients with a normal bronchial tree; however, this needed to be balanced with the availability and suitability of patient samples from either bronchoscopic or surgical lists.

The variability of both basal cell LRIG1 expression and the number of basal cells in each sample may be reflective of the quality of brush biopsy obtained. Three of the samples obtained for the Hoescht 33342 proliferation experiment had to be excluded due to low basal cell numbers and in one of the colony-forming assays a full 96-well plate of cells was not collected due to low basal cell numbers. The basal cells are firmly adherent to the basement membrane and it is possible that the LRIG1-expressing basal cells are those most closely attached to the basement membrane (as this corresponds to the brightest immunofluorescence staining for LRIG1). The effectiveness of the brush (and the technique of the operator) may influence both the number of basal cells and the number of $LRIG1^{+}$ basal cells that go into the cell suspension. Other methods of obtaining airway epithelial cells were

considered, including the use of bronchial biopsies and collecting resected airway samples from surgical procedures. However, both these methods require a digestion step to detach the basal cells and would add 1- 2 hours to the preparation of the samples for flow cytometry. This is likely to influence both the viability of the cells that are ultimately analysed (and the proportion of colonies that form), and the number of cells in the G2/M phase of the cell cycle as seen through Hoescht 33342 uptake.

Whilst a shift in the population of epithelial cells was seen on staining for LRIG1, a clearly defined LRIG1^{+} and LRIG1^{-} population was not detectable. There may be a gradient of LRIG1 expression, with the cells with the 'higher' LRIG1 expression being more clonogenic than those with lower levels. However, (although using low cell numbers) this was not confirmed by index sorting and amongst the LRIG1-positive population there appeared to be no clear threshold above which the cells formed a colony. This contrasts to the mouse data, where an eGFP^{+} and eGFP^{-} cell population was clearly distinguishable.

LRIG1 shRNA knockdown was performed in cultured human basal cells. Although *LRIG1* shRNA knockdown cells formed increased numbers of colonies compared to the non-silencing controls, this failed to reach significance. The power of the experiment may be improved by increasing the number of patient cell lines used for the *LRIG1* shRNA knockdown, but the failure to reach significance may also be explained by heterogeneity within the basal cell population and an incomplete *LRIG1* knockdown. The population of cultured basal cells was considered as a whole, instead of being divided into LRIG1^{+} and LRIG1^{-} populations. Due to the nature of cell culture, cultured basal cells are likely to be more homogeneous than those derived directly from a patient. It was clearly seen by immunoblotting that the parental cell lines expressed LRIG1 prior to knockdown, but whether LRIG1 expression varied across the cultured basal cell population was uncertain. Attempts to assess differences in LRIG1 expression in individual cells by flow cytometry were thwarted by the cleavage of LRIG1 by trypsin (90), and trials using a number of different digestion techniques, including the previously reported thermolysin, with

the aim of preserving the LRIG1 epitope were unsuccessful. To ensure complete knockdown of *LRIG1*, CRISPR-Cas9 technology could be employed (238). A good shRNA knockdown is considered as an 80-90% reduction in protein expression (239) and, as the *LRIG1* shRNA knockdown is incomplete, may explain the only marginal differences seen in EdU uptake at cell confluence. Lu *et al* showed a more marked continued proliferation at cell confluence (104) (using cells from *Lrig1* knockout mice where LRIG1 expression is absent), with a greater proportion of *Lrig1* knockout cells grown at air liquid interface exhibiting BrdU uptake compared to wild-type cells (with 9.7% in the knockout cells and 0.5% in the wild-type) but differences in EdU uptake in these experiments were seen to vary by only 3-4%. Enough residual LRIG1 may be present in the *LRIG1* shRNA knockdown cell lines to ameliorate the effect of *LRIG1* shRNA knockdown on proliferation at cell confluence. CRISPR-Cas9 technology would entirely knockout LRIG1 expression and would give a clearer indication of the effects of LRIG1 loss, not only at cell confluence, but also within the other assays that have been performed. Using CRISPR-Cas9 was initially considered, but due to time limitations was beyond the scope of this thesis. Should time have allowed, and based on the above shRNA data, this could be revisited.

Using the EdU assay to measure continued proliferation at cell confluence may not have been the most appropriate assay. There was evidence of contact inhibition in the 3T3 + Y culture conditions, and even the *LRIG1*-expressing non-silencing control cells continued to proliferate at cell confluence in BEGM. This poses the question as to whether the cells would ever be contact inhibited within BEGM, but would instead undergo apoptosis before this point. To more successfully address whether the loss of LRIG1 leads to a loss of contact inhibition, and would time have allowed I would repeat the assay performed by Lu *et al* that assessed contact inhibition at air-liquid-interface (104).

It is difficult to draw firm conclusions from the invasion assays. There was no evidence of any invasion in samples from PB, which had the best growth of epithelial cells, but in PC and PA, where the epithelial covering was less intact, there was a suggestion of cell encroachment into the matrix. This was not the expected reported

tumour bodies (235), or a tumour 'front' as seen in the positive control samples, but a more random encroachment of cells. The cell encroachment may be an artefact as when the assays are being prepared the cells are loaded onto submerged matrices and an epithelial covering is allowed to form over 72 hours. At 72 hours, this epithelial cell-covered matrix is raised onto scaffolds. The abnormal appearances occur where the epithelial cells are less confluent, which may reflect the exposure of the matrix to air. Following exposure to air there may be breakdown of the matrix, allowing epithelial cell invasion. In retrospect, this assay may not have been the most appropriate to use, whilst the invasive potential of the positive control is clearly visible, no changes in the behaviour of the cell lines were seen on the loss of LRIG1. This may be due to the loss of LRIG1 causing only a subtle increase in the ability of cells to invade, that is not detectable in this assay. An alternative to consider would be a scratch assay (240), where the migratory potential of cells are compared (although the increased rate of growth of the *LRIG1* shRNA knockdown cells would need to be accounted for). To confirm the findings that lentiviral transduction and LRIG1 shRNA knockdown does not affect differentiation potential, cells could be grown either tracheosphere assays or at air-liquid-interface.

Further considerations could include how the loss of LRIG1 leads to the loss of cell-cell contact inhibition and an on-going proliferation at cell confluence (104). Lu *et al* showed through immunoprecipitation experiments performed at cell confluence, in LRIG1-expressing cells, that a ternary complex forms between LRIG1, E-cadherin and EGFR (104). These experiments were performed in A549 cells, an adenocarcinoma cell line that does not express LRIG1. The A549 cells were transduced with LRIG1 protein attached to FLAG (due to difficulties with antibody detection of LRIG1). The formation of the ternary complex may provide a mechanism by which primary epithelial cells are growth inhibited at cell confluence and may explain how LRIG1 loss leads to preinvasive disease. It would be of benefit to assess the formation of a ternary complex within the primary HBECS, as the system would be more relevant than using a cell line transduced to over express LRIG1. Since the Lu *et al* paper (104) has been published there has been the development of antibodies that are more successful in the detection of LRIG1 by immunoblotting (as used in my

experiments), making the use of a FLAG-tagged protein redundant, and time permitting, this is something I would pursue.

Due to the loss of LRIG1 in preinvasive lung cancers it would be useful to obtain bronchial brushings from patients with preinvasive lesions. The LRIG1 expression and behaviour of basal cells (with or without LRIG1 expression) could then be compared in matched samples from areas of normal epithelium to those of preinvasion. To date, it has not been possible to grow preinvasive squamous cell lung cancer cells in culture. Our group has shown that growing cells from preinvasive epithelial brushes or biopsies selects for cells with a normal genotype, without the genetic mutations associated with preinvasive disease. It has been shown that adding LRIG1 to the A549 adenocarcinoma cell line leads to a change in phenotype (by inducing cell-cell contact inhibition at cell confluence), but A549 cells are derived from cancer in a distal epithelial cell that I have shown, in mouse, by immunofluorescence do not express LRIG1. If preinvasive squamous cells could be grown in culture, the effect of LRIG1 re-introduction or knockout could be established.

Consideration of this data as a whole suggests that LRIG1 may act as a possible 'brake' to regulate the airway epithelial stem cell population. In the mouse and human airway, LRIG1 marks a population of basal cells which are more clonogenic and proliferative than LRIG1^{-} basal cells. When *LRIG1* undergoes shRNA knockdown in an LRIG1-expressing basal cell population, the cells become increasingly clonogenic and proliferative. This implies both the loss of a regulator and the removal of a regulatory 'brake'. The 'brake' hypothesis would explain how LRIG1 loss may lead to preinvasive and lung cancer development: LRIG1^{+} basal cells have increased stem cell characteristics, with LRIG1 loss from these basal cells leading to dysregulation, compartment expansion and preinvasive disease. To add support to this hypothesis, the use of LRIG1 knockdown and overexpression within the same parental cell lines would need to be performed. This would allow direct comparison of proliferation and clonogenic capacity in an LRIG1-overexpressing and LRIG1-knockdown assay.

5.5 Summary

- LRIG1 is expressed across the human airway
- LRIG1^{+} basal cells are more proliferative and clonogenic than LRIG1^{-} cells
- shRNA knockdown of *LRIG1* in HBECs leads to increased EGFR signalling
- shRNA *LRIG1* knockdown leads to increased colony-forming efficiency, continued cell proliferation at cell confluence and increased rate of proliferation of HBECs

6. The effect of LRIG1 loss in a murine squamous cell lung cancer model

6. The effect of LRIG1 loss in a murine squamous cell cancer model

6.1 Introduction

The loss of LRIG1 predisposes to malignancy across a range of epithelial types (75, 97, 110, 241) and within the human airway LRIG1 loss has been observed in early, preinvasive squamous cell lung cancers (104). To assess the effect of loss of LRIG1 on the development of preinvasive and squamous cell lung cancers, a murine model of disease is required. By comparing disease in wild-type mice to LRIG1-null mice, the role of LRIG1 in the development of preinvasive lung cancer can be elucidated.

Despite progress with the generation of murine models recapitulating adenocarcinoma, where disruption of a single gene can cause disease, the creation of a robust squamous cell carcinoma model has proved more challenging (242). Simultaneous activation of *Kras*^{G12D} (an activating mutation associated with the development of murine adenocarcinoma) with loss of liver kinase B1 (*Lkb1*) leads to the development of lung tumours including adeno-, adenosquamous and squamous cell lung carcinomas. However, the loss of *Lkb1* in isolation, although lost in human disease, does not lead to squamous lung tumour production in a murine model (243). The mutation of IκB kinase (*IKKα*), through an amino acid replacement in the adenosine triphosphate (ATP) binding site, results in loss of the kinase activity and leads to the formation of squamous lung cancers. However, these animals also develop skin and gut tumours that lead to death, this often occurs before lung tumours can be analysed and restricts their use in a lung cancer model (244). To keep the animals alive long enough to be used in a lung cancer model, the authors expressed wild-type *IKKα* cDNA in the epidermis, under the control of a truncated loricrin promoter, which allowed the assessment of lung disease (244).

Phosphatase and tensin homolog (*PTEN*) is a tumour suppressor whose loss is associated with the development of human squamous cell carcinomas, whilst *SOX2*

overexpression has been shown in the development of both preinvasive invasive and squamous cell carcinomas. However, the loss of *Pten,* or *Sox2* overexpression in mouse models does not lead to the development of significant lesions (227, 245). Overexpression of *Sox2* initiates adenocarcinomas that exhibit some squamous features, including p63 expression and although the loss of *Pten* causes tumour development, only 8% of these lesions are squamous (227, 245).

Combining the loss of *Lkb1* and *Pten* has been shown to lead to development of entirely squamous cell lung cancers after a 40-50 week latency. Tumours initially develop as small nodules at around 30-40 weeks, they then enlarge and progress to lymphovascular invasion and limited metastatic spread (to the chest wall). However, these tumours (that initially develop as nodules) do not progress through the step-wise preinvasive to squamous cell carcinoma sequence seen in human disease (246), where LRIG1 is thought to influence disease progression (104).

More recently, the overexpression of *Sox2* in mice with a conditional loss of both *Pten* and cyclin-dependent kinase inhibitor 2A/B (*Cdkn2ab)* has been shown to lead to squamous cell lung cancer development. *Sox2* overexpression was targeted to either keratin 5 (KRT5)-positive basal cells, surfactant protein C (SPC)-positive cells, alveolar type 2 (AT2) cells or Clara cell 10 (CC10)-positive club cells, and in all cases led to squamous tumours (247). Significant tumour production took over a year to develop, and again there was no indication of a preinvasive disease phase.

The use of a chemical carcinogen to induce murine squamous cell lung cancers was first reported with the use of benzopyrene, a polycyclic aromatic hydrocarbon found in cigarette smoke. Unfortunately, there is no consensus on either the dosing schedule or the application method for benzopyrene, with intraperitoneal injections, intranasal instillation and oral gavage all used with variable success (248, 249). Benzopyrene does lead to both squamous and adenocarcinomas, with the proportion of squamous lesions increasing with benzopyrene dosage (250).

In 2004, Wang *et al* (251) reported that the application of the alkylating agent N-Nitrosotris-(2-chloroethyl)urea (NTCU) to the shaved, dorsal skin of mice recapitulates both preinvasive and invasive squamous cell lung tumours. The regimen consisted of 8 months of twice-weekly NTCU treatments and the investigators noted a large variability in both the severity and the number of lesions that was dependent on mouse strain. More recently, a method was reported that treated animals with 75 µl of 0.013 M NTCU, this was the same dose of NTCU, but the drug was dissolved in a higher volume of solvent. This treatment regimen led to both preinvasive and squamous cell lung cancers developing after a much shorter, 18-week period (252). In contrast to the Wang method, which used continual NTCU dosing over the 8 month study period, the second group's regimen involved only 8 weeks of NTCU application followed by a 10 week 'observation' period prior to culling. Both methods induce comparable levels of disease in the cancer-susceptible A/J strain of mice. Wang *et al*, report that following 8 months of treatment, 100% of animals had developed hyperplasia, metaplasia and carcinoma-in-situ and 75% have invasive tumours (251), whilst following the shorter, 8 weeks of NTCU and 10 weeks of follow-up, animals were shown to exhibit comparable grades of preinvasive disease and 71% had developed tumours (252). NTCU is an alkylating agent, although its mechanism of action is uncertain (249). It has been shown to induce an inflammatory reaction with the plasma interleukin-6 levels elevated in NTCU treated animals compared to controls (253).

Due to time constraints, developing a compound *Lrig1*-knockout transgenic animal lacking both *Lkb1* and *Pten* would be prohibitive, as would an animal with *Pten* and *Cdkn2ab* deletion together with *Sox2* overexpression. As both models only induce invasive squamous cell lesions, they may be best utilised in the assessment of therapeutics and behaviour of established tumours, rather than looking at the progression and evolution of preinvasive disease. LRIG1 loss has been shown in human preinvasive lesions (104), so the mouse model needs to recapitulate the human form of disease. NTCU-treated animals develop the full spectrum of preinvasive disease whilst also developing invasive squamous cell tumours. Therefore, this model more successfully recapitulates the changes that are occurring

in the human airway than any of the previously discussed methods that involve genetically modified mice. By following the shorter, 18 week treatment programme (252), there would be an opportunity for optimisation of a dosing regimen, specific to the colony. A further advantage is that the chemical can be applied directly to the *Lrig1* EGFP-ires-CreERT2 animals, without the need for further genetic manipulations.

To assess the effect of LRIG1 loss in the airway, I used the *Lrig1* EGFP-ires-CreERT2 strain. As previously discussed (Chapter 3, Figure 3.1.B), homozygous mice with two copies of *Lrig1* EGFP-ires-CreERT2 allele are equivalent to LRIG1-null animals, with no LRIG1 protein produced, and LRIG1-heterozygous mice have one copy of the *Lrig1* EGFP-ires-CreERT2 allele and one wild-type *Lrig1* allele.

6.2 Aims

- To set up the NTCU model using the *Lrig1* EGFP-ires-CreERT2 strain
- To validate that any subsequent lesions are either preinvasive or invasive squamous cell carcinomas
- To develop a strategy of lesion assessment
- To compare lesion development in wild-type, LRIG1-heterozygous and LRIG1-null mice

6.3 Results

6.3.1 **NTCU treatment optimisation and establishment of** a treatment protocol

The effects of NTCU on the development of preinvasive and squamous cell cancers are strain specific, with studies identifying A/J mice as sensitive, FVB/N as intermediate and C57BL/6 as resistant to the effects of the carcinogen (251). In the more sensitive A/J mice, dysplastic lesions are seen after just 2 weeks of NTCU (followed by a 16 week follow-up) and 25% of these animals develop invasive

disease (252). When the treatment period was extended to 4 and 8 weeks the number and severity of lesions progressively increased, but a marked 47% mortality was seen following 8 weeks of NTCU treatment (252). On their arrival to the laboratory, the animals containing the *Lrig1* EGFP-ires-CreERT2 allele were on an FVB/N and C57BL/6 mixed background. This indicates their sensitivity to NTCU was likely to fall between that reported in the FVB/N and C57BL/6 mice. To increase the animal's susceptibility to the development of lesions, the initial cross of the *Lrig1* EGFP-ires-CreERT2 was with an FVB/N animal, increasing the FVB/N proportion in the strain. In an effort to limit the variability caused by their mixed background, all animals were used at the same generation.

As NTCU had not previously been used within the group, I set up three preliminary cohorts of mice. The first two cohorts, A and B, were used to ensure that the dosing regimen was appropriate for the mouse strain, and the third cohort, cohort C, examined the effect of extending the observation period. My aim was to determine the dose where preinvasive lesions developed (as I want to investigate whether LRIG1 affects the development of these lesions in humans), whilst balancing the risk of any dose-related mortality. All animals were commenced between 6-8 weeks of age, and only females used, due to their increased predisposition to malignancy (254, 255). Cohort A (Figure 6.1.A), received 4 weeks of NTCU followed by 14 weeks of observation. The short treatment duration was to ensure the mice could tolerate NTCU dosing and would not develop side effects (such as skin irritation). The second group, cohort B, received 8 weeks of NTCU treatment followed by 10 weeks of observation (Figure 6.1.A). Both cohort A and B contained a single mouse of each genotype to give both an indication as to the susceptibility of the strain but also as to whether loss of LRIG1 in the LRIG1-null animals would lead to a dramatic increase in lesion development and necessitate any dosage alterations. Both groups included an acetone-only (vehicle) control. All animals were weighed immediately prior to each NTCU application and then twice weekly weights were continued throughout the observation period.

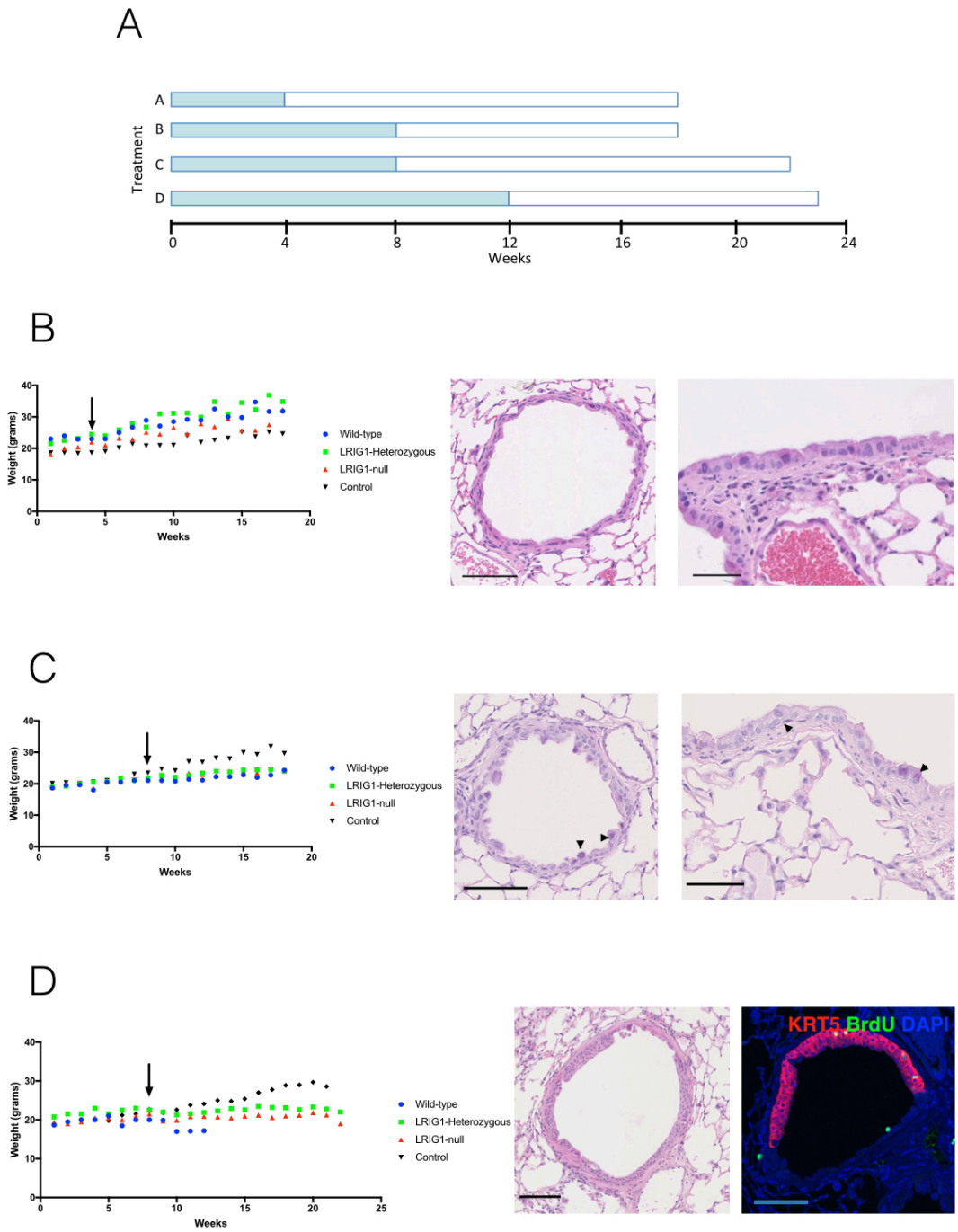

Figure 6.1: Optimisation of NTCU dosing strategy

A) Treatment cohorts, showing NTCU-dosing period (blue bar) and observation period (open bar). B) Weights of cohort A during assessment period, 4 animals were included, one wild-type, LRIG1-heterozygous, LRIG1-null and an LRIG1-heterozygous control. Arrows indicate the length of treatment period. Haematoxylin and eosin (H&E) stain of end-on bronchiole and transverse section from a cohort A mouse, scale bars = 100 µm and 50 µm. C) Weights of cohort B during assessment period, 4 animals were included, one wild-type, LRIG1-heterozygous, LRIG1-null and an LRIG1 heterozygous control. End-on and transverse bronchioles from cohort B animals showing evidence of enlarged hyperplastic basal cells, indicated by arrow heads, scale bars = 100 µm and 50 µm. D) Weights of cohort C animals during assessment, n=2-3 in each group. Bronchiole from cohort C treated animal with evidence of low-grade dysplasia, note multiple layers of epithelial cells and flattening of the nuclei at the luminal edge, scale bar = 50 µm and keratin 5 (KRT5; red) staining of bronchiole from a cohort C animal, BrdU (green) stained cells are seen adjacent to the basement membrane, n = 3, scale bar = 50 µm.

Cohort A displayed no side effects, with no skin irritation or weight loss and the animals remained well throughout the study period. On organ harvest, there were no macroscopic anomalies and histology revealed nothing suggestive of preinvasive lung disease (Figure 6.1.B).

In the 8-week treatment group, cohort B, one of the mice developed skin irritation over the left scapula. This was treated with manuka honey and resolved on grooming of the nails. At the experimental end point, no macroscopic changes were detectable within the lungs, liver or skin of the mice. Review of lung histology (with pathology assistance) identified that NTCU had induced basal cell hyperplasia. This was shown by basal cell enlargement and an increased nuclear to cytoplasmic ratio (Figure 6.1.C). A small difference in weight was seen between the treated animals and control, with the control animal 15% heavier than the treated animals at the experimental end point (Figure 6.1.C).

Cohort C (Figure 6.1.D) consisted of 8 treatment mice (3 LRIG1-null, 3 wild-type and 2 LRIG1-heterozygous animals) alongside two LRIG1-heterozygous controls (acetone only). As the NTCU treatments take a number of weeks, this cohort had commenced and finished the treatment phase prior to the results from cohort B being obtained. This meant the treatment period could not be lengthened, but the observation phase was extended from 10 to 14 weeks. When the lungs from these animals were examined, there was evidence of more advanced preinvasive disease. Low-grade lesions, consisting of multiple layers of cells and flattening of the nuclei at the luminal edge, were seen within the bronchioles (Figure 6.1.D). These low-grade lesions were KRT5-positive, indicating a squamous cell phenotype (256). Cohort C was the first group to exhibit untoward effects and 5 animals, of varying genotypes, were lost (discussed later).

In both cohort B and C, a separation between the weights of the treated and control animals were seen (Figure 6.1.C and 6.1.D). During the first 8- 10 weeks the weights remained similar but, after this point, the weights of the control mice increased whilst the weights of the treated animals remained static.

As low-grade lesions were detectable in cohort C, NTCU was clearly shown to induce lesions in the *Lrig1* EGFP-ires-CreERT2 colony. To assess for differences in the susceptibility to develop preinvasive and squamous cell cancers, the number of lesions needed to be both increased and be of a greater severity. Different strategies were considered to increase lesion frequency. These included the administration of intranasal lipopolysaccharide (LPS) that has been seen to increase NTCU-induced tumour size by enhancing NTCU-induced inflammation (181) and the use of naphthalene that causes airway damage and subsequent epithelial cell proliferation. Naphthalene increases the number of lung adenocarcinomas that develop in a murine genetically-induced *KRas*^{G12D} adenocarcinoma model, through stimulating the proliferation of bronchioalveolar *s*tem cells (BASCs) (129), the putative stem cell population for the distal airway. The origin of the NTCU-induced preinvasive lesions is uncertain, but the triggering of proliferation in the distal airway may lead to increased disease. However, whilst both methods may increase lesion development, to ensure the model remained reproducible and without adding additional confounders, the dosing period was simply extended to 12 weeks, with a 12-week period of follow up.

6.3.2 An optimised treatment course for NTCU

Cohort D (Figure 6.1.A) was initiated where the NTCU dosing period was increased from 8 to 12 weeks and the period of observation from 10 to 12 weeks. In total, the period of assessment was extended from 18 weeks in cohort B to 24 weeks in cohort D. Batches of animals, containing equal number of LRIG1-null, LRIG1-heterozygous and wild-type animals were set up at 3 weekly intervals, allowing closer monitoring of untoward effects and to simplify dosing. The follow-up period was curtailed at 11 weeks, giving a 23 week total treatment period. This was due to breathlessness and a general deterioration within the colony. As the treatments were staggered, I needed to ensure all animals could reach the same end point and would not have to be culled early.

All of the animals showed an initial weight gain and the weights in the treatment and control groups were comparable until 10 weeks (Figure 6.2.A). Beyond 10 weeks, the control mice continued to gain weight whilst the weight of the treatment groups levelled. There was no significant difference in the weights of the wild-type, LRIG1-heterozygous and LRIG1-null treatment arms. By 23 weeks, a difference of 27% was seen between the weights of the control and LRIG1-heterozygous treated animals.

Initially, LRIG1-heterozygous animals were used as controls, as there was a surplus of LRIG1-heterozygous mice (in accordance with the principles of the '3 Rs' (207). However, following the finding by Powell *et al*, that LRIG1-null mice develop gut adenomas, which spontaneously progress to adenocarcinomas (94), LRIG1-null controls were also subsequently included to ensure the LRIG1-null animals did not develop spontaneous lung tumours. The weights of the LRIG1-null control animals mirrored that of the LRIG1-heterozygous controls (Supplementary, Figure 1).

Histology from cohort D showed the animals developed lesions that recapitulated human disease. All grades of lesions were seen across the treatment arms. Low-grade lesions, with multiple layers of cells and retention of organization from the basal layer to cells of a more squamous appearance along the luminal edge were apparent (Figure 6.2.Bi), as was flat atypia (Figure 6.2.Bii), defined through nuclei of abnormal morphology and increased basal cell size. These areas were most clearly identified by staining for KRT5. In healthy mice, KRT5 is not seen beyond the cartilage-containing airways (176), meaning any single layer of KRT5-stained cells beyond the cartilage-containing trachea and the immediate origin of right and left main bronchi is abnormal. This increased KRT5 expression is the first indication of a more squamous phenotype and is classified as flat atypia.

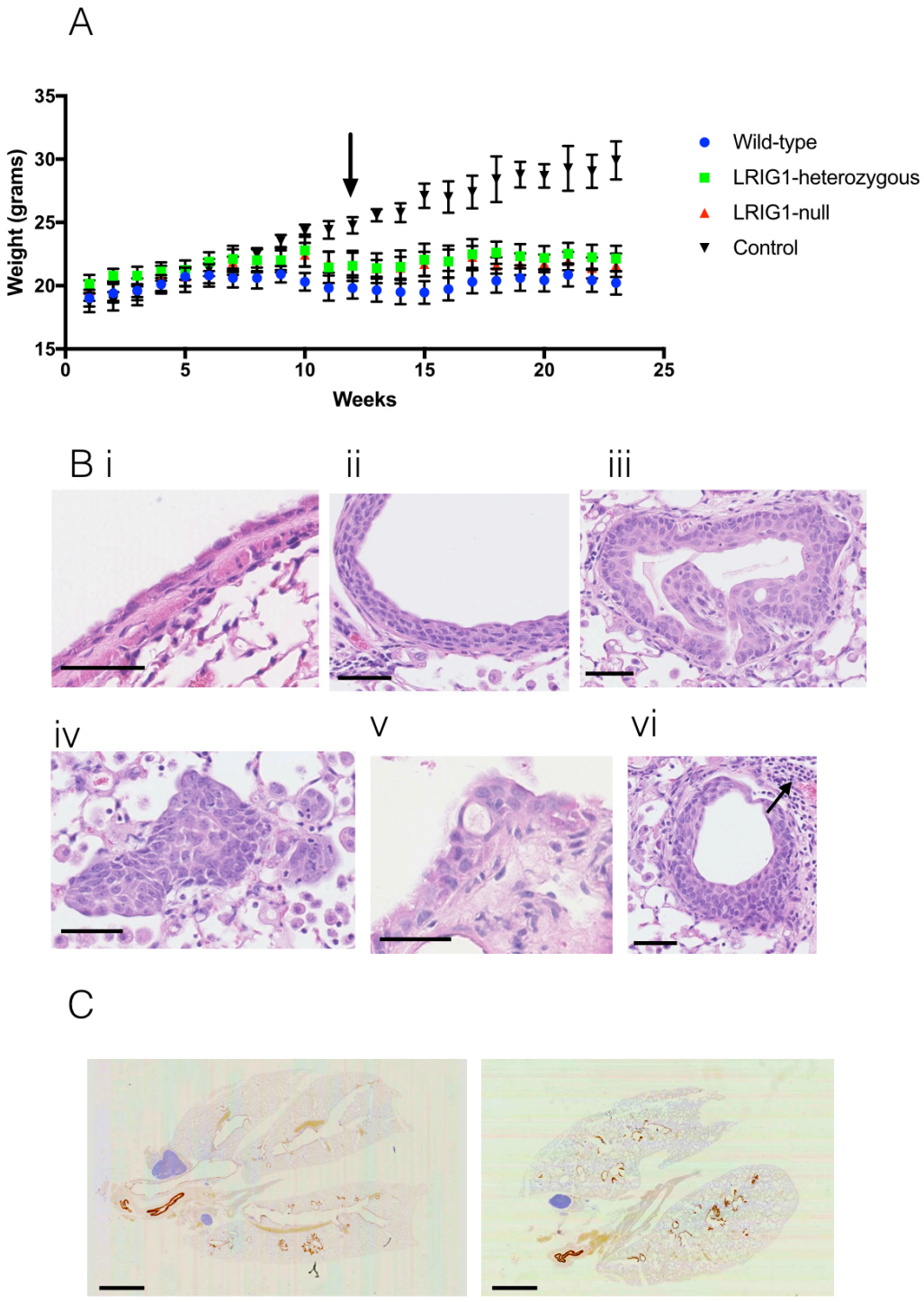

Figure 6.2: Cohort D, the final dosing regimen in the NTCU treated animals

A) Weights of cohort D, NTCU-treated mice and controls. Arrow indicates end of NTCU treatment period. Error bars signify S.E.M, n= 7-10 per group. B) i) Flat atypia, with enlarged, flattened nuclei, and increased nuclear- cytoplasmic ratio, scale bar = 50 μm. ii) Low-grade dysplasia. Multiple, ordered layers of epithelial cells, with clear organisation from the basement membrane to the luminal surface. Note flattened nuclei adjacent to the lumen, scale bar = 50 μm. iii) High-grade dysplasia, with the presence of disordered layers of epithelial cells and multiple enlarged nuclei, scale bar = 50 μm. iv) Invasive squamous cell carcinoma lesion, beginning to fill the alveolar spaces, scale bar = 50 μm. v) Close-up image of a keratin pearl, a characteristic feature of squamous cell carcinoma, scale bar = 50 μm. vi) Bronchiole showing high-grade dysplasia and breakdown of the basement membrane (arrowed). This signifies an early squamous cell carcinoma. Note inflammatory infiltrate in the top right corner, scale bar = 50 μm. Images representative of lesions seen in treated mice of all genotypes. C) Caudal sections of the lung, stained with keratin 5 (KRT5). The KRT5 expression indicates localisation of changes to the distal lung, scale bar = 5 mm.

High-grade lesions were classified as lesions several layers thick, with abnormal cellular morphology and no organization between the basal layer and the luminal cells (Figure 6.2.Biii). Invasive cancers were seen to fill the alveolar spaces and they exhibited large nuclei with increased nuclear-to-cytoplasmic ratio (Figure 6.2.Biv). Keratin pearls, a classical feature of squamous aetiology (251), were visible in the more advanced lesions (Figure 6.2.Bv). Areas where high-grade dysplasias were seen to break the epithelial basement membrane, becoming invasive cancers, were also present (Figure 6.2.Bvi).

Lesions were clearly distributed in the periphery of the lung, beyond the main bronchi (Figure 6.2.C). These formed two main patterns: disease lining the bronchioles and invasive lesions clustered around the distal bronchioles. Invasive disease was seen to occur within the periphery of the lung, rather than arising from the main airway.

No tumours, invasive lesions or basal cell hyperplasia was seen in the control animals. These included animals of both the LRIG1-heterozygous and LRIG1-null genotypes.

6.3.3 NTCU treatment complications

Animal losses occurred across all treatment groups. There was no predilection for the genotype of the mouse (Figure 6.3.A) and no losses occurred in the control groups. The main cause of death was bowel distension. This affected 6 of the 37 animals that were treated as part of cohort D and one of the animals in cohort C. 5 of the 6 animals were culled due to the animals reaching humane end points. The cases all appeared during the monitoring phase of the experiment, after NTCU dosing was complete. A further mouse developed abdominal swelling that was intermittent and did not progress over a 4-week period. This animal completed the observation period and was included in the analysis. The affected animals were not littermates and were from different breeding pairs, making a spontaneous genetic

mutation unlikely. Once the abdomen had begun to swell, other than in the one mouse, it progressed rapidly, was associated with severe breathlessness, lack of movement and grimacing, which necessitated immediate culling. On dissection, the abdomen was markedly distended (Figure 6.3.Bi), with the entire bowel swollen from stomach to colon. It is known that LRIG1-null mice develop spontaneous bowel adenocarcinomas after several months (94), but on removing the bowel, neither a circumferential lesion nor blockage was evident. Samples taken for histology showed necrosis, an inflammatory infiltrate and oedema (Figure 6.3.Bii and 6.3.Biii). Discussion with a pathologist confirmed necrosis, however, no other anomalies such as tumour mucosal deposits were visualised. It was felt the necrosis was secondary to the enormous bowel distension and disrupted blood supply, rather than being the initiating event. The cause of death appeared to be a septic ileus with increased air ingestion. A further discussion with Avrum Spira's group, Boston University, USA, revealed similar complications within their NTCU-treated animals. They attribute this side effect to overwhelming sepsis following an NTCU-provoked systemic inflammatory state.

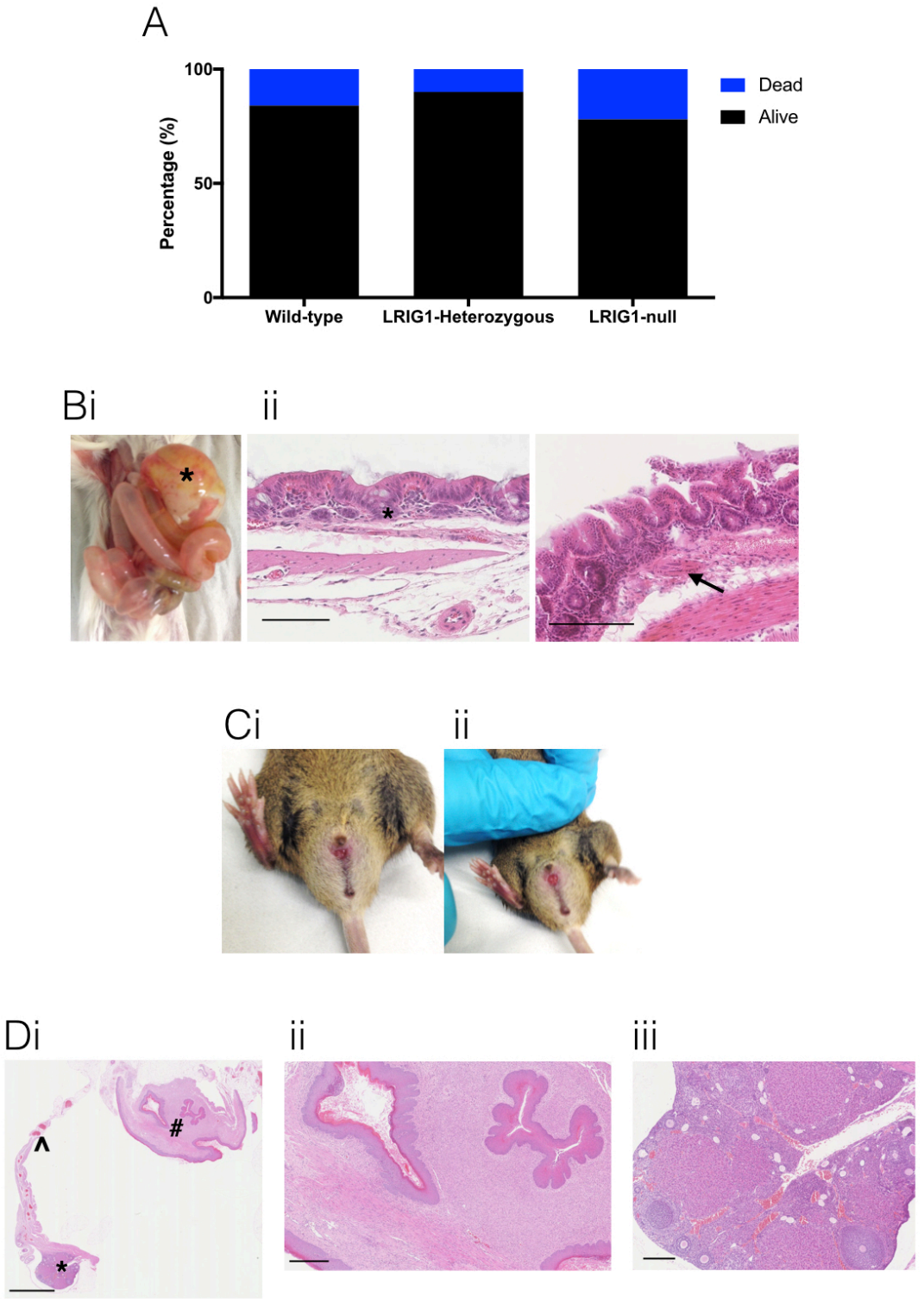

Figure 6.3: Complications of NTCU treatment

A) The number of animals lost from cohort D, according to genotype. B) i) Gross distension of the bowel, with air insufflation and opacity of the walls. Stomach indicated by *. ii) Haemotoxylin and eosin (H&E) staining of the bowel wall, with inflammatory infiltrate, indicated by * and haemorrhage, indicated by arrow, scale bars = 200 µm and 100 µm. C) i) Genital swelling, with distension of soft tissue around the vaginal introitus. ii) Compression on the abdomen increases the genital swelling, implying possible prolapse. D) i) H&E staining of the ovary (*), fallopian tube (^) and uterus (#), revealing no abnormality, scale bar = 2 mm. ii) Close up image of the ovary, with normal follicular appearances, scale bar = 200 µm. iii) Close up of the endometrium, showing no evidence of malignancy, scale bar = 400 µm.

Genital abnormalities were a further complication that had not previously been reported when using the NTCU-model. These changes occurred after the NTCU dosing period and affected both the vulva and vaginal introitus in cohorts C and D (Figure 6.3.C). The swelling was increased by abdominal compression, suggesting the pathology was secondary to a raised intra-abdominal pressure or vaginal prolapse. Although some mouse strains are susceptible to vaginal and rectal prolapse (257, 258), these complications had not previously been seen within the colony. Following discussion with the animal unit NACWOs and veterinary surgeon it was advised to cull the animals and collect their reproductive organs. Histology showed normal ovarian tissue (Figure 6.3.Dii) and a normal endometrium (Figure 6.3.Diii), with no evidence of malignancy. In total, 3 animals from cohort C were culled due to the genital abnormalities, none of which developed weight loss or features of distress. 3 further animals in cohort D showed genital changes, these were managed by close observation and daily application of aqueous cream to the affected areas. The swellings were noted to be intermittent and all three of the cohort D animals reached the experimental end points. There was no correlation of the genital changes with the genotype of the mouse (with the abnormality seen in all genotypes), the degree of the disease seen in the lung or whether the animals were of the same litter.

6.3.4 Investigation for NTCU-associated disease in other organs

Other than skin ulceration (253), NTCU-associated disease in other organs has not been reported. When the animals were culled, they were opened along the midline and no visible intra-abdominal pathology (other than in the animals that failed to reach the experimental end point) was identified. To assess further for disease, both the skin and liver were removed.

The animals were shaved for NTCU application. Once treatment ceased, the fur regrew. Only one animal, from cohort B, developed a skin lesion. This appeared irritation-related and resolved on treatment. When the organs were harvested, the skin was re-shaven and palpated to detect any underlying lesion. The skin was subsequently removed and processed. No macroscopic or microscopic anomalies were detected (Figure 6.4.A).

There were no macroscopic anomalies in the liver, however, microscopically, 4 of the animals had lesions. These lesions were of a different appearance to the normal homogeneous liver architecture, with disorganised cells and visible red blood cells (Figure 6.4.B). There was no association with genotype and the animals had not lost weight. The liver changes were discussed with a liver pathologist and were felt to be consistent with necrosis. The lesions were thought to have occurred pre-mortem, with drug toxicity a probable cause.

The upper part of the trachea, from the midpoint to the larynx was taken for assessment. No evidence of convincing preinvasive disease was seen (Figure 6.4.Ci and 6.4.Cii). The section of trachea from the point of insufflation into the bronchi was damaged following lung insufflation, however, no preinvasive disease was seen. KRT5 staining confirmed the presence of a single layer of KRT5 cells throughout this section of trachea. This excluded the development of any preinvasive lesion other than early flat atypia.

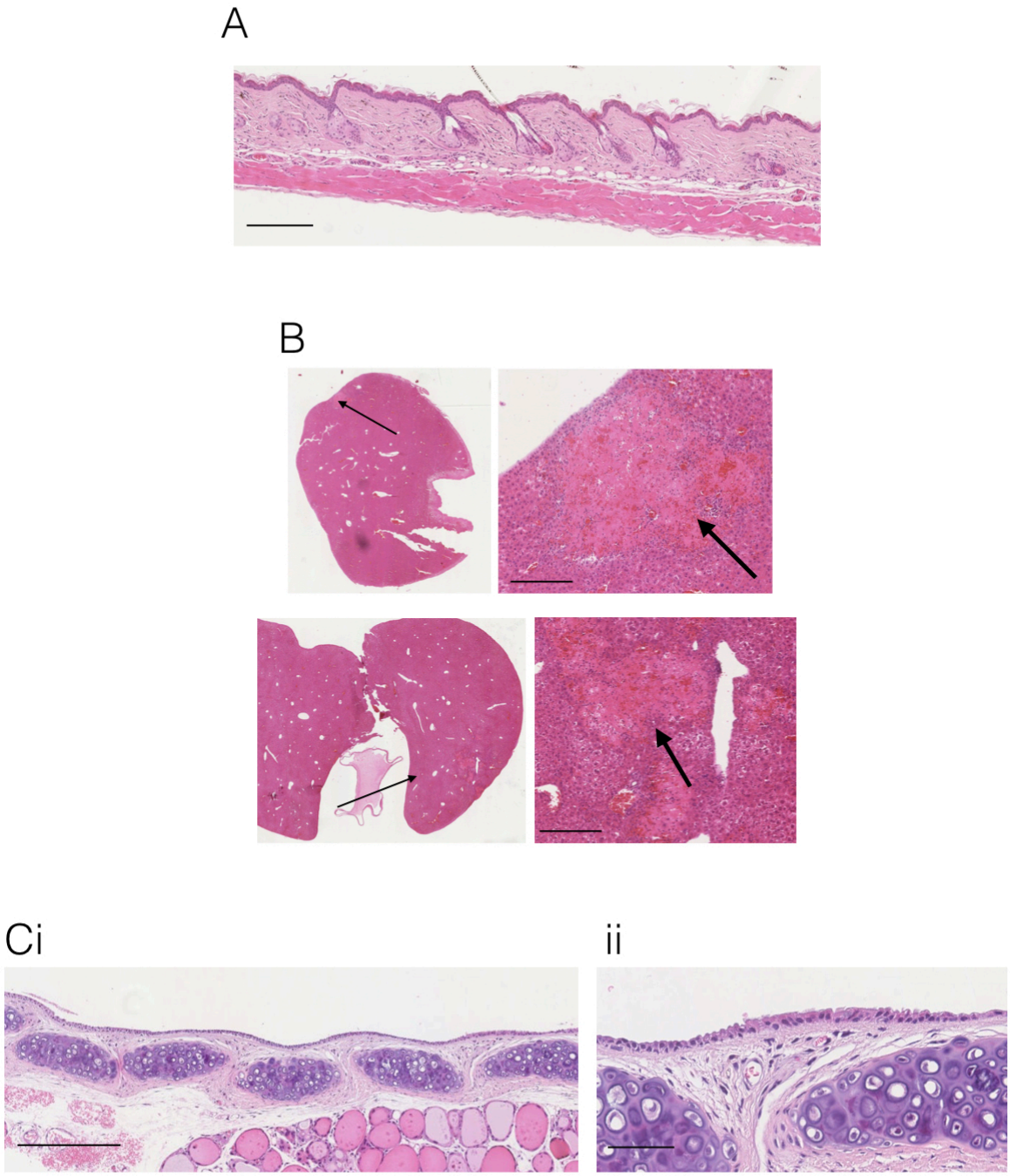

Figure 6.4: Assessment of NTCU-mediated disease outside the lung and in the upper trachea

A) Haemotoxylin and eosin (H&E) staining showing normal structure of the skin. No evidence of hyperproliferation within the epidermis or hair follicle and no tumours visualised, scale bar = 200 μm. B) H&E staining showing liver abnormalities. These are seen as areas of different density within the liver, indicated by arrows. Close up of these areas shows necrosis with loss of the normal liver architecture and an infiltration of red blood cells. Scale bar = 200 μm. C) i) H&E staining of the upper trachea, revealing normal architecture with no evidence of preinvasive lesions or tumours, scale bar= 250 μm. ii) Close up of tracheal epithelium with normal epithelial cells seen, scale bar = 50 μm.

6.3.5 Validation of NTCU-induced preinvasive squamous cell lesions

NTCU is associated with the development of squamous cell lung cancers. To confirm the developing lesions were of a squamous phenotype, the lungs were stained for a number of markers. Both KRT5 and p63 are markers of squamous cell lung cancers and have been used to validate NTCU-induced preinvasive and squamous cell lesions (252, 255, 259, 260).

KRT5 is not expressed beyond the trachea in the normal murine airway (other than rare cells in the distal lung) (176) but clear expression was seen in the peripheral lung in the NTCU treated mice. KRT5 staining was seen across the bronchial tree and marked early, preinvasive, flat atypia lesions (Figure 6.5.A). KRT5 staining was also evident in both low-grade and high-grade lesions (Figure 6.5.Aii) and throughout the cells of invasive squamous cell lung tumours (Figure 6.5.Aiii).

In the normal airway, p63 marks basal epithelial cells that are adherent to the upper airway basement membrane. Interestingly, p63 staining is seen in preinvasive lesions, beyond the trachea, but only within the cells that are in contact with the basement membrane. As the lesions become more advanced with a progressive increase in the number of layers of cells, the p63 expression remains restricted to the cells in contact with the membrane (Figure 6.5.B). When invasive lesions are stained for p63, variable expression is seen within the tumour. The highest levels appear to be in those constrained by the alveolar membranes (Figure 6.5.Biii).

EGFR is overexpressed in preinvasive and squamous cell lung cancers (261). EGFR expression is seen along the basolateral membrane of the epithelium, throughout the bronchial tree. Staining for EGFR confirmed that in both preinvasive lung lesions and lung tumours, EGFR expression had increased, beyond that of basal levels (Figure 6.5.C).

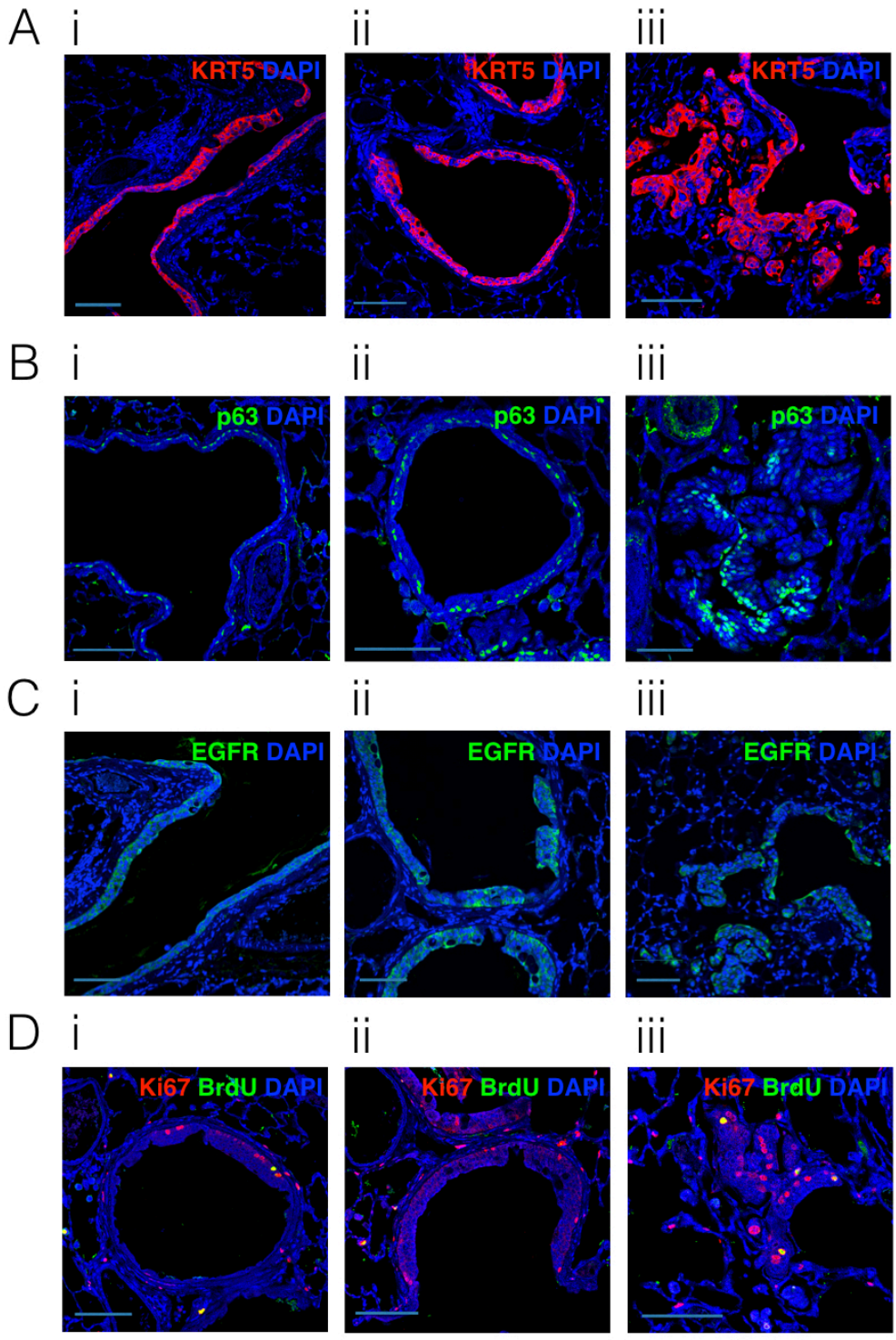

Figure 6.5: Confirmation that preinvasive and invasive lesions have a squamous phenotype

A) Keratin (KRT5) immunofluorescence staining (red) shown in i) flat atypia, with KRT5 expression seen only in those cells adjacent to the basement membrane, in ii) low-grade and high-grade dysplasia where KRT5 is expressed throughout the increased layers of epithelial cells and in iii) an invasive tumour where KRT5 is seen distributed across all abnormal cells. B) p63 immunofluorescence staining (green), demonstrated in i) distal airway flat atypia, ii) in the cells adjacent to the basement membrane in low-grade atypia and in iii) invasive tumours, where the p63 expression is not uniform but appears with highest concentration in the cells along a basement membrane and lining the alveolar surface. C) Epidermal growth factor receptor (EGFR; green), seen in i) low-grade dysplasia and flat atypia, ii) high-grade lesions and iii) within invasive tumours. D) Ki67 (red) and BrdU (green) immunofluorescence staining of i) low-grade lesions and ii) high- grade dysplasia where the proliferative cells are those seen along the basement membrane, and in iii) tumours, where the proliferative cells are distributed throughout the tumour. Ki67 labels a greater number of cells than 4 hours BrdU labelling. In all cases, DAPI used as a counterstain and n= 3, with wild-type, LRIG1-heterozygous and LRIG1-null animals used for comparison. Scale bar = 50 μm.

To assess proliferation, sections were stained for both BrdU and Ki67. BrdU was administered 4 hours prior to sacrifice, but revealed very few proliferative cells within areas of preinvasive disease (Figure 6.5.D). Those that were stained were in contact with the basement membrane. To obtain a clearer indication of proliferation, Ki67 staining was also performed. This staining marked a greater number of cells, and similarly to BrdU, the staining was detected in the cells in contact with the basement membrane. Within the lung tumours there was a suggestion that the cells on the tumour periphery were more proliferative with increased Ki67 staining (Figure 6.11.E).

6.3.6 Assessment for markers of adenocarcinoma

Surfactant protein C (SPC) and thyroid transcription factor 1 (TTF1) are markers of type 2 cells within the distal airway (262). Both are overexpressed in lung adenocarcinoma (256, 262). As NTCU-induced lesions were anticipated to be SPC-negative and had previously been reported to be negative for TTF1 (253, 259), dual staining was performed with either SPC or TTF1 in association with KRT5. The KRT5 staining was used to identify areas of disease.

As expected, the preinvasive lesions were negative for SPC, as were the cells within invasive lesions (Figure 6.6.Aiii). However, the TTF1 staining was unexpected, with TTF1-positive cells detected across all grades of preinvasive and invasive lesions (Figure 6.6.B). TTF1-positive cells within the preinvasive lesions were dual positive for both KRT5 and TTF1. The intensity of TTF1 staining was greatest in the alveolar type 2 cells and was slightly lower in those cells positive for KRT5. However, the co-staining of TTF1 and KRT5 was clearly brighter than both the negative control and the nuclei in the DAPI-stained stromal and alveolar type 1 cells. To further characterise these lesions, combined stains were performed to examine airway marker co-expression.

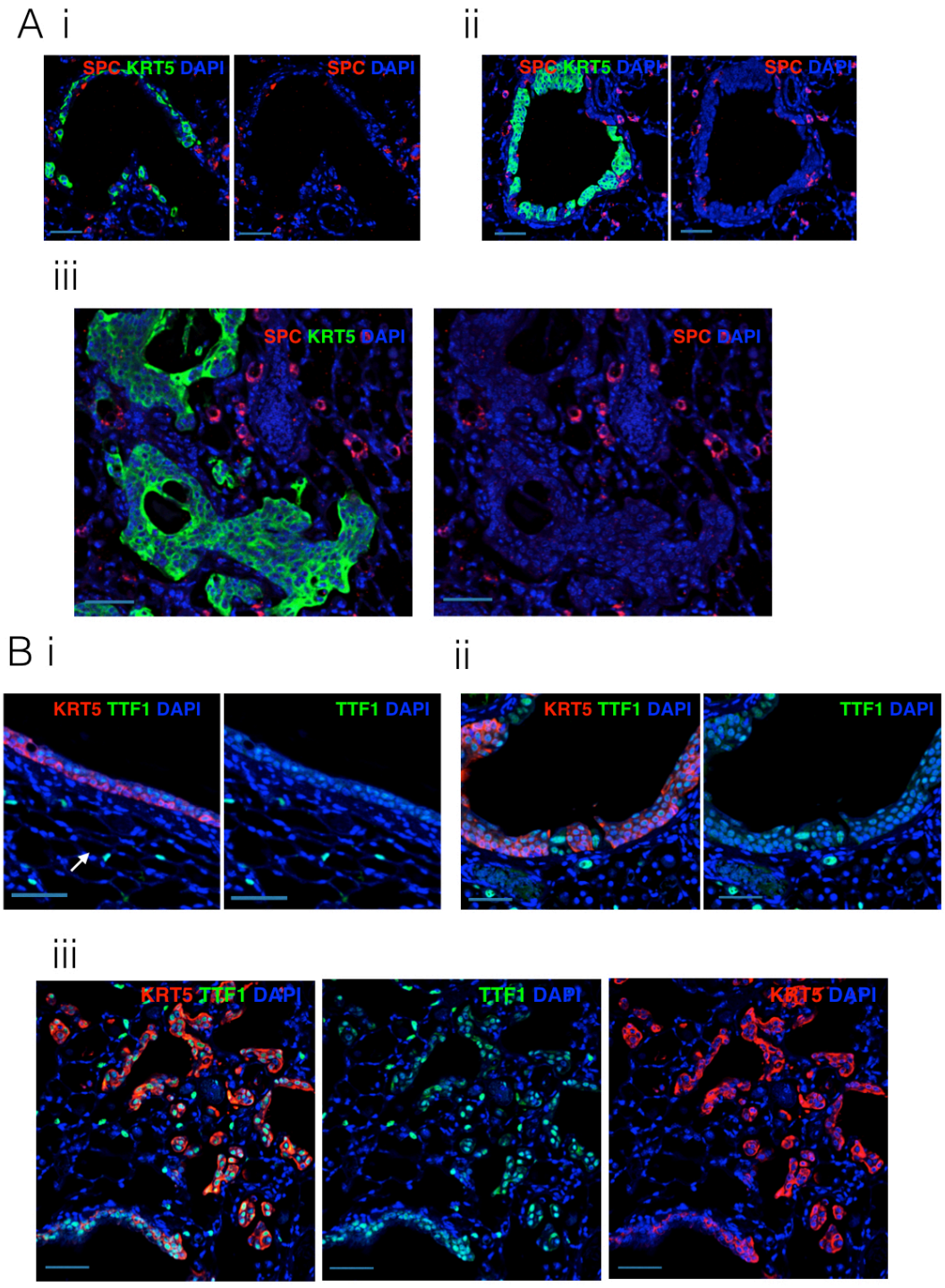

Figure 6.6: Assessment of lesions for the adenocarcinoma associated markers TTF1 and SPC

A) i) Immunofluorescence staining using surfactant protein C (SPC; red) and keratin 5 (KRT5;green) to identify abnormal areas. No SPC positive cells are visible in flat atypia lesions, scale bar = 50 μm, ii) SPC (red) and KRT5 (green) staining of a low-grade lesion. Again, no SPC-positive cells are seen within the lesion, scale bar = 50 μm, iii) SPC (red) and KRT5 (green) staining of tumour, showing no evidence of dual staining for SPC and KRT5, scale bar = 50 μm. B) i) Immunofluorescence staining for thyroid transcription factor 1 (TTF1; green), with KRT5 (red) highlighting areas of abnormal epithelium. In an area of flat atypia, TTF1 staining is seen in association with KRT5. There is a gradient of TTF1 expression with highest intensity seen in the nuclei of alveolar type 2 cells (arrowed), an intermediate level in the dysplastic epithelium and negative staining in the nuclei of surrounding stroma and alveolar type 1 cells. Scale bar = 50 μm. ii) TTF1 (green) and KRT5 (red) staining in a low-grade lesion. Cells are dual stained for both markers, scale bar = 50 μm. iii) TTF1 (green) and KRT5 (red) staining in an invasive tumour. Cells that are dual stained for both markers are clearly visible, scale bar = 50 μm. In all cases DAPI used as a counterstain and n= 3, with staining performed on wild-type, LRIG1-heterozygous and LRIG1-null animals.

6.3.7 Elucidating the possible cell of origin of preinvasive and squamous cell lung cancers

To establish whether a TTF1-positive cell was the origin of the preinvasive lesion, and whether it co-localised with a subpopulation of basal cells, staining for TTF1, KRT5 and p63 was performed. p63 marks an airway basal cell that on airway injury can develop into a keratin 8 (KRT8)-expressing, p63-negative basal cell, and depending on Notch signalling then enters a ciliated or secretory lineage (132). Therefore, to assess the association of TTF1 with the p63 positive basal cells, triple staining was performed. As anticipated, all p63-positive cells within lesions were KRT5 positive and all cells in the preinvasive areas appeared to be TTF1-positive. The p63-positive cells were also TTF1-positive, but the intensity of staining was not increased in this population (Figure 6.7.A). TTF1 was reduced in the preinvasive lesion and tumours compared to the surrounding alveolar type 2 cells. Further co-staining for KRT5, CC10 and TTF1 revealed rare, triple-stained cells (arrowed) (Figure 6.7.B). It has been speculated that the origin of NTCU tumourigenesis is a p63-, CC10-, KRT5-expressing cell (260), however, staining for these markers revealed only one potential cell (Figure 6.7.C), and further areas need to examined.

Bronchioalveolar stem cells (BASCs) are thought to be a stem cell of the distal airway. These are identified through the coexpression of SPC and CC10 (129). BASCs were detectable in the distal lung (Figure 6.7.Di, arrowed) and showed a lower intensity of SPC staining compared to that seen in surrounding AT2 cells, consistent with the reported literature (129). The identified BASCs were not KRT5 stained (and there was no suggestion of any cells being triple stained for SPC, KRT5 and CC10), but the BASCs were consistently shown to be adjacent to areas of preinvasive disease (Figure 6.7.Di). On review of control sections, where animals had not been administered NTCU, lower BASC numbers was seen compared with the NTCU treated mice (Figure 6.7.Dii).

A i

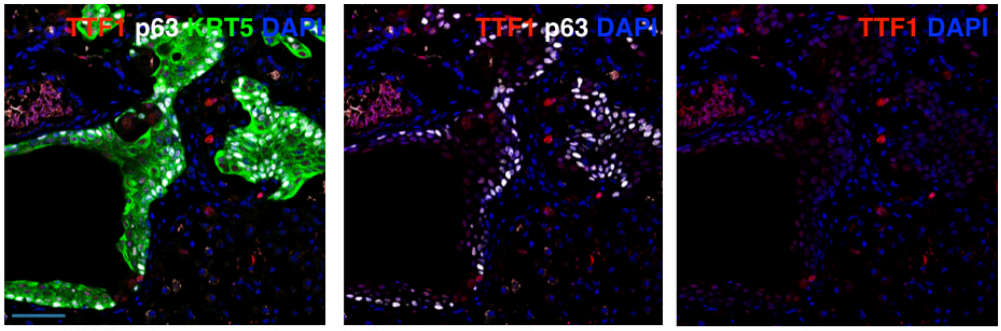
TTF1 p63 KRT5 DAPI
TTF1 p63 DAPI
TTF1 DAPI

ii

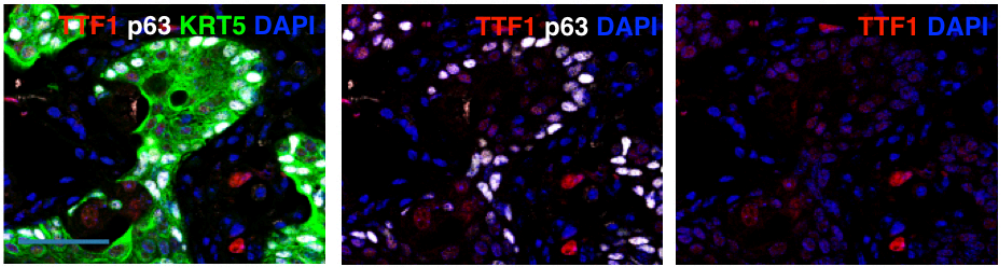
TTF1 p63 KRT5 DAPI
TTF1 p63 DAPI
TTF1 DAPI

B i

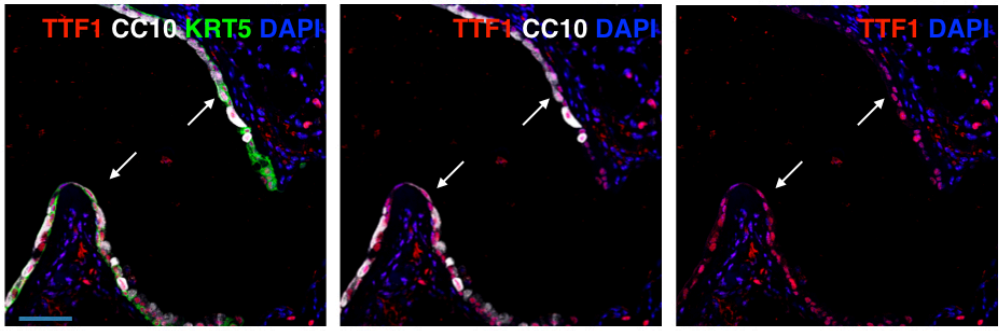
TTF1 CC10 KRT5 DAPI
TTF1 CC10 DAPI
TTF1 DAPI

ii

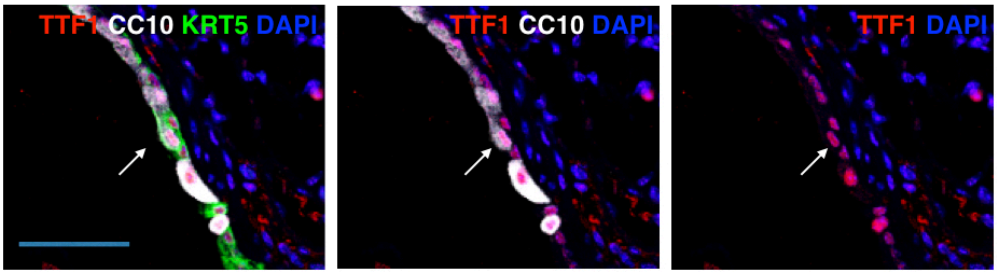
TTF1 CC10 KRT5 DAPI
TTF1 CC10 DAPI
TTF1 DAPI

C

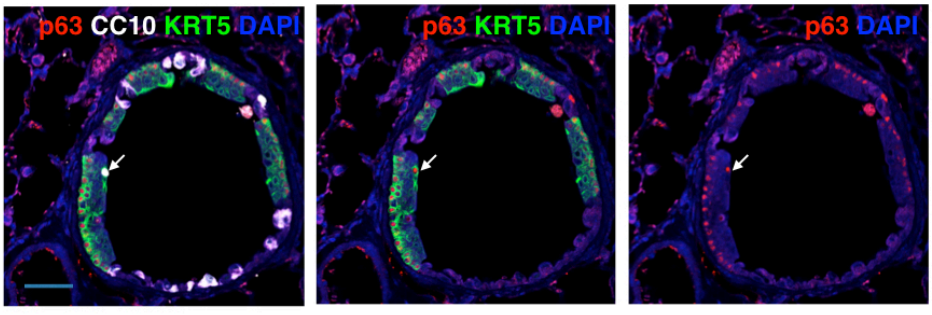
p63 CC10 KRT5 DAPI
p63 KRT5 DAPI
p63 DAPI

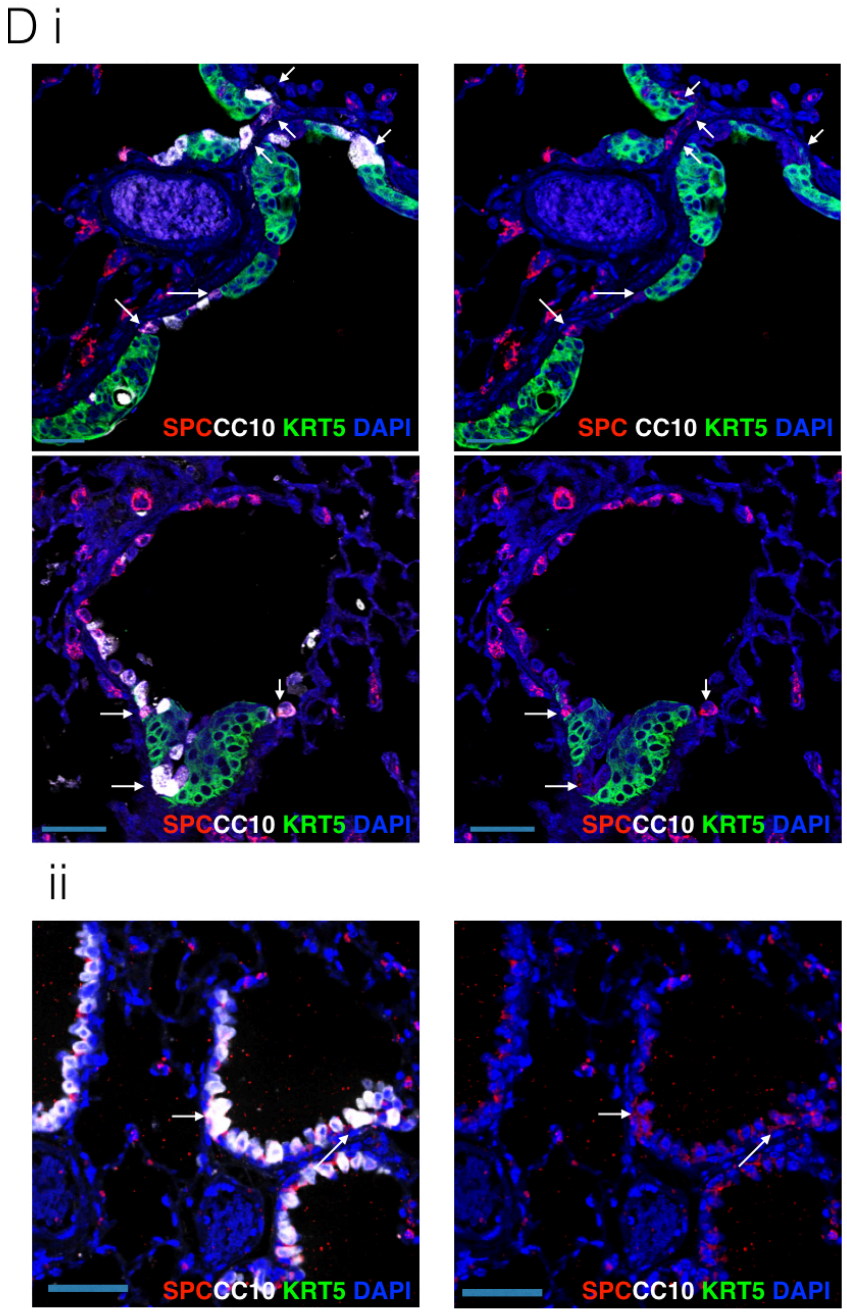

Figure 6.7: Co-staining of epithelial markers within the airway epithelium

A) i) Immunofluorescence staining of a preinvasive lesion for keratin 5 (KRT5; green), p63 (white), and thyroid transcription factor 1 (TTF1; red), indicating triple stained epithelial cells. Combined image on left. Centre shows overlap of p63 (white) and TTF1 (red) expression, whilst right image shows TTF1 staining (red) with DAPI counterstain. The expression of TTF1 can be seen in alveolar type 2 cells and also in dual $p63^{+}/KRT5^{+}$ cells, but at a reduced level. Scale bar = 100 μm. ii) Close up image from i), demonstrating clear triple expression. Scale bar = 50 μm. B) i) Immunofluorescence staining of a preinvasive lesion for KRT5 (green), Clara cell 10 (CC10; white) and TTF1 (red). DAPI used as counterstain. Two $KRT5^{+}CC10^{+}TTF1^{+}$ cells are visible, indicated by arrows. Scale bar = 100 μm ii) Close up image of the $KRT5^{+}CC10^{+}TTF1^{+}$ epithelial cell, showing a clear overlap in staining. Scale bar = 50 μm. C) Immunofluorescence staining of a preinvasive lesion for KRT5 (green), p63 (red) and CC10 (white). Combined triple-stained image on left, centre image showing KRT5 and p63 staining and right image p63 staining. Arrow indicating a $KRT5^{+}p63^{+}CC10^{+}$ triple- stained cell. Scale bar = 50 μm. D) i) Immunofluorescence staining of bronchioalveolar stem cells (BASCs), which show positive staining for CC10 (white) and SPC (red) (arrowed). Areas of preinvasive disease are indicated by staining for KRT5 (green). ii) Immunofluorescence staining in control mice, not treated for with NTCU, showing BASCs, indicated by arrows. In all cases n= 3, with staining undertaken in wild-type animals. Staining performed by Dr Sandra Gomez Lopez.

6.3.8 Development of lung adenocarcinoma

A single mouse in cohort D lost weight rapidly and fell below the 20% acceptable weight loss limits, necessitating culling. In total the mouse had received 12 weeks of treatment followed by 7 weeks of follow up and had a wild-type genotype. On removal of the lungs, a large tumour was seen that encompassed the majority of the right upper lobe (Figure 6.8.A). The histological appearances differed to the previously seen KRT5-positive invasive lesions. The tumour consisted of tightly-packed cells, with large nuclei and a glandular morphology. A further area was present within the leftt upper lobe, which exhibited similar features and had the characteristic glandular organization of a lung adenocarcinoma (Figure 6.8.B).

Both the large right upper lobe tumour and left upper lobe tumour were KRT5-negative, although there were many KRT5-positive, preinvasive lesions at the lung bases (Figure 6.8.C). To confirm the tumour identity, sections were stained for the adenocarcinoma markers TTF1 and SPC and in addition to KRT5, the squamous cell markers p63 and EGFR. The lesions were positive for SPC and TTF1 and negative for KRT5, EGFR and p63, confirming the tumours adenocarcinoma identity (Figure 6.8.D).

Ageing FVB/N mice do develop spontaneous lung adenomas (180) and in NTCU-treated FVB/N animals these adenomas have been observed to progress to adenocarcinomas (259). Only this mouse developed features of lung adenocarcinoma and there was no evidence of lesions in either the control mice (in either the LRIG1-heterozygous or LRIG1-null controls), or in other treated animals. This may have become more problematic should the animals have been treated for longer periods of time.

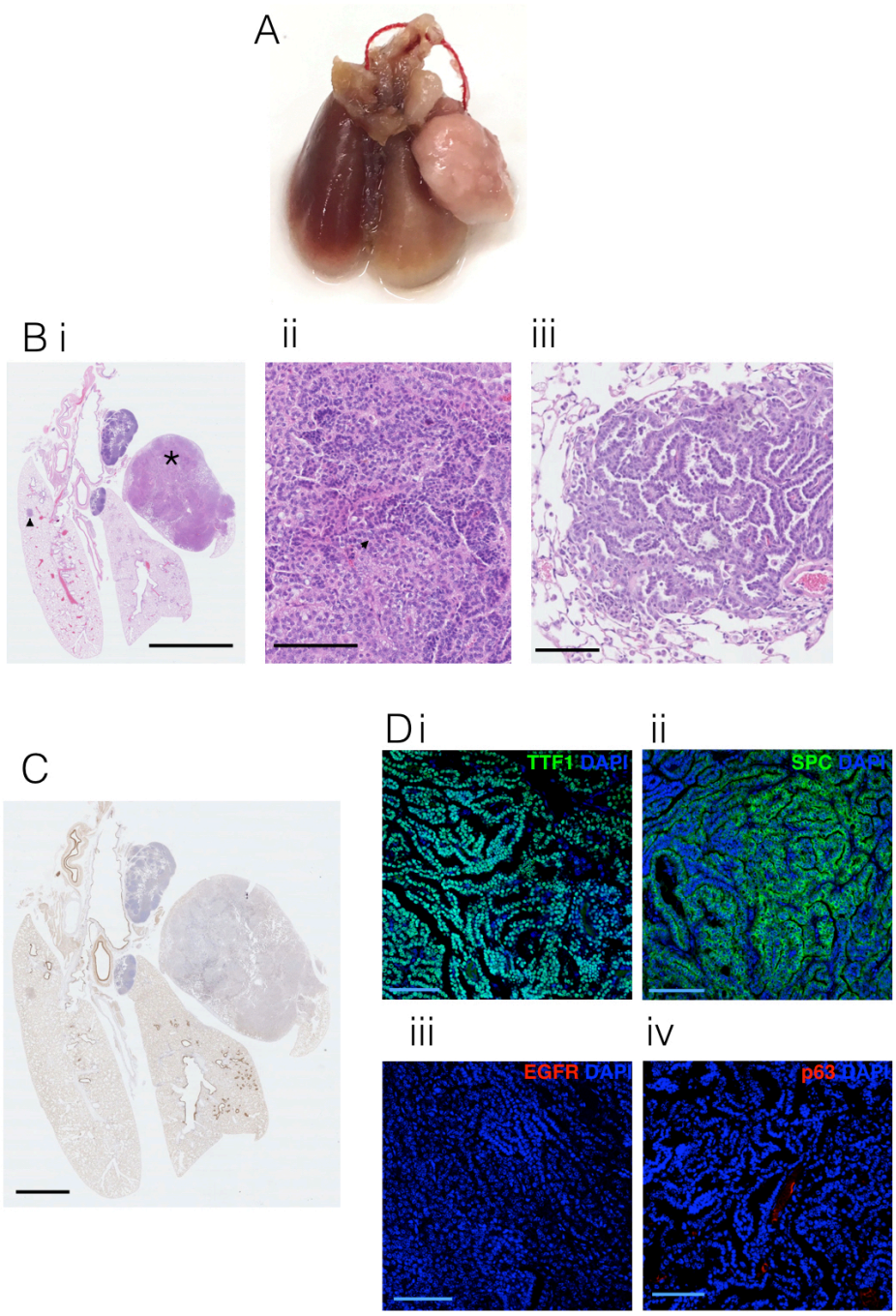

Figure 6.8: Appearance of adenocarcinoma in an NTCU-treated LRIG1-heterozygous animal

A) Large tumour situated within the right upper lobe. The usual smooth surface of the lung seen on the right is replaced by nodular densities. B)i) Haematoxylin and eosin (H&E) staining of a caudal section of lung. Tumour has almost completely replaced the normal architecture of the left upper lobe. A further opacity is present in the right upper zone (arrow head). Scale bar = 0.5 cm. ii) Close up image of left upper lobe tumour, from area marked with '*' in 'i'. Cells have a tightly- packed glandular appearance with an increased nuclear to cytoplasmic ratio, scale bar = 200 µm ii) Close up image of right-sided lesion, marked with an arrow head. Cells are less tightly packed and the glandular structure is apparent, scale bar = 100 µm. C) Keratin 5 (KRT5) staining of lung. Note both the left upper lobe tumour and right sided lesion are negative. KRT5 staining is seen, particularly at the left lung bases and right upper zone. These areas show features characteristic of preinvasive and invasive squamous cell carcinoma, bar = 250 mm. D)i) Staining of tumour for the nuclear protein thyroid transcription factor 1 (TTF1; green), scale bar = 100 µm. ii) Staining of the cytoplasm of the tumour cells for the alveolar type 2 cell associated protein surfactant protein C (SPC; green), scale bar = 100 µm. iii) Tumour negatively stained for epidermal growth factor receptor (EGFR) (red), bar = 100 µm. iv) Tumour negatively stained for p63 (red), bar = 100 µm.

6.3.9 Association of LRIG1 with preinvasive and invasive squamous cell lung tumours

As shown, LRIG1 is not expressed within the distal lung parenchyma, but is seen within the distal airway bronchioles (Chapter 3). To confirm whether LRIG1 expression is detectable when preinvasive lesions develop, slides were co-stained for eGFP (to identify the presence of the eGFP reporter protein, and hence LRIG1) and KRT5 (to identify areas of preinvasive disease). eGFP expression was seen within lung tumours as well as the preinvasive lesions (Figure 6.9.A); the eGFP expression was also seen in LRIG1-null animals (Figure 6.9.B). As expected, this eGFP staining was absent in wild-type mice (Figure 6.9.C).

As LRIG1 is clearly expressed in the distal lung, and the NTCU- induced lesions are developing in the distal airway (instead of the trachea), the effect of the loss of LRIG1 on the development of preinvasive lesions can be assessed in this model. In addition, the expression of eGFP in LRIG1-null mice in the lesions indicates that the *Lrig1* promoter is active and suggests an ongoing biological need for LRIG1.

In the LRIG1-heterozygous animals there is clear eGFP expression (and hence LRIG1 expression) in association with both the preinvasive lesions and tumours. In humans LRIG1 expression is lost in preinvasive lung cancer development (104), but in this mouse model the presence of eGFP indicates that LRIG1 expression is ongoing.

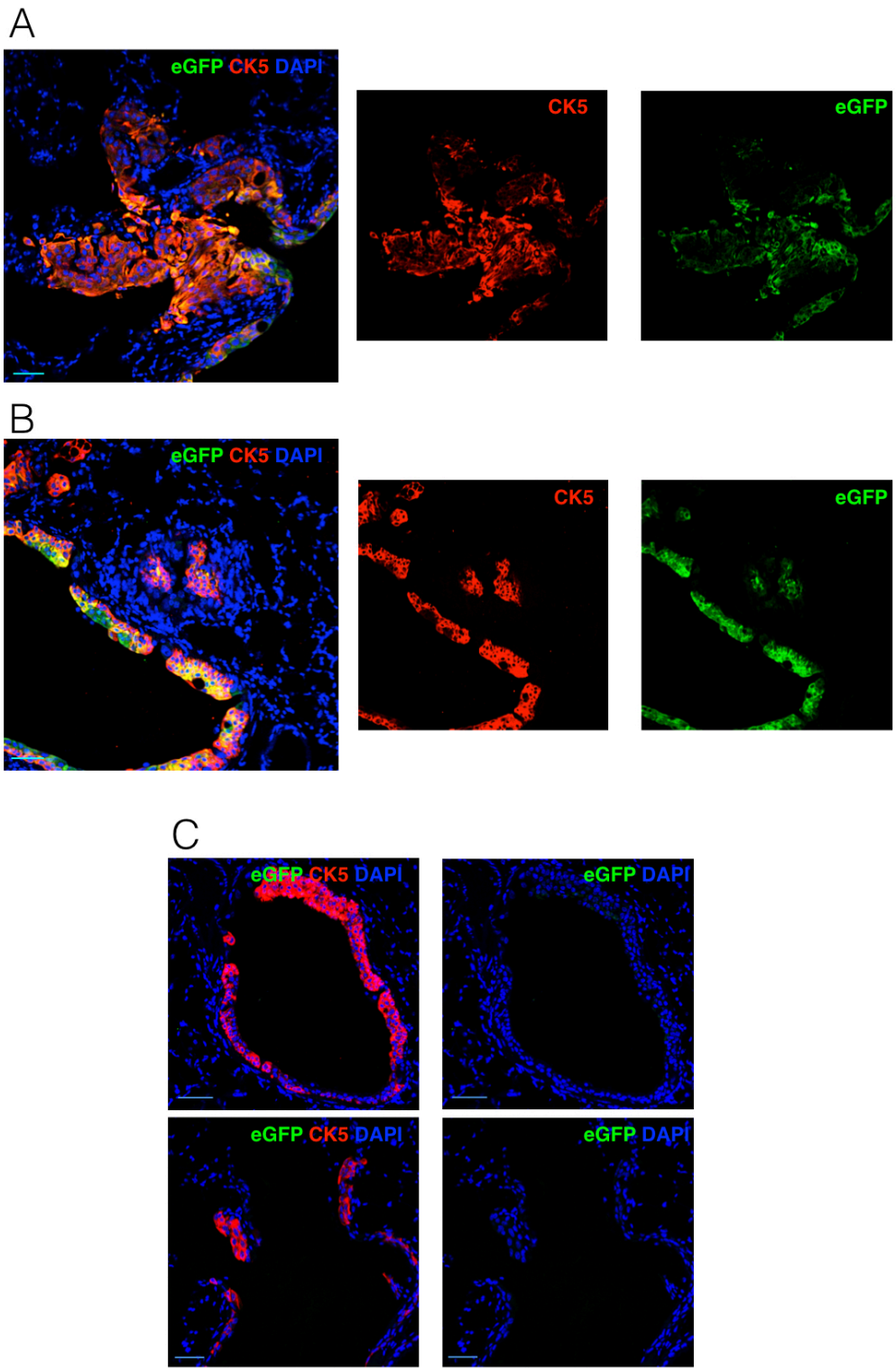

Figure 6.9: Expression of LRIG1 in lesions of the distal airway

A) Immunofluorescence staining of a distal airway tumour in an LRIG1-heterozygous animal. Keratin 5 (KRT5; red) was used to identify abnormal areas, whilst eGFP (green) was used to assess areas of LRIG1 expression. Left image shows combined stains, centre KRT5 staining and right eGFP (LRIG1) expression, scale bar = 50 μm. B) Immunofluorescence staining for KRT5 (red) and eGFP (green) in an LRIG1-null mouse. Both preinvasive and invasive cancers are seen, both expressing KRT5 and eGFP, scale bar = 50 μm. C) No eGFP expression in a wild-type mouse. KRT5 staining has marked the abnormal area. The left image shows both KRT5 and eGFP staining, right image shows eGFP staining, indicating no expression in wild-type preinvasive lesions, scale bar = 50 μm. n=3 and staining performed on wild-type, LRIG1-heterozygous and LRIG1-null animals.

6.3.10 Assessment of the effects of NTCU application

Different methods of quantifying NTCU-induced lesions have been reported. These range from the use of PET-CT (263), to sectioning lesions at intervals and counting areas of disease. Hudish *et al* simply counted the number of each type of preinvasive lesion across 3 sections, 50 µm apart, without considering lesion size (255). Another group analysed the percentage of each bronchiole covered by each type of lesion (low- grade dysplasia, etc.) and then approximated this to the nearest 25% across three sections, 100 µm apart (253).

It was clear that the lesions that developed within my colony were not uniform and were of varying sizes. I was concerned that if I was to simply count the number of lesions I may underestimate the extent to which the airways were affected. Assessing the surface areas of lesions to the nearest 25% also appeared insensitive due to the subtle abnormalities between each section, and counting lesions in sections at only 50 or 100 µm apart seemed to be too narrow a margin. A number of tumours were greater than 50 µm in diameter, so if sections were analysed at only 50 µm apart, some tumours may be counted twice.

To obtain a clear representation of the lungs and bronchial tree, lung blocks were cut until the trachea and main bronchi were reached. Cutting until this point ensured that the greatest visible lung surface area and greatest proportion of the bronchial tree was included. Two sections were analysed at 200 µm apart, with an average taken of the two. KRT5 staining beyond the trachea and left and right bronchi is not seen in the mouse under normal conditions (176), so to assess the degree by which the individual animal had been affected by NTCU application, the percentage of the distal airway (that beyond the trachea and the origin of the right and left main bronchi) that expressed KRT5 out of the total airway was elucidated. The abnormalities were then divided into high-grade, low-grade and flat atypia and the difference between wild-type, LRIG1-heterozygous and LRIG1-null animals compared. To assess invasive lesions, the number of tumours per section was counted and then both their surface area and the total lung surface area recorded.

Dividing the total surface area of tumour by the total surface area of lung allowed the percentage of lung affected by tumour to be calculated.

KRT5 staining in the distal lung showed that, following NTCU treatment the proportion of wild-type and LRIG1-heterozygous airways affected by abnormal epithelium was similar. There was, however, a significant reduction in the proportion of the airway stained by KRT5 in the LRIG1-null mice ($p < 0.05$) (Figure 6.10.A). To assess whether LRIG1-null animals developed lesions of a greater severity, the type of airway lesion was classified and the proportion of the abnormal airway affected by each grade of abnormality was calculated. This demonstrates that, although there is less abnormal airway in the LRIG1-null animals, the degree to which all genotypes are affected by each grade of disease is similar. Notably, there is not an increase in the proportion of high-grade disease in the LRIG1-null mice (Figure 6.10.B). The grading and assessment of lesions was discussed and confirmed with a histopathologist.

By assessing the number of cancerous lesions developing in each genotype, whether LRIG1 influences the progression of areas of dysplasia to invade into the basement membrane could be established. The number of lesions across two sections 200 µm apart was counted. Lesions were considered to be part of one larger lesion if the distance between 2 areas was smaller than 200 µm. The number of invasive lesions that developed in the LRIG1-heterozygous and LRIG1-null mice was similar (Figure 6.11.A). Fewer lesions were seen in the wild-type group, however, the differences between the three groups were not significant.

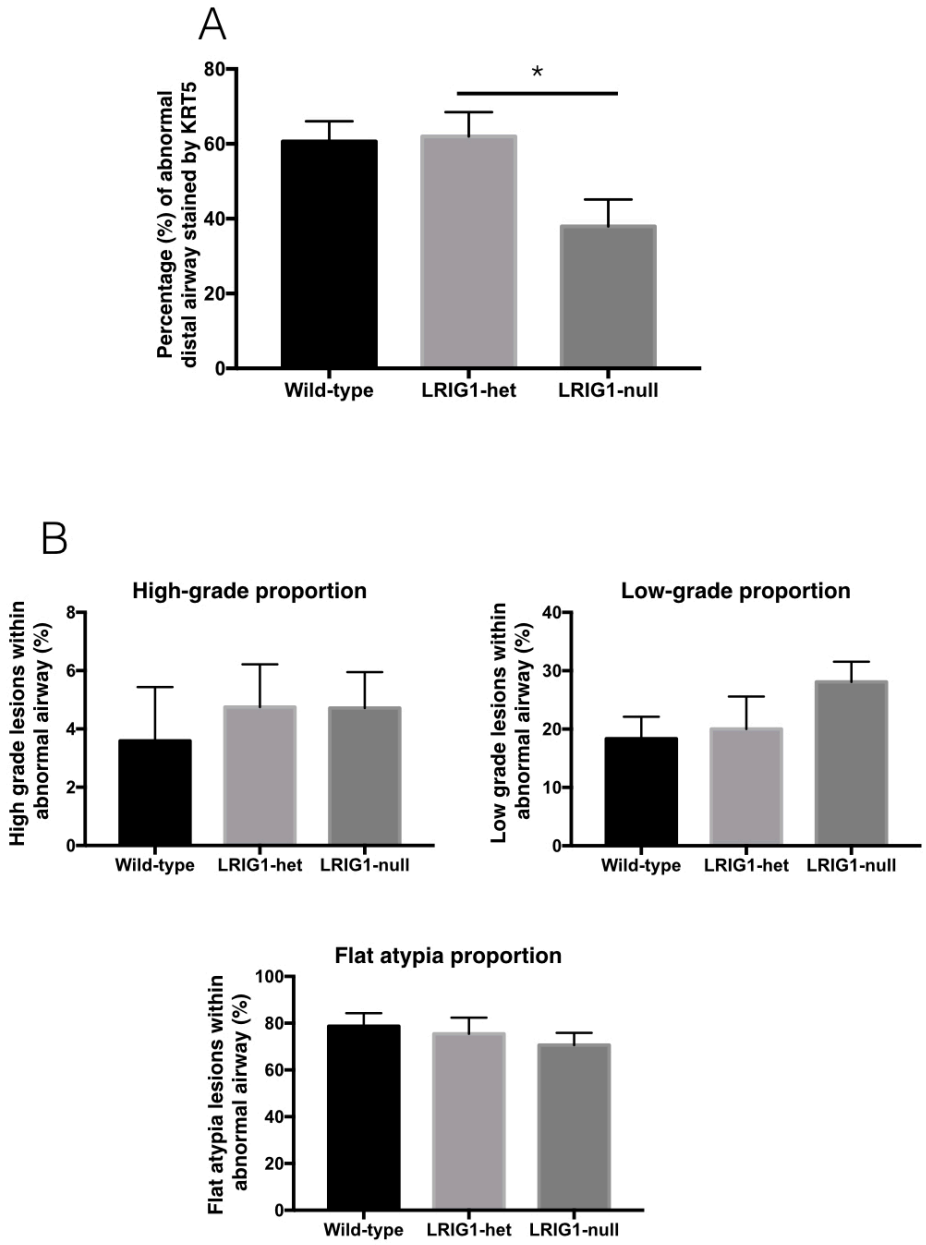

Figure 6.10: The development of NTCU-induced preinvasive lesions in LRIG1-wild-type, LRIG1-heterozygous and LRIG1-null animals

A) Quantification of the percentage of abnormal keratin 5 (KRT5) expression in the distal airway in wild-type, LRIG1-heterozygous and LRIG1-null animals. Statistical analysis was performed using a Kruskal-Wallis test, with Dunn's post- test, following an arcsine transformation; n= 7-10 mice; mean ± SEM; * indicates $p< 0.05$. B) The assessment of proportion of each type of lesion out of the total amount of KRT5- stained abnormal airway in each animal, including high-grade, low-grade and flat-atypia lesions; n = 7- 10 mice; mean ± SEM. Statistical analysis was performed using a Kruskal-Wallis test, following assessment of normality using the D'Agostino & Pearson normality test, with Dunn's post test; n= 7–10 mice; mean ± SEM.

In addition to the cells' ability to invade surrounding tissue, tumour size may be affected by the proliferation of the tumour cells. To assess whether loss of LRIG1 influences tumour size, the surface area of each lesion was calculated. Each tumour size was considered as an independent variable, with the size of each tumour across each of two sections 200 μm apart recorded from wild-type, LRIG1-heterozygous and LRIG1-null mice (Figure 6.11.B). This method of analysis has been used in the determination of clonal sizes (174). Tumour size was significantly increased in LRIG1-null animals (Figure 6.11.C), and the sizes of tumours in mice of this genotype were also more widely distributed with a greater number of LRIG1-null tumours recorded to be over 200,000 μm^2.

Finally, the proportion of the lung affected by tumours was examined (Figure 6.11.B). This allowed the proportion of invasive disease to be normalised to the size of the lung. All mice were of similar weight at the experimental end-point, so a similar lung surface area was anticipated. As only three of the wild-type mice had lung tumours, and many animals had no lesions, the overall percentage of the lung affected by disease was lower. In the LRIG1-heterozygous and LRIG-null animals, the total affected surface area was similar, a result of the number of tumours being greater in the LRIG1-heterozygous mice, but the surface area of the tumours in the LRIG1-null animals being greater, leading to similar proportions of the lung being affected.

6.3.11 Proliferative index of tumours from wild-type, LRIG1-heterozygous and LRIG1-null animals

The tumours that developed in LRIG1-null animals were significantly larger than those occurring in LRIG1-heterozygous and wild-type mice. As *Lrig1* loss appears to increase the proliferation of human epithelial cells (Chapter 5) and cause ongoing murine epithelial proliferation at cell confluence (104), I assessed whether LRIG1 loss was having a proliferative effect in the development of murine lesions and stained tumours from wild-type, LRIG1-heterozygous and LRIG1-null animals for Ki67

expression. To ensure that any increase in proliferation was not negated by tumour cell death, annexin V staining was performed alongside.

Only rare cells were annexin V positive, with staining only detectable in tumours of greater than 150 cells. Most of the annexin V staining was located around the periphery of the lung tumour and not as part of the tumour mass (Figure 6.11.E). The staining of Ki67 staining was greatest towards the edges of tumour, and decreased towards the centre. Comparing the LRIG-heterozygous to the LRIG1-null mice showed that there was no significant difference in the percentage of Ki67-positive cells within the tumours.

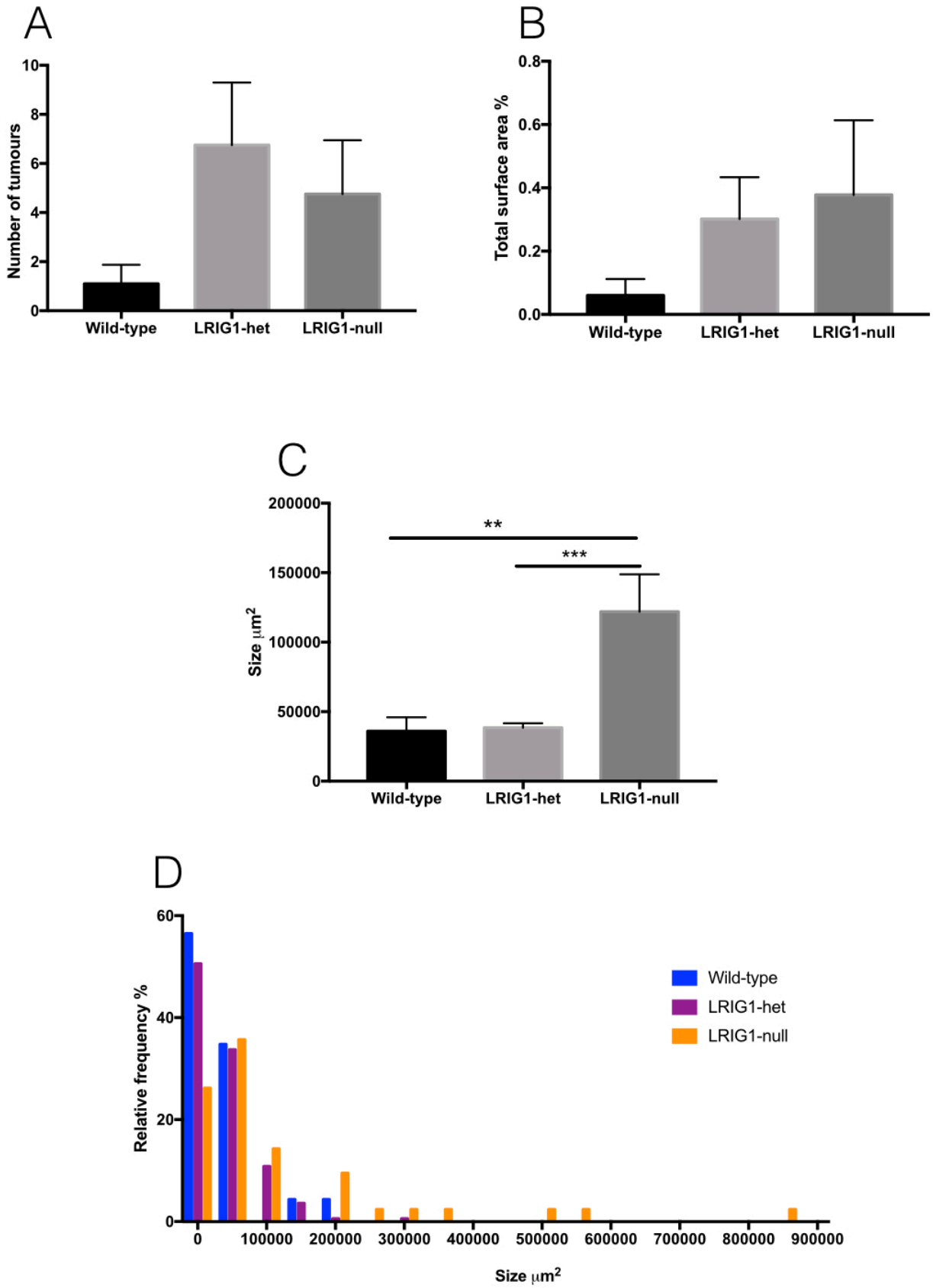
A
Number of tumours
0
2
4
6
8
10
Wild-type
LRIG1-het
LRIG1-null
B
Total surface area %
0.0
0.2
0.4
0.6
0.8
Wild-type
LRIG1-het
LRIG1-null
C
Size µm²
0
50000
100000
150000
200000
**
***
Wild-type
LRIG1-het
LRIG1-null
D
Relative frequency %
0
20
40
60
0
100000
200000
300000
400000
500000
600000
700000
800000
900000
Size µm²
Wild-type
LRIG1-het
LRIG1-null

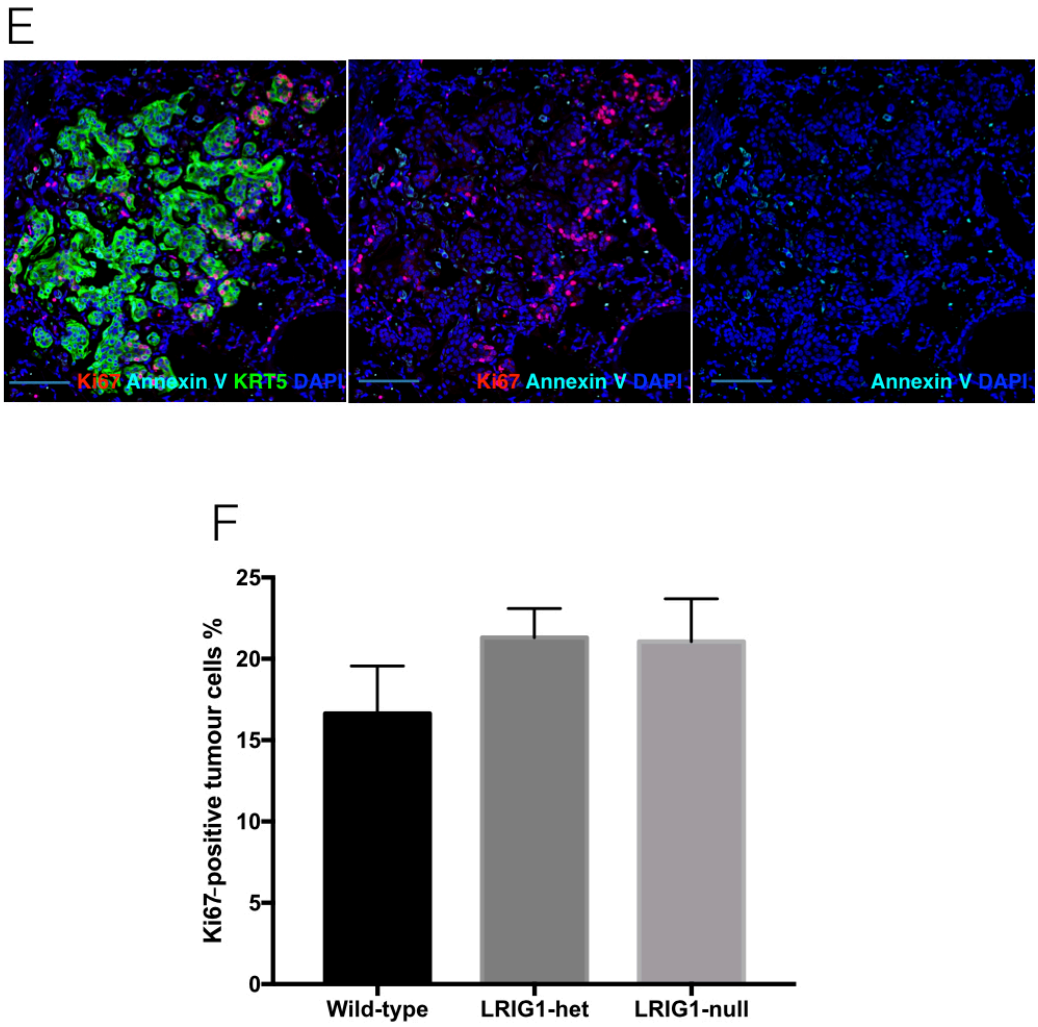

Figure 6.11: The development of invasive lesions in LRIG1-wild-type, LRIG1-heterozygous and LRIG1-null animals

A) Number of tumours found in wild-type, LRIG1-heterozygous and LRIG1-null mice. Statistical analysis was performed using a Kruskal-Wallis test, with Dunn's post test; n = 7-10 mice; mean ± SEM. B) Percentage of lung surface area covered by tumours in wild-type, LRIG1-heterozygous and LRIG1-null animals. Statistical analysis was performed using a Kruskal-Wallis test, with Dunn's post test; n = 7-10 mice; mean ± SEM. C) Size of individual tumours from wild-type, LRIG1-heterozygous and LRIG1-null animals. Statistical analysis was performed using a Kruskal- Wallis test, with Dunn's post test; n = 23-166 tumours; mean ± SEM. D) Histogram showing the distribution of tumour sizes from wild-type, LRIG1-heterozygous and LRIG1-null mice. E) Immunofluorescence staining of a distal airway tumour stained for Ki67 (red), annexin V (cyan), keratin 5 (KRT5) (green) and DAPI (blue). Note the proliferative Ki67 cells are seen at the tumour margins, whilst the annexin V stained cells are seen at the edges of the tumour. F) Graph showing the percentage of Ki67-positive cell per tumour. Statistical analysis was performed using a Kruskal-Wallis test, following assessment of normality using the D'Agostino & Pearson normality test, with Dunn's post test, following an arcsine transformation; 10-46 tumours analysed per group; mean ± SEM.

6.4 Discussion

I have shown that the application of 0.013 M NTCU to the dorsal skin of the *Lrig1* EGFP-ires-CreERT2 mouse strain leads to both preinvasive and invasive squamous cell lung cancers. All phenotypes of human preinvasive disease are recapitulated in this model. Squamous aetiology has been confirmed by the expression of KRT5, p63 and EGFR.

The preinvasive and squamous cell carcinomas arose in the distal airways whereas, in humans, squamous cell cancers are lesions of the upper airways where the basal cells, the putative squamous cancer cell of origin, are concentrated. The distribution of NTCU-induced disease may be related to dilution. When 0.013 M of NTCU is delivered in 75 µl of solvent (252), as used here, peripheral lesions form. However, when 25 µl of 0.04 M NTCU (equating to the same dosage) is applied, tracheal lesions develop (251). The higher volume of administration was selected as lesions are seen after 18 weeks, compared to the 8-month treatment period when using 25 µl volumes. The shorter treatment duration was selected to allow the development of lesions within the time constraints of my PhD. The differences in lesion distribution may relate to how the NTCU is absorbed: NTCU is applied between the shoulder blades of the mouse so when a smaller volume is given the dose is likely to remain more localised and affect a more discrete area of tissue (the trachea), but a larger volume may spread and affect a larger surface area of skin and subsequently lung, causing distal lesions. The cell density is also reduced in the distal airway so may explain the appearance of lesions earlier than when they occur in the trachea, with the NCTU needing to permeate through more layers of tissue in the trachea than more distally.

Whilst the NTCU experiments were underway, a further group reported the development of tracheal lesions in FVB/N mice using 25 µl of 0.02 M NTCU (half the dose as above) (259). Animals were treated twice weekly until the end-point (with no observation phase). Tracheal changes were first detected at 12 weeks, with increased proliferation and a higher number of KRT5-positive basal cells, followed by

bronchial dysplasia at 25 weeks and tumours at 32 weeks (259). This protocol may more effectively recapitulate human disease patterns, and cause a greater disease burden in the upper airway, than the model I have used. Although the time course is more prolonged (needing 32 weeks instead of 23 weeks for lesions to develop), I would consider using this dosing strategy in any further studies.

In the model described here, both the preinvasive and invasive lesions express basal cell markers. Basal cells are considered the origin of squamous cell carcinoma and as the stem cell of the upper airway their highest concentration is seen in the trachea, with few basal cells seen in the distal lung. Therefore, the origins of the KRT5-positive, p63-positive NTCU-induced lesions in the distal airways are of interest. The use of a murine acute respiratory distress syndrome (ARDS) model, where mice are infected with the influenza virus, has shown the development of $p63^{+}KRT5^{+}$ 'pods' in the distal lung (142). During lung repair, these cells expand and through lineage tracing, are seen to regenerate all alveolar cell types. This is consistent with previous reports showing that, following the destruction of naphthalene-sensitive secretory CC10-positive cells, a rare population of basal cells expands within the bronchiolar epithelium to repair the lung damage (264). More recently, extremely rare $p63^{+}KRT5^{+}$ cells have been identified in the distal lung. When a human diphtheria toxin receptor mechanism is used to eradicate these $p63^{+}KRT5^{+}$ cells post influenza virus infection the alveolar regeneration is prevented and fibrosis occurs (265). Consequently, NTCU may either activate the migration of basal cells from the more proximal airways to the sites of chemically induced injury or trigger the proliferation of the rare, distal $p63^{+}KRT5^{+}$ cells. The recent NTCU paper where low NTCU doses are utilised reports changes first in the trachea before the distal lung, indicating the possibility of basal cells migrating outwards in response to NCTU application (259), although I was unable to see any tracheal effects in this NTCU model. Intriguingly, an alternative possibility is raised by a recent publication that targets shows SOX2 overexpression to either KRT5-positive basal cells, or distal airway SPC- or CC10-positive cells in a conditional combined *Pten*- and *Cdkn2ab*-knockout mouse. This model shows that, irrespective of the tumour cell targeted, squamous cell lung tumours develop (247). Whilst highlighting the importance of SOX2 overexpression

in squamous cell development, the results are interesting as they are suggestive that even an SPC- or CC10-positive distal airway cell, when sufficiently antagonised and on the development of a sufficient number of mutations, is capable of obtaining a squamous phenotype and leading to squamous cell carcinoma. SOX2 appears to be the key switch in this change of phenotype. NTCU, with its alkylating effects, may create an environment where multiple mutations occur within the distal airway epithelium, meaning the preinvasive lesion's cell of origin is a distal epithelial cell that has acquired sufficient mutations to develop a squamous phenotype, rather than a basal cell that has travelled distally.

A further consideration in regards to the origin of the distal $KRT5^+$ lesions is the dual expression of TTF1 and KRT5 in preinvasive and invasive squamous cell lesions. This contrasts to previous reports where NTCU-induced lesions were TTF1-negative (253, 255). There appears to be a gradient in the level of TTF1 expression, with alveolar type 2 cells brightly stained and a lower intensity of TTF1 expression in cells co-expressing KRT5. Dual positive KRT5 and TTF1 positive cells are not normally present in the lung, other than during lung development where TTF1 plays a role in lung morphogenesis. In the adult lung, it is localised to the distal airway (266). As TTF1 is expressed in all grades of lesion it is suggestive that the lesions possibly arise from a TTF1-expressing cell. However, notably, there does not appear to be a reduction in the number of $TTF1^+$ $KRT5^+$ stained cells in either the high-grade lesions or invasive tumours that may suggest the lesion has originated from a TTF1-positive cell that is subsequently developing a squamous phenotype. If the origin were a TTF1-positive epithelial cell that had become squamous the TTF1- positive cells would be expected to decrease as the lesions became more advanced with fewer cells seen in more advanced preinvasive lesions and tumours.

A triple-positive $CC10^+p63^+KRT5^+$ cell has been identified in the distal lung (260), these triple-positive stained cells also expressed CD44, a potential cancer stem-cell marker, suggesting that the origin of an NTCU-induced lesion could be a CC10-positive cell. A number of sections were stained for these markers but only one potential triple stained cell was identified. This section was unusual, as in contrast to

all other sections investigated, the p63 positive cell was not adjacent to the basement membrane. This is either an artefact, or indicative of rare p63 positivity in association with CC10 and KRT5 markers and expressed in cells where squamous lesions subsequently develop.

Assessment of the epithelium for BASCs in the NTCU-treated airways has shown the location of BASCs adjacent to areas of preinvasive disease. Their number appears to be increased compared to untreated controls, where BASCs are rare. The BASCs sit at a stem cell niche within the distal airway, and the increase in BASC numbers suggests that either the development of preinvasive disease may arise from the BASC population (although unlikely as no triple-stained $KRT5^{+}SPC^{+}CC10^{+}$ lesions were visible) or that the BASCs facilitate and support the development of preinvasive disease. To investigate this further, the use of naphthalene could be revisited. Naphthalene causes hyperplasia of the BASC population (following the death of $CC10^{+}$ cells) and increases the development of adenocarcinomas in an adenocarcinoma model, so the effects of naphthalene exposure on NTCU-induced lesions would be valuable to determine. If BASCs were the squamous cell of origin or supportive of preinvasive lesion development, then naphthalene in combination with NTCU treatment would be expected to increase the number and severity of NTCU-induced lesions in addition to causing BASC hyperplasia.

To analyse the cell of origin of squamous cell carcinoma in more detail further, methodical sectioning of the airway epithelium is required. This would assess whether triple-positive $CC10^{+}p63^{+}KRT5^{+}$ cells exist in high numbers and the association of BASCs with preinvasive disease. The use of cell counting and mathematical modelling may be of additional benefit in determining the cell of origin of these lesions, this could be combined with lineage tracing models. Lineage tracing in TTF1-, SPC-, CC10- and KRT5- reporter animals following NTCU administration would assist in the elucidation of which cell type is the origin of squamous disease.

LRIG1 is expressed within the bronchioles of the distal airways of mice (Chapter 3), and in the NTCU model both preinvasive and invasive lesions show evidence of LRIG1

expression. It is possible that, lesions do develop from an LRIG1- expressing cell as when the lesions develop, the $p63^{+}/KRT5^{+}$ cells may constitutively express LRIG1 (if they have migrated from the upper airways or developed from the rare distal $p63^{+}/KRT5^{+}$ cells, whose LRIG1 expression is unknown), or if their origin is from the transformation of a distal cell type (such as an LRIG1-positive, TTF1-positive cell) the expression of LRIG1 is maintained with the change in phenotype. Lineage tracing could be used to answer this question, with the activation of a reporter in LRIG1-expressing KRT5-positive cells together with the administration of NTCU.

It is notable that the expression of LRIG1 is not lost in the development of preinvasive lesions in LRIG1-heterozygous mice, as has been seen in the human airway (104). To confirm the relevance of the model to human disease, genomic sequencing of the tumours could be performed. This would necessitate the laser capture of both preinvasive lesions and tumours (267), and give an insight into not only the natural history of mutations in the NTCU model but how closely the NTCU-induced mutations are aligned to those seen in human squamous cell lung cancer, and whether the driver mutations are shared. It would particularly interesting to assess whether SOX2 is overexpressed, as this genetic abnormality appears to be the key 'switch' in the development of squamous lesions when targeted to the varying epithelial cell types of the distal lung one (247).

Contrary to the initial hypothesis, where loss of LRIG1 predisposes to preinvasive disease, LRIG1-null animals do not develop any more preinvasive lesions than the LRIG1-heterozygous or wild-type animals. It is intriguing that the LRIG1-null animals actually show less distal airway KRT5 staining, the marker of the presence of an abnormal epithelium after NTCU treatment than either the LRIG1-heterozygous or wild-type mice. When lesion type is taken into consideration, the proportion of abnormal airway that is affected by high-grade, low-grade dysplasia or flat atypia is similar across the three groups. The similar behaviour of the wild-type and LRIG1-heterozygous animals mirrors my findings of there being no difference in the proliferation of the epithelium between LRIG1-heterozygous and wild-type animals

(Chapter 3). This finding also corresponds to previous research where haploinsufficiency of *Lrig1* has no phenotypic effect (104).

The downregulation of LRIG1 is associated with the increased epithelial-to-mesenchymal (EMT) transition of breast and nasopharyngeal epithelial cells (110, 111) and its loss within the ocular epithelium precipitates progression of surface neoplasia to invasive disease (103). This implies the protein influences the onset of EMT and triggers the invasion of abnormal cells through the basement membrane. Across all three genotypes there is a similar proportion of abnormal airway that is affected by high-grade dysplasia, but although there are more tumours in the LRIG1-heterozygous mice, this is not significantly higher than the LRIG1-null animals. If loss of LRIG1 contributed to EMT it may be expected that the number of invasive lesions in the LRIG1-null group would be higher than that of the LRIG1-heterozygous or wild-type animals. This is not seen, and indicates that in this model LRIG1 does not influence the invasion of abnormal epithelial cells and the number of cancers produced.

The loss of LRIG1 does lead to the development of significantly larger tumours than in LRIG1-heterozygous or wild-type mice. There is also a greater distribution in the number of tumours formed in the LRIG1-null animals. It is known that loss of LRIG1 causes a loss of contact inhibition between epithelial cells (104), so it is possible that, when tumours lack LRIG1, they are not inhibited by cell-cell contact or the airway walls and continue to proliferate beyond the size of that generated by LRIG1-expressing tumours.

To establish whether the larger tumour size in the LRIG1-null mice was a result of increased proliferation, tumours were stained for both Ki67 and annexin V expression. However, no differences in the proliferation of tumours from LRIG1-heterozygous and LRIG1-null mice were detectable, despite the findings in Chapter 5 showing that loss of LRIG1 through shRNA knockdown in human airway epithelial cells leads to increased cell proliferation. The similar proliferation may be explained by the tumour size and the location of the proliferative cells. It is clear from the Ki67

staining that the proliferating cells are at the tumour margins. In a small tumour, the cells around the margin of the tumour are still proliferating. There are very few tumour cells in the centre that are not dividing, so the percentage of proliferating cells for the size of the tumour is high. In a much larger tumour, the cells that are proliferating are still around the periphery, but the number of tumour cells in the centre that are not dividing is increased. Therefore the percentage of proliferating cells in larger tumours is reduced compared to tumours of a smaller size. The presence of large tumours in the LRIG1-null mice may lead to a reduction in the overall number of cells proliferating, and mean the results are comparable in the LRIG1-heterozygous and LRIG1-null animals. To understand how larger tumours develop in the LRIG1-null mice, measurements of tumour size need to take place at several time points in the same animal, giving an indication of tumour growth dynamics. This may be possible through imaging techniques such as micro-CT (268) or PET scanning (263).

Some subtleties within the data may have been missed due to an under-powering of the experiment. During experimental design, the number of animals needed in each group to show a significant difference was calculated at 9. However, there were very few studies on which to base the anticipated likelihood of lesion development. When animal losses occurred, further experimental cages were set up to account for these. However, due to the length of the experiments these, were staggered at several weeks apart. Animals were lost in one of the final cages due to husbandry issues (so that they could not be replaced because of time restrictions), meaning only 7 animals were ultimately included in the LRIG1-null arm. The NTCU when made up in solvent is also extremely volatile, meaning the dosing of animals was difficult before the chemical evaporated. Each cage contained an animal of each genotype, so the animals sequentially rotated for the first, second and third dose. Small dosing inaccuracies may have led to a different dose being administered to each mouse. By increasing the power of the experiment, the effect of these variables may be reduced.

Further bearings on the results may be that the animals have a constitutive loss of LRIG1, and do not lose the protein, as occurs in the development of preinvasive lung cancer. As shown in the experiments that assessed the characteristics of basal cells (Chapter 4), no differences were seen between basal cells from LRIG1-heterozygous and LRIG1-null animals. This raises the possibility that loss of LRIG1 from gestation leads to compensatory mechanisms and that any effect of LRIG1 on the development of malignancy may not be best assessed in this model. The observation that eGFP is expressed (following activation on the *Lrig1* promoter) in LRIG1-null mice implies LRIG1 may still have a biological function and that the animals are suitable for modelling the effects of LRIG1 loss following NTCU treatment. Using NTCU to initiate tumour development in an *Lrig1*-conditional knockout would answer this question more succinctly, and clarify the role of loss LRIG1 in lesion development.

A final caveat is that the mice are on an FVB/N and C57BL/6 mixed background, which may have led to a variable proportion of each genotype within the experimental groups. Whilst animal backcrossing was considered, the time necessary to produce a pure strain and then to optimise the NTCU regimen would not have been available within the constraints of a PhD. The loss of LRIG1 on a pure FVB/N background has also been shown to lead to perinatal death at p10, and would prevent their use in these NTCU experiments (93). To account for the potential effects of the mixed background, animals were pooled from the same generation and littermates included where possible. FVB/N animals are a more sensitive strain than C57BL/6 (251), so if the final proportion of FVB/N was greater within an individual mouse, it may be more susceptible to the development of malignancy and influence the final result. Increasing the power of the experiment would reduce the effect of this potential confounder.

6.5 Summary

- Application of NTCU induces the development of both preinvasive and invasive squamous cell lung cancers which closely models the progression of human disease
- The cell of origin of the squamous cell changes induced by NTCU has yet to be determined.
- There is no effect of the loss of LRIG1 on the development of preinvasive disease.
- Loss of LRIG1 leads to the development of larger squamous cell carcinomas.

7. Summary and Future Directions

7. Summary/ Future Directions

7.1 Summary

LRIG1 is lost in human preinvasive lung cancer lesions (104) and its loss is associated with a worsening prognosis of non-small cell lung cancer (NSCLC) (105). In fact, it is also one of 4 key genes whose loss is associated with a worsening of outcomes across epithelial cancer subtypes, including lung cancer (98). The aim of this work was to elucidate the role of LRIG1 in the airway and how its loss may lead to preinvasive lung cancer.

I have shown that LRIG1 is expressed in the murine airway epithelium. Instead of marking a subpopulation of airway epithelial cells, or being found to mark the airway stem cell population, as it is in other organs, LRIG1 expression is seen across the ciliated, secretory and basal cells. By isolating the airway basal cells, l have shown that only 50% of basal cells are LRIG1-positive. These LRIG1-expressing basal cells exhibit increased stem cell features with an increased colony- and spheroid-forming capacity. LRIG1-expressing basal cells are also more proliferative than LRIG1-negative basal cells. These features are in line with recent research suggesting that the airway basal cell population is more heterogeneous than first appreciated. Interestingly, basal cells isolated from LRIG1-null mice do not show a change in proliferation, colony- or spheroid-forming capacity compared to the LRIG1-expressing basal cells from LRIG1-heterozygous mice. This implies that either LRIG1 is only the marker of a more proliferative and stem-cell like population of basal cells, or that in LRIG1 constitutively-null animals, there is a compensation for absence of LRIG1.

By isolating human airway epithelial cells obtained at bronchoscopy, I have confirmed there is an LRIG1-expressing basal cell population in the human airway and that the characteristics seen in mouse airway basal cells are conserved in the human. The human LRIG1-expressing basal cells show an increased colony-forming

capacity and are more proliferative than LRIG1-negative basal cells. By using shRNA knock down of LRIG1 in cultures of primary human epithelial cells, I have shown that LRIG1 does not simply mark a basal cell population but that loss of the protein affects cell phenotype. *Lrig1* shRNA knocked-down basal cells exhibit an increased proliferation, colony-forming ability and a reduction in cell-cell contact inhibition at cell confluence.

To assess the effects of LRIG1 loss in an *in vivo* animal model, I have optimised the N-Nitrosotris-(2-chloroethyl)urea (NTCU) model for the development of murine squamous cell lung cancers in LRIG1-null, LRIG1-heterozygous and wild-type mice. I have demonstrated that these mice not only develop lung tumours but also that the developing lesions recapitulate all stages of human preinvasive disease. Whilst the absence of LRIG1 does not influence the development of preinvasive lung cancers, significantly larger tumours were detected in LRIG1-null mice. However, in this NTCU model, LRIG1 was not lost in the development of preinvasive lesions or lung tumours. It is possible that in humans, the loss of LRIG1 is not essential or the key event in the development of preinvasive disease.

I have shown that LRIG1, similarly to in the skin and the gut, regulates a stem cell population within the airway. LRIG1-expressing basal cells exhibit a more stem cell-like phenotype, with *LRIG1* shRNA knockdown leading to the dysregulation of these characteristics. Loss of the inhibitory regulation of LRIG1 in the airway stem cell compartment may lead to both the development of preinvasive lesions and lung tumours. An LRIG1-expressing airway basal cell, that exhibits stem cell characteristics, on the loss of LRIG1 may become dysregulated and develop the features of a cancer stem cell. This basal cell may then act as the cell of origin for, initially preinvasive, and later invasive, squamous cell lung tumours. The reduction of cell-cell contact inhibition, seen here and in the work of Lu *et al*, may explain the formation of larger tumours in LRIG1-null mice and the worsening of NSCLC prognosis on LRIG1 loss.

7.2 Future directions

The main aim of this project was to increase our understanding of LRIG1 initially in airway homeostasis, but then to assess the effects of its loss in preinvasive lung cancer, with a view to developing therapeutic candidates.

The comparison of the mouse and human airway suggests that there is compensation in the LRIG1-null mouse, but as there are differences between the wild-type and LRIG1-null mice in the NTCU experiment, this indicates compensation may not be present. To clarify the findings, I could use an *Lrig1*-conditional knockout mouse model which would more closely recapitulate the loss of LRIG1 that occurs in the human airway. To confirm the effect of loss of LRIG1 in the human airway seen by shRNA knockdown I would also perform CRISPR-Cas9 to gene edit and completely remove the effects of LRIG1 expression.

Due to difficulties with the single cell-RNA sequencing data, I was unable to use this data to gain an insight into the gene expression changes that occur on loss of LRIG1 and therefore how this loss might lead to preinvasive disease. Re-exploring gene expression analysis may be of benefit in the identification of pathways downstream of LRIG1 activation that may be targeted for a therapeutic intervention. The use of the above-mentioned *Lrig1*-conditional knockout mouse would be advantageous for any further gene expression analysis.

However, LRIG1 has been identified as a tumour suppressor in the gut and I have shown that the loss of LRIG1 leads to larger lung tumours in LRIG1-null mice, therefore the replacement/administration of LRIG1 may provide a potential therapy to established disease and would provide a natural progression of the project. It is interesting that administration of EGFR receptor antagonists to patients with squamous cell lung cancers leads to small improvements in cancer survival (26,27), so reducing EGFR signalling in lung cancer would be a logical therapeutic target. To date, full-length LRIG1 has been administered to bladder tumour xenografts in mice by the direct injection of LRIG1-producing adenoviruses into an established tumour

bulk (269). This leads to a reduction in tumour mass. The soluble LRIG1 (s-LRIG1) extracellular domain has been explored as a potential therapy and has been delivered to murine glioblastoma models, by using s-LRIG1-producing cells contained within alginate beads (86). Again, this model has been shown to reduce both the size of established tumours and to reduce tumour development when the s-LRIG1-producing beads are implanted simultaneously with the glioblastoma cells.

The optimised NTCU squamous cell lung cancer model could be used to assess LRIG1's potential as a therapeutic agent. LRIG1 could be potentially administered to established squamous cell lung tumours to assess whether tumour growth and development could be reduced. LRIG1 administration may prove challenging in the lung. Initially, the identification of the lesion would necessitate imaging and injecting the LRIG1-producing cells into a tumour mass is would be challenging without direct vision. The use of mesenchymal stem cells to successfully deliver the cancer targeting agent tumour related apoptosis inducing ligand (TRAIL) to the lung in a mesothelioma model has been reported by our research group (270), and will soon move into a clinical trial setting. This strategy may provide a modality by which LRIG1 could be delivered directly to the site of the tumour.

A therapy for patients with preinvasive lesions would be advantageous but would need to be patient-acceptable with minimal side effects (as lesions may never progress to cancer). The NTCU model failed to show an effect of LRIG1 loss on the development of preinvasive lesions, although the model could be optimised further with larger sample numbers and the use of a conditional *Lrig1* knockout targeted to the keratin 5 basal cell population. Confirming the link of LRIG1 to preinvasive disease may provide the option for prophylactic treatment in patients with known lesions. An inhaled therapy would be ideal in targeting the upper airways where the preinvasive lesions are situated, and an inhaled therapy is likely to lead to fewer side effects than systemic medications. However, LRIG1 expression is seen in association with that of EGFR and is localised to the basolateral cell membrane (61), so a significant challenge would be to get LRIG1 to the site of action.

8. Supplementary

8. Supplementary

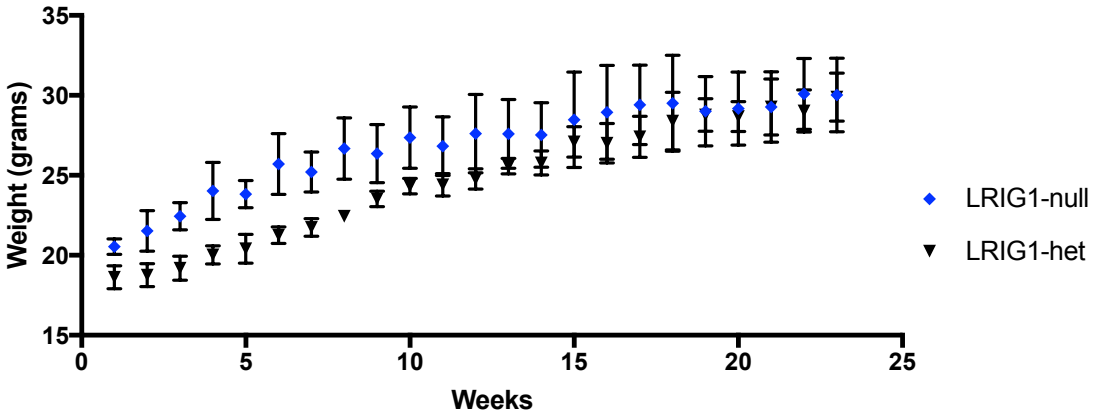

Supplementary Figure 1. Weights of LRIG-heterozygous and LRIG1-null animals.

The LRIG1-null animals initially weigh less than the LRIG1-heterozygous mice, but over the course of the experiment the weights of the two groups equilibrates. Error bars signify the S.E.M, n=3 in each group

Supplementary table 1

1 pack year of smoking equivalent to 20 cigarettes a day for a year

	Gender	Age	History	Smoking, pack years	Site	Histology	Experiment
A	M	65	Left upper lobectomy January 2014. CIS at stump, regressed, now clear	25, ex smoker		Normal epithelium	Cell culture
B	M	54	Foreign body RLL	30, current	Right upper	Normal epithelium	Cell culture
C	F	77	Surveillance	Ex smoker		Normal epithelium	Cell culture
D	M	64	Interventional due to obstructing sarcoma, normal area sampled			Normal epithelium	Cell culture
E	F	58	surveillance RLL CIS	55	Main carina	Normal epithelium	LRIG1 assess
F	M	75	surveillance	40	Main carina	Normal epithelium	LRIG1 assess
G	SF 25/1	57	Surveillance, previous carcinoid tumour		Main carina	Normal epithelium Granulation tissue elsewhere	LRIG1 assess
H	M	54	Foreign body RLL	30, current	Right upper	Normal epithelium	Colony
I	M	58	Haemoptysis	63, ex smoker	Main carina	Normal epithelium	Colony
J	F	76	Surveillance for RMB dysplasis	30, ex smoker	Left upper	Normal epithelium	Colony
K	M	84	Surveillance Previous lung cancer x 2	50, ex smoker	Main carina	Metaplasia	Colony
L	M	70	Haemoptysis	45, current	Main carina	Normal epithelium	Colony
M	F	55	Surveillance RLL CIS	55	Main carina	Normal epithelium	Colony
N	M	54	Lingula hamartoma	50, ex smoker 2002	Main carina	Normal epithelium	Proliferation
O	M	76	Previous squamous cell cancer, CIS at resection margin	current	Left upper	Normal epithelium dysplasia elsewhere	Proliferation
P	M	63	CIS surveillance	60, ex smoker 2011	Right upper lobe	Normal epithelium	Proliferation
Q	F	58	CIS surveillance	50, ex smoker 2000	Right main bronchus	Normal epithelium	Proliferation

9. References

9. References

1. Lung Cancer Incidence Statistics. 2016 [cited 2017 5/1/2017]. Available from: http://www.cancerresearchuk.org/health-professional/cancer-statistics/statistics-by-cancer-type/lung-cancer/incidence.
2. Herbst RS, Heymach JV, Lippman SM. Lung cancer. *N Engl J Med* 2008; 359: 1367-1380.
3. Doll R, Hill AB. Smoking and carcinoma of the lung; preliminary report. *Br Med J* 1950; 2: 739-748.
4. Lantz PM, Mendez D, Philbert MA. Radon, smoking, and lung cancer: the need to refocus radon control policy. *Am J Public Health* 2013; 103: 443-447.
5. Trichopoulos D, Kalandidi A, Sparros L, MacMahon B. Lung cancer and passive smoking. *Int J Cancer* 1981; 27: 1-4.
6. Lee PN, Chamberlain J, Alderson MR. Relationship of passive smoking to risk of lung cancer and other smoking-associated diseases. *British journal of cancer* 1986; 54: 97-105.
7. Travis WD, Giroux DJ, Chansky K, Crowley J, Asamura H, Brambilla E, Jett J, Kennedy C, Rami-Porta R, Rusch VW, Goldstraw P, International Staging C, Participating I. The IASLC Lung Cancer Staging Project: proposals for the inclusion of broncho-pulmonary carcinoid tumors in the forthcoming (seventh) edition of the TNM Classification for Lung Cancer. *J Thorac Oncol* 2008; 3: 1213-1223.
8. Lung Cancer Stages. 2014 [cited 2017 5/1/2017]. Available from: http://www.cancerresearchuk.org/about-cancer/type/lung-cancer/treatment/lung-cancer-staging.
9. Van Schil PE, Balduyck B, De Waele M, Hendriks JM, Hertoghs M, Lauwers P. Surgical treatment of early-stage non-small-cell lung cancer. *EJC Suppl* 2013; 11: 110-122.
10. Reck M, Heigener DF, Mok T, Soria JC, Rabe KF. Management of non-small-cell lung cancer: recent developments. *Lancet* 2013; 382: 709-719.
11. Cancer Genome Atlas Research N. Comprehensive molecular profiling of lung adenocarcinoma. *Nature* 2014; 511: 543-550.
12. Vallath S, Hynds RE, Succony L, Janes SM, Giangreco A. Targeting EGFR signalling in chronic lung disease: therapeutic challenges and opportunities. *Eur Respir J* 2014; 44: 513-522.
13. Sequist LV, Bell DW, Lynch TJ, Haber DA. Molecular predictors of response to epidermal growth factor receptor antagonists in non-small-cell lung cancer. *J Clin Oncol* 2007; 25: 587-595.
14. Maemondo M, Inoue A, Kobayashi K, Sugawara S, Oizumi S, Isobe H, Gemma A, Harada M, Yoshizawa H, Kinoshita I, Fujita Y, Okinaga S, Hirano H, Yoshimori K, Harada T, Ogura T, Ando M, Miyazawa H, Tanaka T, Saijo Y, Hagiwara K, Morita S, Nukiwa T, North-East Japan Study G. Gefitinib or chemotherapy for non-small-cell lung cancer with mutated EGFR. *N Engl J Med* 2010; 362: 2380-2388.
15. Mok TS, Wu YL, Thongprasert S, Yang CH, Chu DT, Saijo N, Sunpaweravong P, Han B, Margono B, Ichinose Y, Nishiwaki Y, Ohe Y, Yang JJ, Chewaskulyong B, Jiang H, Duffield EL, Watkins CL, Armour AA, Fukuoka M. Gefitinib or carboplatin-paclitaxel in pulmonary adenocarcinoma. *N Engl J Med* 2009; 361: 947-957.
16. Kobayashi S, Boggon TJ, Dayaram T, Janne PA, Kocher O, Meyerson M, Johnson BE, Eck MJ, Tenen DG, Halmos B. EGFR mutation and resistance of non-small-cell lung cancer to gefitinib. *N Engl J Med* 2005; 352: 786-792.
17. Pao W, Miller VA, Politi KA, Riely GJ, Somwar R, Zakowski MF, Kris MG, Varmus H. Acquired resistance of lung adenocarcinomas to gefitinib or erlotinib is associated with a second mutation in the EGFR kinase domain. *PLoS Med* 2005; 2: e73.

18. Soda M, Choi YL, Enomoto M, Takada S, Yamashita Y, Ishikawa S, Fujiwara S, Watanabe H, Kurashina K, Hatanaka H, Bando M, Ohno S, Ishikawa Y, Aburatani H, Niki T, Sohara Y, Sugiyama Y, Mano H. Identification of the transforming EML4-ALK fusion gene in non-small-cell lung cancer. *Nature* 2007; 448: 561-566.
19. Shaw AT, Kim DW, Nakagawa K, Seto T, Crino L, Ahn MJ, De Pas T, Besse B, Solomon BJ, Blackhall F, Wu YL, Thomas M, O'Byrne KJ, Moro-Sibilot D, Camidge DR, Mok T, Hirsh V, Riely GJ, Iyer S, Tassell V, Polli A, Wilner KD, Janne PA. Crizotinib versus chemotherapy in advanced ALK-positive lung cancer. *N Engl J Med* 2013; 368: 2385-2394.
20. Graham J, Muhsin M, Kirkpatrick P. Cetuximab. *Nat Rev Drug Discov* 2004; 3: 549-550.
21. Pirker R, Filipits M. Cetuximab in non-small-cell lung cancer. *Transl Lung Cancer Res* 2012; 1: 54-60.
22. Hall PE, Spicer J, Popat S. Rationale for targeting the ErbB family of receptors in patients with advanced squamous cell carcinoma of the lung. *Future Oncol* 2015; 11: 2175-2191.
23. Cancer Genome Atlas Research N. Comprehensive genomic characterization of squamous cell lung cancers. *Nature* 2012; 489: 519-525.
24. Chan BA, Hughes BG. Targeted therapy for non-small cell lung cancer: current standards and the promise of the future. *Transl Lung Cancer Res* 2015; 4: 36-54.
25. Liao RG, Jung J, Tchaicha J, Wilkerson MD, Sivachenko A, Beauchamp EM, Liu Q, Pugh TJ, Pedamallu CS, Hayes DN, Gray NS, Getz G, Wong KK, Haddad RI, Meyerson M, Hammerman PS. Inhibitor-sensitive FGFR2 and FGFR3 mutations in lung squamous cell carcinoma. *Cancer Res* 2013; 73: 5195-5205.
26. Lopez-Malpartida AV, Ludena MD, Varela G, Garcia Pichel J. Differential ErbB receptor expression and intracellular signaling activity in lung adenocarcinomas and squamous cell carcinomas. *Lung Cancer* 2009; 65: 25-33.
27. Hirsch FR, Varella-Garcia M, Bunn PA, Jr., Di Maria MV, Veve R, Bremmes RM, Baron AE, Zeng C, Franklin WA. Epidermal growth factor receptor in non-small-cell lung carcinomas: correlation between gene copy number and protein expression and impact on prognosis. *J Clin Oncol* 2003; 21: 3798-3807.
28. Thatcher N, Hirsch FR, Luft AV, Szczesna A, Ciuleanu TE, Dediu M, Ramlau R, Galiulin RK, Balint B, Losonczy G, Kazarnowicz A, Park K, Schumann C, Reck M, Depenbrock H, Nanda S, Kruljac-Letunic A, Kurek R, Paz-Ares L, Socinski MA, Investigators S. Necitumumab plus gemcitabine and cisplatin versus gemcitabine and cisplatin alone as first-line therapy in patients with stage IV squamous non-small-cell lung cancer (SQUIRE): an open-label, randomised, controlled phase 3 trial. *Lancet Oncol* 2015; 16: 763-774.
29. Pirker R, Pereira JR, Szczesna A, von Pawel J, Krzakowski M, Ramlau R, Vynnychenko I, Park K, Yu CT, Ganul V, Roh JK, Bajetta E, O'Byrne K, de Marinis F, Eberhardt W, Goddemeier T, Emig M, Gatzemeier U, Team FS. Cetuximab plus chemotherapy in patients with advanced non-small-cell lung cancer (FLEX): an open-label randomised phase III trial. *Lancet* 2009; 373: 1525-1531.
30. Boelens MC, van den Berg A, Fehrmann RS, Geerlings M, de Jong WK, te Meerman GJ, Sietsma H, Timens W, Postma DS, Groen HJ. Current smoking-specific gene expression signature in normal bronchial epithelium is enhanced in squamous cell lung cancer. *J Pathol* 2009; 218: 182-191.
31. Alexandrov LB, Ju YS, Haase K, Van Loo P, Martincorena I, Nik-Zainal S, Totoki Y, Fujimoto A, Nakagawa H, Shibata T, Campbell PJ, Vineis P, Phillips DH, Stratton MR. Mutational signatures associated with tobacco smoking in human cancer. *Science* 2016; 354: 618-622.

32. Spira A, Beane J, Shah V, Liu G, Schembri F, Yang X, Palma J, Brody JS. Effects of cigarette smoke on the human airway epithelial cell transcriptome. *Proc Natl Acad Sci U S A* 2004; 101: 10143-10148.
33. Beane J, Sebastiani P, Liu G, Brody JS, Lenburg ME, Spira A. Reversible and permanent effects of tobacco smoke exposure on airway epithelial gene expression. *Genome Biol* 2007; 8: R201.
34. Corner J, Hopkinson J, Fitzsimmons D, Barclay S, Muers M. Is late diagnosis of lung cancer inevitable? Interview study of patients' recollections of symptoms before diagnosis. *Thorax* 2005; 60: 314-319.
35. Birring SS, Peake MD. Symptoms and the early diagnosis of lung cancer. *Thorax* 2005; 60: 268-269.
36. Holiday DB, McLarty JW, Farley ML, Mabry LC, Cozens D, Roby T, Waldron E, Underwood RD, Anderson E, Culbreth W, et al. Sputum cytology within and across laboratories. A reliability study. *Acta Cytol* 1995; 39: 195-206.
37. Nicholson AG, Perry LJ, Cury PM, Jackson P, McCormick CM, Corrin B, Wells AU. Reproducibility of the WHO/IASLC grading system for pre-invasive squamous lesions of the bronchus: a study of inter-observer and intra-observer variation. *Histopathology* 2001; 38: 202-208.
38. Franklin WA. Diagnosis of lung cancer: pathology of invasive and preinvasive neoplasia. *Chest* 2000; 117: 80S-89S.
39. Hirsch FR, Merrick DT, Franklin WA. Role of biomarkers for early detection of lung cancer and chemoprevention. *Eur Respir J* 2002; 19: 1151-1158.
40. Auerbach O, Stout AP, Hammond EC, Garfinkel L. Changes in bronchial epithelium in relation to cigarette smoking and in relation to lung cancer. *N Engl J Med* 1961; 265: 253-267.
41. George PJ. Fluorescence bronchoscopy for the early detection of lung cancer. *Thorax* 1999; 54: 180-183.
42. Lam S, Kennedy T, Unger M, Miller YE, Gelmont D, Rusch V, Gipe B, Howard D, LeRiche JC, Coldman A, Gazdar AF. Localization of bronchial intraepithelial neoplastic lesions by fluorescence bronchoscopy. *Chest* 1998; 113: 696-702.
43. Daniels JM, Sutedja TG. Detection and minimally invasive treatment of early squamous lung cancer. *Ther Adv Med Oncol* 2013; 5: 235-248.
44. Jeremy George P, Banerjee AK, Read CA, O'Sullivan C, Falzon M, Pezzella F, Nicholson AG, Shaw P, Laurent G, Rabbitts PH. Surveillance for the detection of early lung cancer in patients with bronchial dysplasia. *Thorax* 2007; 62: 43-50.
45. van Boerdonk RA, Smesseim I, Heideman DA, Coupe VM, Tio D, Grunberg K, Thunnissen E, Snijders PJ, Postmus PE, Smit EF, Daniels JM, Sutedja TG. Close Surveillance with Long-Term Follow-up of Subjects with Preinvasive Endobronchial Lesions. *Am J Respir Crit Care Med* 2015; 192: 1483-1489.
46. Steiling K, Ryan J, Brody JS, Spira A. The field of tissue injury in the lung and airway. *Cancer Prev Res (Phila)* 2008; 1: 396-403.
47. Pipinikas CP, Kiropoulos TS, Teixeira VH, Brown JM, Varanou A, Falzon M, Capitanio A, Bottoms SE, Carroll B, Navani N, McCaughan F, George JP, Giangreco A, Wright NA, McDonald SA, Graham TA, Janes SM. Cell migration leads to spatially distinct but clonally related airway cancer precursors. *Thorax* 2014; 69: 548-557.
48. McCaughan F, Pole JC, Bankier AT, Konfortov BA, Carroll B, Falzon M, Rabbitts TH, George PJ, Dear PH, Rabbitts PH. Progressive 3q amplification consistently targets SOX2 in preinvasive squamous lung cancer. *Am J Respir Crit Care Med* 2010; 182: 83-91.
49. Keith RL, Miller YE. Lung cancer chemoprevention: current status and future prospects. *Nat Rev Clin Oncol* 2013; 10: 334-343.

50. Lam S, leRiche JC, McWilliams A, Macaulay C, Dyachkova Y, Szabo E, Mayo J, Schellenberg R, Coldman A, Hawk E, Gazdar A. A randomized phase IIb trial of pulmicort turbuhaler (budesonide) in people with dysplasia of the bronchial epithelium. *Clin Cancer Res* 2004; 10: 6502-6511.
51. Lam S, McWilliams A, LeRiche J, MacAulay C, Wattenberg L, Szabo E. A phase I study of myo-inositol for lung cancer chemoprevention. *Cancer Epidemiol Biomarkers Prev* 2006; 15: 1526-1531.
52. Keith RL, Blatchford PJ, Kittelson J, Minna JD, Kelly K, Massion PP, Franklin WA, Mao J, Wilson DO, Merrick DT, Hirsch FR, Kennedy TC, Bunn PA, Jr., Geraci MW, Miller YE. Oral iloprost improves endobronchial dysplasia in former smokers. *Cancer Prev Res (Phila)* 2011; 4: 793-802.
53. Higashiyama S, Iwabuki H, Morimoto C, Hieda M, Inoue H, Matsushita N. Membrane-anchored growth factors, the epidermal growth factor family: beyond receptor ligands. *Cancer Sci* 2008; 99: 214-220.
54. Singh B, Coffey RJ. Trafficking of epidermal growth factor receptor ligands in polarized epithelial cells. *Annu Rev Physiol* 2014; 76: 275-300.
55. Yarden Y, Sliwkowski MX. Untangling the ErbB signalling network. *Nat Rev Mol Cell Biol* 2001; 2: 127-137.
56. Zhang H, Berezov A, Wang Q, Zhang G, Drebin J, Murali R, Greene MI. ErbB receptors: from oncogenes to targeted cancer therapies. *The Journal of clinical investigation* 2007; 117: 2051-2058.
57. Nyati MK, Morgan MA, Feng FY, Lawrence TS. Integration of EGFR inhibitors with radiochemotherapy. *Nat Rev Cancer* 2006; 6: 876-885.
58. Miettinen PJ, Warburton D, Bu D, Zhao JS, Berger JE, Minoo P, Koivisto T, Allen L, Dobbs L, Werb Z, Derynck R. Impaired lung branching morphogenesis in the absence of functional EGF receptor. *Developmental biology* 1997; 186: 224-236.
59. Burgel PR, Nadel JA. Epidermal growth factor receptor-mediated innate immune responses and their roles in airway diseases. *The European respiratory journal* 2008; 32: 1068-1081.
60. Lai HY, Rogers DF. Mucus hypersecretion in asthma: intracellular signalling pathways as targets for pharmacotherapy. *Current opinion in allergy and clinical immunology* 2010; 10: 67-76.
61. Vermeer PD, Einwalter LA, Moninger TO, Rokhlina T, Kern JA, Zabner J, Welsh MJ. Segregation of receptor and ligand regulates activation of epithelial growth factor receptor. *Nature* 2003; 422: 322-326.
62. Kim S, Schein AJ, Nadel JA. E-cadherin promotes EGFR-mediated cell differentiation and MUC5AC mucin expression in cultured human airway epithelial cells. *American journal of physiology Lung cellular and molecular physiology* 2005; 289: L1049-1060.
63. Tyner JW, Kim EY, Ide K, Pelletier MR, Roswit WT, Morton JD, Battaile JT, Patel AC, Patterson GA, Castro M, Spoor MS, You Y, Brody SL, Holtzman MJ. Blocking airway mucous cell metaplasia by inhibiting EGFR antiapoptosis and IL-13 transdifferentiation signals. *The Journal of clinical investigation* 2006; 116: 309-321.
64. Avraham R, Yarden Y. Feedback regulation of EGFR signalling: decision making by early and delayed loops. *Nat Rev Mol Cell Biol* 2011; 12: 104-117.
65. Goh LK, Huang F, Kim W, Gygi S, Sorkin A. Multiple mechanisms collectively regulate clathrin-mediated endocytosis of the epidermal growth factor receptor. *The Journal of cell biology* 2010; 189: 871-883.
66. Roepstorff K, Grandal MV, Henriksen L, Knudsen SL, Lerdrup M, Grovdal L, Willumsen BM, van Deurs B. Differential effects of EGFR ligands on endocytic sorting of the receptor. *Traffic* 2009; 10: 1115-1127.

67. Wilson KJ, Gilmore JL, Foley J, Lemmon MA, Riese DJ, 2nd. Functional selectivity of EGF family peptide growth factors: implications for cancer. *Pharmacol Ther* 2009; 122: 1-8.
68. Segatto O, Anastasi S, Alema S. Regulation of epidermal growth factor receptor signalling by inducible feedback inhibitors. *Journal of cell science* 2011; 124: 1785-1793.
69. Gur G, Rubin C, Katz M, Amit I, Citri A, Nilsson J, Amariglio N, Henriksson R, Rechavi G, Hedman H, Wides R, Yarden Y. LRIG1 restricts growth factor signaling by enhancing receptor ubiquitylation and degradation. *The EMBO journal* 2004; 23: 3270-3281.
70. Zhang X, Pickin KA, Bose R, Jura N, Cole PA, Kuriyan J. Inhibition of the EGF receptor by binding of MIG6 to an activating kinase domain interface. *Nature* 2007; 450: 741-744.
71. Wang Y, Poulin EJ, Coffey RJ. LRIG1 is a triple threat: ERBB negative regulator, intestinal stem cell marker and tumour suppressor. *British journal of cancer* 2013; 108: 1765-1770.
72. Nilsson J, Vallbo C, Guo D, Golovleva I, Hallberg B, Henriksson R, Hedman H. Cloning, characterization, and expression of human LIG1. *Biochemical and biophysical research communications* 2001; 284: 1155-1161.
73. Nilsson J, Starefeldt A, Henriksson R, Hedman H. LRIG1 protein in human cells and tissues. *Cell and tissue research* 2003; 312: 65-71.
74. Laederich MB, Funes-Duran M, Yen L, Ingalla E, Wu X, Carraway KL, 3rd, Sweeney C. The leucine-rich repeat protein LRIG1 is a negative regulator of ErbB family receptor tyrosine kinases. *The Journal of biological chemistry* 2004; 279: 47050-47056.
75. Shattuck DL, Miller JK, Laederich M, Funes M, Petersen H, Carraway KL, 3rd, Sweeney C. LRIG1 is a novel negative regulator of the Met receptor and opposes Met and Her2 synergy. *Molecular and cellular biology* 2007; 27: 1934-1946.
76. Ledda F, Bieraugel O, Fard SS, Vilar M, Paratcha G. Lrig1 is an endogenous inhibitor of Ret receptor tyrosine kinase activation, downstream signaling, and biological responses to GDNF. *J Neurosci* 2008; 28: 39-49.
77. Rondahl V, Holmlund C, Karlsson T, Wang B, Faraz M, Henriksson R, Hedman H. Lrig2-deficient mice are protected against PDGFB-induced glioma. *PLoS One* 2013; 8: e73635.
78. Stutz MA, Shattuck DL, Laederich MB, Carraway KL, 3rd, Sweeney C. LRIG1 negatively regulates the oncogenic EGF receptor mutant EGFRvIII. *Oncogene* 2008; 27: 5741-5752.
79. Jensen KB, Watt FM. Single-cell expression profiling of human epidermal stem and transit-amplifying cells: Lrig1 is a regulator of stem cell quiescence. *Proc Natl Acad Sci U S A* 2006; 103: 11958-11963.
80. Rafidi H, Mercado F, 3rd, Astudillo M, Fry WH, Saldana M, Carraway KL, 3rd, Sweeney C. Leucine-rich repeat and immunoglobulin domain-containing protein-1 (Lrig1) negative regulatory action toward ErbB receptor tyrosine kinases is opposed by leucine-rich repeat and immunoglobulin domain-containing protein 3 (Lrig3). *The Journal of biological chemistry* 2013; 288: 21593-21605.
81. Simion C, Cedano-Prieto ME, Sweeney C. The LRIG family: enigmatic regulators of growth factor receptor signaling. *Endocrine-related cancer* 2014; 21: R431-443.
82. Peschard P, Fournier TM, Lamorte L, Naujokas MA, Band H, Langdon WY, Park M. Mutation of the c-Cbl TKB domain binding site on the Met receptor tyrosine kinase converts it into a transforming protein. *Mol Cell* 2001; 8: 995-1004.
83. Goldoni S, Iozzo RA, Kay P, Campbell S, McQuillan A, Agnew C, Zhu JX, Keene DR, Reed CC, Iozzo RV. A soluble ectodomain of LRIG1 inhibits cancer cell growth by attenuating basal and ligand-dependent EGFR activity. *Oncogene* 2007; 26: 368-381.

84. Yi W, Holmlund C, Nilsson J, Inui S, Lei T, Itami S, Henriksson R, Hedman H. Paracrine regulation of growth factor signaling by shed leucine-rich repeats and immunoglobulin-like domains 1. *Experimental cell research* 2011; 317: 504-512.
85. Li S, Schmitz KR, Jeffrey PD, Wiltzius JJ, Kussie P, Ferguson KM. Structural basis for inhibition of the epidermal growth factor receptor by cetuximab. *Cancer cell* 2005; 7: 301-311.
86. Johansson M, Oudin A, Tiemann K, Bernard A, Golebiewska A, Keunen O, Fack F, Stieber D, Wang B, Hedman H, Niclou SP. The soluble form of the tumor suppressor Lrig1 potently inhibits in vivo glioma growth irrespective of EGF receptor status. *Neuro Oncol* 2013; 15: 1200-1211.
87. Smith A. Glossary A glossary for stem-cell biology. *Nature* 2006; 441.
88. Suzuki Y, Sato N, Tohyama M, Wanaka A, Takagi T. cDNA cloning of a novel membrane glycoprotein that is expressed specifically in glial cells in the mouse brain. LIG-1, a protein with leucine-rich repeats and immunoglobulin-like domains. *The Journal of biological chemistry* 1996; 271: 22522-22527.
89. Suzuki Y, Miura H, Tanemura A, Kobayashi K, Kondoh G, Sano S, Ozawa K, Inui S, Nakata A, Takagi T, Tohyama M, Yoshikawa K, Itami S. Targeted disruption of LIG-1 gene results in psoriasiform epidermal hyperplasia. *FEBS Lett* 2002; 521: 67-71.
90. Jensen KB, Collins CA, Nascimento E, Tan DW, Frye M, Itami S, Watt FM. Lrig1 expression defines a distinct multipotent stem cell population in mammalian epidermis. *Cell stem cell* 2009; 4: 427-439.
91. Page ME, Lombard P, Ng F, Gottgens B, Jensen KB. The epidermis comprises autonomous compartments maintained by distinct stem cell populations. *Cell stem cell* 2013; 13: 471-482.
92. Barker N. Adult intestinal stem cells: critical drivers of epithelial homeostasis and regeneration. *Nat Rev Mol Cell Biol* 2014; 15: 19-33.
93. Wong VW, Stange DE, Page ME, Buczacki S, Wabik A, Itami S, van de Wetering M, Poulsom R, Wright NA, Trotter MW, Watt FM, Winton DJ, Clevers H, Jensen KB. Lrig1 controls intestinal stem-cell homeostasis by negative regulation of ErbB signalling. *Nature cell biology* 2012; 14: 401-408.
94. Powell AE, Wang Y, Li Y, Poulin EJ, Means AL, Washington MK, Higginbotham JN, Juchheim A, Prasad N, Levy SE, Guo Y, Shyr Y, Aronow BJ, Haigis KM, Franklin JL, Coffey RJ. The pan-ErbB negative regulator Lrig1 is an intestinal stem cell marker that functions as a tumor suppressor. *Cell* 2012; 149: 146-158.
95. Poulin EJ, Powell AE, Wang Y, Li Y, Franklin JL, Coffey RJ. Using a new Lrig1 reporter mouse to assess differences between two Lrig1 antibodies in the intestine. *Stem cell research* 2014; 13: 422-430.
96. Nakamura T, Hamuro J, Takaishi M, Simmons S, Maruyama K, Zaffalon A, Bentley AJ, Kawasaki S, Nagata-Takaoka M, Fullwood NJ, Itami S, Sano S, Ishii M, Barrandon Y, Kinoshita S. LRIG1 inhibits STAT3-dependent inflammation to maintain corneal homeostasis. *J Clin Invest* 2014; 124: 385-397.
97. Hedman H, Nilsson J, Guo D, Henriksson R. Is LRIG1 a tumour suppressor gene at chromosome 3p14.3? *Acta oncologica* 2002; 41: 352-354.
98. Rouam S, Moreau T, Broet P. Identifying common prognostic factors in genomic cancer studies: a novel index for censored outcomes. *BMC bioinformatics* 2010; 11: 150.
99. Lindstrom AK, Ekman K, Stendahl U, Tot T, Henriksson R, Hedman H, Hellberg D. LRIG1 and squamous epithelial uterine cervical cancer: correlation to prognosis, other tumor markers, sex steroid hormones, and smoking. *Int J Gynecol Cancer* 2008; 18: 312-317.

100. Guo D, Nilsson J, Haapasalo H, Raheem O, Bergenheim T, Hedman H, Henriksson R. Perinuclear leucine-rich repeats and immunoglobulin-like domain proteins (LRIG1-3) as prognostic indicators in astrocytic tumors. *Acta Neuropathol* 2006; 111: 238-246.
101. Lindquist D, Nasman A, Tarjan M, Henriksson R, Tot T, Dalianis T, Hedman H. Expression of LRIG1 is associated with good prognosis and human papillomavirus status in oropharyngeal cancer. *British journal of cancer* 2014; 110: 1793-1800.
102. Tanemura A, Nagasawa T, Inui S, Itami S. LRIG-1 provides a novel prognostic predictor in squamous cell carcinoma of the skin: immunohistochemical analysis for 38 cases. *Dermatol Surg* 2005; 31: 423-430.
103. Nagata M, Nakamura T, Sotozono C, Inatomi T, Yokoi N, Kinoshita S. LRIG1 as a potential novel marker for neoplastic transformation in ocular surface squamous neoplasia. *PloS one* 2014; 9: e93164.
104. Lu L, Teixeira VH, Yuan Z, Graham TA, Endesfelder D, Kolluri K, Al-Juffali N, Hamilton N, Nicholson AG, Falzon M, Kschischo M, Swanton C, Wright NA, Carroll B, Watt FM, George JP, Jensen KB, Giangreco A, Janes SM. LRIG1 regulates cadherin-dependent contact inhibition directing epithelial homeostasis and pre-invasive squamous cell carcinoma development. *The Journal of pathology* 2013; 229: 608-620.
105. Kvarnbrink S, Karlsson T, Edlund K, Botling J, Lindquist D, Jirstrom K, Micke P, Henriksson R, Johansson M, Hedman H. LRIG1 is a prognostic biomarker in non-small cell lung cancer. *Acta oncologica* 2015; 54: 1113-1119.
106. Thompson PA, Ljuslinder I, Tsavachidis S, Brewster A, Sahin A, Hedman H, Henriksson R, Bondy ML, Melin BS. Loss of LRIG1 locus increases risk of early and late relapse of stage I/II breast cancer. *Cancer Res* 2014; 74: 2928-2935.
107. Krig SR, Frietze S, Simion C, Miller JK, Fry WH, Rafidi H, Kotelawala L, Qi L, Griffith OL, Gray JW, Carraway KL, 3rd, Sweeney C. Lrig1 is an estrogen-regulated growth suppressor and correlates with longer relapse-free survival in ERalpha-positive breast cancer. *Mol Cancer Res* 2011; 9: 1406-1417.
108. Miller JK, Shattuck DL, Ingalla EQ, Yen L, Borowsky AD, Young LJ, Cardiff RD, Carraway KL, 3rd, Sweeney C. Suppression of the negative regulator LRIG1 contributes to ErbB2 overexpression in breast cancer. *Cancer Res* 2008; 68: 8286-8294.
109. Thomasson M, Wang B, Hammarsten P, Dahlman A, Persson JL, Josefsson A, Stattin P, Granfors T, Egevad L, Henriksson R, Bergh A, Hedman H. LRIG1 and the liar paradox in prostate cancer: a study of the expression and clinical significance of LRIG1 in prostate cancer. *Int J Cancer* 2011; 128: 2843-2852.
110. Sheu JJ, Lee CC, Hua CH, Li CI, Lai MT, Lee SC, Cheng J, Chen CM, Chan C, Chao SC, Chen JY, Chang JY, Lee CH. LRIG1 modulates aggressiveness of head and neck cancers by regulating EGFR-MAPK-SPHK1 signaling and extracellular matrix remodeling. *Oncogene* 2014; 33: 1375-1384.
111. Yokdang N, Hatakeyama J, Wald JH, Simion C, Tellez JD, Chang DZ, Swamynathan MM, Chen M, Murphy WJ, Carraway Iii KL, Sweeney C. LRIG1 opposes epithelial-to-mesenchymal transition and inhibits invasion of basal-like breast cancer cells. *Oncogene* 2016; 35: 2932-2947.
112. Lamouille S, Xu J, Derynck R. Molecular mechanisms of epithelial-mesenchymal transition. *Nat Rev Mol Cell Biol* 2014; 15: 178-196.
113. Stuart HM, Roberts NA, Burgu B, Daly SB, Urquhart JE, Bhaskar S, Dickerson JE, Mermerkaya M, Silay MS, Lewis MA, Olondriz MB, Gener B, Beetz C, Varga RE, Gulpinar O, Suer E, Soygur T, Ozcakar ZB, Yalcinkaya F, Kavaz A, Bulum B, Gucuk A, Yue WW, Erdogan F, Berry A, Hanley NA, McKenzie EA, Hilton EN, Woolf AS, Newman WG. LRIG2 mutations cause urofacial syndrome. *American journal of human genetics* 2013; 92: 259-264.

114. Roberts NA, Woolf AS, Stuart HM, Thuret R, McKenzie EA, Newman WG, Hilton EN. Heparanase 2, mutated in urofacial syndrome, mediates peripheral neural development in Xenopus. *Hum Mol Genet* 2014; 23: 4302-4314.
115. Holmlund C, Haapasalo H, Yi W, Raheem O, Brannstrom T, Bragge H, Henriksson R, Hedman H. Cytoplasmic LRIG2 expression is associated with poor oligodendroglioma patient survival. *Neuropathology : official journal of the Japanese Society of Neuropathology* 2009; 29: 242-247.
116. Zhang H, Yan Q, Xu S, Ou Y, Ye F, Wang B, Lei T, Guo D. Association of expression of Leucine-rich repeats and immunoglobulin-like domains 2 gene with invasiveness of pituitary adenoma. *Journal of Huazhong University of Science and Technology Medical sciences = Hua zhong ke ji da xue xue bao Yi xue Ying De wen ban = Huazhong keji daxue xuebao Yixue Yingdewen ban* 2011; 31: 520-523.
117. Hedman H, Lindstrom AK, Tot T, Stendahl U, Henriksson R, Hellberg D. LRIG2 in contrast to LRIG1 predicts poor survival in early-stage squamous cell carcinoma of the uterine cervix. *Acta Oncol* 2010; 49: 812-815.
118. Wang G, Wu J, Song H. LRIG2 expression and prognosis in non-small cell lung cancer. *Oncology letters* 2014; 8: 667-672.
119. Abraira VE, Del Rio T, Tucker AF, Slonimsky J, Keirnes HL, Goodrich LV. Cross-repressive interactions between Lrig3 and netrin 1 shape the architecture of the inner ear. *Development* 2008; 135: 4091-4099.
120. Zhao H, Tanegashima K, Ro H, Dawid IB. Lrig3 regulates neural crest formation in Xenopus by modulating Fgf and Wnt signaling pathways. *Development* 2008; 135: 1283-1293.
121. Muller S, Lindquist D, Kanter L, Flores-Staino C, Henriksson R, Hedman H, Andersson S. Expression of LRIG1 and LRIG3 correlates with human papillomavirus status and patient survival in cervical adenocarcinoma. *Int J Oncol* 2013; 42: 247-252.
122. Guo D, Yang H, Guo Y, Xiao Q, Mao F, Tan Y, Wan X, Wang B, Lei T. LRIG3 modulates proliferation, apoptosis and invasion of glioblastoma cells as a potent tumor suppressor. *J Neurol Sci* 2015; 350: 61-68.
123. Cai M, Han L, Chen R, Ye F, Wang B, Han F, Lei T, Guo D. Inhibition of LRIG3 gene expression via RNA interference modulates the proliferation, cell cycle, cell apoptosis, adhesion and invasion of glioblastoma cell (GL15). *Cancer Lett* 2009; 278: 104-112.
124. Succony L, Janes SM. Airway stem cells and lung cancer. *QJM* 2014; 107: 607-612.
125. Hogan BL, Barkauskas CE, Chapman HA, Epstein JA, Jain R, Hsia CC, Niklason L, Calle E, Le A, Randell SH, Rock J, Snitow M, Krummel M, Stripp BR, Vu T, White ES, Whitsett JA, Morrisey EE. Repair and regeneration of the respiratory system: complexity, plasticity, and mechanisms of lung stem cell function. *Cell Stem Cell* 2014; 15: 123-138.
126. Visvader JE, Clevers H. Tissue-specific designs of stem cell hierarchies. *Nat Cell Biol* 2016; 18: 349-355.
127. Jones DL, Wagers AJ. No place like home: anatomy and function of the stem cell niche. *Nat Rev Mol Cell Biol* 2008; 9: 11-21.
128. Giangreco A, Groot KR, Janes SM. Lung cancer and lung stem cells: strange bedfellows? *American journal of respiratory and critical care medicine* 2007; 175: 547-553.
129. Kim CF, Jackson EL, Woolfenden AE, Lawrence S, Babar I, Vogel S, Crowley D, Bronson RT, Jacks T. Identification of bronchioalveolar stem cells in normal lung and lung cancer. *Cell* 2005; 121: 823-835.
130. Rock JR, Onaitis MW, Rawlins EL, Lu Y, Clark CP, Xue Y, Randell SH, Hogan BL. Basal cells as stem cells of the mouse trachea and human airway epithelium. *Proceedings of the*

National Academy of Sciences of the United States of America 2009; 106: 12771-12775.
131. Rock JR, Gao X, Xue Y, Randell SH, Kong YY, Hogan BL. Notch-dependent differentiation of adult airway basal stem cells. *Cell Stem Cell* 2011; 8: 639-648.
132. Pardo-Saganta A, Law BM, Tata PR, Villoria J, Saez B, Mou H, Zhao R, Rajagopal J. Injury induces direct lineage segregation of functionally distinct airway basal stem/progenitor cell subpopulations. *Cell Stem Cell* 2015; 16: 184-197.
133. Tata PR, Mou H, Pardo-Saganta A, Zhao R, Prabhu M, Law BM, Vinarsky V, Cho JL, Breton S, Sahay A, Medoff BD, Rajagopal J. Dedifferentiation of committed epithelial cells into stem cells in vivo. *Nature* 2013; 503: 218-223.
134. Hajj R, Baranek T, Le Naour R, Lesimple P, Puchelle E, Coraux C. Basal cells of the human adult airway surface epithelium retain transit-amplifying cell properties. *Stem Cells* 2007; 25: 139-148.
135. Teixeira VH, Nadarajan P, Graham TA, Pipinikas CP, Brown JM, Falzon M, Nye E, Poulsom R, Lawrence D, Wright NA, McDonald S, Giangreco A, Simons BD, Janes SM. Stochastic homeostasis in human airway epithelium is achieved by neutral competition of basal cell progenitors. *eLife* 2013; 2: e00966.
136. Rawlins EL, Okubo T, Xue Y, Brass DM, Auten RL, Hasegawa H, Wang F, Hogan BL. The role of Scgb1a1+ Clara cells in the long-term maintenance and repair of lung airway, but not alveolar, epithelium. *Cell Stem Cell* 2009; 4: 525-534.
137. Reynolds SD, Giangreco A, Power JH, Stripp BR. Neuroepithelial bodies of pulmonary airways serve as a reservoir of progenitor cells capable of epithelial regeneration. *Am J Pathol* 2000; 156: 269-278.
138. Hong KU, Reynolds SD, Giangreco A, Hurley CM, Stripp BR. Clara cell secretory protein-expressing cells of the airway neuroepithelial body microenvironment include a label-retaining subset and are critical for epithelial renewal after progenitor cell depletion. *Am J Respir Cell Mol Biol* 2001; 24: 671-681.
139. Giangreco A, Reynolds SD, Stripp BR. Terminal bronchioles harbor a unique airway stem cell population that localizes to the bronchoalveolar duct junction. *Am J Pathol* 2002; 161: 173-182.
140. Zheng D, Limmon GV, Yin L, Leung NH, Yu H, Chow VT, Chen J. A cellular pathway involved in Clara cell to alveolar type II cell differentiation after severe lung injury. *PloS one* 2013; 8: e71028.
141. Rock JR, Barkauskas CE, Cronce MJ, Xue Y, Harris JR, Liang J, Noble PW, Hogan BL. Multiple stromal populations contribute to pulmonary fibrosis without evidence for epithelial to mesenchymal transition. *Proc Natl Acad Sci U S A* 2011; 108: E1475-1483.
142. Kumar PA, Hu Y, Yamamoto Y, Hoe NB, Wei TS, Mu D, Sun Y, Joo LS, Dagher R, Zielonka EM, Wang de Y, Lim B, Chow VT, Crum CP, Xian W, McKeon F. Distal airway stem cells yield alveoli in vitro and during lung regeneration following H1N1 influenza infection. *Cell* 2011; 147: 525-538.
143. Giangreco A, Arwert EN, Rosewell IR, Snyder J, Watt FM, Stripp BR. Stem cells are dispensable for lung homeostasis but restore airways after injury. *Proc Natl Acad Sci U S A* 2009; 106: 9286-9291.
144. Evans MJ, Johnson LV, Stephens RJ, Freeman G. Renewal of the terminal bronchiolar epithelium in the rat following exposure to NO2 or O3. *Lab Invest* 1976; 35: 246-257.
145. Kajstura J, Rota M, Hall SR, Hosoda T, D'Amario D, Sanada F, Zheng H, Ogorek B, Rondon-Clavo C, Ferreira-Martins J, Matsuda A, Arranto C, Goichberg P, Giordano G, Haley KJ, Bardelli S, Rayatzadeh H, Liu X, Quaini F, Liao R, Leri A, Perrella MA, Loscalzo J, Anversa P. Evidence for human lung stem cells. *N Engl J Med* 2011; 364: 1795-1806.

146. Liu Q, Huang X, Zhang H, Tian X, He L, Yang R, Yan Y, Wang QD, Gillich A, Zhou B. c-kit(+) cells adopt vascular endothelial but not epithelial cell fates during lung maintenance and repair. *Nat Med* 2015; 21: 866-868.
147. Lau AN, Goodwin M, Kim CF, Weiss DJ. Stem cells and regenerative medicine in lung biology and diseases. *Mol Ther* 2012; 20: 1116-1130.
148. Visvader JE. Cells of origin in cancer. *Nature* 2011; 469: 314-322.
149. Barth PJ, Koch S, Muller B, Unterstab F, von Wichert P, Moll R. Proliferation and number of Clara cell 10-kDa protein (CC10)-reactive epithelial cells and basal cells in normal, hyperplastic and metaplastic bronchial mucosa. *Virchows Archiv : an international journal of pathology* 2000; 437: 648-655.
150. Beasley MB, Lantuejoul S, Abbondanzo S, Chu WS, Hasleton PS, Travis WD, Brambilla E. The P16/cyclin D1/Rb pathway in neuroendocrine tumors of the lung. *Hum Pathol* 2003; 34: 136-142.
151. Sutherland KD, Proost N, Brouns I, Adriaensen D, Song JY, Berns A. Cell of origin of small cell lung cancer: inactivation of Trp53 and Rb1 in distinct cell types of adult mouse lung. *Cancer Cell* 2011; 19: 754-764.
152. Blanpain C. Tracing the cellular origin of cancer. *Nat Cell Biol* 2013; 15: 126-134.
153. Xu X, Rock JR, Lu Y, Futtner C, Schwab B, Guinney J, Hogan BL, Onaitis MW. Evidence for type II cells as cells of origin of K-Ras-induced distal lung adenocarcinoma. *Proc Natl Acad Sci U S A* 2012; 109: 4910-4915.
154. O'Flaherty JD, Barr M, Fennell D, Richard D, Reynolds J, O'Leary J, O'Byrne K. The cancer stem-cell hypothesis: its emerging role in lung cancer biology and its relevance for future therapy. *J Thorac Oncol* 2012; 7: 1880-1890.
155. Reya T, Morrison SJ, Clarke MF, Weissman IL. Stem cells, cancer, and cancer stem cells. *Nature* 2001; 414: 105-111.
156. Ho MM, Ng AV, Lam S, Hung JY. Side population in human lung cancer cell lines and tumors is enriched with stem-like cancer cells. *Cancer Res* 2007; 67: 4827-4833.
157. Loebinger MR, Giangreco A, Groot KR, Prichard L, Allen K, Simpson C, Bazley L, Navani N, Tibrewal S, Davies D, Janes SM. Squamous cell cancers contain a side population of stem-like cells that are made chemosensitive by ABC transporter blockade. *British journal of cancer* 2008; 98: 380-387.
158. Bertolini G, Roz L, Perego P, Tortoreto M, Fontanella E, Gatti L, Pratesi G, Fabbri A, Andriani F, Tinelli S, Roz E, Caserini R, Lo Vullo S, Camerini T, Mariani L, Delia D, Calabro E, Pastorino U, Sozzi G. Highly tumorigenic lung cancer CD133+ cells display stem-like features and are spared by cisplatin treatment. *Proc Natl Acad Sci U S A* 2009; 106: 16281-16286.
159. Nowell PC. The clonal evolution of tumor cell populations. *Science* 1976; 194: 23-28.
160. Polyak K. Tumor heterogeneity confounds and illuminates: a case for Darwinian tumor evolution. *Nat Med* 2014; 20: 344-346.
161. McGranahan N, Swanton C. Biological and therapeutic impact of intratumor heterogeneity in cancer evolution. *Cancer Cell* 2015; 27: 15-26.
162. Gerlinger M, Rowan AJ, Horswell S, Larkin J, Endesfelder D, Gronroos E, Martinez P, Matthews N, Stewart A, Tarpey P, Varela I, Phillimore B, Begum S, McDonald NQ, Butler A, Jones D, Raine K, Latimer C, Santos CR, Nohadani M, Eklund AC, Spencer-Dene B, Clark G, Pickering L, Stamp G, Gore M, Szallasi Z, Downward J, Futreal PA, Swanton C. Intratumor heterogeneity and branched evolution revealed by multiregion sequencing. *N Engl J Med* 2012; 366: 883-892.
163. Untergasser A, Cutcutache I, Koressaar T, Ye J, Faircloth BC, Remm M, Rozen SG. Primer3--new capabilities and interfaces. *Nucleic acids research* 2012; 40: e115.
164. Koressaar T, Remm M. Enhancements and modifications of primer design program Primer3. *Bioinformatics* 2007; 23: 1289-1291.

165. Rosewell IR, Giangreco A. Murine aggregation chimeras and wholemount imaging in airway stem cell biology. *Methods Mol Biol* 2012; 916: 263-274.
166. Hegab AE, Ha VL, Attiga YS, Nickerson DW, Gomperts BN. Isolation of basal cells and submucosal gland duct cells from mouse trachea. *Journal of visualized experiments : JoVE* 2012: e3731.
167. Hegab AE, Ha VL, Darmawan DO, Gilbert JL, Ooi AT, Attiga YS, Bisht B, Nickerson DW, Gomperts BN. Isolation and in vitro characterization of basal and submucosal gland duct stem/progenitor cells from human proximal airways. *Stem cells translational medicine* 2012; 1: 719-724.
168. A M. Mitogenic reposnse of rat lung and tracheal epithelial cells in monolayer primary cultures- Modulation of TNF-a expression. *Journal of Bioscience* 1994; 19: 11.
169. You Y, Brody SL. Culture and differentiation of mouse tracheal epithelial cells. *Methods Mol Biol* 2013; 945: 123-143.
170. You Y, Richer EJ, Huang T, Brody SL. Growth and differentiation of mouse tracheal epithelial cells: selection of a proliferative population. *Am J Physiol Lung Cell Mol Physiol* 2002; 283: L1315-1321.
171. Butler CR, Hynds RE, Gowers KH, Lee Ddo H, Brown JM, Crowley C, Teixeira VH, Smith CM, Urbani L, Hamilton NJ, Thakrar RM, Booth HL, Birchall MA, De Coppi P, Giangreco A, O'Callaghan C, Janes SM. Rapid Expansion of Human Epithelial Stem Cells Suitable for Airway Tissue Engineering. *American journal of respiratory and critical care medicine* 2016; 194: 156-168.
172. Hynds RE, Butler CR, Janes SM, Giangreco A. Expansion of Human Airway Basal Stem Cells and Their Differentiation as 3D Tracheospheres. *Methods Mol Biol* 2016.
173. van Kuppeveld FJ, van der Logt JT, Angulo AF, van Zoest MJ, Quint WG, Niesters HG, Galama JM, Melchers WJ. Genus- and species-specific identification of mycoplasmas by 16S rRNA amplification. *Appl Environ Microbiol* 1992; 58: 2606-2615.
174. Alcolea MP, Greulich P, Wabik A, Frede J, Simons BD, Jones PH. Differentiation imbalance in single oesophageal progenitor cells causes clonal immortalization and field change. *Nature cell biology* 2014; 16: 615-622.
175. Poulin EJ, Powell AE, Wang Y, Li Y, Franklin JL, Coffey RJ. Using a new Lrig1 reporter mouse to assess differences between two Lrig1 antibodies in the intestine. *Stem cell research* 2014; 13: 422-430.
176. Rock JR, Randell SH, Hogan BL. Airway basal stem cells: a perspective on their roles in epithelial homeostasis and remodeling. *Disease models & mechanisms* 2010; 3: 545-556.
177. Sutherland KD, Berns A. Cell of origin of lung cancer. *Molecular oncology* 2010; 4: 397-403.
178. Hanna JM, Onaitis MW. Cell of origin of lung cancer. *Journal of carcinogenesis* 2013; 12: 6.
179. Hennings H, Glick AB, Lowry DT, Krsmanovic LS, Sly LM, Yuspa SH. FVB/N mice: an inbred strain sensitive to the chemical induction of squamous cell carcinomas in the skin. *Carcinogenesis* 1993; 14: 2353-2358.
180. Mahler JF, Stokes W, Mann PC, Takaoka M, Maronpot RR. Spontaneous lesions in aging FVB/N mice. *Toxicologic pathology* 1996; 24: 710-716.
181. Song JM, Qian X, Teferi F, Pan J, Wang Y, Kassie F. Dietary diindolylmethane suppresses inflammation-driven lung squamous cell carcinoma in mice. *Cancer prevention research* 2015; 8: 77-85.
182. Guo D, Holmlund C, Henriksson R, Hedman H. The LRIG gene family has three vertebrate paralogs widely expressed in human and mouse tissues and a homolog in Ascidiacea. *Genomics* 2004; 84: 157-165.

183. Shimizu T, Nettesheim P, Mahler JF, Randell SH. Cell type-specific lectin staining of the tracheobronchial epithelium of the rat: quantitative studies with Griffonia simplicifolia I isolectin B4. *The journal of histochemistry and cytochemistry : official journal of the Histochemistry Society* 1991; 39: 7-14.
184. Borthwick DW, Shahbazian M, Krantz QT, Dorin JR, Randell SH. Evidence for stem-cell niches in the tracheal epithelium. *American journal of respiratory cell and molecular biology* 2001; 24: 662-670.
185. Schoch KG, Lori A, Burns KA, Eldred T, Olsen JC, Randell SH. A subset of mouse tracheal epithelial basal cells generates large colonies in vitro. *American journal of physiology Lung cellular and molecular physiology* 2004; 286: L631-642.
186. Liu X, Driskell RR, Engelhardt JF. Stem cells in the lung. *Methods in enzymology* 2006; 419: 285-321.
187. Van de Laar E, Clifford M, Hasenoeder S, Kim BR, Wang D, Lee S, Paterson J, Vu NM, Waddell TK, Keshavjee S, Tsao MS, Ailles L, Moghal N. Cell surface marker profiling of human tracheal basal cells reveals distinct subpopulations, identifies MST1/MSP as a mitogenic signal, and identifies new biomarkers for lung squamous cell carcinomas. *Respiratory research* 2014; 15: 160.
188. Brechbuhl HM, Ghosh M, Smith MK, Smith RW, Li B, Hicks DA, Cole BB, Reynolds PR, Reynolds SD. beta-catenin dosage is a critical determinant of tracheal basal cell fate determination. *The American journal of pathology* 2011; 179: 367-379.
189. Hackett TL, Shaheen F, Johnson A, Wadsworth S, Pechkovsky DV, Jacoby DB, Kicic A, Stick SM, Knight DA. Characterization of side population cells from human airway epithelium. *Stem cells* 2008; 26: 2576-2585.
190. Zhu H, Guo ZK, Jiang XX, Li H, Wang XY, Yao HY, Zhang Y, Mao N. A protocol for isolation and culture of mesenchymal stem cells from mouse compact bone. *Nature protocols* 2010; 5: 550-560.
191. Baustian C, Hanley S, Ceredig R. Isolation, selection and culture methods to enhance clonogenicity of mouse bone marrow derived mesenchymal stromal cell precursors. *Stem cell research & therapy* 2015; 6: 151.
192. Yu KR, Yang SR, Jung JW, Kim H, Ko K, Han DW, Park SB, Choi SW, Kang SK, Scholer H, Kang KS. CD49f enhances multipotency and maintains stemness through the direct regulation of OCT4 and SOX2. *Stem cells* 2012; 30: 876-887.
193. Nolan DJ, Ciarrocchi A, Mellick AS, Jaggi JS, Bambino K, Gupta S, Heikamp E, McDevitt MR, Scheinberg DA, Benezra R, Mittal V. Bone marrow-derived endothelial progenitor cells are a major determinant of nascent tumor neovascularization. *Genes & development* 2007; 21: 1546-1558.
194. Tabor DR, Larry CH, Jacobs RF. Differential induction of macrophage GSIB4-binding activity. *Journal of leukocyte biology* 1989; 45: 452-457.
195. Maya, Usha, Nagalakhmi. Mitogenic response of rat lung and tracheal epithelial cells in monolayer primary cultures- Modulation of TNF-a expression. *Journal of Bioscience* 1994; 19: 207-218.
196. Kumar RK, Maronese SE, O'Grady R. Serum-free culture of mouse tracheal epithelial cells. *Experimental lung research* 1997; 23: 427-440.
197. Herbert C, Siegle JS, Shadie AM, Nikolaysen S, Garthwaite L, Hansbro NG, Foster PS, Kumar RK. Development of asthmatic inflammation in mice following early-life exposure to ambient environmental particulates and chronic allergen challenge. *Disease models & mechanisms* 2013; 6: 479-488.
198. Paget C, Ivanov S, Fontaine J, Renneson J, Blanc F, Pichavant M, Dumoutier L, Ryffel B, Renauld JC, Gosset P, Gosset P, Si-Tahar M, Faveeuw C, Trottein F. Interleukin-22 is produced by invariant natural killer T lymphocytes during influenza A virus infection:

potential role in protection against lung epithelial damages. *The Journal of biological chemistry* 2012; 287: 8816-8829.
199. Chiang CF, Okou DT, Griffin TB, Verret CR, Williams MN. Green fluorescent protein rendered susceptible to proteolysis: positions for protease-sensitive insertions. *Archives of biochemistry and biophysics* 2001; 394: 229-235.
200. Soriano P. Generalized lacZ expression with the ROSA26 Cre reporter strain. *Nature genetics* 1999; 21: 70-71.
201. Li X, Zhao X, Fang Y, Jiang X, Duong T, Fan C, Huang CC, Kain SR. Generation of destabilized green fluorescent protein as a transcription reporter. *The Journal of biological chemistry* 1998; 273: 34970-34975.
202. Watson JK, Rulands S, Wilkinson AC, Wuidart A, Ousset M, Van Keymeulen A, Gottgens B, Blanpain C, Simons BD, Rawlins EL. Clonal Dynamics Reveal Two Distinct Populations of Basal Cells in Slow-Turnover Airway Epithelium. *Cell reports* 2015; 12: 90-101.
203. Ghosh M, Brechbuhl HM, Smith RW, Li B, Hicks DA, Titchner T, Runkle CM, Reynolds SD. Context-dependent differentiation of multipotential keratin 14-expressing tracheal basal cells. *Am J Respir Cell Mol Biol* 2011; 45: 403-410.
204. Alcolea MP, Jones PH. Cell competition: winning out by losing notch. *Cell cycle* 2015; 14: 9-17.
205. Lynch TJ, Engelhardt JF. Progenitor cells in proximal airway epithelial development and regeneration. *Journal of cellular biochemistry* 2014; 115: 1637-1645.
206. Mou H, Vinarsky V, Tata PR, Brazauskas K, Choi SH, Crooke AK, Zhang B, Solomon GM, Turner B, Bihler H, Harrington J, Lapey A, Channick C, Keyes C, Freund A, Artandi S, Mense M, Rowe S, Engelhardt JF, Hsu YC, Rajagopal J. Dual SMAD Signaling Inhibition Enables Long-Term Expansion of Diverse Epithelial Basal Cells. *Cell Stem Cell* 2016.
207. Fenwick N, Griffin G, Gauthier C. The welfare of animals used in science: how the "Three Rs" ethic guides improvements. *Can Vet J* 2009; 50: 523-530.
208. McConnell AM, Yao C, Yeckes AR, Wang Y, Selvaggio AS, Tang J, Kirsch DG, Stripp BR. p53 Regulates Progenitor Cell Quiescence and Differentiation in the Airway. *Cell Rep* 2016; 17: 2173-2182.
209. Tadokoro T, Wang Y, Barak LS, Bai Y, Randell SH, Hogan BL. IL-6/STAT3 promotes regeneration of airway ciliated cells from basal stem cells. *Proc Natl Acad Sci U S A* 2014; 111: E3641-3649.
210. Danahay H, Pessotti AD, Coote J, Montgomery BE, Xia D, Wilson A, Yang H, Wang Z, Bevan L, Thomas C, Petit S, London A, LeMotte P, Doelemeyer A, Velez-Reyes GL, Bernasconi P, Fryer CJ, Edwards M, Capodieci P, Chen A, Hild M, Jaffe AB. Notch2 is required for inflammatory cytokine-driven goblet cell metaplasia in the lung. *Cell Rep* 2015; 10: 239-252.
211. Rochat A, Kobayashi K, Barrandon Y. Location of stem cells of human hair follicles by clonal analysis. *Cell* 1994; 76: 1063-1073.
212. Nygaard V, Hovig E. Options available for profiling small samples: a review of sample amplification technology when combined with microarray profiling. *Nucleic Acids Res* 2006; 34: 996-1014.
213. Wu AR, Neff NF, Kalisky T, Dalerba P, Treutlein B, Rothenberg ME, Mburu FM, Mantalas GL, Sim S, Clarke MF, Quake SR. Quantitative assessment of single-cell RNA-sequencing methods. *Nat Methods* 2014; 11: 41-46.
214. Treutlein B, Brownfield DG, Wu AR, Neff NF, Mantalas GL, Espinoza FH, Desai TJ, Krasnow MA, Quake SR. Reconstructing lineage hierarchies of the distal lung epithelium using single-cell RNA-seq. *Nature* 2014; 509: 371-375.

215. Akamatsu T, Arai Y, Kosugi I, Kawasaki H, Meguro S, Sakao M, Shibata K, Suda T, Chida K, Iwashita T. Direct isolation of myofibroblasts and fibroblasts from bleomycin-injured lungs reveals their functional similarities and differences. *Fibrogenesis Tissue Repair* 2013; 6: 15.
216. Cancela L, Hsieh CL, Francke U, Price PA. Molecular structure, chromosome assignment, and promoter organization of the human matrix Gla protein gene. *J Biol Chem* 1990; 265: 15040-15048.
217. Gunning PW, Schevzov G, Kee AJ, Hardeman EC. Tropomyosin isoforms: divining rods for actin cytoskeleton function. *Trends Cell Biol* 2005; 15: 333-341.
218. Ferby I, Reschke M, Kudlacek O, Knyazev P, Pante G, Amann K, Sommergruber W, Kraut N, Ullrich A, Fassler R, Klein R. Mig6 is a negative regulator of EGF receptor-mediated skin morphogenesis and tumor formation. *Nat Med* 2006; 12: 568-573.
219. Sacchetti A, El Sewedy T, Nasr AF, Alberti S. Efficient GFP mutations profoundly affect mRNA transcription and translation rates. *FEBS Lett* 2001; 492: 151-155.
220. McWilliam H, Li W, Uludag M, Squizzato S, Park YM, Buso N, Cowley AP, Lopez R. Analysis Tool Web Services from the EMBL-EBI. *Nucleic Acids Res* 2013; 41: W597-600.
221. Grun D, Lyubimova A, Kester L, Wiebrands K, Basak O, Sasaki N, Clevers H, van Oudenaarden A. Single-cell messenger RNA sequencing reveals rare intestinal cell types. *Nature* 2015; 525: 251-255.
222. Bhargava V, Head SR, Ordoukhanian P, Mercola M, Subramaniam S. Technical variations in low-input RNA-seq methodologies. *Sci Rep* 2014; 4: 3678.
223. Sommer SS, Cohen JE. The size distributions of proteins, mRNA, and nuclear RNA. *J Mol Evol* 1980; 15: 37-57.
224. Saliba AE, Westermann AJ, Gorski SA, Vogel J. Single-cell RNA-seq: advances and future challenges. *Nucleic Acids Res* 2014; 42: 8845-8860.
225. Tan DW, Jensen KB, Trotter MW, Connelly JT, Broad S, Watt FM. Single-cell gene expression profiling reveals functional heterogeneity of undifferentiated human epidermal cells. *Development* 2013; 140: 1433-1444.
226. An Y, Zhao Z, Ou P, Wang G. Expression of LRIG1 is Associated With Good Prognosis for Human Non-small Cell Lung Cancer. *Medicine (Baltimore)* 2015; 94: e2081.
227. Lu Y, Futtner C, Rock JR, Xu X, Whitworth W, Hogan BL, Onaitis MW. Evidence that SOX2 overexpression is oncogenic in the lung. *PloS one* 2010; 5: e11022.
228. Suprynowicz FA, Upadhyay G, Krawczyk E, Kramer SC, Hebert JD, Liu X, Yuan H, Cheluvaraju C, Clapp PW, Boucher RC, Jr., Kamonjoh CM, Randell SH, Schlegel R. Conditionally reprogrammed cells represent a stem-like state of adult epithelial cells. *Proceedings of the National Academy of Sciences of the United States of America* 2012; 109: 20035-20040.
229. Liu X, Ory V, Chapman S, Yuan H, Albanese C, Kallakury B, Timofeeva OA, Nealon C, Dakic A, Simic V, Haddad BR, Rhim JS, Dritschilo A, Riegel A, McBride A, Schlegel R. ROCK inhibitor and feeder cells induce the conditional reprogramming of epithelial cells. *Am J Pathol* 2012; 180: 599-607.
230. van den Bogaard EH, Rodijk-Olthuis D, Jansen PA, van Vlijmen-Willems IM, van Erp PE, Joosten I, Zeeuwen PL, Schalkwijk J. Rho kinase inhibitor Y-27632 prolongs the life span of adult human keratinocytes, enhances skin equivalent development, and facilitates lentiviral transduction. *Tissue Eng Part A* 2012; 18: 1827-1836.
231. Horani A, Nath A, Wasserman MG, Huang T, Brody SL. Rho-associated protein kinase inhibition enhances airway epithelial Basal-cell proliferation and lentivirus transduction. *Am J Respir Cell Mol Biol* 2013; 49: 341-347.
232. Shaykhiev R, Zuo WL, Chao I, Fukui T, Witover B, Brekman A, Crystal RG. EGF shifts human airway basal cell fate toward a smoking-associated airway epithelial

phenotype. *Proceedings of the National Academy of Sciences of the United States of America* 2013; 110: 12102-12107.
233. Palechor-Ceron N, Suprynowicz FA, Upadhyay G, Dakic A, Minas T, Simic V, Johnson M, Albanese C, Schlegel R, Liu X. Radiation induces diffusible feeder cell factor(s) that cooperate with ROCK inhibitor to conditionally reprogram and immortalize epithelial cells. *Am J Pathol* 2013; 183: 1862-1870.
234. Moutasim KA, Nystrom ML, Thomas GJ. Cell migration and invasion assays. *Methods Mol Biol* 2011; 731: 333-343.
235. Jenei V, Nystrom ML, Thomas GJ. Measuring invasion in an organotypic model. *Methods Mol Biol* 2011; 769: 223-232.
236. Li H, Da LJ, Fan WD, Long XH, Zhang XQ. Transcription factor glioma-associated oncogene homolog 1 is required for transforming growth factor-beta1-induced epithelial-mesenchymal transition of non-small cell lung cancer cells. *Mol Med Rep* 2015; 11: 3259-3268.
237. Wansleeben C, Bowie E, Hotten DF, Yu YR, Hogan BL. Age-related changes in the cellular composition and epithelial organization of the mouse trachea. *PLoS One* 2014; 9: e93496.
238. Sander JD, Joung JK. CRISPR-Cas systems for editing, regulating and targeting genomes. *Nat Biotechnol* 2014; 32: 347-355.
239. Rao DD, Vorhies JS, Senzer N, Nemunaitis J. siRNA vs. shRNA: similarities and differences. *Adv Drug Deliv Rev* 2009; 61: 746-759.
240. Liang CC, Park AY, Guan JL. In vitro scratch assay: a convenient and inexpensive method for analysis of cell migration in vitro. *Nat Protoc* 2007; 2: 329-333.
241. Thomasson M, Hedman H, Ljungberg B, Henriksson R. Gene expression pattern of the epidermal growth factor receptor family and LRIG1 in renal cell carcinoma. *BMC research notes* 2012; 5: 216.
242. Meuwissen R, Berns A. Mouse models for human lung cancer. *Genes & development* 2005; 19: 643-664.
243. Ji H, Ramsey MR, Hayes DN, Fan C, McNamara K, Kozlowski P, Torrice C, Wu MC, Shimamura T, Perera SA, Liang MC, Cai D, Naumov GN, Bao L, Contreras CM, Li D, Chen L, Krishnamurthy J, Koivunen J, Chirieac LR, Padera RF, Bronson RT, Lindeman NI, Christiani DC, Lin X, Shapiro GI, Janne PA, Johnson BE, Meyerson M, Kwiatkowski DJ, Castrillon DH, Bardeesy N, Sharpless NE, Wong KK. LKB1 modulates lung cancer differentiation and metastasis. *Nature* 2007; 448: 807-810.
244. Xiao Z, Jiang Q, Willette-Brown J, Xi S, Zhu F, Burkett S, Back T, Song NY, Datla M, Sun Z, Goldszmid R, Lin F, Cohoon T, Pike K, Wu X, Schrump DS, Wong KK, Young HA, Trinchieri G, Wiltrout RH, Hu Y. The pivotal role of IKKalpha in the development of spontaneous lung squamous cell carcinomas. *Cancer cell* 2013; 23: 527-540.
245. Malkoski SP, Cleaver TG, Thompson JJ, Sutton WP, Haeger SM, Rodriguez KJ, Lu SL, Merrick D, Wang XJ. Role of PTEN in basal cell derived lung carcinogenesis. *Molecular carcinogenesis* 2014; 53: 841-846.
246. Xu C, Fillmore CM, Koyama S, Wu H, Zhao Y, Chen Z, Herter-Sprie GS, Akbay EA, Tchaicha JH, Altabef A, Reibel JB, Walton Z, Ji H, Watanabe H, Janne PA, Castrillon DH, Rustgi AK, Bass AJ, Freeman GJ, Padera RF, Dranoff G, Hammerman PS, Kim CF, Wong KK. Loss of Lkb1 and Pten leads to lung squamous cell carcinoma with elevated PD-L1 expression. *Cancer cell* 2014; 25: 590-604.
247. Ferone G, Song JY, Sutherland KD, Bhaskaran R, Monkhorst K, Lambooij JP, Proost N, Gargiulo G, Berns A. SOX2 Is the Determining Oncogenic Switch in Promoting Lung Squamous Cell Carcinoma from Different Cells of Origin. *Cancer cell* 2016; 30: 519-532.

248. Wattenberg LW, Estensen RD. Chemopreventive effects of myo-inositol and dexamethasone on benzo[a]pyrene and 4-(methylnitrosoamino)-1-(3-pyridyl)-1-butanone-induced pulmonary carcinogenesis in female A/J mice. *Cancer research* 1996; 56: 5132-5135.
249. Vikis HG, Rymaszewski AL, Tichelaar JW. Mouse models of chemically-induced lung carcinogenesis. *Frontiers in bioscience* 2013; 5: 939-946.
250. Yoshimoto T, Inoue T, Iizuka H, Nishikawa H, Sakatani M, Ogura T, Hirao F, Yamamura Y. Differential induction of squamous cell carcinomas and adenocarcinomas in mouse lung by intratracheal instillation of benzo(a)pyrene and charcoal powder. *Cancer research* 1980; 40: 4301-4307.
251. Wang Y, Zhang Z, Yan Y, Lemon WJ, LaRegina M, Morrison C, Lubet R, You M. A chemically induced model for squamous cell carcinoma of the lung in mice: histopathology and strain susceptibility. *Cancer research* 2004; 64: 1647-1654.
252. Tago Y, Yamano S, Wei M, Kakehashi A, Kitano M, Fujioka M, Ishii N, Wanibuchi H. Novel medium-term carcinogenesis model for lung squamous cell carcinoma induced by N-nitroso-tris-chloroethylurea in mice. *Cancer science* 2013; 104: 1560-1566.
253. Mazzilli SA, Hershberger PA, Reid ME, Bogner PN, Atwood K, Trump DL, Johnson CS. Vitamin D Repletion Reduces the Progression of Premalignant Squamous Lesions in the NTCU Lung Squamous Cell Carcinoma Mouse Model. *Cancer prevention research* 2015; 8: 895-904.
254. Singh SV, Benson PJ, Hu X, Pal A, Xia H, Srivastava SK, Awasthi S, Zaren HA, Orchard JL, Awasthi YC. Gender-related differences in susceptibility of A/J mouse to benzo[a]pyrene-induced pulmonary and forestomach tumorigenesis. *Cancer letters* 1998; 128: 197-204.
255. Hudish TM, Opincariu LI, Mozer AB, Johnson MS, Cleaver TG, Malkoski SP, Merrick DT, Keith RL. N-nitroso-tris-chloroethylurea induces premalignant squamous dysplasia in mice. *Cancer prevention research* 2012; 5: 283-289.
256. Rekhtman N, Ang DC, Sima CS, Travis WD, Moreira AL. Immunohistochemical algorithm for differentiation of lung adenocarcinoma and squamous cell carcinoma based on large series of whole-tissue sections with validation in small specimens. *Modern pathology : an official journal of the United States and Canadian Academy of Pathology, Inc* 2011; 24: 1348-1359.
257. Uchihashi M, Wilding LA, Nowland MH. Surgical Correction of Rectal Prolapse in Laboratory Mice (Mus musculus). *Journal of the American Association for Laboratory Animal Science : JAALAS* 2015; 54: 433-438.
258. Burkholder T, Foltz C, Karlsson E, Linton CG, Smith JM. Health Evaluation of Experimental Laboratory Mice. *Current protocols in mouse biology* 2012; 2: 145-165.
259. Ghosh M, Dwyer-Nield LD, Kwon JB, Barthel L, Janssen WJ, Merrick DT, Keith RL. Tracheal dysplasia precedes bronchial dysplasia in mouse model of N-nitroso trischloroethylurea induced squamous cell lung cancer. *PloS one* 2015; 10: e0122823.
260. Yamano S, Gi M, Tago Y, Doi K, Okada S, Hirayama Y, Tachibana H, Ishii N, Fujioka M, Tatsumi K, Wanibuchi H. Role of deltaNp63(pos)CD44v(pos) cells in the development of N-nitroso-tris-chloroethylurea-induced peripheral-type mouse lung squamous cell carcinomas. *Cancer science* 2016; 107: 123-132.
261. Kurie JM, Shin HJ, Lee JS, Morice RC, Ro JY, Lippman SM, Hittelman WN, Yu R, Lee JJ, Hong WK. Increased epidermal growth factor receptor expression in metaplastic bronchial epithelium. *Clinical cancer research : an official journal of the American Association for Cancer Research* 1996; 2: 1787-1793.

262. Chen Z, Fillmore CM, Hammerman PS, Kim CF, Wong KK. Non-small-cell lung cancers: a heterogeneous set of diseases. *Nature reviews Cancer* 2014; 14: 535-546.
263. Ambrosini V, Nanni C, Pettinato C, Fini M, D'Errico A, Trepidi S, Spinelli A, Al-Nahhas A, Rubello D, Zompatori M, Fabbri M, Franchi R, Fanti S. Assessment of a chemically induced model of lung squamous cell carcinoma in mice by 18F-FDG small-animal PET. *Nuclear medicine communications* 2007; 28: 647-652.
264. Hong KU, Reynolds SD, Watkins S, Fuchs E, Stripp BR. Basal cells are a multipotent progenitor capable of renewing the bronchial epithelium. *The American journal of pathology* 2004; 164: 577-588.
265. Zuo W, Zhang T, Wu DZ, Guan SP, Liew AA, Yamamoto Y, Wang X, Lim SJ, Vincent M, Lessard M, Crum CP, Xian W, McKeon F. p63(+)Krt5(+) distal airway stem cells are essential for lung regeneration. *Nature* 2015; 517: 616-620.
266. Yatabe Y, Mitsudomi T, Takahashi T. TTF-1 expression in pulmonary adenocarcinomas. *Am J Surg Pathol* 2002; 26: 767-773.
267. Tang X, Shigematsu H, Bekele BN, Roth JA, Minna JD, Hong WK, Gazdar AF, Wistuba, II. EGFR tyrosine kinase domain mutations are detected in histologically normal respiratory epithelium in lung cancer patients. *Cancer research* 2005; 65: 7568-7572.
268. Namati E, Thiesse J, Sieren JC, Ross A, Hoffman EA, McLennan G. Longitudinal assessment of lung cancer progression in the mouse using in vivo micro-CT imaging. *Med Phys* 2010; 37: 4793-4805.
269. Li F, Ye ZQ, Guo DS, Yang WM. Suppression of bladder cancer cell tumorigenicity in an athymic mouse model by adenoviral vector-mediated transfer of LRIG1. *Oncol Rep* 2011; 26: 439-446.
270. Sage EK, Kolluri KK, McNulty K, Lourenco Sda S, Kalber TL, Ordidge KL, Davies D, Gary Lee YC, Giangreco A, Janes SM. Systemic but not topical TRAIL-expressing mesenchymal stem cells reduce tumour growth in malignant mesothelioma. *Thorax* 2014; 69: 638-647.